Late Quaternary ice-ocean interactions in central West Greenland

MCCARTHY, DAVID,JOHN

Abstract

A greater knowledge of the interactions between the Greenland Ice Sheet and climate is critical to understanding the possible impacts of future global warming, including ice sheet contribution to global sea-level rise and perturbations to ocean circulation. Recent acceleration, thinning and retreat of major tidewater glaciers in Greenland and Antarctica during the past two decades demonstrate the potential for ice sheets to respond to climate change much faster than previously assumed. One approach to understanding the role of atmospheric and oceanic warming to ice sheet dynamics is to investigate how ice sheets responded to past periods of climate change.

This thesis uses benthic foraminifera as a proxy to reconstruct past changes in the temperature of the relatively warm West Greenland Current, to investigate the possible influence of ocean warming on ice sheet dynamics during the initial marine-based deglaciation phase, and throughout the Holocene, when the ice was positioned close to the present margin. This thesis finds that the marine-based ice sheet in central West Greenland collapsed rapidly due to a combination of high relative sea-level and ice sheet thinning due to climatic warming. Foraminiferal evidence does not support a major influence of ocean forcing on initial deglaciation. However, Holocene changes in the relative temperature of the West Greenland Current may have had a more significant influence on ice stream dynamics following the marine-based ice retreat, when outlet glaciers were positioned within coastal fjords. Changes in the relative temperature of the West Greenland Current are determined “upstream” by wider scale changes in the North Atlantic region.

Department of Geography

Late Quaternary ice-ocean interactions in central West Greenland

David John McCarthy

Grey College

May 2011

Submitted for the degree of Doctor of Philosophy

Table of Contents

List of Tables

List of Figures

Chapter 1

Chapter 2

Chapter 3

Chapter 4

Chapter 5

Chapter 6

Chapter 7

Chapter 8

List of Abbreviations

AA	Agglutinated assemblage
A.D.	*Anno Domini*
AMOC	Atlantic meridional overturning circulation
AO	Arctic Oscillation
B2k	before A.D. 2000
BC	Baffin Current
Ka BP	thousand years before present, where 'present' is defined as A.D. 1950
CA	Calcareous assemblage
CTD	Conductivity, temperature, depth
(D)(p)CCA	(Detrended) (partial) canonical correspondence analysis
DBD	Dry bulk density
DCA	Detrended correspondence analysis
DSOW	Denmark Strait Overflow Water
EDA	European Dark Ages
EGC	East Greenland Current
FAZ	Foraminiferal assemblage zone
G (suffix)	Gravity core
GICC05	Greenland Ice Core Chronology 2005
GrIS	Greenland Ice Sheet
HML	Holocene Marine Limit
HTM	Holocene thermal maximum
IC	Irminger Current
IRD	Ice-rafted debris/detritus
LIA	Little Ice Age
LGM	Last Glacial Maximum
LOI	Loss-on-ignition
LSW	Labrador Sea Water
MC (suffix)	Multicore

MCE	maximum counting error (in years)
MRE	Marine reservoir effect
MS	Magnetic susceptibility
MWGC	Mixed-West Greenland Current
MWP	Mediaeval Warm Period
NAC	North Atlantic Current
NADW	North Atlantic Deep Water
NAO	North Atlantic Oscillation
NeoG	Neoglaciation
PW	Polar Water
RMSEP	Root mean square error of prediction
RSL	Relative sea-level
RWP	Roman Warm Period
SD	Standard deviation
SW	Surface Water
TA	Total assemblage
TLDA	Total (living+dead) assemblage
(V)DPB	Vienna Pee Dee Belemnite
WA	Weighted-averaging
WA-PLS	Weighted-averaging partial least squares
WGC	West Greenland Current
XRF	X-ray fluorescence
YD	Younger Dryas

Declaration

I confirm that no part of the material presented in this thesis has previously been submitted by me or any other person for a degree in this or any other institution. In all cases, where relevant, material from the work of others has been acknowledged.

This thesis benefits from data provided by several project collaborators. Where additional data has been used, this has been acknowledged at the beginning of each chapter, and within the main text itself. Contributions from collaborators are briefly acknowledged below. Unpublished modern foraminifera data analysed in Chapter 4 have been provided by Jeremy M. Lloyd. This enhances the modern database presented in Lloyd (2006a). Environmental data associated with foraminifera surface sample assemblages collected during the R.V. "Porsild" cruise during September-August 1999 were provided by Jeremy M. Lloyd, and are published in Lloyd (2006a). CTD data (water temperature and salinity) was collected during the cruises of the R.V. "Porsild" and R.V. "Maria S. Merian" (June-July 2007). XRF and magnetic susceptibility core scanning data was undertaken aboard the R/V "Maria S. Merian" shortly after core retrieval. Kerstin Perner and Matthias Moros (Leibniz-Institut für Ostseeforschung Warnemünde - IOW) provided digital X-ray radiographs of core MSM-343340_G (Chapter 5) and MSM-343520_G (Chapter 6) grain size data obtained by sieving of coarse grain size fractions. Kerstin Perner provided loss-on-ignition and moisture content data from core MSM-343520-G (Chapter 6). Noortje Dijkstra (University of Amsterdam) provided grain size (laser diffraction) data for core MSM-343520_G (Chapter 5). David H. Roberts provided unpublished cosmogenic radionuclide dates from the Uummannaq terrestrial margin, which are used in Chapter 6. Camilla S. Andresen (GEUS) provided sedimentological (sieving of coarse grain size fractions and clast counts), petrological, and magnetic susceptibility core scanning data from core DA06-139G used in Chapter 7. This data is presented in Andresen et al. (2011). Some of this data is also shown in the summary chapter (Chapter 8).

Statement of Copyright

Signed:

David John McCarthy
University of Durham
May 2011

Acknowledgements

Firstly, I would like to thank my supervisors, Dr. Jeremy Lloyd, Dr. David Roberts, and Dr. Andreas Vieli, for their valuable advice, support, and patience during my PhD, and at times going beyond the call of duty. A special thank you to Jerry for the time you have dedicated to getting me to the finishing line.

Funding provided by a Durham Doctoral Fellowship made it possible to undertake this PhD research. Isotope analyses on calcareous foraminifera were funded by a NERC award (IP/1046/0508) and analysed by Melanie Leng and colleagues at the NERC Isotope Geoscience Laboratory (NIGL) in Keywoth. The Dudley Stamp Memorial Fund kindly provided funding towards laboratory visits to sub-sample core material in Germany. The Quaternary Research Association and National Science Foundation provided funds that allowed me to present some of my findings in this thesis at very enjoyable conferences.

I would like to thank friends, colleagues, and collaborators working on the wider research project in West Greenland. This thesis has benefited from data provided by, and discussions with Jerry Lloyd, Dave Roberts (Durham), Matthias Moros, Kerstin Perner, Nicolas Krauß (IOW), Antoon Kuijpers, Camilla Andresen (GEUS), Ian Snowball (University of Lund), Anne Jennings (University of Colorado at Boulder); Noortje Dikstra and Simon Troelstra (Univeristy of Amsterdam). Neil Tunstall, Amanda Hayton, and Martin West provided valuable help and advice with regards to lab analyses in the Geography Department, Durham University.

Matthias Moros and Thomas Leipe invited me to experience the Baltic Sea during December aboard the FS "Professor A. Penck" before it was decommissioned. Thanks to cruise members for an enjoyable experience, and a slightly unusual birthday. Thanks also to Antoon Kuijpers for the experience of dodging icebergs, spotting whales, seeing a spectacular *Aurora Borealis*, and collecting a few marine samples in front of Jakobshavn Isfjord, and for the company of Naja Mikkelsen and Simon Troelstra, and crew, while aboard the RV “Porsild”.

Thanks to all those who helped make my time at Durham so enjoyable; including Steve Dugdale, Natasha Barlow, Chris Brodie (and for his critiques of science!), Ed Garrett, and all those who shared many, many hours in SRIF looking down a microscope, and the top floor SRIF 'crew' for providing cake to keep us going! Thanks to all those who have provided a bed for the night (or much more!) on various ventures; Kerstin, for an extended stay in her living room, Matthias and Claudia, when the Penck broke down; Kerstin, Ed and Caroline, Chris and Rachel, Steve and Claire.

To Jeay, thank you for the many happy memories of our time together, and the love and support you gave me through the most difficult period of my life.

Finally, thank you Mum and Dad for encouraging me to pursue my interests, supporting me when things did not quite go to plan, and looking after me while I acquired a colourful medical history.

For Mum and Dad

Chapter 1

Introduction

Introduction

1.1 Introduction

The Greenland Ice Sheet (GrIS) (*Fig. 1.1*) is the only great northern hemisphere ice sheet that has survived to the present day. The modern GrIS contains more than 7 m equivalent sea level (Lemke *et al.*, 2007), and contributes approximately 0.5 mm a^{-1} to global mean sea-level rise (Shepherd and Wingham, 2007). A greater knowledge of the interactions between the GrIS and climate is critical to understanding the possible impacts of future global warming, including ice sheet contribution to global sea-level rise and perturbations to ocean circulation (Alley *et al.*, 2005). It has become apparent that since the mid-1990s, the GrIS has been losing mass at an accelerating rate (Krabill *et al.*, 2000; Krabill *et al.*, 2004; Chen *et al.*, 2006; Ramillien *et al.*, 2006; Velicogna and Wahr, 2006; Luthcke *et al.*, 2007). Rapid instabilities in fast-flowing ice stream systems, the main outlets by which the GrIS evacuates ice to the oceans, appear to be the main source of this mass imbalance (Rignot and Kanagaratnam, 2006). The acceleration, thinning and retreat of major tidewater glaciers in Greenland during the past two decades demonstrates the potential for ice sheets to respond to climate change much faster than previously assumed (Zwally *et al.*, 2002; Krabill *et al.*, 2004; Rignot and Kanagaratnam, 2006; Howat *et al.*, 2007; Luthcke *et al.*, 2006). Jakobshavn Isbræ, which drains approximately 7% of the GrIS into Disko Bugt, central West Greenland, is one such glacier that underwent significant changes between 1997 and 2003, including a near doubling in velocity and the collapse of the floating marine-based terminus (Bindschadler, 1984; Abdalati and Krabill, 1999; Thomas *et al.*, 2003; Joughin *et al.*, 2004; Podlech and Weidick, 2004; Thomas, 2004). However, the driving mechanisms behind these changes remain poorly understood.

A key uncertainty is the role of atmospheric versus oceanic forcing influencing ice sheet dynamics. Atmospheric warming may drive rapid instabilities through enhanced ablation and subsequent meltwater penetration to the ice sheet bed, leading to basal lubrication and acceleration of ice streams (e.g. Zwally *et al.*, 2002; Thomas *et al.*, 2003). Alternatively, warmer ocean temperatures may cause abrupt changes in ice sheet behaviour by enhancing basal

melting of the marine-based portions of the ice sheet, resulting in thinning of floating ice, enhanced calving, and ice stream acceleration (Payne *et al.*, 2004; Bindschadler, 2006; Holland *et al.*, 2008).

A robust approach to understanding the role of atmospheric and oceanic warming to ice sheet dynamics is to investigate how ice sheets responded to past periods of climate change. The presence of two large trough mouth fans that extend 400 km west of the present ice sheet margin in the Disko Bugt and the Uummannaq area, suggests the GrIS expanded on to the outer continental shelf in the past, and possibly during the last glacial advance. It is likely that large ice stream systems draining into these two areas were a major influence on GrIS dynamics in the past. Previous research in central West Greenland investigating deglacial and Holocene ice sheet history has been largely limited to the terrestrial ice-free margin and the inner continental shelf of Disko Bugt, and has focused on the latter stages of deglaciation. However, there has been little offshore research from the outer shelf in these areas to constrain past ice sheet extent and retreat history.

In light of these shortcomings in our current knowledge, this study seeks to investigate the timing and nature of ice retreat during the early stages of deglaciation, and the possible role of ocean forcing on ice sheet stability during deglaciation and throughout the Holocene.

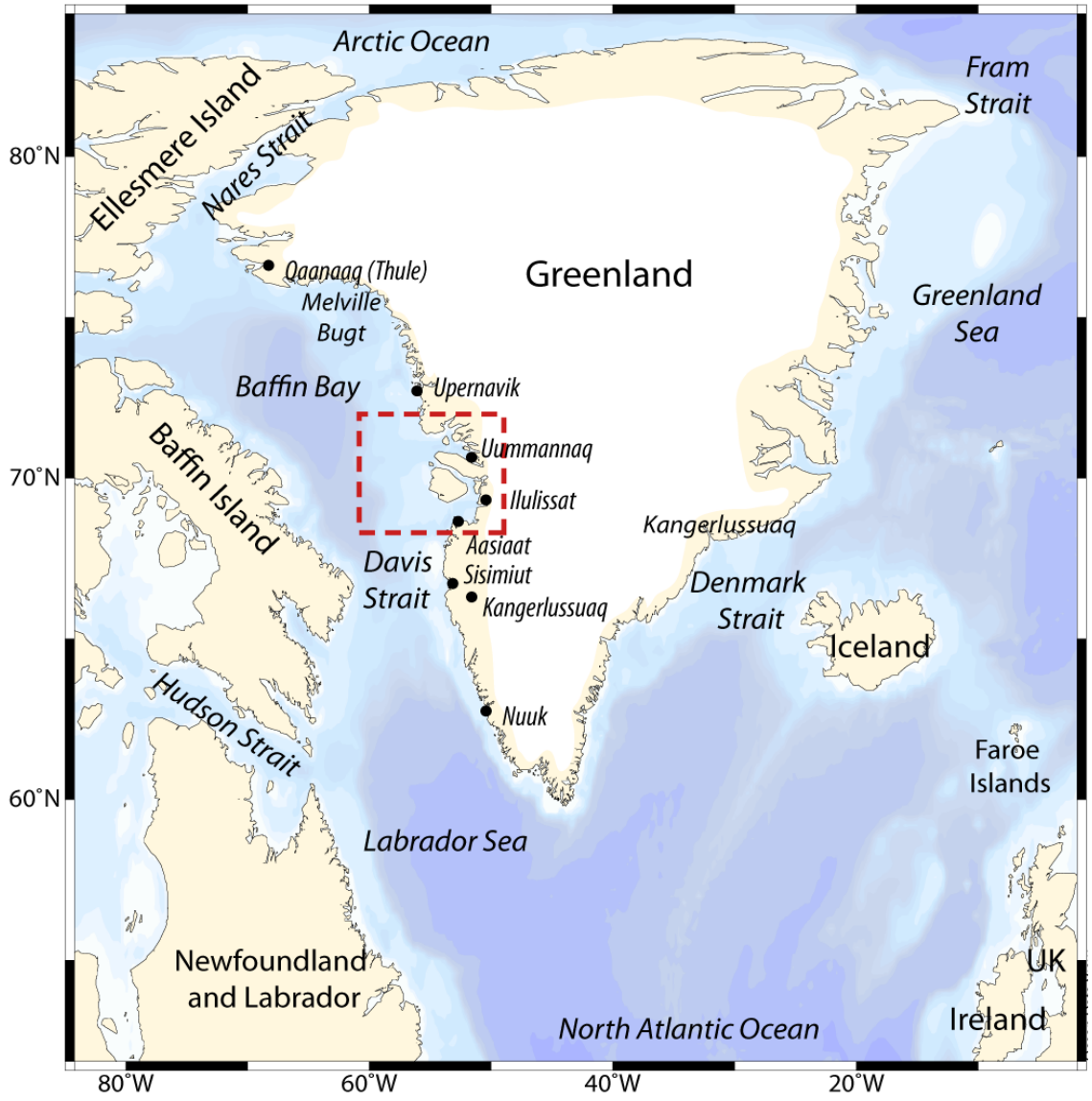

Figure 1.1 Map of Greenland showing location of study area in red box (illustrated in *Fig. 1.2*).

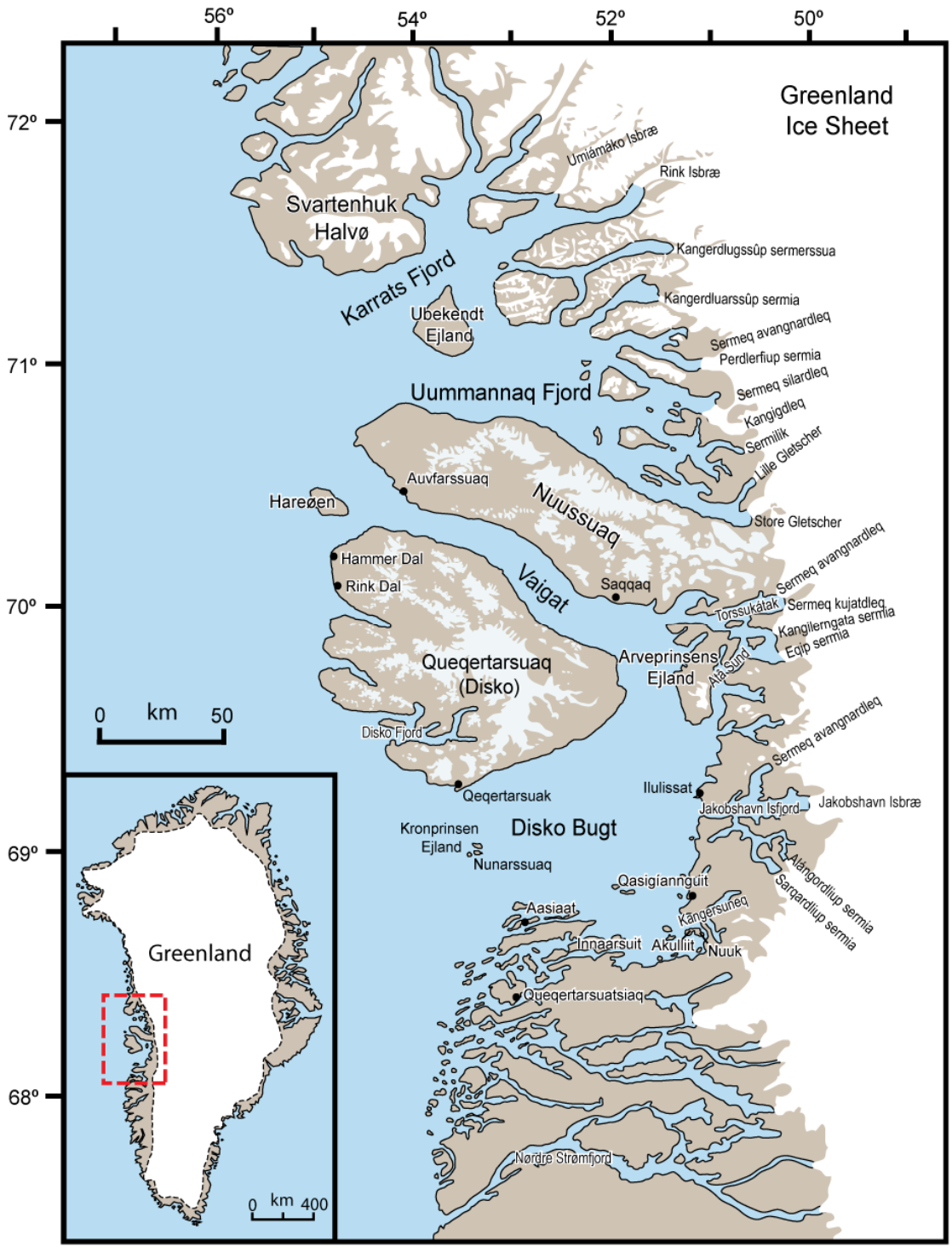

Figure 1.2 Map showing location of major settlements, outlet glaciers, fjords, and study sites mentioned in text.

1.2 Research aims and objectives

The overarching aim of this thesis is to investigate deglacial and Holocene changes in the activity of major West Greenland ice streams, and identify possible interactions between climate, ocean circulation, and ice sheet dynamics.

This broad aim is investigated using proxy evidence from offshore geological records (sediment cores) from three key locations, and is addressed with reference to five specific objectives outlined below:

i) To investigate the ecology of modern benthic foraminifera assemblages in central West Greenland in order to more reliably reconstruct past environmental changes from fossil foraminifera assemblages.

ii) To assess fossil sediment cores for evidence of reworking and their suitability for high-resolution palaeoceanographic reconstructions, and identify changes in glacimarine sedimentation linked to major West Greenland ice streams.

iii) To assess Funder and Hansen's (1996) model for deglaciation in the central west sector of the Greenland Ice Sheet, and to identify alternative driving mechanisms for ice retreat where the pattern of deglaciation differs from this model.

iv) To establish high resolution deglacial and Holocene records of changes in local and regional water mass characteristics from marine records representative of proximal and distal locations to the Greenland Ice Sheet

v) To compare these new marine records documenting changes in ocean circulation and ice stream activity to other published marine, terrestrial and ice core records, in order to identify and evaluate possible driving mechanisms of ice stream behaviour.

1.3 Wider justification and context for research

Over the past 100 years, the Arctic has warmed at nearly twice the global average rate (Serreze and Francis, 2006; Trenberth *et al.*, 2007; Kaufman and Arctic Lakes 2k Project Members, 2009). Since 1950, average Arctic temperatures have increased by 2-3°C and winter temperatures have risen by up to 4°C (Huntingdon and Weller, 2004). The Arctic is warmer at the present than at any time in the preceding 1300 years, and climate projections indicate this warming trend will continue in future decades (Trenberth *et al.*, 2007).

While ice sheet mass balance estimates vary (e.g. Thomas *et al.*, 2008), there is a consensus that the GrIS is losing mass, and that the rate of ice loss has increased in the past decade. Ice losses are due to surface ablation at low altitudes and acceleration of outlet glaciers at the ice margin (Luthcke *et al.*, 2006). Two-thirds of ice mass loss is believed to be due to ice dynamics (Rignot and Kanagaratnam, 2006). There is growing evidence of ocean forcing on ice margin stability (e.g. Rignot and Jacobs, 2002; Payne *et al.*, 2004; Luckman *et al.*, 2006; Walker *et al.,* 2007; Holland *et al.*, 2008; Hanna *et al.*, 2009; Nick *et al.*, 2009; Rignot *et al.* 2010). In Greenland, marine-terminating glaciers have accelerated, thinned, and retreated much faster than land-terminating glaciers (Sole *et al.*, 2008; Moon and Joughin, 2008). There also appears to be a trend of marine-terminating glacier acceleration spreading northwards (e.g Rignot and Kanagaratnam, 2006). Thomas (2004) identified average ice shelf thinning of 80 m a^{-1} immediately preceding the acceleration and collapse of Jakobshavn Isbræ's floating ice tongue, which took place between 1997 and 2003. These rates are considerably higher than thinning rates of nearby grounded ice, suggesting that basal melting due to warmer ocean temperatures may be responsible. Holland *et al.* (2008) found that a pulse of warm sub-surface water was transported northwards along the West Greenland coast, and entered Disko Bugt and Jakobshavn Isfjord in 1997, coinciding with initial rapid changes in ice stream behaviour. Recent studies in Greenland and Antarctica suggest ocean forcing may be an important influence on modern ice stream stability (e.g. Jenkins *et al.*, 1997; Payne *et al.*, 2004; Walker *et al.*, 2007; Holland *et al.*, 2008; Straneo *et al.*, 2010; Rignot *et al.*, 2010). It is therefore likely that ocean temperature changes have influenced ice margin dynamics over longer timescales.

Understanding the driving mechanisms behind collapses of marine-based ice is a key societal concern. This is particularly pertinent for the West Antarctic Ice Sheet, which is grounded below sea level, contains 5.6 m sea level equivalent, and is the world's most unstable ice sheet and a large potential contributor to future sea level rise (e.g. Vaughan and Spouge, 2002; Overpeck, *et al.*, 2006). Recent research in Antarctica has identified similar accelerations and thinning of ice streams to those observed in Greenland (Rignot, 2001; Shepherd *et al.*, 2001; Rignot *et al.*, 2002). However, the rapid response of inland ice to the loss of ice-shelves in Greenland and Antarctica indicates that ice grounded above sea level is also vulnerable to future perturbations (e.g. Rignot *et al.*, 2002; Shepherd *et al.*, 2002; de Angelis and Skvarca, 2003). Warming subsurface ocean temperature is one cause of ongoing ice loss (Rignot and Jacobs, 2002; Shepherd *et al.*, 2004). However, the potential for warmer subsurface waters to drive large-scale changes in ice dynamics is at present poorly understood.

1.4 Rationale behind research objectives

1.4.1 Objective (i)

To investigate the ecology of modern benthic foraminifera assemblages in central West Greenland in order to more reliably reconstruct past environmental changes from fossil foraminifera assemblages.

Identifying environmental controls on modern benthic foraminifera provides a foundation for correctly interpreting fossil benthic foraminiferal assemblages and reconstructing palaeoenvironmental change. Data from other studies of modern and fossil benthic foraminifera from high-latitude shelf and fjord environments will supplement interpretations of modern foraminiferal assemblages from central West Greenland. Statistical analyses on the recently extended modern foraminifera dataset will assess whether benthic foraminifera from the central West Greenland shelf may be a reliable and robust proxy that can be used to semi-quantitatively reconstruct environmental parameters from fossil foraminifera assemblages. This may aid our understanding of the characteristics of intermediate waters impinging on the seafloor in central West Greenland.

1.4.2 Objective (ii)

To assess fossil sediment cores for evidence of reworking and their suitability for high-resolution palaeoceanographic reconstructions, and identify changes in glacimarine sedimentation linked to major West Greenland ice streams.

Sediment reworking (e.g. sediment-gravity flows, turbidity currents, bioturbation, iceberg scouring) is common in high-latitude continental shelf settings influenced by rapid sediment accumulation. It is therefore necessary to assess sedimentary deposits for evidence of reworking, since this has important implications for palaeoceanographic reconstructions using proxy evidence (e.g. Ó Cofaigh *et al.*, 2002). Changes in glacimarine sedimentation may reflect changes in glacial activity at the ice terminus. These may be driven by internal ice sheet dynamics, or external factors such as climate and ocean temperature changes. The characteristics of glacimarine sediments may be used to interpret relative changes in the position of the ice front and/or changes in glacier activity. An understanding of changes in glacimarine sedimentation, which exert a strong influence on surface water conditions, turbidity in the water column, and sedimentation rates, may therefore aid interpretations of foraminiferal assemblages.

1.4.3 Objective (iii)

To assess Funder and Hansen's (1996) model for deglaciation in the central west sector of the Greenland Ice Sheet, and to identify alternative driving mechanisms for ice retreat where the pattern of deglaciation differs from this model.

This study seeks to assess Funder and Hansen's (1996) two-stage deglacial model for Greenland which proposes deglaciation took place in two distinct phases; firstly, an early and rapid clearance of marine-based ice driven by eustatic sea-level rise from *ca.* 15 ka BP, followed by slower land-based ice retreat driven by atmospheric warming. Basal ages from cores collected from deep offshore troughs on the West Greenland shelf will provide minimum ages to constrain the pattern of fast-flowing ice retreat during deglaciation. The timing and nature of GrIS retreat across the shelf will be identified by comparing basal ages from cores

from the mid-shelf to nearby minimum ages for deglaciation. A robust dating framework allows faunal and sedimentological changes in cores from this study to be compared against other local and regional proxy climate records to help establish driving mechanisms of deglaciation.

A greater knowledge of spatial and temporal differences in deglaciation is a key requirement for validating ice sheet models (e.g. Tarasov and Peltier, 2002; Fleming and Lambeck, 2004; Simpson *et al.*, 2009). Constraining the timing and magnitude of ice sheet, and hence ice volume changes, enables a greater understanding of the role of climate and ocean forcing on modern ice-sheet changes, and improving the predictability of ice sheet response to future climate change and contribution to sea level rise.

1.4.4 Objective (iv)

To establish high-resolution records of deglacial and Holocene changes in local and regional water mass characteristics from marine records representative of proximal and distal locations to the Greenland ice sheet.

By comparison with terrestrial and ice core records, high-resolution records of marine temperature changes during deglaciation and the Holocene will help establish linkages between ice-ocean-climate interactions on ice margin dynamics. A particular focus is to identify the potential influence of relatively warm and saline West Greenland Current (WGC) waters on ice sheet retreat. Links with air temperatures are often well established, though the role of ocean temperatures on ice margin stability is in its infancy. Records in close proximity to ice margins are relatively few in number, and local-to-regional scale variations in ocean circulation patterns present additional challenges to identifying changes in ocean forcing. This is particularly true along the West Greenland shelf, where temperatures at the seafloor are influenced by changes in the influence of Polar and Atlantic-sourced Water.

Current ice-sheet models incorporate reconstructed air temperatures based on ice core data as ‘forcing parameters’ for ice sheet response to climate change. To improve predictability and reduce uncertainty in future ice-sheet models, high quality records of ocean temperature

changes must be incorporated. These records must be collected from shelf locations, such as those used in this thesis, in relatively close proximity to the ice sheet margin.

1.4.5 Objective (v)

To compare these new marine records documenting changes in ocean circulation and ice stream activity to other published marine, terrestrial and ice core records, in order to identify and evaluate possible driving mechanisms of ice stream behaviour.

A robust dating framework allows faunal and sedimentological changes in cores from this study to be compared against other local and regional proxy climate records to help establish forcing mechanisms on ice margin position. Comparing reconstructed changes in the temperature of waters impinging on the West Greenland shelf against other proxy records may help identify how these waters are influenced by wider-scale climate changes in the North Atlantic and Arctic region. Temperature changes in sub-surface waters along West Greenland have been linked to changes in the phase of the North Atlantic Oscillation (NAO) (e.g. Hakkinen and Rhines, 2003; Holland *et al.*, 2008). The penetration of relatively warm Atlantic Water into Jakobshavn Isfjord, where it subsequently enhanced basal melting beneath the floating ice tongue of Jakobshavn Isbræ in Disko Bugt (*Fig. 1.2*), has been traced to an increase in Irminger Current water entrained in the West Greenland Current during a negative NAO phase (Holland *et al.*, 2008). A greater understanding of the linkages between variability in sub-surface WGC water temperatures and wider scale changes in North Atlantic Ocean and atmospheric circulation patterns (e.g. the NAO/Arctic Oscillation) may help identify conditions under which enhanced Atlantic Water may be propagated northwards in the WGC, and potentially influence ice margin stability. Identifying the possible role of warmer ocean temperatures on ice margin stability over longer timescales will improve our understanding of mechanisms of deglaciation and how ice sheets may respond to future oceanic and climate warming.

1.5 Thesis structure

Chapter 2 introduces the West Greenland study area. In order to provide context for interpreting the results of this study, the geological, climatic, oceanographic, and glacial setting of central West Greenland is summarised. Relative ocean temperatures on the West Greenland shelf are strongly influenced "upstream" in the Atlantic and Arctic Ocean. Changes in ice stream activity of the GrIS may also affect global ocean circulation "downstream" through meltwater fluxes to locations of deep-water formation. Therefore, variability in wider-scale oceanography, and how this is manifested in West Greenland waters, is also summarised. Finally, current knowledge concerning deglaciation of the Baffin Bay region, and subsequent ice marginal changes in central West Greenland, are reviewed, and limitations to our understanding are identified.

The material and methods used in this study are introduced in Chapter 3. A synopsis of the location and importance of each core site is given, and the sampling strategy used for each core with respect to addressing the research questions for this thesis is given. The methods used to approach these questions are introduced and briefly reviewed to provide context for the analysis and interpretation of the results. Methods of statistical modelling (multivariate methods) are also introduced.

In Chapter 4, the relationships between modern benthic foraminifera and environmental variables are explored using multivariate methods. This identifies the major controls on the distribution of modern benthic foraminifera in central West Greenland, particularly the relationship of benthic foraminifera to water mass characteristics (i.e. temperature and salinity of water impinging on the shelf). These data provide a basis for interpreting past changes in the relative temperature of the basal water mass impinging on the seafloor of the West Greenland continental shelf. A preliminary transfer function is also developed that may be applied to fossil benthic foraminifera assemblages to provide estimates of past water temperatures. Discussion of the results is supplemented with reference to other benthic foraminiferal investigations from high latitude shelf locations.

In each of Chapters 5, 6, and 7, the results of analyses on marine sediment cores from key sites on the mid-shelf west of Disko Bugt, in the Vaigat, and the mid-shelf west of Uummannaq Fjord, respectively, are presented. The three key locations are presented and discussed individually since each core is investigated with respect to different research objectives. The timing and nature of deglaciation, and ocean conditions during initial deglaciation west of Disko Bugt (as the ice sheet retreats from an 'ice-proximal' position) is investigated in Chapter 5. Chapter 6 provides constraints of the timing of initial deglaciation on the Uummannaq shelf, investigates marine conditions during the early stages of deglaciation, and provides a more regional scale reconstruction for possible marine forcing when the ice sheet has retreated landwards to an 'ice-distal' location. Chapter 7 focuses on mid- to late-Holocene conditions in Vaigat. The core from this location provides a link between the southerly core outside Disko Bugt and the northerly core west of Uummannaq. This is because both the relatively warm and saline waters that circulate and may influence ice dynamics in Disko Bugt, and the icebergs calving from marine terminating glaciers in Disko Bugt, exit the bay through this sound, and can be linked to marine and sedimentological influences on conditions on the Uummannaq shelf.

Finally, in Chapter 8, the results from the preceding three chapters are discussed with respect to the main research aim of this thesis, and placed within a wider context. Discussion focuses on Late Quaternary ice-ocean interactions in central West Greenland. This is divided into two parts. Firstly, regional differences in timing and nature of deglaciation of the shelf are identified, and the possible driving mechanisms for this are discussed. Secondly, Holocene oceanographic changes in central West Greenland, and linkages between ice margin changes, climate, and ocean circulation, are discussed. To conclude, the main findings of this thesis are summarised.

All dates in this thesis are reported in calibrated years before present (where present is defined as A.D. 1950), which is abbreviated to "ka BP", unless otherwise explicitly stated. Age ranges are quoted at the two-sigma level.

Chapter 2

Study area and background

Chapter 2
Study area and background

2.1 Introduction

The Greenland Ice Sheet plays an important role in climate dynamics and ocean circulation on a regional to global scale. This chapter provides an overview of the current glacial, oceanographic and climatic setting in the central West Greenland study area. The tightly coupled ice-ocean-atmosphere system responds to external forcings over a range of timescales through complex positive and negative feedbacks. This chapter explores the modern oceanography and climate, and their possible influences on ice-margin dynamics in order to contextualise sub-centennial scale oceanographic changes in marine fossil records from the West Greenland shelf. While an exhaustive review of modern ice-ocean-atmosphere interactions is beyond the scope of this chapter, knowledge of modern (spanning instrumental records) processes operating in the North Atlantic region that may impact upon marine proxy records in central West Greenland is important to make informed interpretations of fossil archives. Therefore, the characteristics, origins and variability of water masses entrained in the West Greenland Current (WGC) are summarised to understand possible causes of changes in the character of this current. Since past climatic extremes beyond modern limits of variability may have been associated with different ocean circulation patterns, it is important to understand regional scale climatic, oceanographic, and glacial influences from the broader North Atlantic and Arctic region that determine the 'downstream' characteristics of the WGC. This provides a firm basis and context for identifying past controls on the relative temperature and salinity of the WGC, which is a strong influence on West Greenland climate, and possibly on dynamics of marine-terminating glaciers during and after the last deglaciation.

2.2 Extent of past research in West Greenland

Although Norse settlers in southwest Greenland made anecdotal descriptions of ice and climatic conditions between the 10th and 15th Centuries, it wasn't until the 1700s that pioneering researchers began to record observations of ice rafting activity and frontal position of local outlet glaciers, including Jakobshavn Isbræ (Weidick and Bennike, 2007). Regular mapping of the

Jakobshavn Isbræ ice front began when H.J. Rink visited in 1850-1851 (Weidick *et al.*, 2003). From 1875, ice velocity measurements were made for outlet glaciers in Disko Bugt (Helland, 1876, cited in Weidick and Bennike, 2007), and instrumental climate records from the Disko Bugt-Uummannaq region extends back to 1807, though almost continuous annual records are only available from 1840 (Box, 2002; Vinther *et al.*, 2006). In recent decades, a particular research focus has been to understand Late Quaternary ice sheet history and environmental changes. Numerous studies have investigated ice-sheet marginal fluctuations (e.g. Weidick, 1968; Weidick, 1972b; Ten Brink and Weidick, 1974; Kelly, 1985; Weidick, 1985; Warren and Hulton, 1990; Weidick, 1996; Long and Roberts, 2002, 2003; Long *et al.*, 2006), changes in climatic conditions (e.g. Fredskild, 1984; Anderson and Leng, 2004), and relative sea-level histories (e.g. Donner and Jungner, 1975; Rasch and Nielsen, 1994, 1995; Rasch *et al.,* 1997; Rasch and Jensen, 1997; Long *et al.*, 1999; Rasch, 2000; Long and Roberts, 2002). While many land-based studies have investigated Holocene environmental change, marine investigations over the past decade have been limited to inner Disko Bugt (e.g. Kuijpers *et al.*, 2001; Park, 2003; Lloyd *et al.*, 2005; Lloyd, 2006b) and local fjord systems (e.g. Gilbert *et al.*, 1998; Desloges *et al.*, 2002; Moros *et al.*, 2006; Lloyd *et al.*, 2007).

2.3 West Greenland

2.3.1 Central West Greenland study area

In this study, central West Greenland refers to the terrestrial and offshore shelf areas between 68°30'N and 72°00'N encompassing Disko Bugt and the Uummannaq area, and the outlet glaciers that feed into fjords in these bays (*Fig. 2.1*). Whereas the continental shelf of Baffin Island on the western margin of Baffin Bay is narrow (typically *ca*. 50 km), the continental shelf off much of West Greenland is relatively wide at more than 150 km. Two large trough mouth fans extend up to a further 100 km off the coast west of Disko Bugt and Uummannaq Fjord (see *Fig. 2.1*). The presence of large sediment fans and deep glacially eroded transverse troughs in Disko Bugt, Vaigat, and Uummannaq extending to the shelf break along the West Greenland continental margin (Zarudzki, 1979) in addition to submarine moraine systems (Brett and Zarudzki, 1979) are suggestive of an extensive offshore GrIS configuration in the past (*Fig. 2.1*).

2.3.2 Geological setting

Knowledge of the Disko Bugt-Uummannaq area geology is of particular importance for identifying sediment provenance and dispersal mechanisms. Three distinct geological areas define Disko Bugt and Uummannaq (*Fig.* 2.2*)*. The mainland (including adjacent smaller islands) and the eastern part of Nuussuaq peninsula form part of the Precambrian basement, consisting of Late Achaean (*ca*. 2800 Ma) orthogneisses, including Atâ tonalite and local granites (Garde and Steenfelt, 1999). The geology of Disko Island is largely composed of Cretaceous-Tertiary clastic sediments in the eastern and northeastern areas, and Tertiary flood basalts and picritic lavas to the west (Henriksen *et al.*, 2000). Quaternary deposits overlie large parts of northern Disko Island and immediately south of Disko Bugt. There is a northern continuation of Lower Tertiary basalts in the western parts of the Uummannaq area, dominating the geology of Ubekendt Ejland and the Svartenhuk Halvø area. Quaternary deposits overlie the basement geology in western Nuussuuaq, eastern Ubekendt Ejland and the eastern part of Svartenhuk Halvø to the north. While the geology of the terrestrial margin is well defined, there is limited data available for the subglacial and offshore geology. Bonow (2005) provides an overview of the general submarine geology in Disko Bugt, shown in *Fig. 2.2*. Tertiary basalts dominate the outer continental shelf west of Kronprinsens Ejland, forming part of a basalt ridge across outer Disko Bugt between Queqertarsuaq and Aasiaat, as well as the western margin of Vaigat and northwards from Nuussuuaq to Svartenhuk Halvø via Ubekendt Ejland (Henriksen *et al.*, 2000). Inner Disko Bugt and the Vaigat consist of Cretaceous-Paleocene sediments, while a continuation of the Precambrian basement is found at the seafloor in southeastern Disko Bugt (Bonow, 2005).

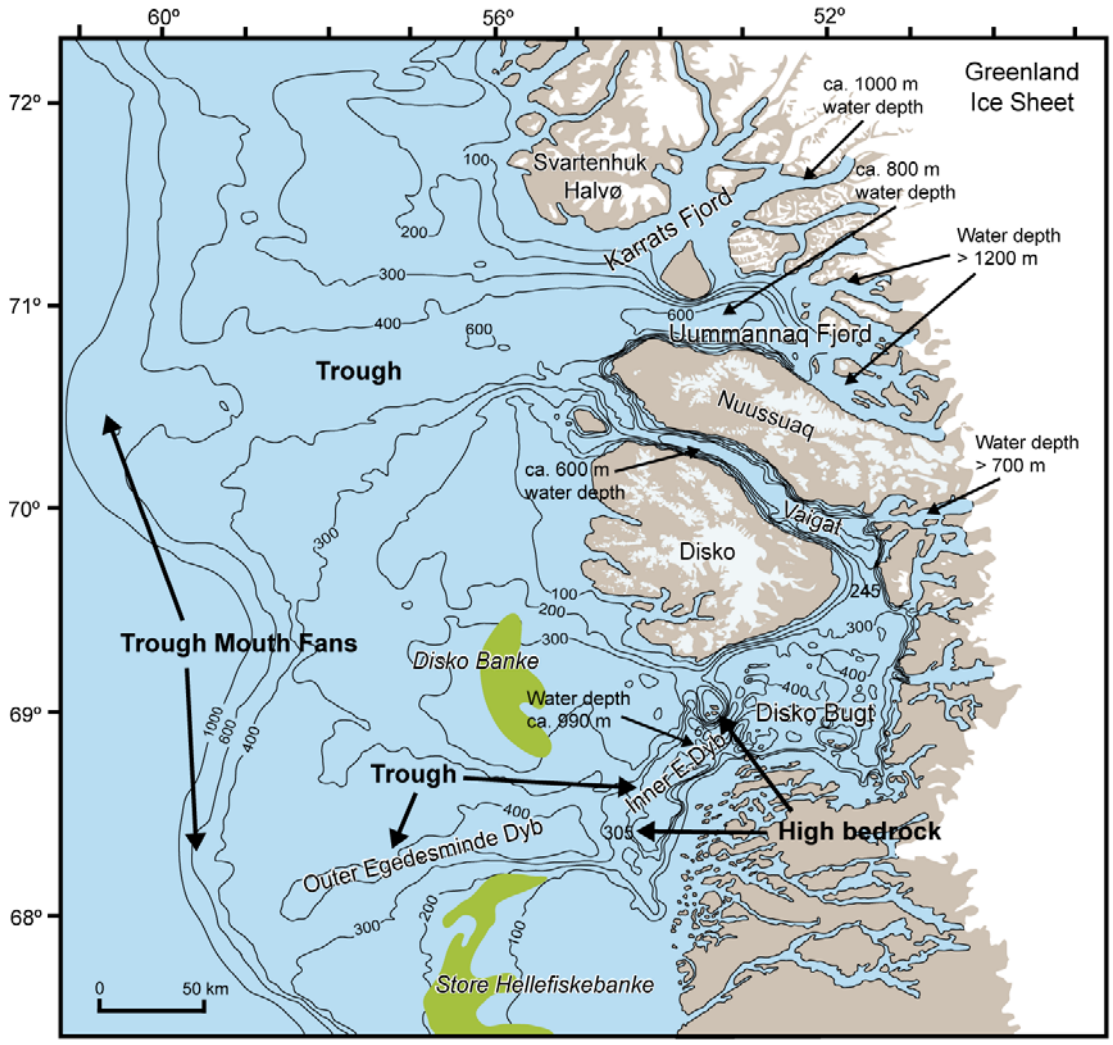

Figure 2.1 Bathymetric map of central West Greenland shelf, showing positions of key features mentioned in text. Green shading marks the position of the Hellefiske moraines. Arrows indicating approximate water depths are based on multibeam echosounding data from Harff (2007) and Ó Cofaigh (2009).

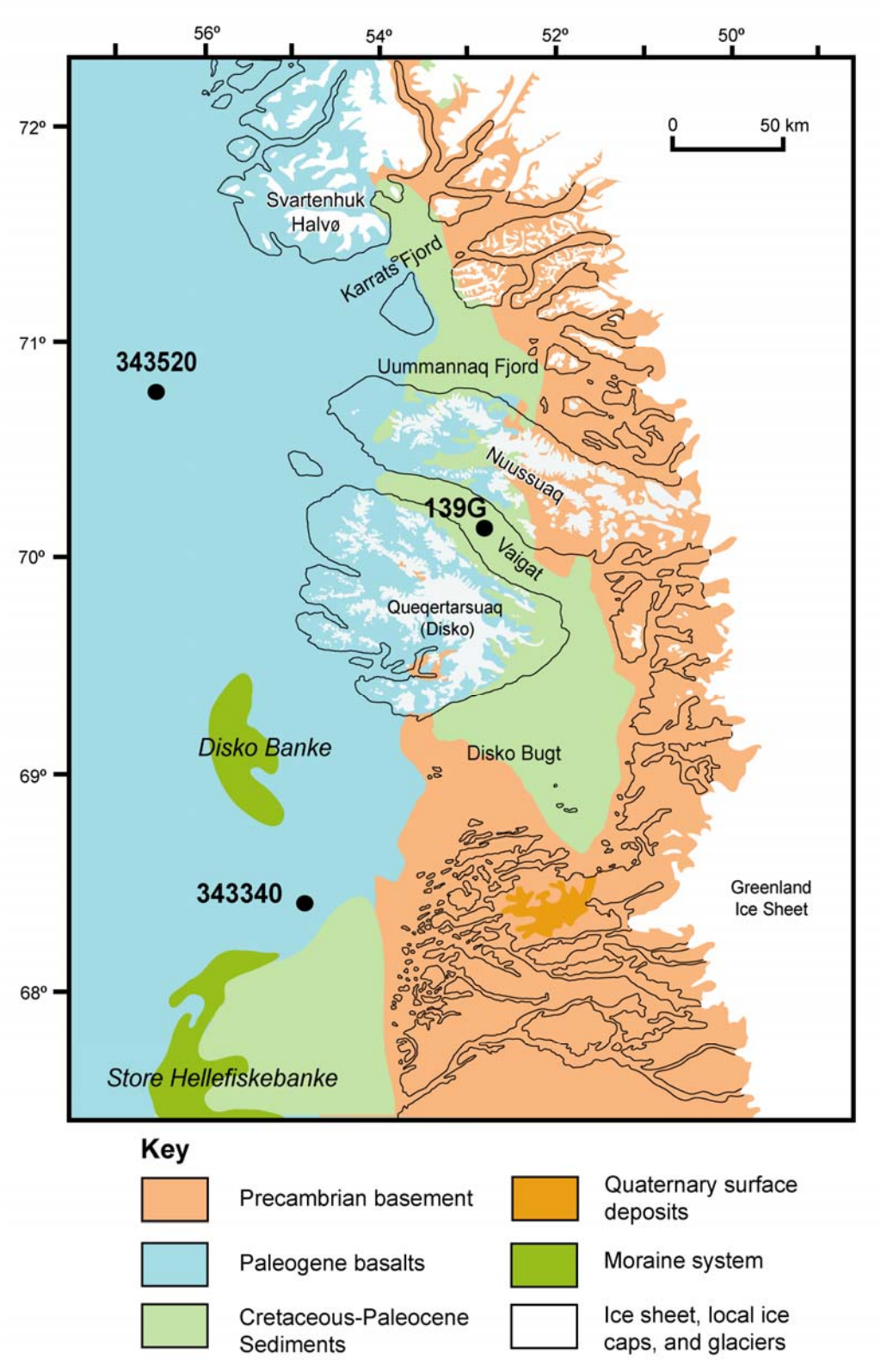

Figure 2.2 Map showing onshore and offshore geology for central West Greenland. Modified from Bonow (2005) and Bonow *et al.* (2006).

2.3.3 West Greenland climate

The climate of Baffin Bay region is strongly influenced by the North American continent, the Greenland Ice Sheet, and surrounding water masses. In Baffin Bay, mean summer temperatures are typically less than 5°C and winter temperatures range between -20°C and -40°C (Valeur *et al.*, 1996). Mean annual air temperatures in West Greenland are consistently 8°C higher than in western Baffin Bay due to the warming influence of the WGC (Williams and Bradley, 1985). Disko Bugt has an arctic marine climate. Mean monthly temperatures range from -15.2°C in March to 8.0°C in July at Ilulissat (Norwegian Meteorological Institute, 2010). Although cyclones are dominantly routed from Newfoundland over southern Greenland towards Iceland, some follow a ridge of low pressure along the West Greenland coast (Valeur *et al.*, 1996). These depressions cause strong southerly winds along West Greenland compared to the moderate winds that usually persist in Baffin Bay. Annual precipitation is typically 200-300 mm in the Disko Bugt area (compared to *ca.* 1000 mm in southwest Greenland), and is greatest during late summer/autumn corresponding with open water conditions and frequent cyclonic activity (Valeur *et al.*, 1998).

A combination of the relative warmth of the WGC and atmospheric forcing determine winter sea-ice extent and duration in Baffin Bay (Stern and Heide-Jørgensen, 2003). Sea-ice (the so-called "Westice") in western Baffin Bay (along the path of the cold Baffin Current; *Fig. 2.3*) is relatively stable, and is partly occupied by multi-year sea-ice sourced from Nares Strait and the Arctic Ocean (Valeur *et al.*, 1996). Sea-ice conditions along West Greenland are more dynamic due to the variable oceanographic conditions (Stern and Heide-Jørgensen, 2003). Sea-ice typically develops in Baffin Bay and Davis Strait during mid-October due to declining insolation and air temperatures, reaching a maximum extent during March, before receding to the west and north. Eastern Baffin Bay is typically ice-free by mid-August (Valeur *et al.*, 1996). In Disko Bugt, sea-ice usually forms between late December and early February (normally mid-January). Sea-ice and the seasonal thermocline break up between early May and late June (normally late May), as insolation and air temperatures increase (Nazareth and Steensboe, 1998). The timing of sea-ice break-up depends on the severity of the winter, which is in part controlled by wind stress and the relative strength of the WGC (Valeur *et al.*, 1996). Sea-ice cover develops

earlier (*ca*. 2 weeks) in Uummannaq Fjord (Nazareth and Steensboe, 1998). In more southerly waters, pack ice drift ("Storis") along the East Greenland coast to Cape Farewell (and occasionally off southwest Greenland) has a cooling and freshening influence on surface waters (Buch and Nielsen, 2001). Decadal variability in Baffin Bay sea-ice cover trends show a strong relationship with the North Atlantic Oscillation (NAO), with greater sea-ice cover in Baffin Bay and Labrador Sea linked to a strongly positive NAO (Mysak *et al.*, 1996; Stern and Heide Jørgensen, 2003). Sea-ice extent and duration determines the availability of a moisture source for West Greenland, and hence is important for precipitation levels (Williams and Bradley, 1985). While Southwest Greenland experiences high levels of precipitation (> 700 mm a^{-1}) due to open water conditions throughout the year, seasonal sea-ice conditions cause precipitation levels in West Greenland to be much lower (200 to 400 mm) (Williams and Bradley, 1985).

2.3.4 West Greenland oceanography

Baffin Bay has a three-layer water mass structure; a cold, fresh surface layer overlies warm and saline intermediate water, with cold fresh deep and bottom water underneath (Tang *et al.*, 2004). The circulation and distribution of water masses in Baffin Bay is determined by the inflow of water masses originating either from the Arctic Ocean through the Canadian Archipelago to the north, or from the Atlantic region through Davis Strait to the south (*Fig. 2.3*). Sills shallower than 700 m depth restrict deep-water exchanges between Baffin Bay, which is locally more than 2300 m deep, and the Arctic Ocean and Labrador Sea (Aksu, 1983; Ingram and Prinsenberg, 1998).

The major influence on West Greenland oceanography and climate is the West Greenland Current (WGC), which enters Baffin Bay through eastern Davis Strait (*Fig. 2.3*) and flows northwards along the West Greenland coast in surface and intermediate layers (Chapman and Beardsley, 1989). The convergence of the cold, fresh East Greenland Current (EGC) and the relatively warm, saline Irminger Current (IC) as they round Cape Farewell at the southern tip of Greenland (*Fig. 2.3*), form the key components of the WGC (Bersch *et al.*, 1999).

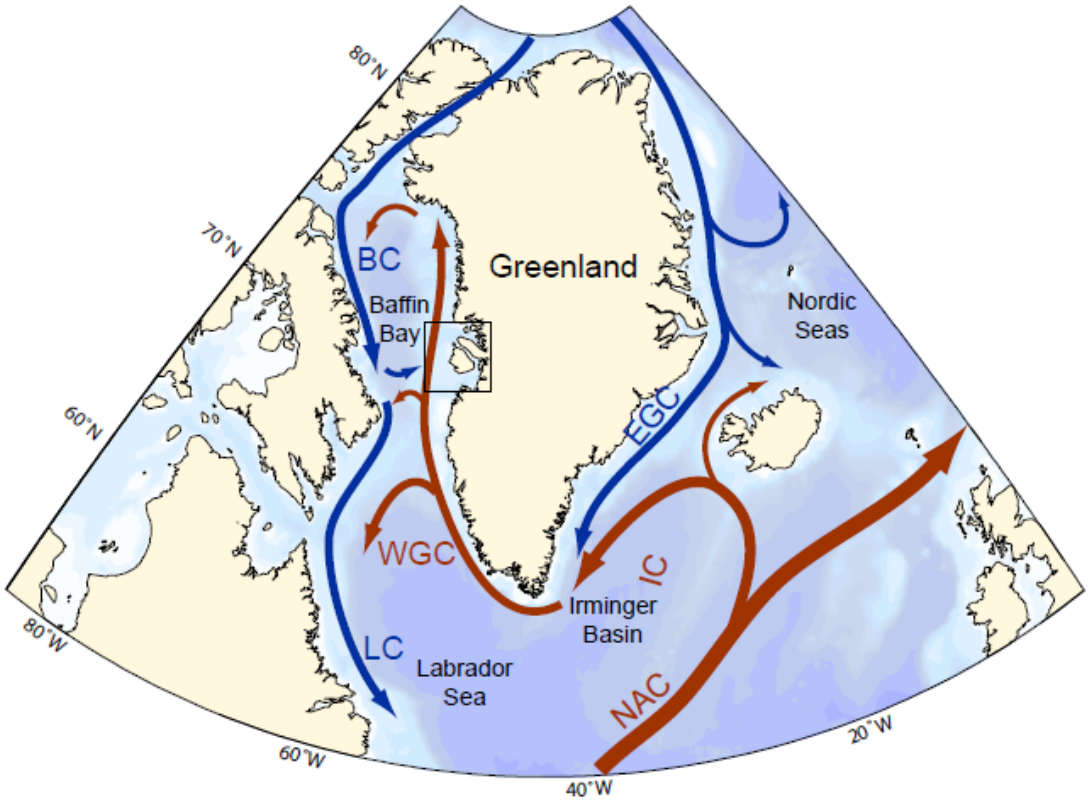

Figure 2.3 Bathymetric map of the North Atlantic with schematic of major surface currents. Red arrows indicate warm currents and blue arrows indicate cold currents. The boxed area shows the study area shown in *Fig.* 2.1. Abbreviations used are: BC, Baffin Current; EGC, East Greenland Current; IC, Irminger Current; NAC, North Atlantic Current; WGC, West Greenland Current.

The EGC is responsible for exporting cold Polar Water (<0°C, 33.5-34.8 psu) from the Arctic Ocean via the Fram Strait and into the Subpolar Basins (Iceland, Irminger, Labrador Basins) through Denmark Strait (Aagaard and Carmack, 1989; Curry and Mauritzen, 2005; Sutherland and Pickart, 2008). Polar Water transported in the EGC system is progressively warmed and freshened between Denmark Strait and Cape Farewell due to meltwater contributions from inland ice, melting sea-ice and icebergs, and net precipitation increases (Bersch *et al.*, 1999; Sutherland and Pickart, 2008).

The IC, on the other hand, transports relatively warm and saline Atlantic Water. The mixing of subtropical water in the NAC with cooler and fresher subpolar water as it is transported northwards by Atlantic meridional overturning circulation (AMOC) produces a water mass

transitional in nature, and described here as “Atlantic Water” (Hansen and Østerhus, 2000). Part of the Atlantic Water that circulates within the Subpolar Basins is redistributed by the IC, which branches off the NAC (*Fig. 2.3*) (Hansen and Østerhus, 2000). The majority of Atlantic Water advected by the IC is deflected southwards at Denmark Strait where it flows alongside the East Greenland Current parallel to the Greenland coast (Bersch, 1995; Hansen and Østerhus, 2000). The water mass characteristics of Atlantic Water in the WGC may be influenced by entrainment of water sourced from the Irminger Basin and Labrador Sea into the IC (e.g. Buch, 1993; Sutherland and Pickart, 2008).

Along West Greenland, the cold and low-salinity Polar Water component of the WGC flows closer to the surface and nearer the shore, while the relatively warm and saline Atlantic Water component flows below and to the west (Andersen, 1981a). After rounding Cape Farewell, the Polar Water component, no longer confined against the coast, becomes laterally more extensive (Buch and Nielsen, 2002; Myers *et al.*, 2009). At Cape Farewell, the warm core in the Atlantic Component of the WGC (5-6°C) is located at 100-200 m water depth (Buch and Nielsen, 2002). At Davies Strait, the warm core of the WGC is located off the shelf (300-600 m water depth, *ca*. 4.5°C, >34.9 psu) and is able to penetrate into Baffin Bay (Tang *et al.*, 2004; Cuny *et al.*, 2005).

As the WGC flows northwards, the Atlantic and Polar Water components are partly mixed, and freshened by meltwater flux from the Greenland ice-sheet and the melting of seasonal sea-ice, though individual water masses remain distinguishable on the shelf in central West Greenland (Chapman and Beardsley, 1989). WGC water is regularly deflected westwards in anticlockwise gyres as it flows north along West Greenland, weakening the transport of Atlantic-sourced waters to northern Baffin Bay. Water advected westwards from the WGC merges with the south-flowing Baffin Current, which is composed of cold, fresh Polar Water from the Arctic Ocean (Ingram and Prinsenberg, 1998). Cold Polar Water is also deflected eastwards from the Baffin Current, and has been found north of Egedesminde (area around Egedesminde Dyb in *Fig. 2.1*) between 40-150 m depth, where it becomes entrained in the WGC (Buch and Nielsen, 2002). The interplay between changes in freshwater from terrestrial and ice-sheet sources, and

changes in the strength of the WGC are responsible for determining the temperature and salinity of sub-surface waters impinging on the shelf in the Disko Bugt-Uummannaq area. Wider scale influences on characteristics of sub-surface waters transported by the WGC are discussed in *section 2.4* below.

2.3.5 Oceanographic setting of Disko Bugt and Uummannaq Fjord

The core of the Atlantic Water component of the WGC is typically found at *ca.* 300 m depth as it passes west of northern Store Hellefiskebanke, controlled by the shallower topography (see *Fig. 2.4c*). Glacially eroded deep-water troughs play an important role in the routing and circulation of relatively warm and saline subsurface waters into the inner continental shelf (*Fig. 2.4e* and *2.5*). West of Disko Bugt, the Atlantic Water component of the WGC flows between 300 and 600 m, with the warm core centred at 300-400 m (2.5-3.5°C) and a saline core at 400-600 m (34.5-34.8 psu). These subsurface waters follow the path of outer Egedesminde Dyb (*ca*. 550 m deep) and penetrate into Disko Bugt after passing over a shallow ridge (*ca*. 305 m depth) to gain access to the much deeper (locally > 900 m water depth) inner Egedesminde Dyb (*Fig. 2.4e* and *2.5*) (Andersen, 1981a). Smith *et al.* (1937, cited in Andersen, 1981a) estimate that approximately 1/3 of the WGC passing Egedesminde enters Disko Bugt. The warmest temperatures are found in southwest Disko Bugt since more northerly waters are cooled by iceberg melting and upwelling (Andersen, 1981a). Stable and relatively fresh surface waters formed from summer meltwater flow northwards out of Disko Bugt through the Vaigat with the deeper WGC water (Andersen, 1981a).

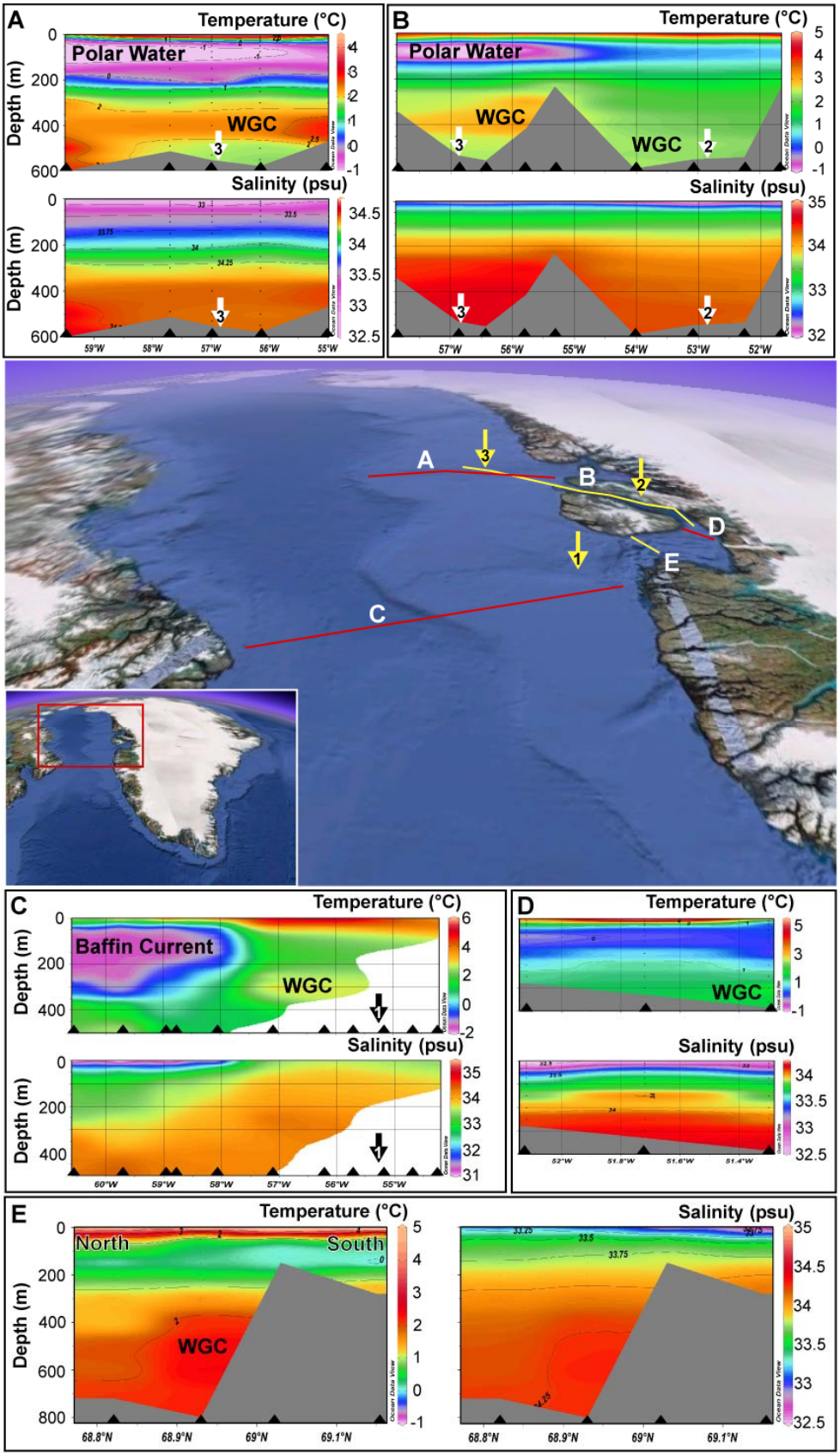

Figure 2.4 (caption below)

Figure 2.4 (above) Interpolated temperature and salinity section profiles in central West Greenland and Davis Strait (triangles indicate CTD sampling stations). Temperature and salinity are plotted on a common depth scale. All other scales differ. Illustrated profiles are marked the Google Earth (2010) image of Baffin Bay; (**a**), Uummannaq shelf (July, 1987); (**b**), Vaigat (1971); (**c**), Davis Strait (July, 1987); (**d**), northeastern Disko Bugt (July, 1987); e, central Disko Bugt (July, 1987). Cores investigated in this study are indicated by numbered (**1-3**) arrows; (**1**), core MSM-343340 (this core is located north of section shown and in deeper water); (**2**), core DA06-139G; (**3**), core MSM-343520. Data are stored in the World Ocean Database 2005, and were retrieved online from the National Oceanographic Data Centre, NOAA (http://www.nodc.noaa.gov), and graphed using Ocean Data View (Schlitzer, 2007).

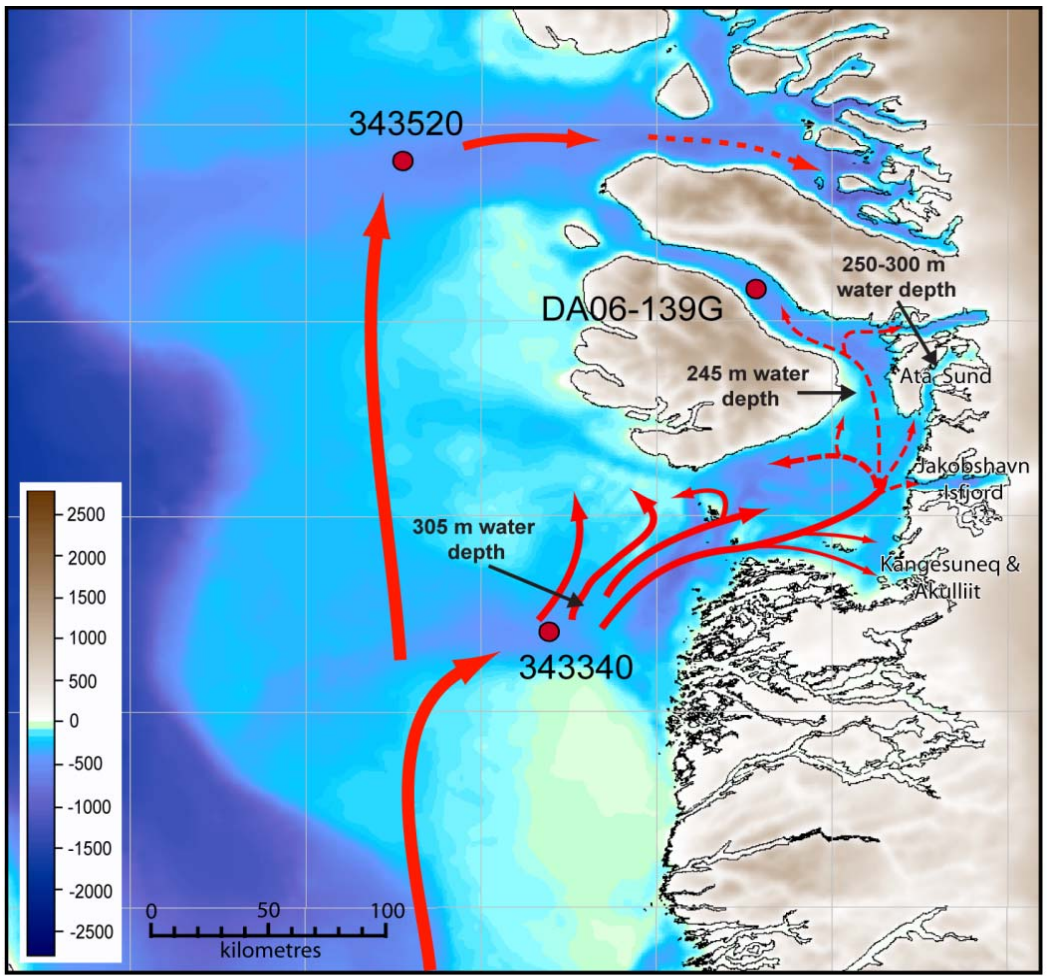

Figure 2.5 Pathways of WGC intrusion into Disko Bugt and Uummannaq Fjord at intermediate depths (200 m). Solid red arrows show the main WGC pathways; dashed arrows show weaker/episodic intrusions of WGC into inner shelf area and fjords. Modified from Andersen (1981a) with additional data from Lloyd (2006a) and Harff (2007).

The WGC penetrates into fjords with relatively open or exposed locations and orientations, including fjords on the west coast of Disko, and over-sill penetration into mainland fjords, such as Jakobshavn Isfjord, Akulliit, and Kangasuneq (*Fig. 2.7*; Deslodges *et al.*, 2002; Harff, 2007; Holland *et al.*, 2008; Lloyd *et al.*, 2007). Importantly, this indicates that warmer WGC water can gain access to the base of tidewater glaciers, and subsequently enhance basal melt rates of floating ice tongues (e.g. Holland *et al.*, 2008). Shallow sills restrict two-way water exchanges at fjord heads, while shallow topography in Atâ Sund (250 m to 300 m depth) and at the entrance to Vaigat (245 m depth) (*Fig. 2.5*) restricts the inflow of relatively warm and saline WGC water into the Vaigat and glacier fjords in northeastern Disko Bugt (Andersen, 1981a). However, Atlantic-sourced water is able to penetrate north into these areas (Harff, 2007; Rignot *et al.*, 2010). Only the upper part of the Atlantic-sourced WGC water enters the Vaigat (*Fig. 2.4b,d*), and can be identified flowing along the Nuussuaq peninsula shoreline, where it mixes with overlying cold water (Andersen, 1981a). Warm Atlantic Water (generally below 250 m) does not always cross the 245 m deep threshold (*Fig. 2.5*) into the *ca.* 500 m deep Vaigat, though in years where this does happen, bottom water temperatures below the threshold depth are increased by up to 2°C (Andersen, 1981a).

North of Uummannaq, the core of Atlantic Water deepens to 400-500 m depth (*Fig. 2.4a*), as the overlying surface waters are cooled and freshened (*ca*. 2°C, <33.5 psu) by the melting of icebergs and winter sea-ice, and the advection of Polar Water from the Baffin Current (Andersen, 1981a). On the outer shelf, the Uummannaq trough is *ca.* 600 m deep, and provides an unobstructed pathway for WGC water to penetrate into the inner shelf towards the base of marine-terminating glaciers.

Andersen (1981a) suggests that the relatively warm, saline WGC prevents cold Polar Water from the Baffin Current from entering inner shelf areas. Thickening of the Polar Water layer due to advection of cold, fresh water from the Baffin Current may result in a deepening of the warm core of the underlying Atlantic Water. This may restrict inflows of the warmest Atlantic-sourced water to inner shelf areas, where there are shallow topographic barriers to cross (i.e. entrance to Disko Bugt). In the deeper Uummannaq trough, however, basal water temperatures may

increase through a deepening of the warm core of the WGC, since this usually lies 100-200 m above the seafloor.

2.4 Wider scale changes in North Atlantic

Long-term changes in the characteristics of the WGC reflect the wider oceanography and climatic variability in the North Atlantic region. Therefore, establishing climatic and oceanographic variability that influences the relative contribution of water transported in the EGC and IC current systems to the WGC (*Fig. 2.3*) is important for understanding the possible causes of water mass changes identified in the palaeoenvironmental record.

The AMOC transports warm, saline subtropical surface and intermediate waters to high latitudes where they cool, sink and return south as cold, saline deep water. Heat redistributed through the AMOC (via the North Atlantic Drift) warms North Atlantic air temperatures by up to 10°C (Macdonald and Wunsch, 1996; Ganachaud and Wunsch, 2000). Denmark Strait Overflow Water (DSOW) and the less dense Labrador Sea Water (LSW), the two main constituents of North Atlantic Deep Water (NADW), form in the Nordic and Labrador Seas, respectively (e.g. Weaver *et al.,* 1999; Rahmstorf, 2002; Straneo, 2006; Kuhlbrodt *et al.*, 2007). These locations are climatically important because the cooling and sinking of dense saline water drives global thermohaline circulation, which redistributes heat to higher latitudes (Weaver *et al.,* 1999; Rahmstorf, 2002; Straneo, 2006; Kuhlbrodt *et al.*, 2007). Freshwater perturbations to sites of Deep Water formation in the North Atlantic region are a possible cause of Holocene climate fluctuations (e.g. Nesje *et al.*, 2004; Denton and Broecker, 2008). Meltwater from the western part of the Greenland Ice Sheet is routed to areas of NADW formation in the Labrador Sea first by the WGC, and then southwards via the Baffin Current and Labrador Current (*Fig. 2.3*). Changes in the volume of freshwater (due to direct melting of the GrIS and/or increased calving flux from tidewater glaciers) from West Greenland may therefore influence LSW formation.

2.4.1 The North Atlantic Oscillation (NAO)

The NAO, which is the most prominent indicator of large-scale atmospheric circulation changes in the North Atlantic region (Ambaum *et al.*, 2001), significantly contributes to interannual/decadal climate variability in the northern hemisphere (Hurrell, 1996). The position of the North Atlantic subtropical high-pressure cell (Azores high) and the subpolar low-pressure cell (Icelandic low) determine changes in the strength of westerly winds (illustrated schematically in *Fig. 2.6b* and *d*). Changes in the strength of westerly winds subsequently affect the pathways and strength of North Atlantic surface currents, which, in turn, alter the temperature and salinity of the WGC (Hurrell & van Loon, 1997; Greatbach, 2000; Blindheim *et al.*, 2001; Furevik and Nilsen, 2005). Stronger-than-normal westerly winds are characteristic of a high/positive NAO index, whereas weaker-than-normal westerly winds typify a low/negative NAO index (Greatbach, 2000). Positive phases of the NAO are associated with more severe than normal conditions in West Greenland and eastern Canada. An increase in westerly wind stress under positive NAO conditions causes a narrowing and strengthening of the North Atlantic Current (NAC) (*Fig. 2.6a* and *b*), resulting in both a weakening of the Irminger Current (IC) and East Greenland Current (EGC), although the EGC component dominates the WGC (*Fig. 2.6c* and *d*) (Blindheim *et al.*, 2001; Buch, 2002). Under negative NAO conditions, the weaker westerly winds result in a much broader NAC and an increase in strength of westward branches of Atlantic Water, particularly the transport of IC water (*Fig. 2.6c*) (Blindheim *et al.*, 2001; Buch, 2002).

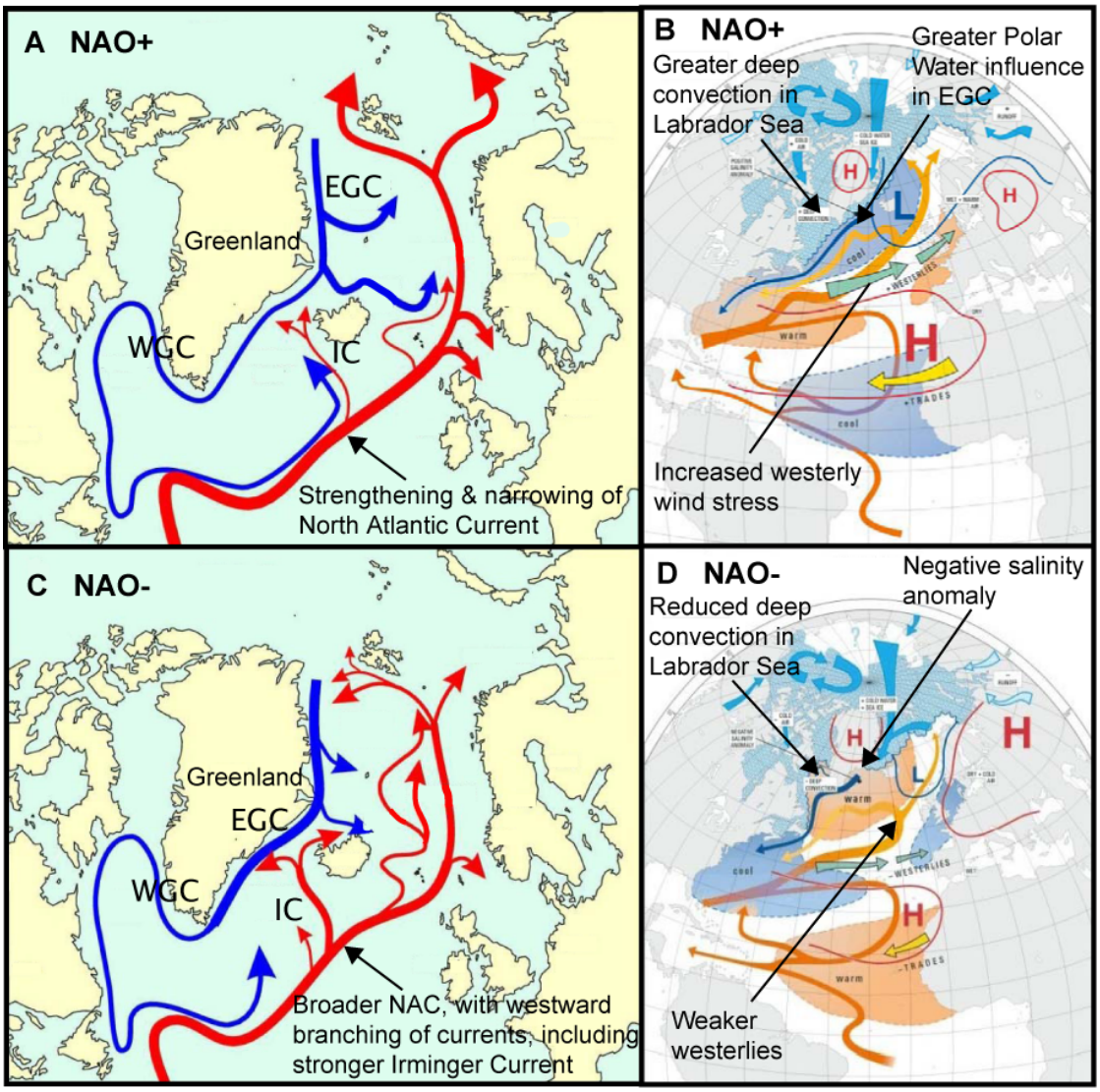

Figure 2.6 The pattern of ocean surface currents associated with changes in the position of the North Atlantic subtropical high-pressure cell (Azores high) and the subpolar low-pressure cell (Icelandic low). (**A, B**) Atmospheric and oceanic conditions associated with a positive NAO; (**C, D**) Atmospheric and oceanic conditions associated with a negative NAO. Cartoons modified from Blindheim *et al.* (2001) and Climatology/Meteorology Research Group (2004).

2.4.2 Great Salinity Anomalies and the NAO

Recent observations report a freshening of North Atlantic waters (Belkin *et al.*, 1998; Dickson *et al.*, 2002; Curry *et al.*, 2003**;** Curry and Mauritzen, 2005). Advection of relatively fresh waters to the Labrador and Nordic Seas, and North Atlantic subpolar gyre, have been linked to changes in freshwater flux (associated with glacial melt, river runoff, and changes in ocean circulation) to these sites, and phase changes in the NAO. Between 1965 and 1995, an additional 19,000 ± 5,000 km^3 of freshwater entered the Nordic Seas through Fram Strait (Curry and Mauritzen,

2005), via the EGC, as a series of pulses during the 1970s, 1980s, and 1990s, that have been described as Great Salinity Anomalies (GSAs) (Dickson *et al.*, 1988; Belkin, 2004). Nearly 80% of this flux penetrated into the eastern Subpolar Basins, freshening surface waters, and through vertical mixing, deeper waters (Curry and Mauritzen, 2005; Peterson *et al.*, 2006). The source of each GSA is debated, though Belkin *et al.* (1998) suggest the larger 1970s anomaly is primarily the result of freshwater outflows from the Arctic Ocean caused by an intensification of northerly winds over the Greenland Sea. The 1980s GSA, however, was probably formed in the Labrador Sea following severe winters in the Labrador and Baffin Bay region (Belkin *et al.*, 1998). Changes in ocean circulation during GSA events may provide insights into how the WGC system may have responded to large freshwater fluxes into the polar and sub-polar region during the Holocene.

Dickson *et al.* (1996) suggest a deep-sea convection seesaw exists between the Labrador Sea and Greenland Sea, and is controlled by the NAO. During a period of reduced overturning with warmer winters and weaker winds in the Greenland Sea during the 1970s and 1990s, a strengthening of deep convection (LSW formation), cooler air temperatures and increased storminess occurred in the Labrador Sea (Dickson *et al.*, 1996). This antiphase relationship has been linked to freshwater flux through Denmark Strait (Oka *et al.*, 2006). Peterson *et al.* (2006) argue that increased freshwater transport to the Labrador Sea is linked to a strong positive NAO phase. Model-based studies indicate that the NAO is linked to convection in Labrador Sea, but not directly related to overturning in the Greenland Sea (Oka *et al.*, 2006). The volume of cold and fresh dense water propagated during the 1988-1994 GSA appears to be exceptional during most of the 20th Century (Yashayaev *et al.*, 2003). The propagation of GSAs coincide with a strongly positive NAO index, which is related to increased sea-ice extent in Baffin Bay (Chapman and Walsh, 1993), and a corresponding reduction in mean annual air temperature in West Greenland (Drinkwater, 1996). The advection of freshwater anomalies and subsequent reduction in deep convection in the Labrador Sea creates a thermohaline contrast across the NAC, which leads to a greater entrainment of warm, saline IC water to the Labrador Sea (Belkin *et al.*, 1998). The switch to warmer, more saline waters in the Labrador Sea and reduced LSW formation in the 1990s is linked to weakening of the North Atlantic subpolar gyre circulation.

These negative-NAO conditions are linked to reduced transport of cold, fresh Polar Water in the EGC, and a trend of increasing heat transport in the WGC, which has extended into the 2000s, consistent with an increase in Irminger Water influence (Hakkinen and Rhines, 2004; Myers *et al.*, 2009).

Since WGC water deflected westwards at Davis Strait may be the main source of freshwater and heat flux to the Labrador Sea (Myers *et al.*, 2009), changes in LSW formation may be closely linked to sub-surface temperatures of WGC water on the West Greenland shelf. There is no evidence that the magnitude of recent GSA events are large enough to reduce the strength of the Gulf Stream (Peterson *et al.*, 2006), and cause more extreme climate responses, though Hátún *et al.* (2005) suggest this is because the increasing salinity of Atlantic water entering the Nordic Seas and Arctic Ocean may counteract these freshwater fluxes. Despite this, changes in the freshwater balance of the North Atlantic contribute to the modification of the composition of the WGC.

2.5 Recent changes in the Greenland Ice Sheet

Although ice-sheet mass balance estimates vary widely between studies, there is a consensus that the Greenland Ice Sheet has been losing mass at an accelerating rate since the mid-1990s (e.g. Krabill *et al.*, 2000; 2004; Velicogna and Wahr, 2005; 2006; Chen *et al.*, 2006; Luthcke *et al.*, 2006; Ramillien *et al.*, 2006). The major source of these mass balance losses is thinning at the ice sheet margin (Krabill *et al.*, 2000; Abdalati *et al.*, 2001; Rignot and Kanagaratnam, 2006; Thomas *et al.*, 2006). While peripheral thinning was initially restricted to southern Greenland (e.g. Velicogna and Wahr, 2006), observations show this has extended northwards. Recent climatic warming in the North Atlantic region can only explain half of the increased ice mass losses (Krabill *et al.,* 2004). The remainder appears to be the result of increased ice flux through calving due to the recent acceleration and thinning of outlet glaciers draining the Greenland ice-sheet (Krabill *et al.*, 2004).

In West Greenland, Jakobshavn Isbræ showed the most dramatic acceleration, thinning and subsequent retreat, beginning in 1997 (Thomas *et al.*, 2003; Joughin *et al.*, 2004). Major outlet

glaciers in East Greenland, including Kangerdlugssuaq and Helheim (Krabill *et al.*, 1999; Howat *et al.*, 2005, 2007, 2008), have since experienced similar ice dynamic changes. The emerging trend shows accelerations in outlet glaciers, and hence increases in ice discharge, have spread northwards to 70°N (Rignot and Kanagaratnam, 2006). Although retreat from pinning points may explain changes in ice dynamics for individual glaciers (e.g. Thomas *et al.*, 2000; 2003; 2004; Joughin *et al.*, 2004), it is unlikely to explain the widespread observed pattern of ice stream acceleration and thinning in both Greenland and Antarctica (e.g. Rignot, 1998; Shepherd *et al.*, 2001). Instead, many authors suggest that an external driver such as atmospheric and/or ocean warming may be responsible (Luckman *et al.*, 2006; Bamber *et al.*, 2007).

Whilst thinning rates of up to 10 m a^{-1} have been measured in peripheral areas of the Greenland Ice Sheet, enhanced surface melting alone is unlikely to explain thinning exceeding 1 m a^{-1}, especially at high (>1500 m) altitudes (Abdalati *et al.*, 2001). However, increased ablation and meltwater delivery to the ice-bedrock interface may cause enhanced basal-sliding (e.g. Zwally *et al.*, 2002; Howat *et al.*, 2008). Despite an increase in the number of summer meltwater lakes on the surface of the Greenland ice-sheet in recent years (Kjær and Korsgaard, 2009), no direct relationship linking atmospheric warming with ice stream acceleration has been found (Luckman *et al.*, 2006). Indeed, Joughin *et al.* (2008) suggest fast-flowing outlet glaciers are relatively insensitive to meltwater-driven basal lubrication compared to the slow-moving ice sheet. Since the late-1990s, marine-terminating outlet glaciers have thinned significantly, while land-terminating glaciers have undergone only negligible changes (Sole *et al.*, 2008). Indeed, many authors favour a mechanism that causes perturbations at the calving margin resulting in reduced back-stresses and ice front retreat (Thomas, 2003; 2004; Howat *et al.*, 2005, 2007; Luckman *et al.*, 2006; Nick *et al.*, 2008). Reduced sea-ice in front of the ice margin linked to warmer sea-surface temperatures (Sohn *et al.*, 1998; Luckman *et al.*, 2006) is one possible cause. Alternatively, basal melting of those parts of marine-terminating glaciers at the terminus in contact with warming subsurface ocean waters may be important (Payne *et al.*, 2004; Shepherd *et al.*, 2004; Bindschadler, 2006; Rignot *et al.*, 2010; Straneo *et al.*, 2010). Based on studies from an Alaskan Fjord, Motkya *et al.* (2003) proposed a model of salinity-driven fjord circulation, with surface meltwater flux from the glacier strengthening the sub-surface

circulation, allowing incoming warm, saline deep waters to penetrate over the sill at the fjord mouth. Warm ocean waters mix with subglacial meltwater to melt submarine ice, and increase meltwater flux. In Sermilik Fjord, East Greenland, Straneo *et al.* (2010) suggest that circulation is driven by the ocean temperature and salinity of waters on the shelf, because meltwater-driven circulation is not strong enough to account for the rapid incursion of a large body of warm water observed between July and September 2008. Straneo *et al.* (2010) suggest that flushing of warm waters into the fjord could take place over just a few days. Northeasterly winds along the East Greenland coast were suggested to be important for establishing the ideal marine conditions for this to take place (Straneo *et al.*, 2010).

2.5.1 Glacial setting of Disko Bugt and Uummannaq Fjord

Central and southwest Greenland (south of 72°N) produces approximately one-third of all calf ice from the Greenland Ice Sheet (Reeh, 1985, 1994; Bigg, 1999). The outlet glaciers feeding into the Disko Bugt-Uummannaq area are responsible for the majority of this iceberg production (Weidick, 1995). Past estimates suggest that tidewater glaciers from this catchment (eight in Disko Bugt, eleven in Uummannaq, *Fig. 1.2*) contribute between 82 (1957) and 93 $km^3\ a^{-1}$ (1964) of water equivalent to global sea level (Bauer et al, 1968; Carbonnell and Bauer, 1968). Calf-ice production in Disko Bugt and the Uummannaq area are broadly similar (Carbonnell and Bauer, 1968). More recent estimates by Rignot and Kanagaratnam (2001) do not account for ice discharge from all the marine-terminating glaciers in Disko Bugt (33.6 $km^3\ a^{-1}$in 1996) and Uummannaq (14.2 $km^3\ a^{-1}$ in 1996).

Disko Bugt is a large marine embayment (approximately 10,000 km^2; 68°30'N to 70°00'N, 50°00'W to 54°00'W), with typical water depths of around 400 m (*Fig. 2.1*). Egedesminde Dyb, a deep-water trough between Jakobshavn Isfjord and the shelf break in Disko Bugt (*Fig. 2.1*), bisects shallow (< 100 m water depth) offshore banks. It is likely that a major ice stream, possibly an extension of Jakobshavn Isbræ, drained onto the continental shelf through this channel at the LGM (Long and Roberts, 2003; Roberts and Long, 2005). Modern tidewater glaciers draining the Greenland Ice Sheet are restricted to fjord systems.

The Uummannaq area (*Fig.2.1*; approximately 8,000 km^2; 70°20'N to 72°00'N, 50°00'W to 55°00'W) is characterised by the high concentration of tidewater glaciers that drain the central West sector of the Greenland Ice Sheet. The most important glaciers in terms of calf-ice production in this region are Sermeq Kujalleq (Store Gletscher), which drains into Uummannaq Fjord, and Rink Isbræ, which drains into Karrats Fjord to the north. Uummannaq Fjord (*Fig. 2.1*) is more than 800 m deep (Harff, 2007; Ó Cofaigh, 2009), although several areas of shallow topography (in places < 300 m depth) identified in multibeam data (Harff, 2007), in addition to the many islands in the inner shelf area, may have acted as ice stream pinning points during the last deglaciation.

2.5.2 Ice stream activity

The central West sector of the GrIS has the highest concentration of calving glaciers in Greenland (see *Fig. 1.2*) (Reeh, 1985). The total calf-ice production in Disko Bugt and the Uummannaq ice stream complex are broadly comparable, each producing *ca. 4*5 km^3 a^{-1} (Weidick, 1995). The volume of calf ice produced by the two major ice streams in the Uummannaq ice stream complex, Rink Isbræ (10.5-16.7 km^3 a^{-1}) and Store Gletscher (13.2-17.5 km^3 a^{-1}) totals *ca.* 25.7-34.2 km^3 a^{-1} (Carbonell and Bauer, 1968; Bauer *et al.*, 1968). This estimate is broadly comparable to the estimated iceberg flux of Jakobshavn Isbræ (26-44 km^3 a^{-1}) before the recent acceleration experienced in the past decade. Calf ice flux is low for outlet glaciers south of Jakobshavn isbræ, though there are two significant glaciers (Sermeq avangnardleq and Sermeq Kujatdleq) calving into Torsukattak, in northeastern Disko Bugt, that each produces an iceberg flux of up to 10 km^3 a^{-1}. In recent decades, ice margin changes have been asynchronous in this region. The two outlet glaciers immediately south of Jakobshavn Isbræ have been relatively stationary since the 1920s, while, ice streams in northeastern Disko Bugt retreated slightly from the 1960s to 1990s, and Equip sermia advanced during the same period. Weidick (1963) provides a more detailed account of historic glacier margin fluctuations in central West Greenland.

Jakobshavn Isbræ is by far the most important glacier at present in central West Greenland, and one of the most important outlet glaciers in Greenland. It has been a research focus for

many years because of the potential impact of sea-level rise and thermohaline circulation by a collapse of the ice front and drawdown of inland ice. Jakobshavn Isbræ drains nearly 7% of the Greenland Ice Sheet into Disko Bugt through a deep subglacial trough that extends more than 100 km inland from the present ice front to depths exceeding 1000 m below sea level (Bindschadler, 1984; Echelmeyer *et al.*, 1991; Clarke and Echelmeyer, 1996). The ice stream grounding line is located at 800 m below sea level, in the uniformly deep Jakobshavn Isfjord (Holland *et al.*, 2008). Current iceberg discharge from Jakobshavn Isbræ has doubled to approximately 50 $km^3 a^{-1}$ of calf-ice since the ice stream began accelerating in 1997 (Carbonnell and Bauer, 1968; Holland *et al.*, 2008). In northeastern Disko Bugt, Eqip Sermia drains into Atâ Sund, and Sermeq Avangnardleq and Sermeq Kujatdleq, feed into Torssukátaq (*Fig. 1.2*). Torssukátaq is a deep fjord system with water depths exceeding 1000 m, separated from northeastern Disko Bugt and the Vaigat by a shallow sill.

Historical observations suggest Jakobshavn Isbræ gradually advanced from the A.D. 1700s (Weidick *et al.*, 2004), and periods of moraine-forming glacier advances in West Greenland occurred at *ca.* A.D. 1840-1850, 1880-1890, and a smaller advance at *ca.* A.D. 1920 (Weidick, 1972). Jakobshavn Isbræ reached its Little Ice Age maximum at around A.D. 1850 (Weidick and Bennike, 2007; Young *et al.*, 2011). Jakobshavn Isbræ gradually retreated *ca.* 26 km between A.D. 1851 and 1953 (Weidick, 1995). While there has been a general retreat of West Greenland glaciers since A.D. 1920 (Weidick, 1972), the position of the ice front of Jakobshavn Isbræ was relatively stable between the 1950s and 1990s (Weidick, 2004). Following a period of relatively slow ice flow and ice stream thickening into the 1990s, Jakobshavn Isbræ experienced a significant acceleration (5.7 km a^{-1} to 12.6 km a^{-1}), dynamic thinning and calving margin retreat between 1997 and 2003 (Thomas *et al.*, 2003; Joughin *et al.*, 2004). Holland *et al.* (2008) recently demonstrated that the initial thinning of the ice tongue in 1997 corresponds to an abrupt increase in subsurface water temperatures (150-400 m depth) from a mean of 1.7°C in 1995 to 3.3°C in 1998 in their study area. Holland *et al.* (2008) argued that gradual changes in atmospheric temperatures could not explain the large and abrupt ice stream changes, including thinning rates of 80 m a^{-1} (Thomas *et al.*, 2003). Thomas *et al.* (2009) found that near-synchronous high-magnitude changes are occurring in marine-terminating glaciers with deep

grounding lines throughout Greenland, while those without deep beds are thinning slowly. This suggests that warming ocean temperatures may indeed be driving higher basal melt rates; accelerating thinning and causing the catastrophic break up of ice fronts, as happened to the floating ice tongue in front of Jakobshavn Isbræ in the late 1990s (Weidick *et al.*, 2003). The plausibility of this mechanism depends on the ability of warm subsurface waters to overtop submarine sills at fjords mouths and gain subglacial access (Bindschadler, 2006). Holland *et al.* (2008) demonstrate that warm subsurface waters are present both outside and throughout Jakobshavn Isfjord, having penetrated over the relatively shallow sill of Isfjeldbanken (the sill at the eastern end of Jakobshavn Isfjord).

2.6 Glacial history since the LGM

2.6.1 Greenland Ice Sheet history since the LGM

The Greenland Ice Sheet is the only Northern Hemisphere ice sheet to survive the climatic amelioration following the Last Glacial Maximum (LGM). The equivalent of 7 m global (eustatic) sea-level rise remains locked in the Greenland Ice Sheet (Lemcke *et al.*, 2007). The maximum extent of the Greenland LGM ice margin and the timing of subsequent ice recession continue to be widely debated. Bennike and Björck (2002) argue for an extensive glaciation of the Greenland shelf at the LGM, reaching the shelf break in northeastern and southern Greenland, and potentially in West Greenland. Others, however, place an offshore Greenland ice margin closer to the present outer coast, for example, in Northeast, West, and central East Greenland (Funder and Hansen, 1996; Funder *et al.*, 1998). A late deglaciation has been suggested for Northeast and Southwest Greenland due to wide shelf area (Bennike and Björck, 2002), while an early deglaciation of the Scoresby Sund area during the Allerød period has been hypothesized (Dowdeswell *et al.*, 1994).

Funder and Hansen (1996) proposed a two-phase model for the deglaciation of Greenland following the LGM (*Fig. 2.7*). Ice is suggested to have expanded out to the shelf edge at the LGM in southeastern and southwestern Greenland. The glaciation of north and northeastern Greenland was less extensive, to the modern coastline and inner fjords. In central West Greenland, the ice sheet is suggested to have reached the mid-shelf area, with a large outlet

glacier extending out of Disko Bugt, possibly to the shelf edge. The large outlet glacier in the Uummannaq area is suggested to be smaller, and less extensive (*Fig. 2.7*). The first stage in Funder and Hansen's (1996) model suggests eustatic sea-level rise rapidly cleared marine-based ice on the Greenland shelf between *ca.* 15 and 10 ka BP, mainly in central East and central West Greenland, and areas to the south. The second stage of the model suggests a slower land-based deglaciation continued from *ca.* 10 ka BP, with ice retreat driven by surface thinning due to atmospheric warming. The terrestrial phase of deglaciation was most extensive in central East Greenland and central West/southwest Greenland.

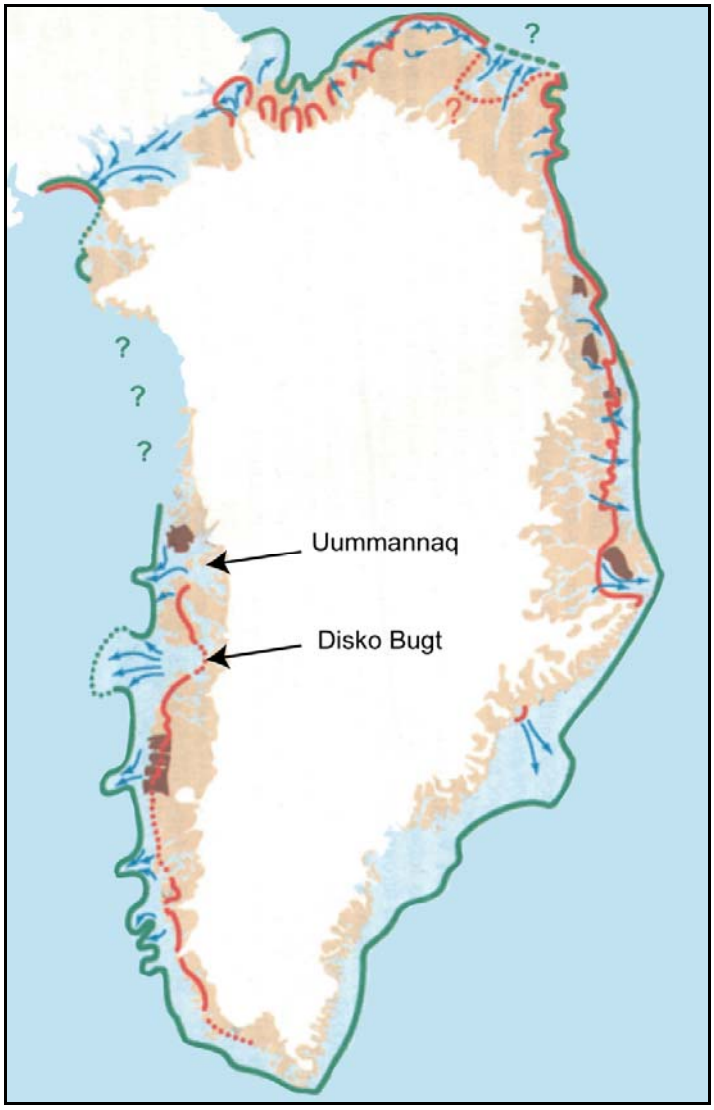

Figure 2.7 Funder and Hansen's (1996) two-stage model for marine-based deglaciation from the continental shelf at *ca.* 15 ka BP (from green line), and land-based deglaciation of the Greenland Ice Sheet from *ca.* 10 ka BP (from red line).

2.6.2 Deglaciation in the Baffin Bay region

Constraining the ice-sheet retreat histories for locations throughout the Baffin Bay region enables us to assess possible mechanisms responsible for deglaciation. The extent of glaciation in northern Baffin Bay has been widely debated (e.g. Blake, 1970; England, 1976; 1983; 1999; Miller *et al.*, 2002). Recent investigations support extensive ice cover at the LGM, with coalescent Greenland and Innuitian ice sheets in Nares Strait until around 10 ka BP (Zreda *et al.*, 1999; England, 1999). Since Nares Strait is one of the main paths for Polar Water export from the Arctic Ocean (Aagaard and Carmack, 1989), and Dyke *et al.* (2002) suggest calving rates must have been low to permit an extensive LGM ice-sheet configuration, freshwater inputs to northern Baffin Bay would have been low during the LGM. At this time, cold and fresh Polar Water circulated within the Arctic Ocean, while a weak WGC circulated in Baffin Bay (Aksu and Piper, 1979; Aksu and Mudie, 1985). Deglaciation of Nares Strait between *ca.* 10-9 ka BP (Zreda *et al.*, 1999; England, 1999) would have allowed cold, fresh Polar Water to enter Baffin Bay from the Arctic Ocean. This would have had a significant oceanographic impact on Baffin Bay. The strengthening of gyre circulation in Baffin Bay by a stronger south-flowing Baffin Current as the Arctic channels opened may have helped initiate or strengthen the north-flowing WGC.

Research suggests the ice margin in northwest Greenland (from Melville Bugt to Thule, see *Fig. 1.1*), north, and northeast Greenland has changed relatively little in extent compared to other parts of the Greenland Ice Sheet (Kelly and Bennike, 1992; Funder and Hansen, 1996). The apparently minimal ice margin retreat since the LGM in northwest Greenland may reflect reduced Holocene deglaciation and/or greater ice expansion in this sector of the Greenland Ice Sheet than elsewhere during the late Holocene Neoglaciation (Kelly, 1980). It is possible that the warming influence of the WGC in northern Baffin Bay continued to provide an open water moisture source in close proximity to the ice sheet during a period of low Neoglacial air temperatures (Levac *et al.*, 2001), and helped maintain a positive ice sheet mass balance in this region.

2.6.3 Deglaciation of the central west sector of the Greenland Ice Sheet

Kelly (1985, p. 477) labelled central West Greenland a 'classic area' for studying the Greenland ice-sheet deglacial history because of the wealth of glacial landforms and dateable material found in the relatively wide (up to 200 km) ice-free terrestrial margin. In Disko Bugt, the current deglacial chronology is based on radiocarbon dates from marine sediment cores (e.g. Lloyd *et al.*, 2005), raised marine deposits (e.g. Ingólfsson *et al.*, 1990; Bennike *et al.*, 1994), and basal gyttja in lakes above the local marine limit (e.g. Long *et al.*, 1999, 2003; Long and Roberts, 2002, 2003). There is greater uncertainty concerning the deglacial chronology for the less-studied Uummannaq region, where there is little data to constrain both the extent of LGM ice and the timing of deglaciation. The current chronology is limited to just two radiocarbon dates in the whole Uummannaq area (Símonarson, 1981; Bennike, 2000) of 10.6 ka BP and 10.4 ka BP on the central-northern shore of Nuussuaq peninsula and Svartenhuk Halvø respectively, though ongoing projects are using cosmogenic exposure dating to directly date deglaciation (D.H. Roberts, personal communication).

Little is known about the offshore deglacial history (i.e. maximum ice extent and subsequent timing and nature of deglaciation) in central West Greenland. The presence of crystalline erratics sourced from mainland Greenland on the basalt plateux of southern Disko Island suggests ice formerly extended out into Disko Bugt (Frich, and Ingólfsson, 1990). Funder and Hansen (1996) hypothesized that ice streamed out of Disko Bugt, calving at or near to the shelf edge during the LGM. Intensive scouring by deep-draft icebergs (>340 m) adjacent to outer Egedesminde Dyb supports ice sheet expansion onto the outer shelf at the LGM (Brett and Zarudzki, 1979), since this can only be explained by icebergs calving from inland ice sitting west of the 300 m deep threshold between inner and outer Egedesminde Dyb (*Fig. 2.1*). Two major offshore moraine complexes, the Hellefiske moraines, located *ca.* 100 km offshore, and the Sisimiut moraines, located *ca.* 40 km offshore (*Fig. 2.1*), indicate that inland ice did indeed extend out onto the shelf in the past (Brett and Zarudzki, 1979; Zarudzki, 1980; Risum *et al.*, 1980; Kelly, 1985). While their ages remain unknown, Kelly (1985) suggests the Hellefiske moraines formed during pre-LGM Weichselian glacial advances or earlier, and the Sisimiut moraines formed *ca.* 14 ka BP. Van Tatenhove *et al.* (1996) speculates that the Hellefiske

moraines correspond to the maximum advance of the Greenland Ice Sheet during the Weichselian between 19 and 13 ka cal. BP, and the Sisimiut moraines are linked to extensive ice cover between 13.8 and 11.8 ka cal. BP. However, there is increasing support for the Hellefiske moraines marking the extent of a Younger Dryas ice readvance (Rinterknecht *et al.*, 2009; Simpson *et al.*, 2009; Roberts *et al.*, 2009).

Bennike *et al.* (1994) interpret rhythmically bedded glaciolacustrine sediments, together with kame deposits and features on western Disko Island, as evidence for an extensive ice shelf west of Disko Island before the last deglaciation. Based on the degree of weathering, Bennike *et al.* (1994) reason that these features are similar in age as glacial striae and Pjetursson's moraine in Blæsedalen, near Queqertarsuaq (*Fig. 2.8*), which Ingólfsson *et al.* (1990) attribute to the Godhavn Stade (the LGM on Disko Island), though no dating evidence exists to test this. A raised marine delta located at the marine limit in the Hammers Dal area, however, has been dated to *ca.* 10.2 ka cal BP (10,530-9,811 cal. yr BP; 9370±140 ^{14}C yr BP, Ingólfsson *et al.,* 1990). The delta appears to be partly reworked by marine processes, possibly suggesting open water conditions characterised the shelf area to the west of Disko Island at this time.

Many authors have argued either for a rapid (e.g. Funder and Hansen, 1996; Long and Roberts, 2003) or slower, punctuated deglaciation of Disko Bugt and the nearby shelf (e.g. Ingólfsson *et al.*, 1990; Weidick, 1996, Rasch, 2000). The current deglacial chronology is largely developed using terrestrial-based evidence found in the wide ice-free margin in central West Greenland. Moraine systems have been tenuously correlated based on morphological similarities, often over distances of 10 km to 100 km. These have been dated using *in situ* marine material, or where this is absent, linked to relative sea-level (RSL) curves (e.g. Weidick, 1972a; 1972b; Ten Brink and Weidick, 1974; Donner and Jungner, 1975; Ten Brink, 1975; Kelly, 1985; Long and Roberts, 2002; Long *et al.*, 2006). The Holocene marine limit (HML; the maximum height of a former RSL) is thought to have formed almost synchronously with deglaciation, as isostatic uplift accompanied ice sheet down wasting during initial deglaciation. Dating of the marine limit is often based on extrapolation from local RSL curves where *in situ* dateable material is absent

(e.g. Donner and Jungner, 1975; Donner, 1978), or dating the onset of organic accumulation in lakes above the marine limit (Long and Roberts, 2003; Weidick and Bennike, 2007).

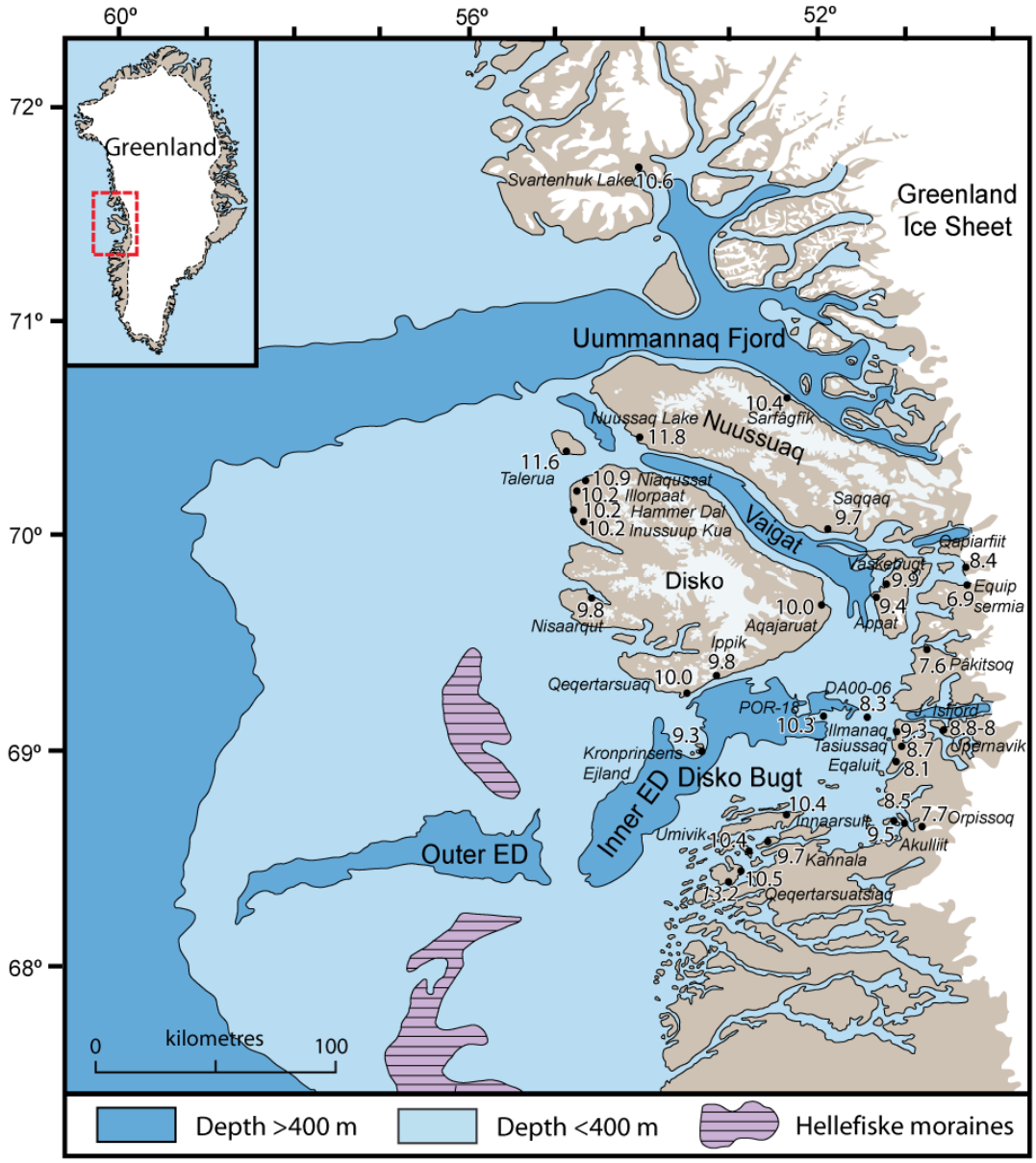

Figure 2.8 Radiocarbon dates from central West Greenland providing minimum ages for deglaciation. Updated from Bennike (1994), Rasch (1997), Long and Roberts (2002), Long *et al.* (2003; 2006), Lloyd *et al.* (2005). Dates are given as mean ages in thousand cal. yr BP. Inner ED and Outer ED refer to the two parts Egedesminde Dyb; the deep trough in the Disko Bugt area.

The earliest date for the minimum age of deglaciation comes from southwestern Disko Bugt (Qeqertarsuatsiaq, *Fig. 2.8*). The age of *ca.* 13.2 ka cal. yr BP, obtained from lacustrine basal gyttja collected from above the marine limit, is a few thousand years older than other dates

collected in Disko Bugt (*Fig. 2.*8). While this may suggest an early initial deglaciation followed by very slow retreat from outer Disko Bugt, or even a stillstand during deglaciation, much later dates obtained for the minimum age of deglaciation in more recent work by Long and Roberts (2003), suggest that the age of 13.2 ka BP must be wrong. Dating of the marine limit indicates that deglaciation of western Disko Bugt took place around 11-10.2 ka BP (Long and Roberts, 2003), with similar ages for marine limits in eastern Disko Bugt (e.g. Long and Roberts, 2002; Long *et al.*, 2003) suggesting deglaciation across the bay was extremely rapid. The minimum ages for deglaciation in this area are comparable to dates from Nunarssuaq, Kronprinsens Ejland (*Fig. 2.8*), of 9.3 ka cal. yr BP (8690±90 ^{14}C yr BP; Bennike *et al.*, 1994) and 10-9.8 ka BP from southern Disko Island (Ingólfsson *et al.*, 1990).

The timing of ice retreat through the Vaigat is poorly understood. Glacial till, composed partly of easterly-sourced gneisses, underlies a raised beach at Hammers Dal, northwest Disko Island (*Fig. 2.8*). While it is likely that ice moving through Vaigat deposited this till, there are no age constraints available (Ingólfsson *et al.*, 1990). A raised marine delta/alluvial fan complex at the marine limit on the western tip of Nuussuaq Peninsula (*ca*. 60 m a.s.l.) was formed when outlet glaciers flowed through Vaigat sound and Uummannaq Fjord (Bennike *et al.*, 1994). Dated molluscs found in the deposits up to 48 m a.s.l. returned infinite ages (>33,540 and >40,000 ^{14}C yrs), possibly suggesting that ice expansion in the Vaigat and Uummannaq did not coalesce at the LGM.

Roberts and Long (2005) suggest that greater ice thicknesses and convergent ice flow from across the Disko Bugt area at the LGM would have facilitated topographically routed ice streaming onto the west Greenland continental slope. Weidick (1994) proposed that enhanced ice stream flow velocities from Sermeq avangnardleq and Sermeq kujatdleq occurred during glacial conditions at the expense of ice flux from Jakobshavn Isbræ. Roberts and Long (2005), however, suggest the confluence of these glacier systems south of Aasiaat (*Fig. 1.2*) may have encouraged a regional drawdown of ice and increased ice flow velocities.

While the available terrestrial-based dates in Disko Bugt provide minimum ages for ice retreat at the fringes of Disko Bugt, they do not permit us to address the timing and nature of deglaciation for faster flowing ice occupying Egedesminde Dyb, the deep water trough that runs through Disko Bugt and out to the shelf edge (*Fig. 2.8*). At present, there are only two marine dates from Disko Bugt (from cores POR 18 and DA00-06, Lloyd *et al.*, 2005) that provide minimum ages for the deglaciation of the faster moving outlet glacier that occupied Disko Bugt.

Lloyd *et al.* (2005) found that the marine-based ice in Disko Bugt had retreated to the eastern part of the embayment by 10.3 ka BP (POR-18). This was followed by a period of relative ice stream stability that lasted around 1000 years before the ice retreated landwards. The DA00-06 core site became deglaciated shortly before 8.3 ka BP (*Fig. 2.8*) (Lloyd *et al*, 2005), as ice retreated onto Isfjeldbanjken, a shallow sill at the mouth to Jakobshavn Isfjord. The final retreat of Jakobshavn Isbræ back into the Isfjord at *ca*. 7.8 ka BP is clearly identified by sedimentological and foraminiferal changes (Lloyd *et al*, 2005). As the ice retreated off Isfjeldbanken there was a major fall in sedimentation and a marked relative increase in coarse sedimentation. This reflects the significant decline in fine-grained sediments ejected at the glacier terminus being deposited from suspension at the core site (Lloyd *et al*, 2005).

2.7 Ice-ocean-atmosphere interactions in the North Atlantic

Oxygen isotope measurements in Greenland ice cores show that large and repeated climate shifts of cooling followed by abrupt warming characterised the last glacial period (Dansgaard *et al.*, 1982; 1993; NGRIP members, 2004). These Dansgaard-Oeschger-type cycles can also be identified in North Atlantic marine sediment records, and show that progressively cooler D-O cycles end with massive iceberg discharges into the North Atlantic called Heinrich events (Heinrich, 1988; Broecker, 1991; Bond *et al.*, 1992; 1993; Bond and Lotti, 1995). The cause of these Heinrich events has been widely debated. One explanation is that internal dynamics of the Laurentide Ice Sheet cause ice stream surges and massive iceberg discharges through the Hudson Strait (MacAyeal, 1993). An alternative explanation is that Heinrich events are a response to external climate forcing (Bond and Lotti, 1995; Bond *et al.*, 1999; Dowdeswell *et al.*, 1995). While IRD layers are largely composed of detrital carbonate sourced from Hudson Strait

(Andrews and Tedesco, 1992; Bond *et al.*, 1993), material originating from the eastern North Atlantic can also be identified (Bond and Lotti, 1995; Bond *et al.*, 1997; 1999; Scourse *et al.*, 2000). Apparently-synchronous ice sheet responses in disparate regions suggest that an external driver may be responsible. Hulbe *et al.* (2004) hypothesize that periodic collapses of Canadian ice shelves in front of Hudson Strait were primarily responsible for the extensive IRD layers in the North Atlantic. Ice-shelf collapses may be a response to gradual rather than abrupt climate warming (Hulbe *et al.*, 2004). The freshwater released from melting icebergs caused rapid reorganizations of North Atlantic thermohaline circulation, including a shutdown of NADW formation (Broecker, 1994; Keigwin and Lehman, 1994; Bard *et al.*, 2000; Rahmstorf, 2002).

While formerly considered to have a relatively stable climate, lower amplitude Dansgaard-Oeschger cycles have continued throughout the Holocene at intervals of 1470±500 years (O'Brien *et al.*, 1995). These are correlated to drift-ice episodes to locations in the North Atlantic presently under the influence of the NAC and IC (Bond *et al.*, 1997; 2001). The composition of IRD from these events suggests past circulation regimes in the North Atlantic may have been vastly different to the modern one (Bond *et al.*, 1997). Haematite-stained IRD suggest ice-laden surface waters originating from the Nordic Seas advected southwards with a coincident shift in the polar front (Bond *et al.*, 1997) and a reduction in NADW formation (Bianchi and McCave, 1999, Bond *et al.*, 1999; Denton and Broecker, 2008). Central West Greenland is an important source of modern iceberg and meltwater fluxes. However, the possible influence of icebergs originating from the Baffin Bay region during the Holocene is poorly constrained. Changes in solar irradiance have been suggested as the primary cause of Holocene millennial-scale climatic variability (Bond *et al.*, 1997; 2001). The climatic response to short periods of reduced solar irradiance is likely to resemble a negative phase of the NAO (Shindell *et al.*, 2001), and cause a weakening in NADW formation similar to the recent GSAs described above (Bond *et al.*, 1997).

Chapter 3

MATERIAL AND METHODS

Chapter 3

Material and methods

3.1 Introduction

In this chapter, the materials and methods used to address the research objectives set out in Chapter 1 are summarised. The rationale for site selection is outlined together with an overview of the physical setting at the core sites. Secondly, the methods used to investigate past changes in sub-surface water mass characteristics and sedimentary environments, and the dating methods used to place these changes within a chronological framework, are outlined.

3.2 Material

Fossil sediment cores collected from three sites in the Disko Bugt-Uummannaq region of West Greenland during cruises of the RV *Dana* in September 2006 (Core DA06-139G) and RV *Maria S. Merian* in June-July 2007, leg 05/03, (Cores MSM-343340 and MSM-343520) provide study material for this investigation. Long sediment records spanning the Holocene were collected using gravity corers (identified with 'G' suffix) at all sampling stations. A short multicore retrieved from the core station MSM-343520 (identified with 'MC' suffix) preserves the sediment-water interface at the seafloor and provides an undisturbed record of recent oceanographic changes.

Core name	Core type	Location	Position		Water depth (m)	Core length (cm)
			Latitude	Longitude		
DA06-139G	Gravity	Vaigat	70°05'47.90"	52°53'43.00"	384	444
MSM-343340-5_G	Gravity	Outer Egedesminde Dyb	68°36'55.00"	55°19'59.00"	461.2	1074
MSM-343520-2-1_MC	Multicore	Uummannaq shelf	70°48'57.00"	56°50'53.64"	545.3	42
MSM-343520-3_G	Gravity	Uummannaq shelf	70°48'57.06"	56°50'53.88"	545.7	989

Table 3.1 Details of fossil cores collected during cruises of the RV *Dana* (09/2006) and RV *Maria S. Merian* (06/2007).

3.2.1 Site selection

There has been significant interest in research in the Disko Bugt-Uummannaq area over recent years investigating the interaction between the Greenland Ice Sheet and ocean circulation. Recent marine-based investigations in the Disko Bugt-Uummannaq area are largely confined to fjord environments (e.g. Deslodges *et al.*, 2002; Gilbert *et al.*, 2002; Park, 2003; Moros *et al.*, 2006; Lloyd *et al.*, 2007) and inner Disko Bugt (e.g. Lloyd *et al.*, 2005; Lloyd, 2006a, Moros *et al.*, 2006; Lloyd *et al.*, 2007; Seidenkrantz *et al.*, 2008; Krawczyk *et al.*, 2010). The timing and mechanisms of deglaciation of the Greenland Ice Sheet in central West Greenland are widely debated (e.g. Funder and Hansen, 1996; Bennike and Björck, 2002; Long and Roberts, 2003). The current deglacial chronology (discussed in Chapter 2) of marine-based ice in Disko Bugt is limited to dates from the terrestrial margins and two dates from marine cores DA00-06 (7843±72 ^{14}C yrs BP, 69°10.21'N, 51°23.71'W) and POR18 (9483±65 ^{14}C yrs BP, 69°10.54'N, 51°49.38'W) in inner Disko Bugt (Lloyd *et al.*, 2005). Although geophysical surveys have identified moraines on the shelf west of Disko Bugt to the north and south of Outer Egedesminde Dyb (Brett and Zarudzki, 1979; see green shading in *Fig. 3.1*), there are at present no dates to constrain the timing of early deglaciation. Further north, there are even fewer dates to constrain the timing of deglaciation in the Uummannaq region (Bennike and Björck, 2002).

To investigate the timing and nature of deglaciation of the outer shelf west of Disko Bugt and Uummannaq Fjord, gravity cores MSM-343340_G and MSM-343520_G are used. Following deglaciation of the marine-based portion of the ice sheet, these cores provide records of changes in bottom water conditions that reflect regional oceanographic trends. Coring locations were selected based on parasound surveys undertaken during the cruise which identified deep-water basins where continuous and relatively undisturbed sedimentation may have taken place during the Holocene.

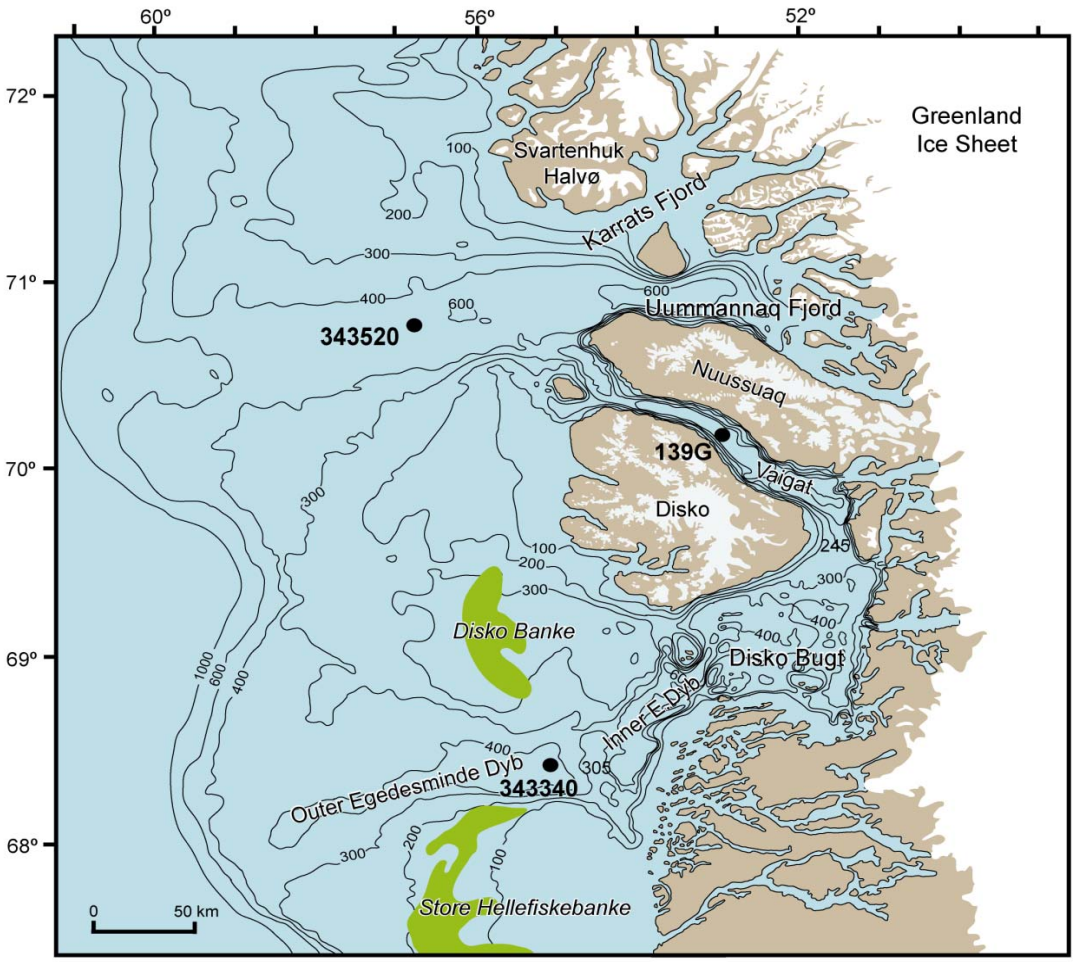

Fig. 3.1 Location of core stations (black circles) and continental shelf bathymetry of the Disko Bugt-Uummannaq area in central West Greenland, showing troughs from inner shelf extending to trough mouth fans and location of moraine banks (highlighted in green). Spot depths mark thresholds into Disko Bugt and the Vaigat.

MSM-343340, Outer Disko Bugt

Core MSM-343340_G (see *Table 3.1* and *Fig. 3.1*) was collected from a water depth of 461.2 m using a 12 m gravity corer (125 mm diameter). MSM-343340 was retrieved from the centre of a small basin located in the outer part of Egedesminde Dyb (*Fig. 3.2*). Egedesminde Dyb is a deep-water trough extending from west of Jakobshavn Isfjord to the shelf break. This trough is bisected by high bedrock (305 m water depth) east of the core site (see *Fig 3.1*). Egedesminde Dyb is thought to have routed the glacial Jakobshavn Isbrae to the outer shelf at the Last Glacial Maximum (Long and Roberts, 2003). However, streamlined bedrock terrain in southwest Disko Bugt suggests that ice streaming under glacial conditions was not restricted to this deep-water trough, and may have extended over a much wider area (Roberts and Long,

2005). Consequently, this site provides the opportunity to assess the timing and nature of deglaciation of fast-flowing ice, compared to the slower-moving main body of the ice sheet in the Disko Bugt area.

The shallow threshold located east of core MSM-343340 is the final barrier that the Atlantic water component of the WGC must overtop in order to enter the main area of Disko Bugt. This core is therefore well situated to record changes in the relative temperature of Atlantic water entering Disko Bugt that has the potential to reach the calving margin of tidewater glaciers in Disko Bugt and influence glacier dynamics. Site MSM-343340 is located within the depth range of the warm core of the WGC, and therefore changes in benthic fauna should reflect changes in the relative temperature of the WGC.

MSM-343520, Uummannaq shelf

Core MSM-343520_G (see *Table 3.1* and *Fig. 3.1*) was collected from a water depth of 545.7 m using a 12 m gravity corer. In order to sample an undisturbed record at the sediment-water interface a multicore (MSM-343520_MUC) was collected from the same site. This core is located mid-way across the shelf west of Uummannaq Fjord (*Fig. 3.1*). Parasound surveying shows that this site lies on a small plateaux (*Fig. 3.3*). The seafloor deepens landwards to depths locally exceeding 1000 m on the inner shelf (Harff, 2007).

Site MSM-343520 is a key site for investigating both deglaciation of the central sector of the Greenland Ice Sheet and the palaeoceanographic evolution of the WGC north of Disko Bugt. While the understanding of deglaciation in the Uummannaq region is poorly constrained, Bennike and Björck (2002) have suggested deglaciation of Uummannaq Fjord occurred around 1000 years earlier than Disko Bugt, though the dating evidence for this is tenuous. Core MSM-343520_G therefore provides the opportunity to assess the relative timing of deglaciation of the mid-shelf area of Uummannaq compared to Disko Bugt. The location of this core will allow investigation of the driving mechanisms of early deglaciation in the Uummannaq area. Following deglaciation, core sediments should provide a record of oceanographic evolution at core sites, and in particular sub-surface temperature changes in the area. Furthermore, the

location of sites MSM-343340 versus MSM-343520 allows a qualitative assessment of changes in water temperature (relative cooling/dilution of WGC) between outer Disko Bugt and the Uummannaq shelf. This is important in assessing the possible role of ocean temperature changes forcing ice margin dynamics in the two regions.

DA06-139G, Vaigat

DA06-139G is located in the central part of the Vaigat fjord (see *Table 3.1* and *Fig 3.1*). The Vaigat is the main conduit through which icebergs and meltwater exit Disko Bugt. The majority of icebergs originate from Jakobshavn Isbræ, although Sermeq Avannarleq and Sermeq Kujalleq in Torsukattak also produce a significant volume of calf-ice. This core is therefore appropriately sited for investigating the changes in iceberg discharge from tidewater glaciers in Disko Bugt that can be compared against sedimentological records from MSM-343520.

Sub-surface water in Disko Bugt flows back into Baffin Bay via the Vaigat. Sub-surface waters must overtop a shallow sill (245 m water depth, see *Fig. 3.1*) in order to enter the Vaigat from the eastern margin of Disko Bugt (Andersen, 1981a). In view of the difficulties of retrieving sediment cores in fjord areas immediately in front of major ice streams, this site may provide the closest analogue for bottom-water conditions in more ice-proximal locations, and the potential for warm WGC incursion over shallow sills with a large meltwater layer at the surface. Sedimentological analyses of core DA06-139G further allows an investigation of the Holocene evolution of iceberg rafting from Disko Bugt.

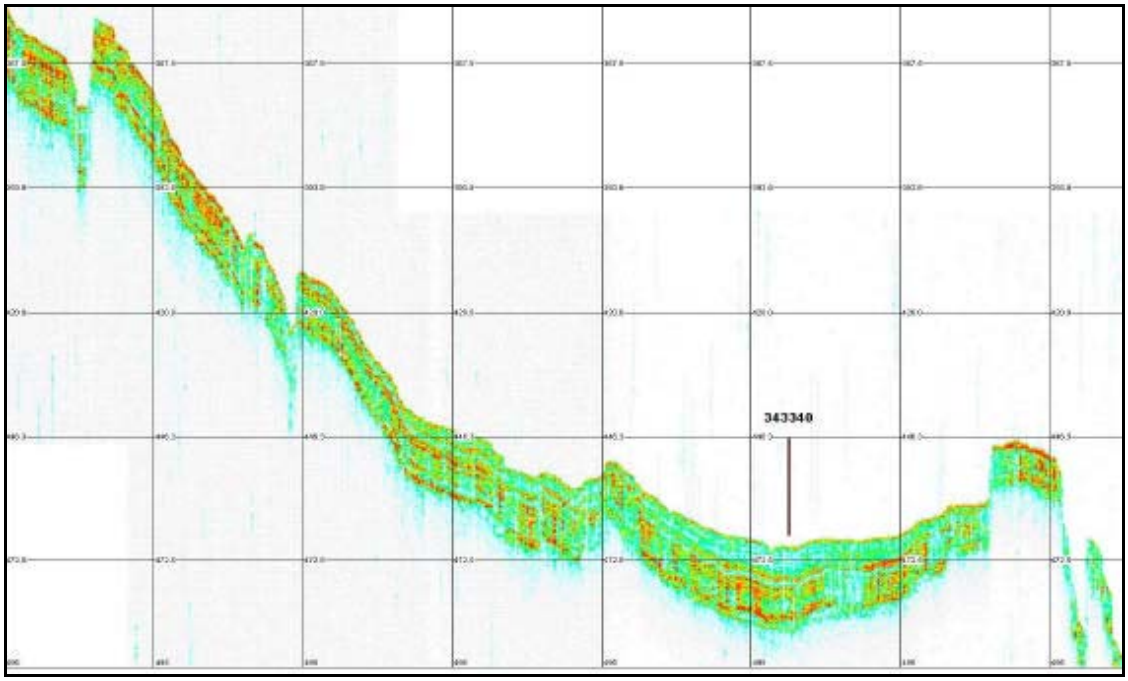

Figure 3.2 Parasound record at station MSM-343340, from southwest (left) to northeast (right), going towards Disko Bugt. Vertical line marks position of core.

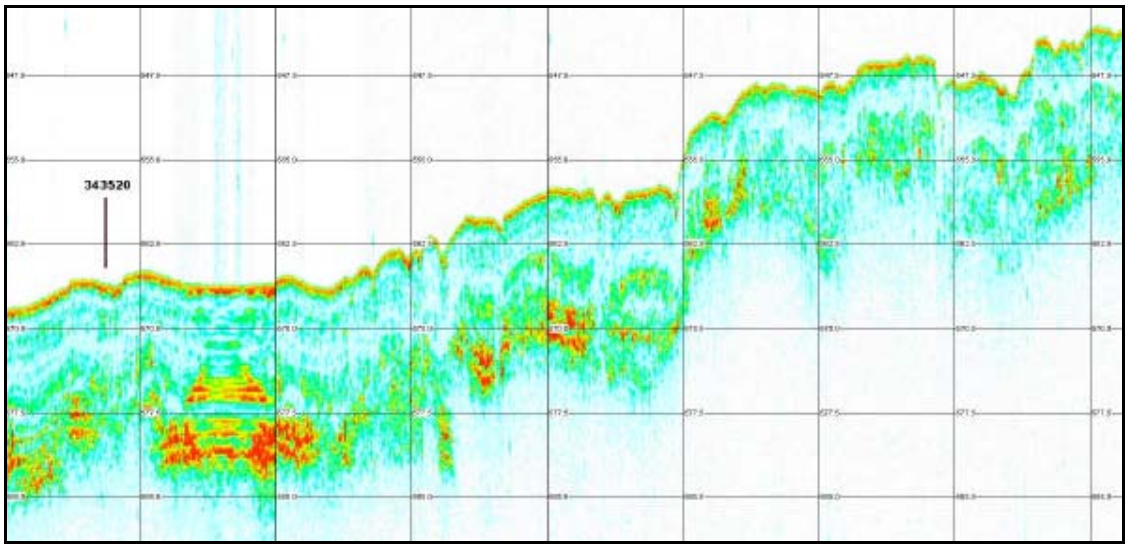

Figure 3.3 Parasound record at station MSM-343520, from east (left) to west (right), showing shoaling towards the shelf edge. Vertical line marks position of core.

3.3 Methods

Table 3.2 details the analyses performed on each core, and data used in this thesis provided by project collaborators. Each sample from gravity cores are analysed in 2 cm 'slices' unless otherwise noted, while multicore samples are analysed in 0.5 cm slices from 0 cm to 11 cm, and 1 cm thereafter, unless otherwise specified.

Analysis	DA06-139G	MSM-343340_G	MSM-343520_MC	MSM-343520_G
Foraminifera	8-16 cm	16 cm	0.5-1 cm	4 cm
Grain size (sieving)	5 cm*	X	X	1 cm***
Grain size (LD)	8-16 cm	0.5-1 cm**	0.5-1 cm**	10 cm****
Clast counts	2 cm*	4 cm	X	4 cm
Petrologic counts	5 cm*	X	X	X
Dry bulk density (DBD)	X	8-16 cm	0.5-1 cm	8-16 cm
Water content	X	8 cm	0.5-1 cm	1 cm***
Mag. Sus.	5 cm*	0.5 cm	X	0.5 cm
LOI	X	8-16 cm	X	1 cm***
XRF (core scanning)	1 cm*	1 cm	X	1 cm
TIC	X	X	X	#
TN	X	X	X	4-16 cm
TC	X	X	0.5-1 cm**	4-16 cm
$\delta^{18}O$	X	X	X	2 cm (max.)
$\delta^{13}C$	X	X	X	2 cm (max.)

Table 3.2 Details of analyses performed on each core, and the resolution of these analyses.
* Data provided by C.S. Andresen (GEUS). Further information about methods detailed in Andresen *et al.* (2011).
** Analyses available in Krauß (2009), though no use of this data has been made in this thesis.
*** Data provided by K. Perner and M. Moros (IOW). Additional water content measurements made at a higher sampling resolution.
**** Data provided by N. Dijkstra (University of Amsterdam).
# Test analyses performed on selected samples from core.
X No analyses performed.

3.3.1 Core sedimentology

Each core was visually logged to identify major changes in sedimentology (Eyles *et al.*, 1983; Ó Cofaigh *et al.*, 2001), including textural changes, sedimentary structures, sediment colour and presence of shell and plant material. X-ray radiographs (see below) were also used to aid the description of sedimentary structures. Sediment reworking by various processes, including sediment-gravity flows, turbidity currents, bioturbation, and iceberg scouring, is commonplace in

high-latitude continental shelf settings, particularly in locations influenced by high sedimentation rates (e.g. Pereira *et al.*, 1988; Ó Cofaigh *et al.*, 2002; Kuijpers and Werner, 2007; Kuijpers *et al.*, 2007). Sediments may be deposited, eroded, or disturbed by these processes (Ó Cofaigh *et al.*, 2002), and this consequently has repercussions for the interpretation and resolution of palaeoceanographic reconstructions (Gutt, 2001; Ó Cofaigh *et al.*, 2002). Given that the sediment cores investigated in this study were collected from basins with steep sides (particularly in outer Egedesminde Dyb, illustrated in the parasound record shown in *Fig. 3.2*), sediment reworking processes may be particularly active. A thorough characterisation of core sedimentology is therefore important for reliably interpreting palaeoceanographic records. Each core was subject to a number of analyses. Details of the methods used are briefly elaborated upon below.

Moisture content (%) was calculated for samples in cores MSM-343340 and MSM-343520 to aid interpretations of X-ray radiographs and core scanning data, and identify sedimentological changes. Core MSM-343520 was sampled at 16 cm intervals and at higher resolution (contiguous in places) for the lower 1.4 m in order to capture sedimentary changes at the base of the core. Core MSM-343340 was sampled at 8 cm intervals. Samples were oven-dried at 110 ºC for 24 hours and re-weighed to determine sediment moisture content (%). Moisture content (%) was calculated using the equation:

$$M_n = [(n_w - n_d)/ n_w] \times 100 \qquad (1)$$

Where M is the moisture content (%) of sample *n*, n_w is the wet sample mass (g), and n_d is the dry sample mass (g). As part of the preparation for ^{210}Pb dating for core MSM-343520_MC (see 3.3.5 below), dry bulk density was measured by calculating the volume of the wet sediment using electronic callipers before freeze drying to remove all moisture. Dry-bulk density, defined as the dry sediment mass divided by the total wet sediment volume (Dadey *et al.*, 1992), is calculated as:

$\gamma_n = m_d / V_w$ (2)

Where γ is the dry bulk density (g/cm^3) of sample *n*, m_d is the dry sediment mass (g), and V_w is the volume (cm^3) of the wet sediment sample (Hobbs, 1983).

Samples for core MSM-343520 at a 1 cm resolution (data provided by K. Perner and M. Moros, IOW) were analysed for loss-on-ignition (LOI) to help provide insights into changes in, for example, particulate organic carbon flux to the seafloor, pertaining to changes in water mass characteristics, and possible changes in sedimentation diluting the organic carbon content in the sediments. Approximately 7 g of wet sediment (typically *ca*. 3.5 g dry mass) was analysed.

LOI (% weight) was determined by heating sediment samples in a furnace at 550 ºC for 5 hours (Dean, 1974), and was calculated as:

LOI (% wt) = $[(n_d – n_a) / n_d] \times 100$ (3)

Where n_a is ash sample mass (g) after heating in furnace.

Grain size analysis

Grain size analyses are used to help understand sediment transport, deposition, and post-depositional processes on the Uummannaq shelf since deglaciation. Grain size analyses determined using three methods, by laser diffraction of the finer than 2000 µm fraction, sieving of sand fractions, and clast counts from X-ray radiographs, are presented in this study. In this study, the full suite of analyses has thus far only been applied to core MSM-343520_G, though clast counts are available for core MSM-343340_G and DA06-139G. The combinination of analyses allows the full range of sediment sizes within the core to be analysed. The three methods used to obtain these data are summarised below:

(i) Clast counts of particles greater than 2 mm

Counts of clasts greater than 2 mm were made from X-ray radiographs, as advocated by Grobe (1987). Counts for DA06-139G, provided courtesy of Camilla Andresen (Andresen *et al.*, 2011), were made from 10x1 cm samples every 2 cm downcore. Since the digital X- radiographs for cores MSM-343520_G and MSM-343340_G do not span the whole core width, clasts were counted in contiguous 4 cm 'long' samples downcore, with a uniform width of 4 cm. This provides a more representative indication of IRD content, though at the expense of temporal resolution.

(ii) Grain size analysis by laser diffraction of particles smaller than 2 mm

The grain size fraction smaller than 2000 µm in surface samples collected in central West Greenland during the MSM 05/03 cruise were analysed at Durham University using a LS13320 Coulter Laser Granulometer. For each sample, approximately 0.5 g of sediment was placed in a 50 ml tube, and immersed with 20 ml of 20 % hydrogen peroxide. Samples were covered with aluminium foil and placed in a boiling water bath until all organic matter dissolved. Samples were centrifuged (4000 rpm for 4 minutes) and supernatant liquid decanted off. This was repeated, and then 20 ml of distilled water and 2 ml of sodium hexametaphosphate solution (a dispersant) was added to samples. The treated sediment samples were analysed by the Coulter granulometer. Each sample was analysed twice and averaged. Where repeat runs were poorly matched, additional analyses were made. Samples from core MSM-343520_G were analysed by Noortje Dijkstra (Marine Biogeology, Faculty of Earth and Life Sciences, VU University of Amsterdam) at 10 cm intervals using a HELOS KR (Sympatec) laser-diffraction particle sizer.

(iii) Dry sieving of coarse fractions greater than 63 µm and 150 µm

Dry sieving of coarse grain size fractions, carried out by K. Perner and M. Moros (IOW), was used to analyse the percentage weight components of sediment fractions. Samples were dried at 60°C, weighed, and then wet sieved through mesh sizes of 63 µm and 150 µm, dried at 60°C, then reweighed. Wet samples masses were typically *ca.* 35 g. The weight of each grain size fraction was calculated as a percentage of the total dry weight.

X-ray radiographs

Differential attenuation of incident X-rays produce radiographs which primarily reflect bulk sediment density (St-Onge *et al.*, 2007). Changes in grain size, water content, and lithology therefore influence the grey scale intensity in X-ray radiographs. Sediment reworking affects both the interpretation and resolution of palaeoceanographic records (Ó Cofaigh *et al.*, 2002). The possible influences of current activity, turbidity, and bioturbation are therefore qualitatively assessed using X-ray radiographs.

An ITRAX core scanner (Institute of Geology and Mineralogy, University of Cologne) captured 20 mm wide digital X-ray radiographs of the archive half of sediment cores MSM-343340 and MSM-343520. All core sections were X-rayed using a step size of 500 µm, while the bottom metre of core MSM-343520 was X-rayed at a higher-resolution using a step size of 200 µm. X-ray radiography used excitation conditions of 55 kV and 50 mA, with a measuring time of 3000 ms and 4000 ms for measurements at step-sizes of 500 µm and 200 µm respectively. Image processing procedures (e.g. image stacking, enhancing contrast) were applied to the digital X-ray radiographs using the ImageJ software package (version 1.41, Rasband, 2008) to allow identification of different lithofacies.

3.3.2 Geochemical analyses

Sediments were analysed using a variety of geochemical methods, as detailed below.

X-Ray Fluorescence (XRF) core scanning

XRF core scanning is becoming more widely used as it provides a fast, economical method for determining relative abundances of elements in fossil sequences. Data from XRF core scanning is used semi-quantitatively in this study to identify possible changes in sediment provenance, grain size, and biological productivity.

A containerized Avaartech X-ray fluorescence (XRF) core scanner (from the Royal Netherlands Institute for Sea Research) onboard the *RV Maria S. Merian* enabled analysis of sediment cores MSM-343340 and MSM-343520 at 1 cm resolution within hours to days of collection during the

MSM-05/03 cruise. Smoothing and covering the sediment surface with plastic film helped reduce the impact of surface roughness on XRF analysis. XRF scanning of core DA06-139G was undertaken at 1 cm intervals two years after collection (data provided by C.S. Andresen and A. Kuijpers, GEUS, Copenhagen). The Avaartech XRF core scanner measures bulk intensities (concentration) of major elements in counts per second. Nine elements (Al, Ca, Cl, Fe, K, Mn, S, Si, Ti) were analyzed, although analysis focuses on the elemental ratios [S/Al], [Si/Al], and [K/Ti]. Using normalized (ratio) X-ray fluorescence (XRF) elemental intensities, rather than just intensity data from XRF core scanners, is recommended because core-scanners provide relative rather than absolute elemental data (e.g. Croudace *et al.*, 2006; Richter *et al.*, 2006; Calvert and Pedersen, 2007; Rothwell *et al.*, 2006). Richter *et al.* (2006) provide a good review of the capabilities, limitations, and applications of the Avaartech XRF core scanning data.

Magnetic susceptibility

Magnetic susceptibility measures the degree to which material can be magnetized (Thomson and Oldfield, 1986), and is the sum of all magnetically susceptible sediment components (Dearing, 1999). Magnetic susceptibility may be used to identify changes in sediment provenance, though scanning sensor measurements are affected by grain size and water content.

The split core was smoothed and covered by a thin plastic film to reduce the effect of surface roughness on magnetic susceptibility. A Bartington Instruments MS2E1 high-resolution surface scanning sensor connected to a TAMISCAN-TS1 automatic logging conveyor measured surface magnetic susceptibility at 1 cm intervals (Harff, 2007). Multicore sediments (0.5 to 1 cm intervals) were placed in Petri dishes, covered with plastic film, and measured using a MS2E1 surface scanning sensor connected to a MS2 meter. Volumetric magnetic susceptibility, K, expressed using the SI convention, is herein referred to as magnetic susceptibility.

Magnetic susceptibility and XRF core-scanning data provide a semi-quantitative means of assessing sediment provenance and making time-transgressive correlations between cores to supplement foraminiferal data.

Total carbon (TC) and total nitrogen (TN)

Samples from MSM-343340 and MSM-343520 were prepared at 8 cm intervals for total carbon, total nitrogen, and total inorganic carbon analysis. Samples were freeze-dried then ground and homogenized using an agate pestle and mortar. Total carbon (TC %) and total nitrogen (TN %) in samples was analysed by combustion in a Costech elemental analyser. A sediment mass of approximately 50 mg was placed in tin capsules and weighed on a microbalance. Tin capsules were sealed, compressed, and loaded into a carousel. Measurements were calibrated using one blank (empty tin capsule) and four Sulfanilamide standard samples (0.5, 1, 1.5, 2 mg). Analytical precision was checked using an analytical quality control (AQC) sample (1.5 mg of the Sulfanilamide standard), a certified reference material sample (15 mg of high organic content sediment standard OAS - B2150), and a blank, in the middle and at the end of the run. Analytical precision determined by analysis of the CRM was better than 5 % for carbon and nitrogen in all batch runs. Total inorganic carbon (TIC) was analysed by digestion in orthophosphoric acid in a Thermo Finnigan TOC 1200 analyser. A stock inorganic carbon calibration standard was prepared using 4.4122 ± 0.0001 g anhydrous sodium carbonate and 3.4970 ± 0.0001 g anhydrous sodium hydrogen carbonate dissolved into 500 ml of deionised water. 100 µl of the calibration standards (prepared to concentrations of 0, 10, 20, 50, 100, 150 mg/l) were analysed to produce a calibration curve. Sample masses typically varied between 10-20 mg depending on inorganic carbon content. Samples were digested for a maximum of 500 seconds. This allowed CO_2 to reach background levels for most samples, and where this was not attained, the unanalysed carbonate contribution was negligible. Calcium carbonate (calcite) is the primary form of inorganic carbon in samples, although minor quantities of less reactive forms (e.g. dolomite, $CaMgCO_3$) may be present. Regular AQC (100 µl) samples indicated analytical precision for TIC was better than ±5 %. Total organic carbon (TOC %) was then calculated as the difference between total carbon (TC %) analysed by combustion and total inorganic carbon (TIC %) measured by digestion. Since TIC was low (typically <0.004 %)

in a selection of samples analysed in MSM-343520_G, the proportion of TIC was considered to be negligible, and C/N ratios were therefore based on total carbon (%) / total nitrogen (%). The weight or atomic ratio of carbon to nitrogen (C/N) is commonly used to calculate the proportion of terrestrially derived carbon in subaqueous sediments (e.g. Lazerte, 1983; Hedges *et al.*, 1988; Prahl *et al.*, 1994). C/N ratios are used to assess relative changes in the contribution of marine versus terrestrial organic inputs. C/N ratios also help identify relative changes in terrestrial sediment delivery, which reflects changes in ice margin activity or changes in terrestrially-sourced sediment fluxes.

3.3.3 Foraminiferal biostratigraphy

A number of factors control the distribution and abundance of benthic foraminifera, including food supply, oxygen content, substrate type, water temperature, and salinity (Murray, 1991). Many studies have reconstructed water mass characteristics (i.e. temperature and salinity) based on benthic foraminifera assemblages from high-latitude shelf locations, which support analysis of foraminiferal assemblages in this thesis (e.g. Lagoe, 1979; Schafer and Cole, 1982; 1986; Hald and Vorren, 1984; Osterman *et al.*, 1989; Schröder-Adams *et al.*, 1990; Corliss, 1991; Scott and Vilks, 1991; Hald and Steinsund, 1992; Jennings and Helgadottir, 1994; Korsun and Hald, 1998; 2000; Rytter *et al.*, 2002; Husum and Hald, 2004; Jennings *et al*, 2004). Recent studies have found organic flux (i.e. food supply), oxygenation, and species competition may be more important than temperature and salinity in controlling benthic foraminifera distribution and abundance (Van der Zwaan, *et al.*, 1999). However, warmer, more saline Atlantic water is responsible for delivering nutrient-rich water to the West Greenland shelf (Carmack, 2007), and consequently, benthic foraminifera show a strong correspondence with the relative temperature of the West Greenland Current (Lloyd, 2006a).

Sampling strategy

Details of the sampling strategy are summarised in *Table 3.*2. The sampling strategy allows research objective (ii) to be addressed. A sampling resolution of 8-16 cm for core DA06-139G was suitable to identify mid- to late-Holocene sub-surface palaeoceanographic trends in the Vaigat. A lower sampling resolution of every 16 cm was used for core MSM-343340 since the

sedimentation rate is, for the majority of the core, an order of magnitude greater than core MSM-343520 and DA06-139G. This sampling frequency is suitable for reconstructing changes in water mass characteristics (i.e. temperature and salinity) through a deglacial sequence, which reflect the balance between meltwater fluxes from the ice margin during deglaciation, and the relative strength of the WGC circulation. Because of the fairly high and consistent sedimentation rate throughout core MSM-343520_G, a sampling interval of every 4 cm allows the interplay between meltwater fluxes and WGC circulation to be investigated during initial deglaciation, followed by a high resolution record of changes in the WGC throughout the Holocene. Each time-averaged assemblage reflects approximately 20-40 years of sediment accumulation. Sub-centennial Holocene trends in water temperature and salinity should be identifiable, and so this core should provide a regional scale record of detailing the potential ocean forcing on ice margin stability.

Sample preparation

Foraminiferal samples were prepared by leaving a measured volume of wet sediment (typically 5 cm^3) to soak and disaggregate in water overnight. Samples were gently washed through a 63 µm and 500 µm sieve and residues preserved in vials with ethanol. Wet residues were transferred to a picking tray by pipette and foraminifera identified using a binocular microscope at 30x to 100x magnification. Foraminifera were handpicked, transferred to Chapman slides, then sorted and identified. Reference to type slides maintained taxonomical consistency. Calcareous foraminifera provided material for isotope analysis and radiocarbon dating. Foraminifera taxonomy follows a number of Arctic studies, including Vilks (1969), Feyling-Hanssen (1980), Vilks *et al.* (1982), Schafer and Cole (1986), Schröder-Adams *et al.* (1990a), Corliss (1991), Scott and Vilks, (1991), Hald and Steinsund (1992), Seidenkrantz and Knudsen (1993), Jennings and Helgadottir (1994), Seidenkrantz (1995), Ishman and Foley (1996), Murray and Pudsey (2004), Jennings *et al.* (2004).

A target of 300 specimens was counted where abundance was sufficient (e.g. Knudsen *et al.*, 2004; 2008a; Eiríksson *et al.*, 2000). Higher counts do not significantly increase data reliability (Phleger, 1960). In samples with low foraminiferal abundance, counts of at least 100 individuals

were made where possible. This provides a 95 % confidence level for species making up at least 3 % of the assemblage (Dennison and Hay, 1967) and is adequate for detecting more than 99 % of species that make up ≥ 5 % of an assemblage (Fatela and Taborda, 2002). Since fossil assemblages are subject to variable preservation (e.g. dissolution of calcareous fauna, destruction of arenaceous tests during burial), 100 specimens of calcareous and agglutinated species were counted where foraminiferal abundance was sufficient. Foraminiferal counts are recorded as percentages for the total assemblage (TA; agglutinated+calcareous species), and individually for both agglutinated and (AA) calcareous foraminifera (CA). Individual components therefore aid interpretations where there may be a systematic loss of certain species. The number of individuals counted in a known fraction of wet residue (based on initial sample volume) is used to estimate foraminiferal concentration, expressed as specimens per ml (individuals per cm^3) for the total assemblage. Counts of foraminifera test linings provide an indication of species loss by dissolution. Although not included in the foraminifera sum, the test lining count is may be used as an indicator of the size of the 'lost' calcareous assemblage by expressing test lining counts as a percentage of the total calcareous foraminifera and test linings. Summary data is provided for percentage agglutinated versus calcareous foraminifera and for groups of species (percentage sum of selected taxa) whose distributions are associated with different water masses. While Lloyd (2006a) classifies species associated with Atlantic, 'intermediate', Arctic, and glaciomarine water mass influences, and a group of 'indifferent' species with no obvious affiliation to water mass characteristics, faunal trends in gravity cores are more simplistically grouped into either Arctic- or Atlantic-influenced fauna, or 'indifferent' fauna. The additional 'intermediate' group is used for core MSM-343520_MC to better highlight the faunal trends.

Modern foraminifera assemblage data presented in Chapter 4 is provided courtesy of J.M. Lloyd (University of Durham). The data set constitutes samples collected in 1999 (see Lloyd, 2006a) and new surface samples (top 2 cm of sediment accumulation) collected during the MSM 05/03 cruise in 2007. These surface samples were collected using a multicorer to preserve the sediment-water interface. Foraminiferal samples were stained with Rose Bengal in the field to

identify living specimens, and preserved with ethanol. Foraminiferal samples are based on counts of at least 100 specimens and more than 300 where possible.

3.3.4 Stable isotope analysis of benthic foraminifera

Oxygen and carbon stable isotope analyses of foraminifera are widely used in palaeoceanographic investigations since calcareous tests preserve a record of the stable isotopic composition of the ambient water in which they grow (Murray, 1991). Consequently, variations in isotope values primarily reflect changes in environmental conditions (Katz *et al.*, 2003). Oxygen isotope ratios in biogenically precipitated calcite are particularly useful, and reflect both the temperature and isotopic composition of the ambient seawater in which foraminifera grow (Urey, 1947; Emiliani, 1955).

A monospecific oxygen and carbon isotope record was constructed for core MSM-343520, with a resolution of up to 2 cm. The species *Nonionella labradorica* was selected for analysis since this was present in adequate abundance throughout most of the core. Although *Nonionella labradorica* has been recorded as deep-infaunal (up to 8 cm depth) at some locations (e.g Ivanova *et al.*, 2008), most foraminifera are likely to live in the top 1 cm of surface sediment (Murray, 1991). In general, 3 or 4 clean intact tests (approximately 70 µg), free of observable diagenetic affects, were used in each analysis. Similar sized tests were selected for each sample to increase the likelihood that these tests represent the same generation or environmental conditions during test secretion, and minimize the affect of species vital effects. Stable isotope analyses were performed at the NERC Isotope Geoscience Laboratory (NIGL), Keyworth, using an IsoCarb common acid bath (reacted at 90°C) connected to a VG Optima mass spectrometer. Isotope ratios are expressed using the δ notation:

$$\delta\,‰ = \frac{\mathrm{R(sample)} - \mathrm{R(standard)}}{\mathrm{R(standard)}} \times 1000 \qquad (4)$$

as relative deviations (per mil) from $^{18}O/^{16}O$ and $^{13}C/^{12}C$ ratios (R) of the Vienna Pee Dee Belemnite (VPDB) standard by reference to an internal laboratory working standard (KCM)

calibrated against the reference material NBS-19 calcite. Repeat measurements of KCM indicated that sample precision was better than ±0.05 ‰ for $\delta^{18}O$ and ±0.02 ‰ for $\delta^{13}C$ at the 1 σ level. The mean standard deviation for repeat analyses on 50 samples at 22 discrete sampling depths was better than ±0.13 ‰ for $\delta^{18}O$ and better than ±0.23 ‰ for $\delta^{13}C$. Ivanova *et al.* (2008) found that *Nonionella labradorica* calcifies in isotopic disequilbrium with ambient seawater, and a correction factor of +0.28 ‰ may be applied to the $\delta^{18}O$ value to account for this. However, this translation has not been applied to data in this study, since past variability of this effect is not known.

3.3.5 Chronological framework

In order to address objectives (iii) to (v), a dating framework combining radionuclide dating of bulk sediment (for upper multicores sediments) and radiocarbon dating of benthic foraminifera, bivalves, molluscs, and plant fragments is used to provide a chronology for each core. A robust chronology will allow a fuller understanding of the timing of palaeoenvironmental changes, and allow comparisons between other archives.

Lead-210 (^{210}Pb) and Caesium-137 (^{137}Cs) radionuclide dating

^{210}Pb (half-life of 22.26 ± 0.22 years) is the last unstable daughter isotope in the ^{238}Uranium decay series. Two types of ^{210}Pb (constituting total ^{210}Pb activity) exist in recently (last *ca*. 150 yrs) deposited sediments; supported ^{210}Pb (in equilibrium with its parent ^{238}U) formed through *in situ* decay of ^{226}Ra, and unsupported or excess ^{210}Pb produced by natural fallout of unsupported ^{210}Pb (Appleby and Oldfield, 1992). The latter is produced in the atmosphere by decay of gaseous ^{222}Rn (half-life 3.8 days) released from surface sediments. Unsupported ^{210}Pb radionuclides return to the earth's surface through precipitation, and are incorporated into marine and terrestrial sediments (Appleby and Oldfield, 1992). Unsupported ^{210}Pb is determined as the difference between supported ^{210}Pb activity from *in situ* decay of ^{222}Rn (measured in older sediments) from the total ^{210}Pb activity in each sample. It takes about 7 half-lives (approx. 156 yrs) for ^{210}Pb in a sample to reach near-zero activity. However, the maximum reliable dating range is approximately 5 half-lives (*ca*. 1895 AD to present).

Sub-sampling of core MSM-343520_MC in slices of 0.5 cm thickness at intervals of 0.5 cm to 1 cm (from 0 to 10 cm depth) and 1 cm thick slices at 2 cm intervals (from 10 to 21 cm depth) provided material for ^{210}Pb dating. Dry bulk density calculations for each sample follow the method as described above. Sediment samples were freeze-dried, ball milled, placed in sealed vials, and left to equilibriate for 21 days. This allows ^{226}Ra and ^{214}Pb to equilibrate prior to gamma analysis, and hence ^{214}Pb emitted from each sample records the supported decay caused by ^{226}Ra rather than atmospheric fallout. ^{210}Pb and ^{137}Cs activities were determined by gamma spectrometry by placing sealed vials in an Ortec GWL p-type Series Germanium gamma ray spectrometer. Count times ranged between 114091 and 349479 seconds (1.3 to 4 days), and errors were typically 5.4% (1 σ). Supported ^{210}Pb activity was determined via ^{214}Pb counted from sediment in sealed vials. Supported specifics activities were between 12.99 and 36.55 mBq g^{-1}.

AMS ^{14}C Radiocarbon dating

Radiocarbon dates were analysed at four laboratories; NERC Radiocarbon Facility, UK (dates identified with "SUERC" prefix), Lund Univeristy Radiocarbon Dating Laboratory, Sweden ("Lus"), Poznań Radiocarbon Laboratory, Poland ("Poz"), and The Aarhus AMS 14C Dating Centre, Denmark ("AAR"). Marine radiocarbon dates are calibrated using the Marine09 calibration curve (Reimer *et al.*, 2009) in the calibration programme Oxcal v4.1 (Bronk Ramsey, 2009). An ocean-atmosphere box diffusion model converts the atmospheric ages from the IntCal09 calibration curve to the surface ocean ^{14}C ages in the Marine09 calibration curve. The Marine09 curve is offset from the IntCal09 curve by a time-dependent global marine reservoir age, "R". Modelled variations in the Marine09 curve are smoothed and attenuated compared to annually-resolved atmospheric ^{14}C records (Reimer *et al.*, 2009). This better simulates mixing from ocean circulation, thus avoiding a large number of intercepts and unrealistically precise calibrated ages afforded by using a constant offset from the atmospheric curve. Between 0 and 12.5 ka cal. BP, the Marine09 curve is corrected for changes in atmospheric ^{14}C production (resolved using tree-ring chronologies). After 12.5 ka cal. BP, a constant 405±22 ^{14}C yrs (i.e. no correction for atmospheric ^{14}C production) is added to the IntCal09 curve to produce the Marine09 curve.

The regional marine reservoir age is assumed to have remained constant along West Greenland since the LGM. However, it is noted that changes in ocean circulation and ventilation patterns may have significantly altered the marine reservoir effect (MRE) in West Greenland waters, particularly during the Late Glacial and Early Holocene. Large temporal and spatial variability in the MRE has been reported in the North Atlantic region (e.g. Bard *et al.*, 1994; Bondevik *et al.*, 2006; Ascough *et al.*, 2007; Cao *et al.*, 2007).

Chapter 4

ENVIRONMENTAL CONTROLS ON MODERN DISTRIBUTION OF BENTHIC FORAMINIFERA IN CENTRAL WEST GREENLAND

All counts of foraminiferal assemblages presented in this chapter were undertaken by Jeremy M. Lloyd (Durham University). Environmental data associated with foraminifera surface sample assemblages collected during the R.V. "Porsild" cruise during September-August 1999 were provided by Jeremy M. Lloyd, and are published in Lloyd (2006a). CTD data (water temperature and salinity) was collected during the cruises of the R.V. "Porsild" and R.V. "Maria S. Merian" (June-July 2007).

Chapter 4

Environmental controls on modern distribution of benthic foraminifera in central West Greenland

4.1 Introduction

Modern distributions of benthic foraminifera offer the potential to be useful indicators of wide-ranging environmental changes in marine and marine-influenced environments. Factors that may influence the distribution of benthic foraminifera include bottom-water temperature and salinity, substrate type, food type and supply, turbidity, and oxygen concentration (Murray, 1991; Jorissen *et al.*, 1995). These factors may limit distributions (e.g. temperature and salinity) or influence abundance (e.g. food supply) (Murray, 1991, Smart and Gooday, 1997; Wollenburg and Mackensen, 1998; van der Zwann *et al.*, 1999). Identifying environmental controls on modern distributions of benthic foraminifera is critical to reliably reconstructing palaeoenvironmental change.

There is an increasing wealth of information about microhabitat preferences of benthic foraminifera in high-latitude settings. Several ecological studies have been carried out from the Arctic Ocean and Canadian Arctic (Vilks, 1969, 1989; Scott and Vilks, 1991; Mackensen *et al.*, 1993; Bergsten, 1994; Wollenburg and Mackensen, 1998; Korsun and Hald, 1998), Svalbard shelf and fjords (Hansen, 1995; Hald and Korsun, 1997; Korsun and Hald, 2000), Norwegian shelf (Mackensen *et al.*, 1985), Labrador Sea and Nova Scotian shelf (Bilodeau *et al.*, 1994), and the East Greenland shelf (Jennings and Helgadottir, 1994; Madesen and Knudsen, 1994; Jennings and Wiener, 1996). Parker and Jones (1865) conducted early studies of benthic foraminifera in Baffin Bay. More recent investigations in the Baffin Bay region have focused on the Canadian Archipelago (e.g. Phleger, 1952; Schröder-Adams *et al.*, 1990a, 1990b; Hunt and Corliss, 1993) and Baffin Island fjords (e.g. Schafer and Cole, 1986). Studies of modern benthic foraminifera distributions on the West Greenland continental shelf, however, are rather more limited; Herman *et al.* (1972) investigated foraminifera assemblages collected from fjords in

southwest Greenland, and Lloyd (2006a) investigated samples collected from Disko Bugt, central West Greenland.

New surface samples collected during summer 2007 extend the database of modern foraminifera assemblages presented by Lloyd (2006a). In total, thirty-two surface samples were collected during cruises of the *R.V. Porsild* (August-September 1999) and the *R.V. Maria S. Merian* (June-July 2007), and are distinguished using POR and MSM prefixes (*Fig. 4.1*). In light of this new data, it is necessary to review and improve our understanding of environmental controls on modern distributions of benthic foraminifera in West Greenland waters. For each surface sample, the benthic foraminifera assemblage and eight environmental variables (temperature, salinity, water depth, total nitrogen, total organic carbon, clay, silt, sand) were analysed. During the cruises, water depth measurements were recorded for each site, and CTD hydrographic profiles, providing temperature and salinity data, were collected using a Sea-Bird Electronics systems (SeaLogger 25 system during the 1999 cruise, and 911*plus* system during the 2007 cruise). Analysis of sedimentological properties (TN, TOC, and grain size) follows methods described in Chapter 3.

The aims of this chapter are threefold; firstly, to identify primary controls on foraminifera distribution in West Greenland, secondly, to assess individual species relationships with environmental parameters, and thirdly, to consider whether a reliable transfer-function can be developed using the available data for application to nearby fossil cores.

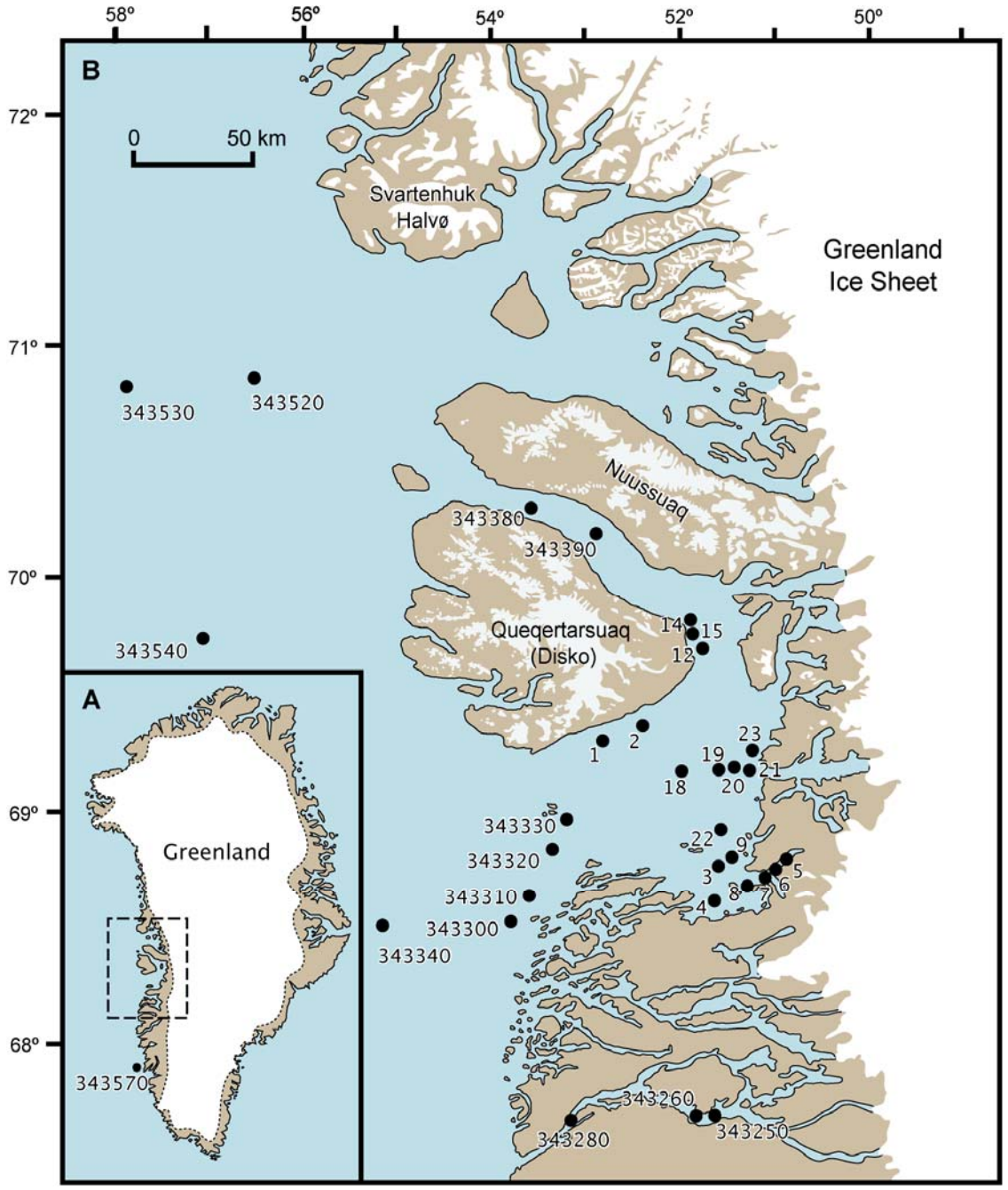

Fig. 4.1 Map showing location of modern surface samples with associated environmental data from the 1999 *R.V. Porsild* cruise (Lloyd, 2006a) and 2007 *Maria S. Merian* cruises. The majority of samples are located in the Disko Bugt-Uummannaq area (B), though the approximate location of one sample (343570), located in a trough on the shelf west of Nuuk, is shown in the inset map (A).

4.2 Numerical analyses

4.2.1 Foraminifera samples

Statistical analyses on two groupings of benthic foraminifera, the total assemblage (TLDA), and the agglutinated assemblage (AA) are presented below. In this chapter, the total assemblage (TLDA) refers to all specimens counted in a surface sample, whether the foraminifera were living or already dead at time of collection. The agglutinated assemblage refers to all agglutinated specimens in a surface sample. The motivations for this are briefly described below.

The primary focus of this chapter is on the influence of environmental controls on the total assemblage (TLDA). The major advantage of analysing the total assemblage is that this is more likely to closely resemble time-averaged fossil foraminifera assemblages. While separate analyses of living and dead foraminifera in surface samples may help identify taphonomic processes affecting the fossilisation potential of individual species (Murray and Alve, 1999), Lloyd (2006a) noted it was difficult to identify living agglutinated specimens because these foraminifera do not easily take up the Rose Bengal stain. This is particularly problematic on the West Greenland shelf because agglutinated foraminifera are dominant in most modern samples. The preservation of calcareous fauna in fossil cores from central West Greenland is a major problem, and is discussed in subsequent chapters. Consequently, for the purposes of developing a transfer function that may be applied to core intervals where the calcareous foraminifera are poorly preserved, or completely absent from the biostratigraphy, multivariate analyses of agglutinated assemblages accompany TLDA analyses where appropriate.

Only samples collected from depths exceeding 100 m are analysed in this study. This is because marine fossil cores from central West Greenland are located at depths exceeding 300 m, where sub-surface (intermediate) waters influence modern benthic foraminifera distributions, and would have also done so during deglaciation and throughout the Holocene. The inclusion of samples under the influence of seasonally-variable surface waters (< 100 m) would most likely reduce the predictability of the transfer function for reconstructing palaeoenvironmental conditions at the seafloor.

4.2.2 Statistical methods

A comprehensive understanding of environmental influences on modern benthic foraminifera distribution is critical if benthic foraminifera are to be used as a reliable proxy for reconstructing water mass characteristics from the geologic record. The statistical approach to investigating relationships between foraminifera species and environmental variable data is described below, and is used to address research objective (i).

The decision-making process followed for investigating species-environment relationships and developing a preliminary transfer function is outlined here. A number of statistical techniques have been employed to analyse the data. Multivariate methods of ordination allow multidimensional data to be summarised, making it easier to explore relationships between benthic foraminifera assemblages (the 'total' assemblage expressed as percentage abundances) and environmental parameters in a two dimensional space. Multivariate analyses are performed using the CANOCO version 4.51 program (ter Braak and Šmilauer, 2002).

A square root transformation was applied to foraminifera species data before analysis, to stabilise variances, increase their signal-to-noise ratio, and reduce the impact of dominant taxa on ordination (Prentice, 1980; ter Braak and Šmilauer, 2002). Rare species (abundance less than one-fifth of the most common specie in a sample) are empirically down-weighted in proportion to their frequency in the CANOCO program so they do not disproportionately influence ordination (ter Braak and Šmilauer, 2002; Legendre and Legendre, 1998). Environmental variables are automatically centred (means equal to zero) and standardized (variances equal to one) in CANOCO before analysis (ter Braak and Šmilauer, 2002).

The steps outlined below allow the following aims to be fulfilled:

(a) Identify appropriate approaches to modelling species-environment relationships.

(b) Identify the relative importance of individual environmental variables for explaining species distributions.

(c) Identify the importance of groups of variables for explaining species distributions, for example, the importance of water mass characteristics (temperature and salinity) versus sedimentological characteristics (grain size).

(d) To construct a transfer-function that may be applied to fossil foraminfera assemblages in order to produce estimates for past bottom-water temperatures on the central West Greenland shelf.

(i) Step 1: Detrended Correspondence Analysis

Detrended correspondence analysis (DCA) is a method of indirect gradient analysis (unconstrained ordination) that assesses heterogeneity in species data (Lepš and Šmilauer, 2003), and thereby indicates whether linear or unimodal constrained ordination methods are suitable for modelling species-environment relationships. Species data was detrended-by-segments with non-linear (Hill's scaling) rescaling (Hill, 1979; ter Braak and Šmilauer, 2002). The length of the longest ordination axis represents the extent of species turnover (i.e. the beta diversity) in standard deviation (SD) units along an independent synthetic gradient (Hill and Gauch, 1980). DCA axis 1 gradient length is 2.6 SD units for the total assemblage. Gradient lengths between 2 and 3 SD units lie within a 'grey zone' where it is unclear whether linear or unimodal methods of constrained ordination best model species-environment relationships (cf. Birks, 1995; ter Braak and Šmilauer, 2002).

(ii) Step 2: Canonical Correspondence Analysis

Studies indicate canonical correspondence analysis (CCA) is suitable for analyzing both linear and unimodal data (ter Braak and Verdonschot, 1995; ter Braak and Šmilauer, 2002), and therefore can be applied to species data with relatively short (<3 SD units) gradient lengths (ter Braak and Šmilauer, 2002). In CCA, compositional data (species, samples) are positioned along synthetic gradients (ordination axes) that represent linear combinations of environmental variables (ter Braak, 1986; Legendre and Legendre, 1998). An initial CCA using all available environmental variables identifies relationships between foraminifera species and explanatory variables (ter Braak, 1986; ter Braak and Verdonschot, 1995).

(iii) Step 3: Stepwise forward selection in CCA

High variance inflation factors (>20) calculated during the CCA ordination indicate autocorrelation (and hence redundancy) between environmental variables (ter Braak and Šmilauer, 2002). The stepwise forward selection procedure in CCA identifies which environmental variables are statistically significant for explaining species distribution on the West Greenland shelf (ter Braak, 1990; Bocard *et al.*, 1992; Lepš and Šmilauer, 2003), and removes redundant, highly correlated variables, thus avoiding artificially increasing the explained variance (Bocard *et al.*, 1992; Birks, 1996).

The first step involves the selection of the variable that best explains patterns in species data. Subsequent explanatory variables are added to the regression model one at a time based on the additional explained variance they contribute. These are called their 'conditional effects' because they are conditional on the variance explained by already-selected variables. At each step, a Monte Carlo permutation test (9999 unrestricted permutations, reduced model) assesses the statistical significance of the variance contributed to the regression model by the selected environmental variable. Permutation tests performed using the reduced model minimises type I errors (i.e. rejecting null hypothesis when it is true), where the null hypothesis states that there is no relationship between compositional data and the environmental variable tested. Rejecting the null hypothesis indicates that foraminifera species respond to measured environmental variables at the 5% significance level. Forward selection identifies four variables (temperature, water depth, salinity, sand) that explain variation in species data at the 5% significance level.

(iv) Step 4: Partial CCA

Partial CCA assessed the independent contribution of each environmental variable to the proportion of species variation (ter Braak, 1988; Bocard *et al.*, 1992; ter Braak and Verdonschot, 1995). Species data was analysed by CCA constrained to one environmental variable at a time. Variation explained by the explanatory variable is calculated as the first axis canonical (constrained to an environmental variable) eigenvalue divided by the total inertia (total variation) of the species data. The proportion of variation explained by all environmental variables is

simply the sum of all canonical eigenvalues in CCA run with all environmental variables relative to the sum of all eigenvalues (total variation).

Furthermore, partial CCA enabled partitioning of variation explained by different sets of environmental variables (see aim 'c' above), following Bocard *et al.* (1992). This identified variation explained by subsets of environmental variables (X_1), after removing the effect of covariables in X_2 ($X_1|X_2$). A second partial CCA identifies variation explained by explanatory variables in group X_2 with members of X_1 specified as covariables ($X_2|X_1$). Variance shared by these subsets of variables ($X_1 \cap X_2$) is the total constrained variation (sum of all canonical eigenvalues when all variables are analysed in CCA) minus the unique variation explained by each subset of variables. Four sets of variables were analysed. The variables in the first analysis help assess the unique variance of environmental variables identified by forward selection and the shared variances with variables not selected during this procedure. The second analysis investigates the unique spatial effect of depth after accounting for other environmental variables. A third analysis assesses variance explained by substrate variables since these are highly correlated, and partial CCA of individual sediment fractions probably overestimates the total variation explained. Finally, variance partitioning gives an indication of the shared variance between temperature and salinity.

(v) Step 5: Transfer-function development

Transfer functions allow environmental variables from fossil records to be reconstructed using compositional data from fossil assemblages. This process involves two steps, calibration and regression. In the first step (calibration), the relationship between modern species data (benthic foraminifera assemblages) and their associated environmental data (e.g. temperature, salinity) is statistically modelled, producing the transfer function. The second step involves regression of this transfer function. Birks (1994) found that rare taxa contribute meaningful ecological information and help reduce prediction errors during the development of transfer function models. An environmental gradient of 3 SD units for the total assemblage and 2.2 SD units for the agglutinated assemblage (untransformed data, no species down-weighting), calculated by detrended canonical correspondence analysis (DCCA) constrained to temperature, indicates

unimodal methods are suitable for modelling foraminifera data when developing transfer functions (Birks, 1995). Transfer functions for summer bottom water temperature were developed in the C2 version 1.5 program (Juggins, 2003) using the weighted averaging (WA) (ter Braak, 1987) and weighted averaging partial least squares (WA-PLS) (ter Braak and Juggins, 1993; ter Braak *et al.*, 1993) regression. Two transfer function models were developed; one using the total assemblage data (TA model), and a second using the agglutinated assemblage (AA model), based on recalculated percentages from the original species counts. Developing the AA model may permit reliable reconstructions of bottom water temperature during fossil core intervals characterised by calcareous dissolution. All taxa and samples were included in the TA model. Two samples were removed from the AA model (sample 3 and 7) based on a low count of agglutinated specimens.

Prediction error estimates calculated by cross-validated transfer functions are more reliable and realistic (Birks, 1995). This study uses the bootstrapping method with 1000 cycles to cross-validate transfer-function models. The coefficient of correlation (r^2) and the root mean square error of prediction (RMSEP) statistics help assess the performance of the transfer function model. The most precise bootstrapped-models have a high coefficient of correlation (r^2) and a low root mean square error of prediction (RMSEP) (Birks, 1995).

The WA model with classical deshrinking appeared to perform best for both total assemblage and agglutinated data. *Table 4.4* details the model performance statistics. Both transfer-function models (TA and AA) were applied to fossil foraminifera samples from multicore MSM-343520 to reconstruct bottom-water temperature changes. Lack-of-fit measures assess how closely fossil assemblages resemble modern assemblages, and therefore identify if modern species-environment relationships are suitable for reconstructing fossil samples. The suitability of fossil data for reconstruction purposes is assessed using the minimum dissimilarity coefficient (MinDC) calculated by the modern analogue technique (MAT) in the C2 programme. This assesses the reliability of the reconstructions of fossil samples by identifying if there are any similar modern assemblages. The MAT compares each fossil sample to the ten most similar modern samples, producing a dissimilarity coefficient for each sample. Woodroffe (2009) use

the largest dissimilarity coefficient calculated between all modern samples as a cut-off between a 'good' and 'poor' match for fossil samples.

4.3 Results

4.3.1 Circulation of water masses in central West Greenland

It is important to review the characteristics of water masses in central West Greenland because these potentially influence the composition of benthic foraminifera assemblages. Understanding the relationships between foraminifera distribution and overlying water mass characteristics is critical to achieving the main aim of this thesis, as this will aid palaeoceanographic interpretations, and hence allow the potential role of temperature forcing on influencing ice sheet stability to be investigated.

Figure 4.2 shows a compilation of historical measurements collected in the Davis Strait and central West Greenland area, highlighting the distinct nature of Atlantic and Polar Waters in Baffin Bay (all the samples shown in *Fig. 4.2a* and graphed in *Fig. 4.2 d* and e). *Figure 4.2c* shows the samples collected from the mid- to outer-shelf of central West Greenland, and the temperature profile at sites MSM-343340 and MSM-343340. Lloyd (2006a) presents CTD data collected during the 1999 *R.V. Porsild* cruise in the inner part of Disko Bugt. Additional new data presented in this chapter are from the outer western parts of Disko Bugt, Vaigat, and further offshore. The CTD data collected during the 2007 *Maria S. Merian* cruise (see selected CTD profiles in *Fig. 4.3*) show the three distinct water masses previously identified in West Greenland (e.g. Andersen, 1981a; Buch and Stein, 1989; Buch, 1993; Buch and Nielsen, 2002; Lloyd, 2006a); surface water, Polar Water and Atlantic Water. Surface waters occupying the upper 50 m of the water column along West Greenland are generally warm (temperature 1-8°C) and relatively fresh (typical salinity 11-33.5 psu) during the summer. The low salinity character of surface waters results from melting of seasonal sea ice, melting icebergs, and meltwater fluxes from inland ice, while warm water temperatures during the summer is due to increased solar insolation. The surface water layer at stations located closer to the ice sheet margin in Nordre Strømfjord is much thicker (*ca.* 60 m) compared to the western parts of the fjord (<10 m), indicating a greater meltwater influence at the two easternmost sites. A steep thermocline

between surface water and the underlying Polar Water is characteristic of temperature profiles for the majority of stations, with the exception of 343380 and 343390 in the Vaigat, where there is a greater mixing between surface waters and underlying Polar Waters to a depth of nearly 80 m.

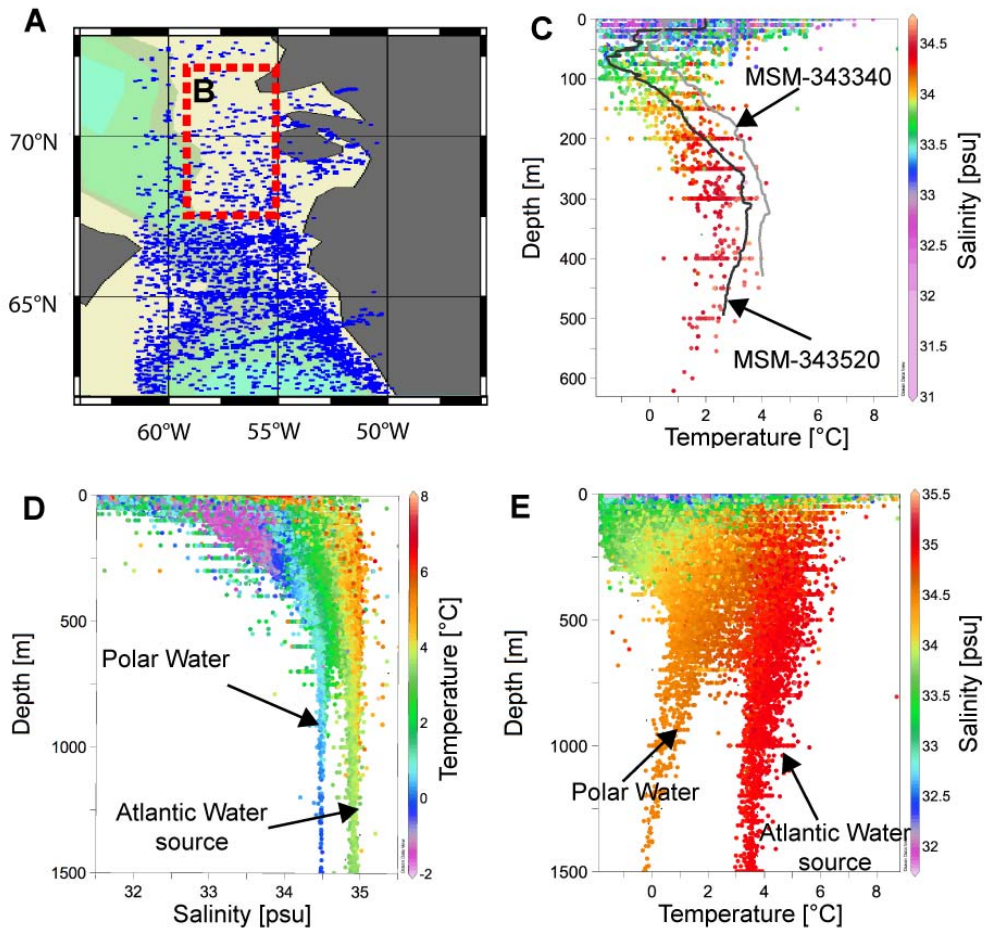

Figure 4.2 Compilation of CTD data from cruises between June 1908 and June 1997 in WOD05; (**a**), location of sampling stations in West Greenland/Davis Strait area; (**b**) inset, showing selected profiles from West Greenland shelf shown in (**c**); (**c**), shows the temperature profile (with colour of dots reflecting salinity) for locations marked by blue dots in inset of (**d**). The temperature profiles for sample stations MSM-343340 and MSM-343520 (Harff, 2007) have been included as grey and black lines, respectively, for easy comparison. (**d**, **e**), compilation of all data shown by blue dots in (**a**), clearly identifying distinct Atlantic and Polar Water components in West Greenland/Davis Strait waters. Data available at: ttp://www.nodc.noaa.gov.

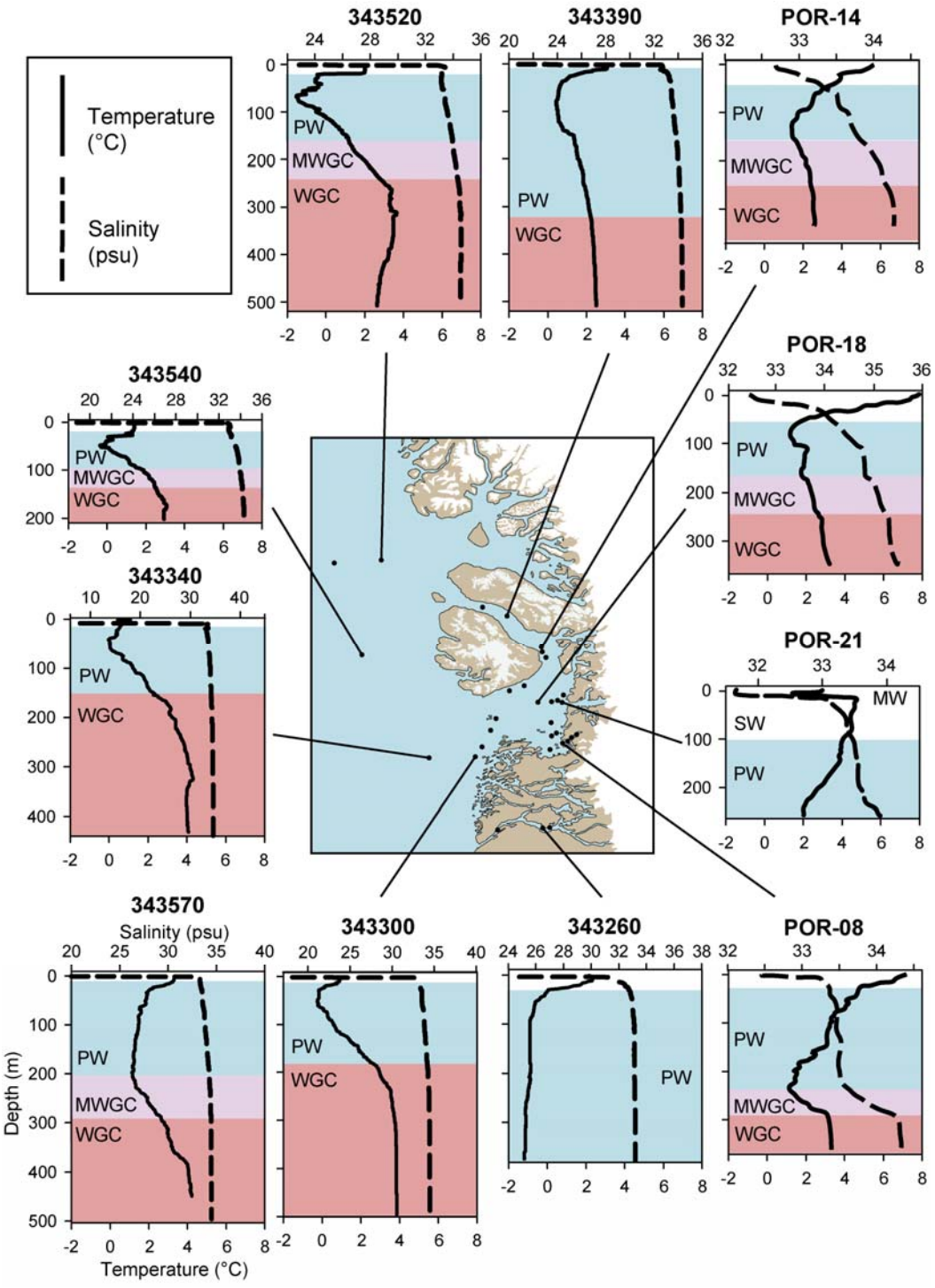

Figure 4.3 Selected temperature (ºC) and salinity (psu) profiles for sites from MSM 05/03 cruise, and POR-99 data from Lloyd (2006a). Note the common temperature scale (bottom axis) and depth scale, and variable salinity scale (top axis). Five water masses are identified; meltwater (MW), surface water (SW; both not shaded), Polar Water (PW, blue shading), Mixed WGC (MWGC, purple shading), West Greenland Current (WGC, red shading). Site 343570 is located in the trough on the shelf west of Nuuk (see *Fig. 4.1*).

Polar Water (temperature -1.6 to 3°C, salinity 32.7 to 33.9 psu) along West Greenland is primarily sourced from the cold, low salinity East Greenland Current (EGC) that forms the upper water mass in the West Greenland Current (WGC) as it rounds southern Greenland. Polar Water lies below surface water, and is present down to depths between *ca.* 180 m and 310 m in shelf areas, and deeper in Nordre Strømfjord, where the water column is uniformly cold and low salinity. Temperatures throughout the water column at stations closer to the head of the fjord (343250 and 343260) are much colder, with a minimum temperature of -1.24°C and salinity of 31.19 psu, compared to a minimum temperature of 0°C and salinity of 33.13 psu at 343280 closer to the fjord mouth. The Polar Water layer (*ca.* 220-30 m) at station 343570 west of Nuuk has a minimum temperature and salinity of 1.1°C and 33.3 psu, respectively. However, minimum temperatures of -0.2°C at 343300 and 0.4°C at 343310 indicates much cooler Polar Waters outside Disko Bugt. This likely reflects additional cooling and mixing of Polar Water with meltwater from the Greenland Ice Sheet as it flows northwards, possibly with a weak influence of Polar Water advected from western Baffin Bay. On the Uummannaq shelf to the north, Polar Water occupies the top 150-220 m of the water column, and has water temperatures in the upper 100 m as cold as -1.6°C. This is far colder than near-surface waters in the Vaigat and at southerly sites along the West Greenland margin, and most likely indicates the influence of cold, low salinity Polar Water from the south-flowing Baffin Island Current, which is deflected eastwards at Davis Strait, and re-circulates as part of the WGC.

A transitional water mass, termed mixed-WGC (Lloyd, 2006a), lies between the Atlantic-sourced water and the overlying Polar Water layer. The characteristics of this water mass are particularly evident in *Fig. 4.4*, which shows the basal temperature and salinity for all samples in this study. The nature of this water mass varies by location; at station 343340 in outer Egedesminde Dyb, water temperatures cool gradually by more than 4°C from 325 m to 50 m depth. However, there is a reduced temperature gradient in inner Egedesminde Dyb, indicating greater mixing between waters of polar and Atlantic origin. The more homogenized water mass structure is suggestive of continued mixing of Polar and Atlantic waters within Disko Bugt, though cooling and freshening by meltwater and icebergs directed through the Vaigat are likely to be a strong influence on the character of the upper part of the water column. Lloyd (2006a)

suggests a larger mixed WGC water mass is found in relatively sheltered locations, where water masses continue to mix. The CTD profiles from outside Disko Bugt and Uummannaq Fjord certainly support this interpretation, with more abrupt changes between Polar and Atlantic Water.

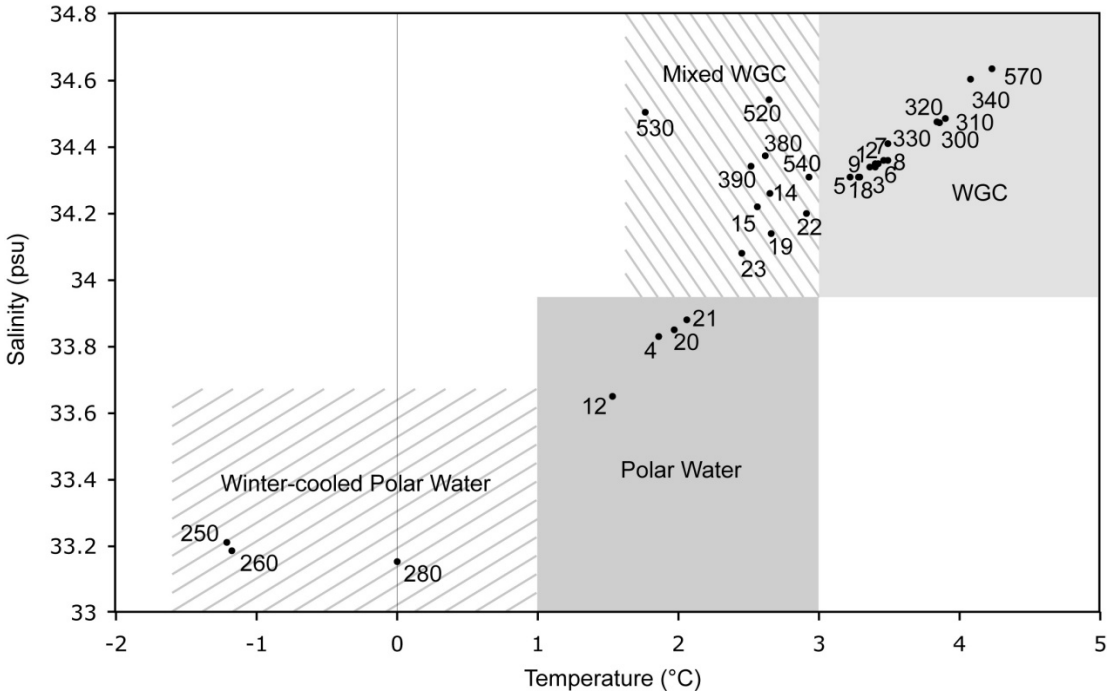

Figure 4.4 Temperature-salinity diagram of bottom-water characteristics at the sample locations (all samples >100m water depth). Boxed areas distinguish the different basal water masses impinging on the shelf in central West Greenland; West Greenland Current water (WGC; Atlantic water influence), Mixed WGC water; Polar Water, and winter-cooled Polar Water.

Relatively warm and saline water of Atlantic origin lies below 200 m depth, and has a temperature exceeding 2.5°C and a salinity greater than 34 psu. In the trough west of Nuuk, the warm core of the WGC is located below *ca*.380 m with a temperature 4-4.2°C and a salinity of 34.6 psu. At station 343340, located in outer Egedesminde Dyb, maximum water temperatures exceed 4.3°C at 325 m depth. This warm and saline basal water cools very slightly as it flows eastwards into Disko Bugt, with maximum temperatures dropping to 3.5°C (salinity 34.4 psu) below 680 m depth at station 343330. The bottom waters in the Vaigat (stations 343380 and 343390) has a weaker Atlantic signature, with a maximum temperature and salinity of 2.6°C and 34.4 psu, indicating further cooling as the water mass circulates and mixes in the embayment. A distinct warm core of the WGC is recognisable at the northernmost

stations located in the Uummannaq trough, with temperatures of 3.5-3.8°C between 210 and 310 m depth at station 343530, and temperatures of 3.3-3.7°C between 250 and 420 m at station 343520. The warmest waters at this latitude remain warmer than more intensely mixed subsurface waters in Disko Bugt. Interestingly, the warm core of the WGC during summer 2007 remains positioned relatively high in the water column, despite a presumed northwards thickening in the Polar Water layer due to meltwater influxes and mixing between water masses. On the Uummannaq shelf, water temperatures cool significantly below the warm core, with basal temperatures of 1.8°C at station 343530 and 2.6°C at station 343520, though salinity remains relatively high and stable (34.5-34.6 psu) below 250-300 m.

4.3.2 Surface foraminiferal assemblages

Seventy-three benthic foraminifera species (30 agglutinated and 43 calcareous) were identified in modern surface samples, and are shown in *Fig. 4.5*. Thirty-eight species occur in abundances greater than 2% in the total assemblage and in more than one sample. Modern species data was square-root transformed using chord distance (Cavalli-Sforza and Edwards, 1967) and modern surface samples grouped into six distinct faunal zones based on unconstrained cluster analysis in CONISS (Grimm, 1987). Cluster analysis groups and orders assemblages based on similarity, so that the most similar assemblages are most closely linked on a dendrogram (see *Fig. 4.5*) (Kovach, 1995). These cluster zones have been plotted on a map with the modern surface samples (*Fig. 4.6*) to highlight the geographic trends in the data linked to different environmental conditions. Detrended correspondence analysis (DCA) was performed on the foraminifera data using the CANOCO version 4.51 program (ter Braak and Šmilauer, 2002). The graphical output from DCA (*Fig 4.7b*) makes it easy to identify similar (closely spaced) and dissimilar (far apart) samples. Each sample in the DCA plot is positioned at the centroid of the species that occur in it (*Fig. 4.7b*). DCA results in clusters of samples that closely resemble the results of cluster analysis, and therefore support faunal groupings in *Fig 4.*5. The overlap of samples in FAZ 1 and 2 in the DCA results do, however, highlight similarities in species composition of these samples. It is apparent that the faunal classification closely groups samples according to temperature and salinity at the seafloor (cf. *Fig. 4.4*).

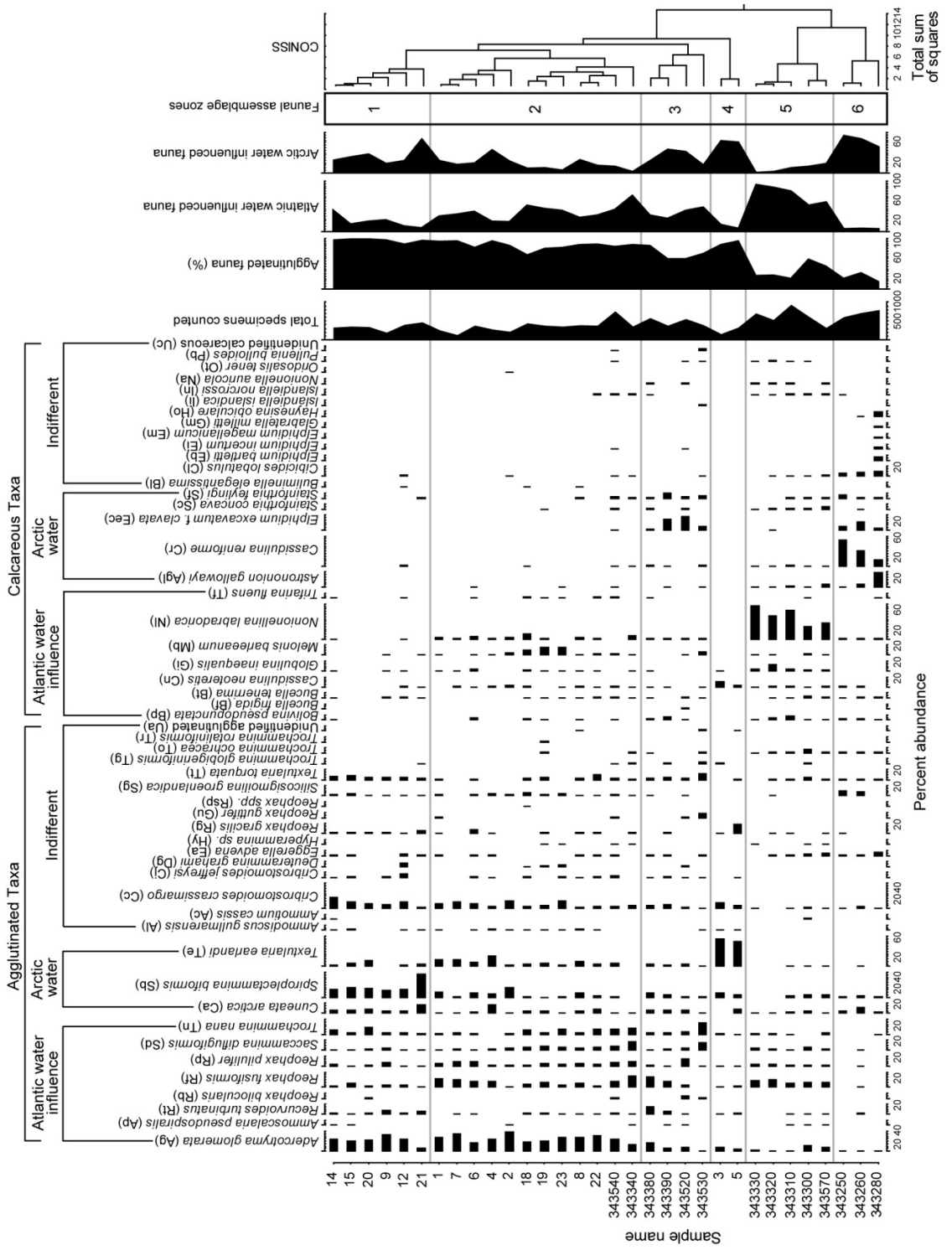

Figure 4.5 Modern foraminiferal assemblages from sites in central West Greenland, classified into six distinct faunal assemblage zones (FAZ) based on unconstrained cluster analysis of square-root transformed species data. Only species greater than 1% are illustrated. Also shown are summary plots of species associated with Arctic and Atlantic waters, based on ecological affiliations identified in this investigation and other high-latitude studies.

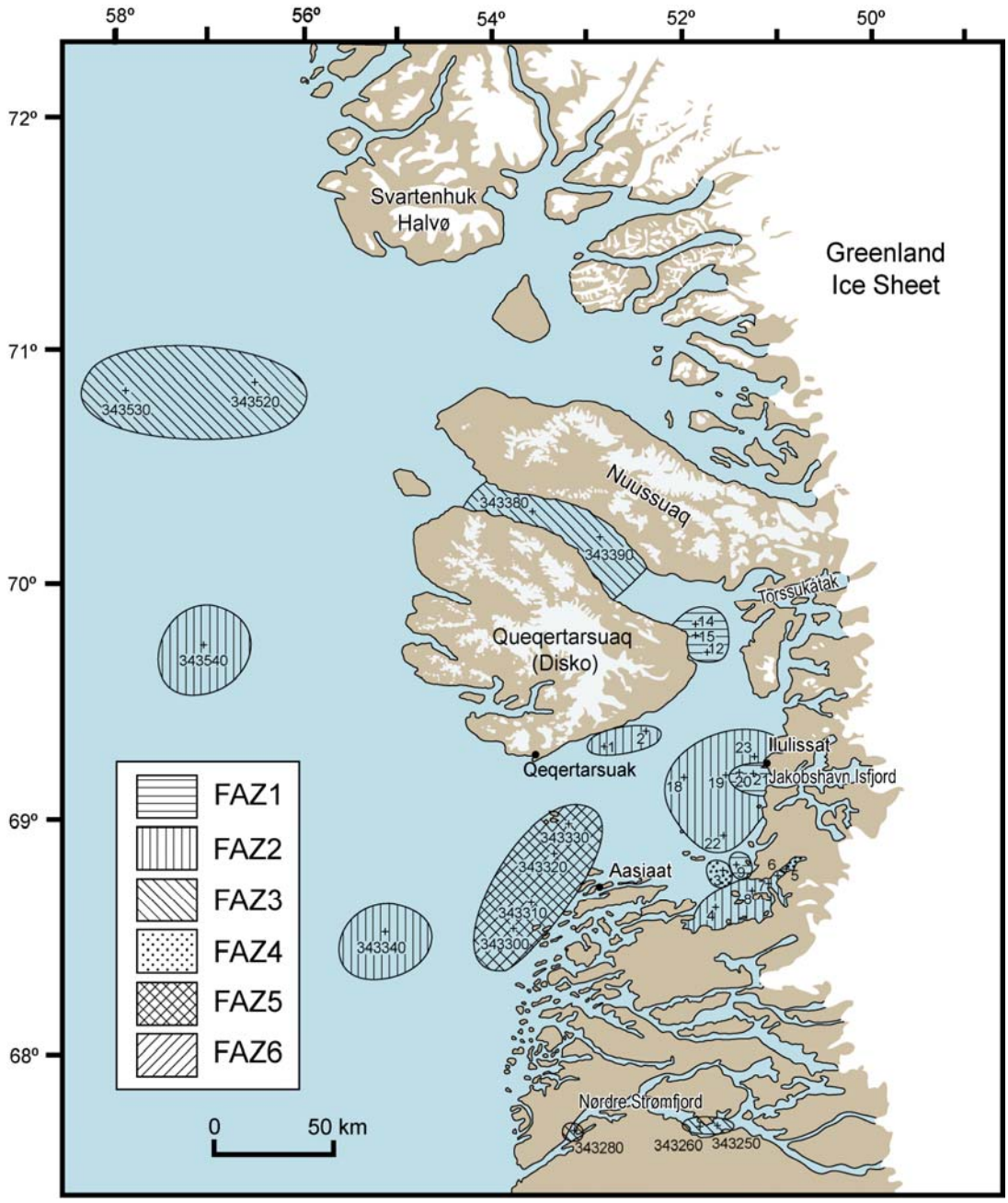

Figure 4.6 Location of surface samples (+) in central West Greenland study area grouped into faunal assemblage zones (FAZs) identified by cluster analysis. Sample 343570, located in a trough on the shelf west of Nuuk (see *Fig. 4.1*), is grouped in FAZ 5.

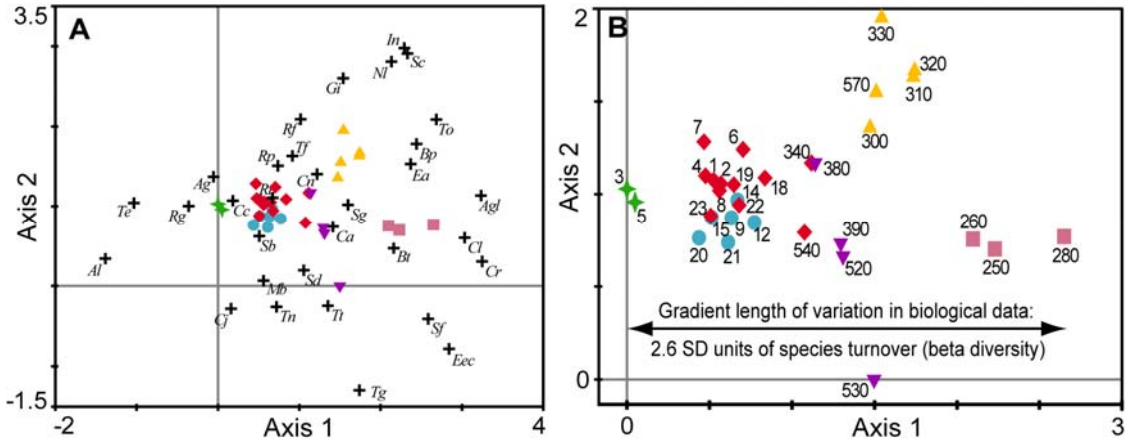

Figure 4.7 DCA ordination diagrams for axis 1 versus axis 2 scores (square-root transformed species data), which explains 30.6% of species variability, showing (**A**) species-sample relationships and (**B**) DCA sample scores only. Assemblages are grouped according to cluster analysis (see *Fig. 4.6*); Blue circles – FAZ 1, red diamonds – FAZ 2, purples triangles – FAZ 3, green stars – FAZ 4, orange triangles –FAZ 5, pink squares – FAZ 6. For clarity, the sample prefixes (343-) for 2007 cruise data have been removed.

Agglutinated foraminifera are dominant in 25 of 32 samples. These samples are grouped into faunal zones 1 to 4, typically comprising more than 80% of specimens counted in the majority of samples. The samples grouped in FAZ 1 have the highest agglutinated foraminifera component, and are found at sites under the influence of Polar Water during the summer. Dominantly calcareous foraminifera samples are found under the influence of both relatively warm, saline water and extremely cold, lower salinity bottom waters. Assemblages in FAZ 5 and 6 are characterised by the highest calcareous foraminifera content. However, the basal water masses influencing these assemblages are at opposite extremes of water mass characteristics in central West Greenland; assemblages in FAZ 5 are influenced by relatively warm and saline waters (>3.4°C , >34.3 psu) at the seafloor, while assemblages in FAZ 6 are influenced by cold, low salinity waters (<0°C, <33.3 psu). The composition of assemblages in these faunal zones, identified by numerical analyses, is briefly described below.

FAZ 1 comprises six samples dominated by agglutinated foraminifera (90-100%), and only isolated occurrences of calcareous fauna. *Adercotryma glomerata* (6-24%) and *Spiroplectammina biformis* (15-46%) are the most abundant taxa. *C crassimargo* (2-21%), *C. arctica* (4-16%), and *T. nana* (2-14%) are also important species. Samples in this zone under

Polar Water influence, including sites close to Jakobshavn Isfjord and in southeast Disko Bugt, primarily because of the shallower water depths of the sample sites.

FAZ 2 contains twelve samples, with *A. glomerata* (13-35%) being the most important species. *C. crassimargo, R. fusiformis*, *R, pilulifer, S. difflugiformis, T. nana* and *T earlandi* are also common in this faunal zone. There is a slightly greater calcareous foraminifera presence (4-22%) in FAZ 2, particularly *M. barleeanum* (up to 15%) and *N. labradorica* (up to 11%). Samples in this zone are found in a number of relatively shallow locations in Disko Bugt (*Fig. 5.1*), and are influenced by slightly warmer bottom-waters than samples in FAZ 1.

FAZ 3 is characterised by high calcareous foraminifera abundance (13-40%). *E. excavatum* f. *clavata* (2-28%) is an important taxon in this faunal zone, with *S. feylingi* (1-9%) an important accessory species. Abundances of *A. glomerata* are lower in FAZ 3 compared to FAZ 1 and 2. There are significant occurrences of *R. fusiformis, R. turbinatus, R. pilulifer, S. difflugiformis, T. nana,* and *T. torquata* within the four samples in this zone. Samples in this zone are from deeper locations in the Vaigat and on the shelf west of Uummannaq.

FAZ 4 contains two samples both with low species diversity and dominated by *T. earlandi* (49-55%). *R. gracilis* (18%) and *C. neoteretis* (11%) are common in individual samples, while *A. glomerata, C. crassimargo* and *S. bifomis* are accessory species. These samples are located in southeast Disko Bugt under relatively warm, saline bottom waters with a muddy substrate.

FAZ 5 contains five samples dominated by calcareous foraminifera (41-79%), particularly *N. labradorica* (32-66%). *R. Fusiformis* is common (7-14%), while *G. inaequalis* and *B. pseudopunctata* are accessory species. These samples were collected from deep trough locations. Samples 343300 to 343330 are located in Egesdesminde Dyb, the deep trough that provides a pathway for warm, saline WGC water into Disko Bugt, while sample 343570 is located in a trough south of Disko Bugt (west of Godthab), where Atlantic subsurface waters are warmer due to reduced mixing with Polar Waters.

FAZ 6 contains three samples from Nordre Strømfjord under the influence of extremely cold and low salinity water dominated by *C. reniforme.* Samples in this zone have the highest abundance of calcareous foraminifera (68-86%), and there are significant occurrences of *S. groenlandica, A. gallowayi, C. lobatulus* and *E. excavatum* f. *clavata.*

4.3.3 Ordination of compositional and environmental data

Table 4.1 shows the modern environmental data used in ordination. Ordination scores focuses on inter-species distances using biplot scaling since this is more quantitative and most suited to compositional data with short gradients (<3 SD) (ter Braak and Šmilauer, 2002). In species scaling, the weighted-average optima of species are located as points within the ordination diagram, with samples it occurs in scattered nearby (ter Braak and Šmilauer, 2002). According to the biplot rule, the location of species points with respect to the origin (0,0) of the ordination diagram indicate the rate of change of fitted species abundance along each axis (ter Braak and Šmilauer, 2002).

Forward selection in CCA identifies temperature, salinity, water depth and sand as significant explanatory variables, accounting for 40.5% of variability (75.4% of explained variance). *Figure 4.8a* illustrates the results of forward selection, with common species, samples and environmental variable vector arrows. The directions of arrows identify gradients of maximum change for individual environmental variables, while arrow lengths are proportion to the rate of change. The first two axes of CCA explain 29.6% of species data and 73.1% of species-environment relationships. Variability along axis 1 of CCA is negatively correlated with bottom-water temperature (-0.71) and salinity (-0.59). The second axis is highly correlated with water depth (0.83), while bottom-water temperature (0.69) and salinity (0.65) also have a strong association with this axis. Long arrow lengths for temperature, salinity and water depth variables indicate that these are the most important variables for explaining variation in species data. The comparatively short arrow for a sandy substrate indicates that this variable does not have as large an influence on species composition.

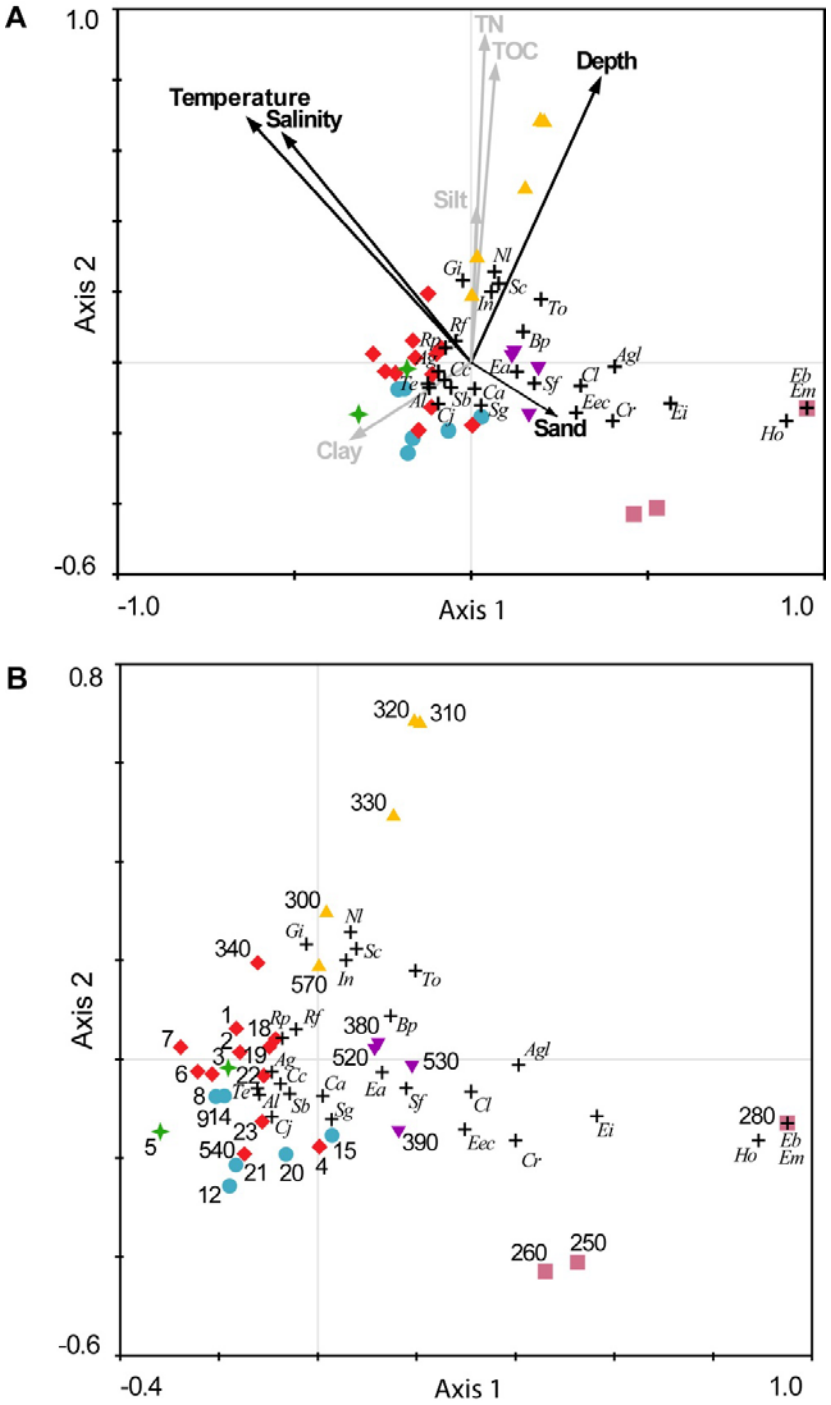

Figure 4.8 Ordination diagrams of CCA results; (**A**), triplot of species-samples-environmental variables; (**B**), Species-samples plot. All samples are shown. Only species that occur in abundances greater than 2% and have a greater than 20% fit to environmental data are shown in both plots. In (**A**) the environmental variables selected by the forward-selection procedure are black. Variables that do not significantly contribute additional data are shown in grey. See *Fig. 4.5* for species codes.

Name	Depth (m)	Temp. (°C)	Salinity (psu)	TN (%)	TOC (%)	Clay (%)	Silt (%)	Sand (%)	C/N ratio
1	356	3.40	34.35	0.19	1.44	25.80	69.90	4.30	7.58
2	355	3.36	34.34	0.18	1.67	25.60	71.70	2.70	9.28
3	331	3.40	34.34	0.22	1.58	53.20	44.70	2.10	7.18
4	198	1.86	33.83	0.22	1.17	50.80	46.60	2.60	5.32
5	260	3.22	34.31	0.10	0.69	54.80	43.80	1.40	6.9
6	327	3.42	34.35	0.16	1.16	46.80	50.40	2.80	7.25
7	338	3.46	34.36	0.17	0.89	52.20	46.10	1.70	5.24
8	358	3.49	34.36	0.19	1.55	56.90	41.70	1.40	8.16
9	318	3.29	34.31	0.20	1.68	52.40	45.20	2.00	8.4
12	112	1.53	33.65	0.07	0.44	9.1	24.2	60.2	6.29
14	331	2.65	34.26	0.12	1.00	22.20	45.60	28.80	8.33
15	245	2.56	34.22	0.10	0.80	17.00	42.80	38.60	8.0
18	343	3.28	34.31	0.20	1.31	35.40	52.30	12.30	6.55
19	353	2.66	34.14	0.20	1.09	40.80	58.30	0.90	5.45
20	286	1.97	33.85	0.10	0.92	45.30	52.00	2.70	9.2
21	254	2.06	33.88	0.07	0.55	48.40	51.60	0.00	7.86
22	302	2.91	34.20	0.22	1.39	45.60	51.40	3.00	6.32
23	253	2.45	34.08	0.05	0.29	16.40	20.80	58.40	5.8
343250	361	-1.21	33.21	0.07	0.67	41.20	56.48	2.32	9.57
343260	373	-1.18	33.19	0.03	0.44	47.29	52.28	0.43	14.67
343280	301	0.00	33.15	0.15	0.74	9.20	18.10	72.70	4.93
343300	496	3.86	34.47	0.35	2.42	30.29	60.08	9.62	6.91
343310	820	3.90	34.49	0.43	2.81	24.19	66.57	9.24	6.53
343320	804	3.84	34.48	0.49	3.21	25.86	73.67	0.47	6.55
343330	738	3.49	34.41	0.35	2.47	28.38	65.46	6.16	7.06
343340	432	4.08	34.60	0.26	1.95	24.70	65.88	9.42	7.5
343380	551	2.62	34.37	0.13	1.51	27.59	60.85	11.57	11.62
343390	508	2.52	34.34	0.12	2.35	28.08	63.26	8.66	19.58
343520	508	2.65	34.54	0.22	1.77	35.07	61.16	3.78	8.05
343530	616	1.76	34.50	0.09	0.95	21.93	76.48	1.60	10.56
343540	202	2.93	34.31	0.13	1.13	28.81	62.97	8.22	8.69
343570	446	4.23	34.64	0.21	1.51	29.53	38.28	32.19	7.19

Table 4.1 Surface samples and associated environmental variable data. C/N ratios are included for informational purposes, but are not included in multivariate analyses.

Table 4.2 lists the order of environmental variables according to their conditional and marginal effects. The unique contributions of individual environmental variables to species variation, their marginal effects, indicate that temperature, followed by salinity then water depth, are the most important variables. Forward selection re-orders explanatory variables according to their conditional effects, with the best fitting variable selected first, and subsequent variables added according to the additional explained variance they contribute to the model. Reordering of explanatory variables based on their conditional effects indicates water depth is more important to explaining species variability than salinity after accounting for temperature. This is not surprising since temperature and salinity are highly correlated (r = 0.91). However, a higher ranking of sandy substrate indicates TN and TOC explain little additional variability to temperature, salinity, and water depth explanatory variables.

Marginal Effects					Conditional Effects			
Variable	**λ1**	**r**	**Exp. var. (%)**	**Sig.**	**Variable**	**λA**	**P**	**F**
Temperature	0.2	0.888	14.6	<0.001	Temp.	0.2	0	5.13
Salinity	0.173	0.859	12.6	<0.001	Depth	0.18	0	5.41
Depth	0.167	0.872	12.2	<0.001	Salinity	0.11	0	3.25
TN	0.149	0.885	10.9	0.001	Sand	0.06	0.003	2.26
TOC	0.134	0.849	9.8	0.001	TN	0.04	0.137	1.31
Clay	0.083	0.66	6.1	0.022	TOC	0.04	0.262	1.17
Silt	0.09	0.807	6.6	0.019	Clay	0.03	0.424	1.01
Sand	0.081	0.758	5.9	0.046	Silt	0.08	0	2.82

Table 4.2 Marginal and conditional effects from forward selection in CCA. [Marginal effects in pCCA table as well] λ_1, canonical eignevalues; r,species-environment correlation; (variance of species data) explained variation (%); significance (P); lambda; P-ratio; F-statistic. Sum of all eignevalues. 1.369, canon. 0.736. Marginal effects are results of partial CCAs. Highlighted variables are not significant at the 1 % level.

Partitioning of variance in CCA identifies the relative importance of environmental variables and their shared variances. Water depth, a variable describing spatial structure in the species data, appears to have little influence on foraminifera distribution (3% unique contribution) once the effects of other measured variables have been taken into account (*Table 4.3*). After removing depth from the analysis, substrate type accounts for 14% of variation in foraminifera data, and

shares 7.5% of variation with the remaining environmental variables (temperature, salinity, TN, TOC). Partitioning of variance in CCA indicates temperature and salinity environmental variables together account for 21.8% of variance (*Fig. 4.9*).

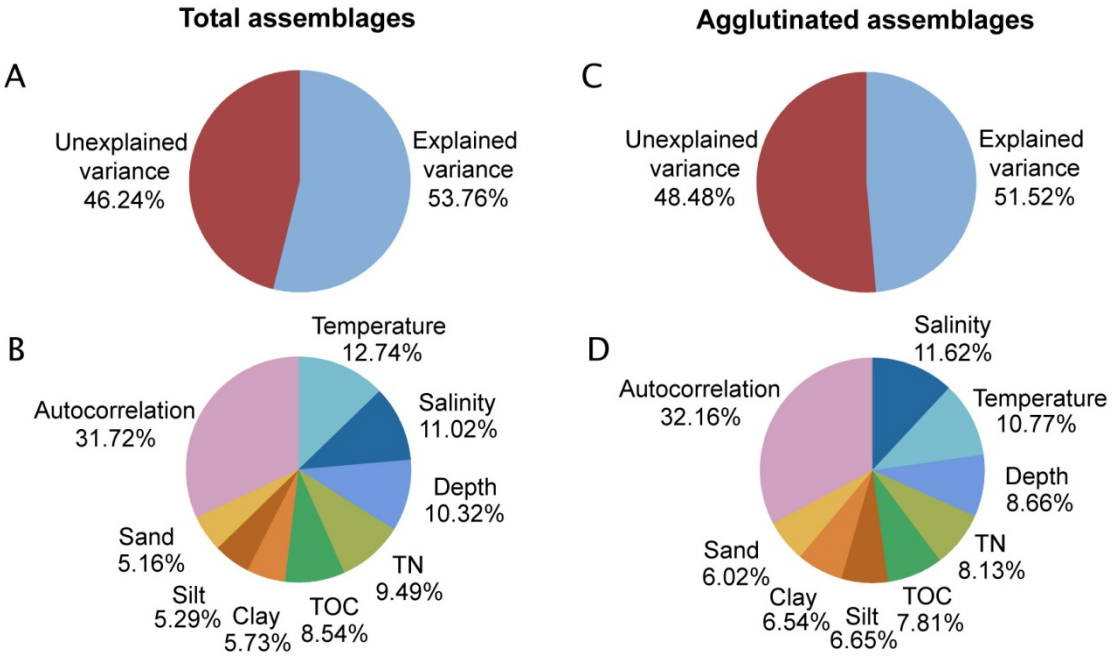

Figure 4.9 Pie charts showing (**A**, **C**) the explained and unexplained variation in the foraminiferal data and (**B**, **D**) the unique contribution of individual environmental variables and the autocorrelation between these to the explained variance.

Partial CCA assessed the contribution of individual environmental variables to the explained variance in the species data. This reaffirms the importance of water mass characteristics, with bottom-water temperature identified as the most important variable (12.7% for TA and 11.6% for AGG; *Fig.4.9*), closely followed by salinity (11%), and water depth (10.3%). In general, substrate type appears to have relatively little influence on foraminiferal composition. The measured environmental variables explain 53.8% of species variability in the total assemblage and 51.5% in the agglutinated assemblage (*Fig.4.9*), while interactions between environmental variables account for nearly a third of explained variance.

				Total variation			Proportion of explained variation (%)		
Subset X1	**Subset X2**	**Exp. variation**	**Unexp. variation**	**X1|X2**	**X2∩X2**	**X2|X1**	**X1|X2**	**X2∩ X2**	**X2|X1**
T, S, Depth, Sand	TN, TOC, Clay, Silt	0.736 (53.8%)	0.633 (46.2%)	0.392 (28.6%)	0.163 (11.9%)	0.181 (13.2%)	53.3	22.1	24.6
EV	Depth	0.736 (53.8%)	0.633 (46.2%)	0.569 (41.6%)	0.023 (1.7%)	0.041 (3%)	77.3	3.1	5.6
T, S, TN, TOC	Sub-strate	0.695 (50.8%)	0.674 (49.2%)	0.401 (29.3%)	0.103 (7.5%)	0.191 (14%)	57.7	14.8	27.5
T	S	0.298 (21.8%)	1.071 (78.2%)	0.125 (9.1%)	0.075 (5.5%)	0.098 (7.2%)	41.9	25.2	32.9

Table 4.3 Decomposition of variance in CCA. The total variation is equal to the eigenvalue of 1.369. Shared variance (X2∩X2) is the variance shared between the two sets of identified environmental variables. The residual variance i.e. unexplained variance, unexp. variance) is the variance not accounted for by the specified environmental variables. T, bottom-water temperature; S, bottom-water salinity; EV, All other remaining measured environmental variables.

4.3.4 Transfer function model and reconstruction performance

Partial CCA indicates that bottom-water temperature appears to be the greatest single influence on variation in species data. However, a CCA plot of modern samples with the first CCA axis constrained to temperature indicates that there is significant variability along the second axis. While some samples have a strong negative correlation with temperature, no samples have a strong positive correlation with bottom-water temperature. The results of CCA indicate that TN, TOC and water depth are highly correlated with axis two. The bootstrapped transfer function models are shown in *Fig.4.10* and *Fig.4.11*. Performance statistics calculated for the transfer functions indicate that the training set species data can be modelled to provide relatively precise and reliable temperature estimates. The selected transfer function models (*Table 4.4*) have r^2 values of 0.79 for the TA model and 0.65 for the AA model, with RMSEP values of 0.81°C and 0.98°C for the TA and AA model, respectively. These results indicate that the TA model should perform better than the AA model. The RMSEP as a percentage of the temperature gradient length (5.44°C) is 14.9% for the total assemblage WA (Classical) model and 18% for the agglutinated only assemblage WA (Classical) model. These values are relatively high when

compared to other studies using benthic foraminifera for various applications; Woodroffe (2009), for example, reports RMSEP values between 7.2% and 10.1% for different models.

Total assemblage model

Environmental gradient: 5.44°C, 1.79 SD units

Model	Component	Boot R2	RMSE s1	RMSE s2	RMSEP
WA	Inv	0.78	0.46	0.66	0.81
WA	Cla	0.79	0.54	0.61	0.81
WA	TOL_Inv	0.80	0.47	0.84	0.96
WA	TOL_Cla	0.80	0.57	0.75	0.94
WA-PLS	1	0.78	0.45	0.68	0.82
WA-PLS	2	0.75	0.53	0.67	0.85
WA-PLS	3	0.76	0.60	0.65	0.88

Agglutinated assemblage model

Environmental gradient: 5.44°C, 1.43 SD units

Model	Component	Boot R2	RMSE s1	RMSE s2	RMSEP
WA	Inv	0.64	0.47	0.86	0.98
WA	Cla	0.64	0.55	0.81	0.98
WA	TOL_Inv	0.69	0.48	0.93	1.05
WA	TOL_Cla	0.69	0.59	0.87	1.05
WA-PLS	1	0.63	0.46	0.87	0.99
WA-PLS	2	0.63	0.54	0.82	0.99
WA-PLS	3	0.62	0.60	0.83	1.02

Table 4.4 Performance statistics for transfer functions developed using the unimodal methods of weighted averaging (WA) and weighted averaging partial least squares (WA-PLS) for the TA and AA model. Shading highlights best performing TA and AA model.

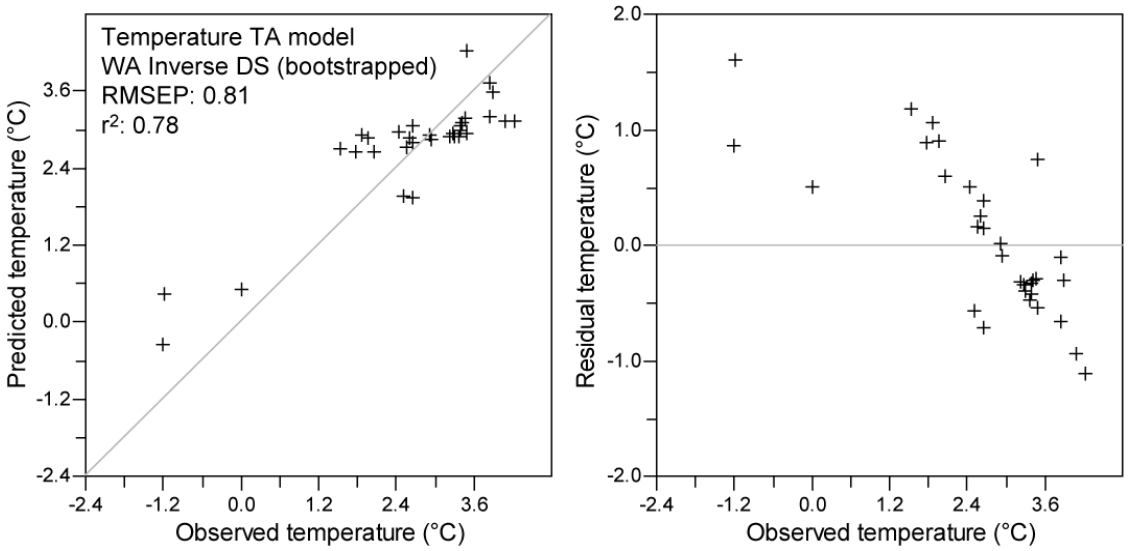

Figure 4.10 Transfer function model for temperature using total assemblage and the bootstrapped weighted averaging model (inverse deshrinking).

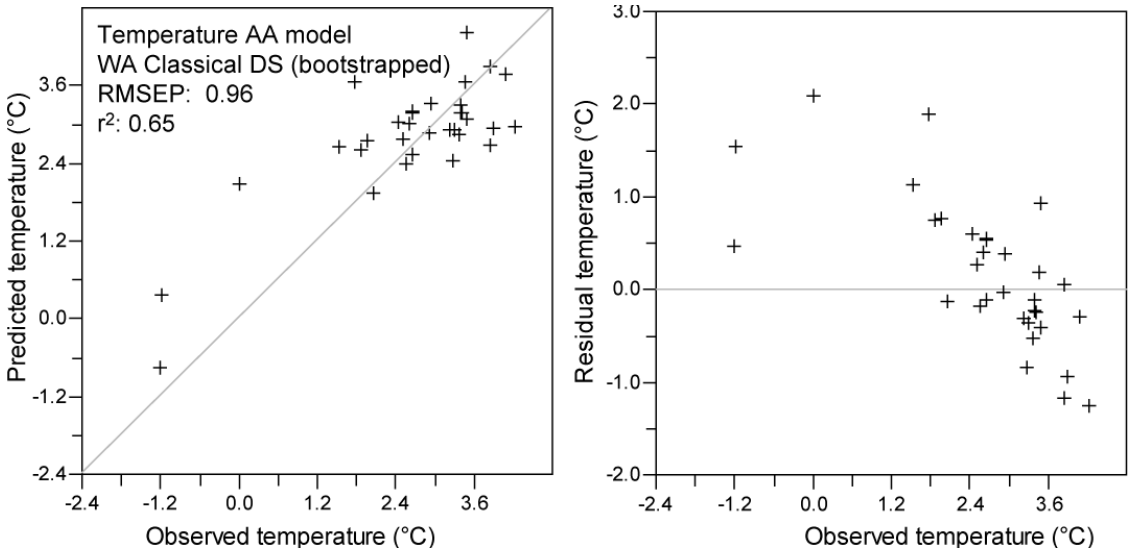

Figure 4.11 Transfer function model for temperature using agglutinated assemblage and the bootstrapped weighted averaging model (classical deshrinking).

4.4 Discussion

4.4.1 Primary environmental controls on foraminifera distribution

In total, measured environmental variables account for 53.8% of variation in species data, while the subset of significant variables identified by forward-selection explains only 40.5% of variation in species data. There remains a significant proportion of unexplained variation (at least 46.2%) in the species data, most likely a combination of other environmental controls that

exist and have not been measured, and a significant amount of random variation in the data. Temperature and salinity are the two most important explanatory variables when considered independently. However, taking the conditional effects of environmental variables into account indicates depth explains greater additional variance than salinity. When assessed independently, a sandy substrate is the least important environmental variable. However, a sandy substrate explains more additional variance than surface sediment TN and TOC content, potential sources of food for benthic foraminifera, after accounting for variability explained by temperature, salinity, and depth. This indicates bottom-water temperature, salinity or water depth explain the similar patterns in species variation as TN and TOC content, and thus suggests a link between food supply to the benthos and water mass characteristics.

Variance partitioning indicates that the forward selected environmental variables explain 28.6% of variation in species data, sharing 11.9% of their variance with non-selected variables, which uniquely contribute 13.2% to species variation. After accounting for other environmental variables, the unique contribution of depth to variation in assemblage composition is small (3.8%). This may be expected because water masses vary by depth, while higher levels of TN and TOC are found in deeper surface sediments. Substrate (clay, silt, sand) has a weak influence on foraminifera distribution, together accounting for 14% of species variance, compared to 29.3% of variance accounted for by temperature, salinity, TN and TOC, all possible indicators of water mass characteristics. Finally, independent of other environmental variables, temperature and salinity uniquely explain 9.1% and 7% of species variance, respectively, and together explain 21.8% of species variation.

The results of multivariate analyses clearly indicate that of the measured environmental variables, bottom-water temperature has the greatest influence on foraminifera distribution, indicating the potential for foraminifera to reliably reconstruct bottom-water temperature changes on the continental shelf of West Greenland.

4.4.2 Ecological preferences of benthic foraminifera in central West Greenland

Species that commonly occur together show a close grouping in DCA (*Figure 4.7*). CCA further explores these species groupings and their associations to measured environmental parameters.

The results of CCA indicate abundances of *Cassidulina reniforme* and *Elphidium excavatum* f. *clavata* increase under cold, low-salinity conditions characterised by reduced nutrient levels. *Cassidulina reniforme* and *Elphidium excavatum* f. *clavata* are common arctic species found in a range of microhabitats in fjord and shelf environments (Mackensen *et al.*, 1985; Corliss, 1991; Hald *et al.,* 1994; Jennings and Helgadottir, 1994; Hald and Korsun, 1997). High abundances of *Elphidium excavatum* f. *clavata* are found at sites influenced by cold, low salinity waters in Nordre Strømfjord, though the highest abundances are found in samples from the Vaigat and Uummannaq shelf under the influence of mixed-WGC water during the summer (2.5 – 2.7 ºC, 34.3 – 34.5 psu). *Elphidium excavatum* f. *clavata* is highly tolerant of ecologically stressful environmental conditions, particularly close to glacier calving margins subject to cold bottom waters, and large shifts in salinity and sediment supply (Hald *et al.*, 1994; Hald and Korsun, 1997; Korsun and Hald, 2000; Jennings *et al.,* 2004). In these locations, *E. excavatum* f. *clavata* flourishes despite hampered primary productivity in the photic layer caused by turbid meltwater plumes (Korsun and Hald, 2000). The transfer function predicted temperature and salinity optima of *ca.* 1°C and 34 psu, respectively, with wide ecological tolerances, appears to confirm the opportunistic nature of this species, and its preference for cold, low-salinity environments.

Cassidulina reniforme is dominant in samples from Nordre Strømfjord (FAZ 6) influenced by low-salinity (<33.2 psu) and extremely cold (<0 ºC) bottom-water conditions. Its distribution is reported to be similar to *E. excavatum* f. *clavata* (e.g. Nagy, 1965; Elverhøi *et al.*, 1980; Hald *et al.*, 1994; Hald and Steinsund, 1996; Hald and Korsun, 1997), which is indicated by the close proximity of these species in the CCA plot (*Figure 4.8*). Abundances of *C. reniforme* exceed *E. excavatum* f. *clavata* in locations with reduced glacier influence (lower sedimentation rate, enhanced food supply) (Korsun and Hald, 2000). *Cassidulina reniforme* is tolerant of high

concentrations of suspended particulate matter, indicating lower phytoplankton abundance and organic carbon content in surface sediments (Korsun and Hald, 1998). *Cassidulina reniforme* and *E. excavatum* f. *clavata* dominate samples in fjord sites influenced by stable warm, saline bottom waters in north Iceland (*ca.* 5°C, 34.7 psu; Jennings *et al.*, 2004) and northern Norway (6-6.9°C, 34-34.75 psu; Husum, 2002, in Jennings *et al.*, 2004), indicating these species have wide ecological tolerances, as shown in *Figure 4.12*.

Stainforthia feylingi, *Silicosigmolina groenlandica* and *Cuneata arctica* have positive axis 1 scores and negative axis 2 scores, indicating an inverse relationship with temperature and salinity. The results of CCA indicate the habitat of *Stainforthia feylingi* (= *Stainforthia fusiformis, Fursenkoina fusiformis*) is similar to *E. excavatum* f. *clavata* and *C. reniforme*, though the association with cooler and lower salinity conditions is not as strong. *Stainforthia feylingi* is a common opportunistic shelf and fjord species in Europe and the Canadian Arctic (Murray 1991, 1992; Alve, 1995). *Stainforthia feylingi* reproduces rapidly in response to organic enrichment from a range of food sources (Alve, 1994) and throughout the year (Murray, 1992). This species also tolerates low oxygen conditions and successfully colonizes formerly anoxic environments (Gooday, 1993; Alve, 1995; Gooday and Alve, 2001). Neither depth nor TN/TOC appears to influence the distribution of *S. feylingi*. While *S. feylingi* abundance increases under cooler bottom-water conditions, the closer position of this species to the centre of the CCA plot compared to *E. excavatum* f. *clavata* and *C. reniforme* may reflect the opportunistic nature of this species, tolerating a range of environmental conditions.

The calcareous species *Globulina inaequalis*, *Islandiella norcrossi, Nonionellina labradorica,* and *Stainforthia concava* show a strong relationship to higher nitrogen and organic carbon in surface sediments, indicated by high CCA axis 2 scores. Transfer function models predict the warmest temperature optima (> 3.5°C) for these species, with relatively high salinity (>34.4 psu). The distribution of *I. norcrossi* is usually interpreted to reflect cold Arctic Waters (e.g. Rytter *et al.*, 2002), and occurs as an ice-distal species following glacier-proximal peaks of *C. reniforme* and *E. excavatum* f. *clavata* (Osterman and Nelson, 1989; Korsun and Hald, 1998). Silis (1993) interpret *I. norcrossi* to reflect influxes of glacial meltwater. Feyling-Hanssen (1990)

interprets fossil samples dominated by *I. norcrossi* in the Thule area, northwest Greenland, to reflect high-Arctic conditions. However, modern occurrences of *I. norcrossi/helenae* in central West Greenland are found under the influence of relatively warm Atlantic-sourced water and are strongly related to organic carbon and nitrogen content of surface sediments. High abundances of *I. norcrossi* are found under the influence of cold bottom water temperatures with a high and stable salinity (Mudie *et al.*, 1983; Austin and Kroon, 1996; Korsun and Hald, 1998) and not under Atlantic water (Hald and Steinsund, 1992; 1996; Ivanova *et al.*, 2008 in SW Barents Sea). Peak abundances of *Islandiella norcrossi* on the Arctic shelf are linked to phytodetritus pulses to the seafloor under high surface primary productivity, including at edge of sea-ice (Korsun and Polyak, 1989; Hald and Steinsund, 1992, 1996; Steinsund and Hald, 1994). Along the West Greenland margin, the distribution of *I. norcrossi* reflects higher levels of organic matter, which are interpreted to be related to influxes of warm WGC water. The weighted averaging optimal temperature and salinity reaffirm such an interpretation. However, *I. norcrossi* has wider tolerances than the other species it occurs with, suggesting that it is tolerant of Polar Water influence.

Nonionellina labradorica is typically a deep endobenthic species (up to 8-10 cm) associated with areas of high seasonal productivity and fresh phytodetritus fluxes to the seafloor, particularly in the Polar Frontal Zone and at the summer sea-ice edge (Cedhagen, 1991; Hunt and Corliss, 1993; Hald and Steinsund, 1992, 1996; Polyak *et al.*, 2002; Rytter *et al.*, 2002; Jennings *et al.*, 2004). In central West Greenland, *N. labradorica* dominates samples in Egedesminde Dyb (FAZ 5), the deep trough at the southeast entrance to Disko Bugt FAZ 5. Lloyd (2006a) interprets the distribution of *N. labradorica* to reflect enhanced nutrient delivery via the warm Atlantic component of the WGC relative to the Arctic Water component. A number of studies find *N. labradorica* associated with warm Atlantic water (temperature 3 - 4°C, salinity >34.5 psu) on the Labrador shelf between *ca.* 500 and 600 m water depth (Vilks, 1980; Mudie *et al.,* 1983; Scott *et al.*, 1984). In the Disko Bugt-Uummannaq region, temperature and organic carbon/nitrogen content are highly correlated, supporting a link between *N. labradorica* and bottom-water temperatures. However, two samples (343340 and 343570) influenced by the warmest subsurface waters at the time of collection have lower abundances of *N. labradorica*

(particularly 343340), suggesting the relationship between this species and Atlantic Water influence is not straight forward. It is possible that *N. labradorica*-dominated samples reflect enhanced surface primary productivity, particularly since these sites are located beyond the influence of productivity inhibiting meltwater from tidewater glaciers in Disko Bugt (Söderkvist *et al.*, 2006). However, it appears most likely that *N. labradorica* abundance corresponds to the higher nutrient levels in the Atlantic-sourced component of the WGC compared to nutrient poor Polar Water (e.g. Jennings *et al.*, 2004).

Cuneata arctica (= *Reophax arctica*) shows a negative relationship with temperature and salinity in CCA. This is in agreement with Schafer and Cole (1988), who find higher abundances (10-25%) of *C. arctica* present under cold water influence (*ca.*-1 to -1.5°C) in fjords of Baffin Island. While weighted averaging predicts a warmer nice for *C. arctica* (*ca.* 2.2°C), this remains among one of the "coldest-water" species in this study, and therefore is associated with Polar Water. *Spiroplectammina biformis* and *Textularia earlandi* have been associated with cold, Polar water influence (e.g. Lagoe, 1979; Schafer and Cole, 1988; Ishman and Foley, 1996). However, *T. earlandi* shows a weak positive relationship with temperature and salinity. Despite this, *Cuneata arctica, S. biformis* and *T. earlandi* show an inverse relationship to TN/TOC-enriched sediments, which may reflect the influence of nutrient-poor Polar waters on these species. Negative axis 1 and 2 CCA species scores for *S. biformis* indicate a poor relationship with temperature and salinity. Schafer and Cole (1982) suggest *S. biformis* has a wide ecological niche, though a maximum abundance of 25% is found under water at *ca.* 500 m depth with a temperature and salinity of 3.2°C and 34.8 psu, respectively. However, in the Amerasian Basin in the Arctic Ocean, *S. biformis* is a dominant taxon under cold, low salinity waters (temperature *ca.* 0.5°C, salinity >34.5 psu). The results of CCA suggest that *S. biformis* prefers environments characterised by a fine-grained substrate, along with a number of other species, including *Trochammina nana, Recurvoides turbinatus, Cribrostomoides* sp., and *Adercotryma glomerata. Spiroplectammina biformis* is relatively ubiquitous in central West Greenland, though is absent (or in low abundance) at sites influenced by warm WGC water, and relatively low abundance under extremely cold Polar Water in Nordre Strømfjord.

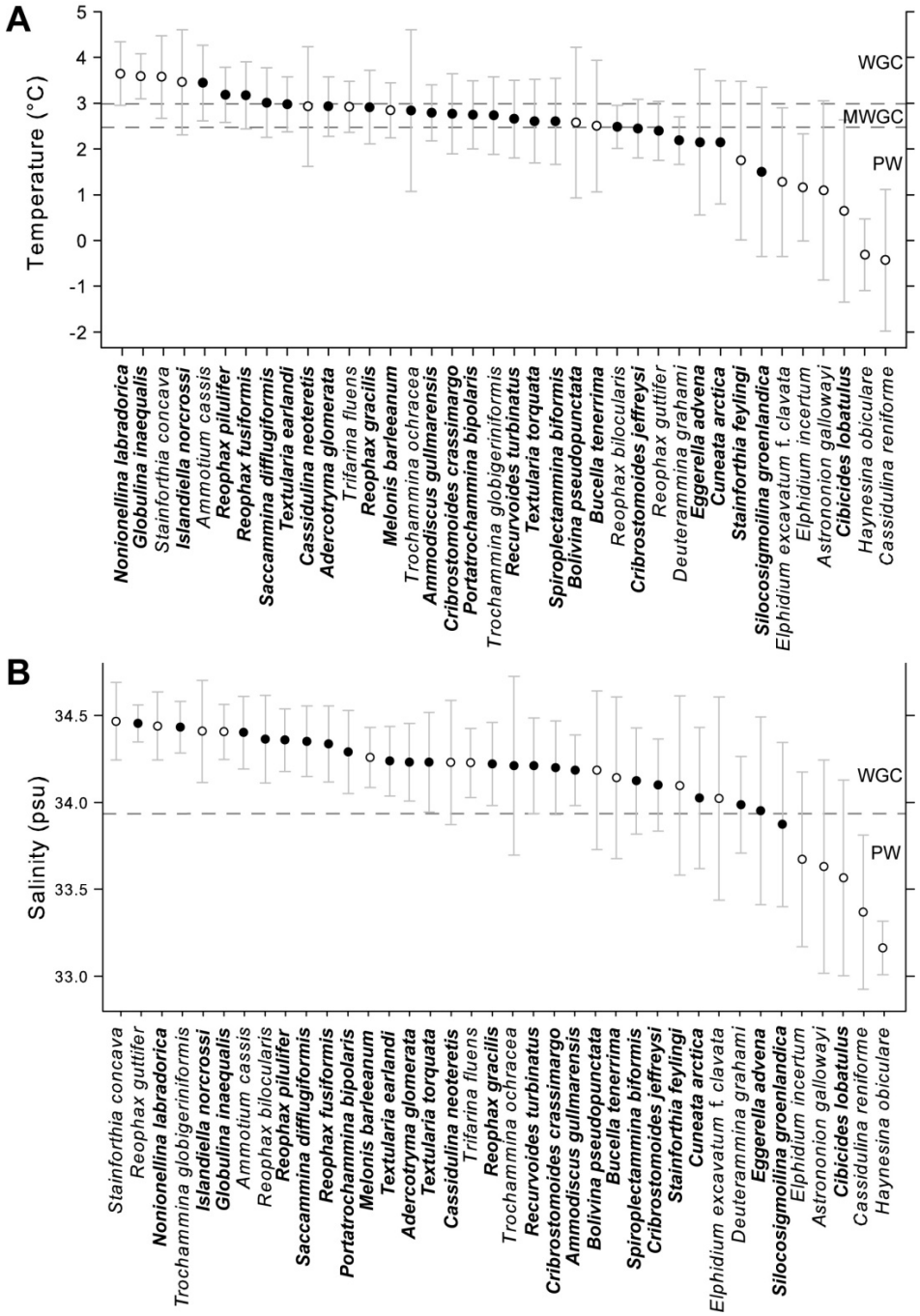

Figure 4.12 (**A**) Temperature and (**B**) salinity bootstrapped weighted average optima and tolerances of benthic foraminifera occurring in at least two samples and abundances exceeding 2% in the modern training set. Species with a bold typeface have more than five N2 occurrences (Hill, 1973), and are therefore can be more reliably predicted. Filled circles indicate agglutinated species and empty circles indicate calcareous species. Dashed lines indicate approximate boundaries between different water masses in West Greenland, though note that these do overlap. WGC, West Greenland Current influence; MWGC, Mixed WGC influence; PW, Polar Water influence.

The results of CCA (*Fig. 4.8*) indicate that the distribution of four species, *Reophax pilulifer*, *Reophax fusiformis*, *Saccammina difflugiformis*, and *Melonis* barleeanum, are closely related to bottom-water temperature and salinity (i.e. close proximity to the variable arrow indicating the direction of the maximum rate of change). *Saccammina difflugiformis* (=*Saccammina atlantica*) has been linked to Atlantic Water on the continental slope of north Svalbard, in Fram Strait, and on the Yermak Plateau (Scott and Vilks, 1991; Bergsten, 1994). However, in Baffin Island fjords, Schafer and Cole (1988) found *S. difflugiformis* associated with cold water present at intermediate depths (temperature ≤ -1°C and depth 50-200m), though abundances do increase with distance from fjord heads. Ecological studies indicate higher abundances of *M. barleeanum* are found in environments influenced by altered (slightly decomposed) marine organic matter (e.g. Corliss, 1985; Caralp, 1989a, 1989b), and shows a strong relationship with TOC, and therefore cannot tolerate high sedimentation rates, particularly in locations influenced by seasonal meltwater (Caralp, 1989). Ivanova (2006; cited in Ivanova *et al.*, 2008) links higher abundances of *M. barleeanum* to the influence of Atlantic Water at the sediment-water interface in the Barents Sea (Ivanova, 2006, cited in Ivanova *et al.*, 2008).

Adercotryma glomerata is a common Arctic species (e.g. Schafer and Cole, 1982). According to Wollenburg and Mackensen (1998a), *Adercotryma glomerata* avoids warmer water masses. However, Schafer and Cole (1982) found high abundances of *A. glomerata* (33%) between 500-530 m depth under the influence of Labrador Current water with a temperature of 3.2°C and a salinity of 34.8 psu. Vilks (1980) also found *A. glomerata* to be important on the Labrador Shelf under relatively warm water (temperature 3-4°C, salinity >34.5 psu). CCA suggests a weak positive relationship to temperature and salinity, and indeed temperature and salinity optima are calculated to be close to 3°C and 34.2 psu, respectively, indicating a preference for relatively warm WGC waters. However, the results of CCA also suggest a negative relationship to organic matter and depth, indicating this species tolerates Polar Water influence.

Based on results from this chapter and other published records from Arctic shelf settings, *Table 4.5* lists the groups of foraminiferal species that will be used in palaeoenvironmental

reconstructions from marine fossil cores to summarise relative temperature changes in the West Greenland Current.

Atlantic Water Group:	Atlantic/Intermediate:	Arctic Water Group:
Ammoscalaria pseudospiralis	*Adercotryma glomerata*	*Cuneata arctica*
Reophax bilocularis		*Spiroplectammina biformis*
Reophax fusiformis		*Textularia earlandi*
Saccammina difflugiformis		*Astrononion gallowayii*
Bolivina psedopunctata		*Cassidulina reniforme*
Bucella frigida		*Elphidium excavatum* f. clavata
Bucella tenerrima		*Islandiella norcrossi/helenae*
Cassidulina neoteretis		*Stainforthia concava*
Globulina inequalis		*Stainforthia feylingi*
Melonis barleeanum		
Nonionellina labradorica		
Trifarina fluens		

Table 4.5 List of foraminifera used to identify Atlantic, “intermediate”, and Arctic Water influence on the continental shelf in central West Greenland.

4.4.3 Can a reliable transfer function model be developed?

Multivariate analyses suggest benthic foraminifera on the central West Greenland shelf are reliable indicators for reconstructing former bottom water temperatures. Many species are highly correlated (positively or negatively) with temperature and salinity, or TN/TOC. A strong correlation between these sets of variables suggests that TN/TOC content in surface sediments corresponds to the influence of different water masses at particular sites. However, CCA with the first axis constrained to temperature (*Fig. 4.13*) indicates a significant amount of unexplained variation (i.e. variation along axis 2 in CCA), though this is not surprising. However, only samples from Nordre Strømfjord show a strong (negative) relationship to temperature, suggesting that periods of significant warming may not be captured by the reconstruction estimates.

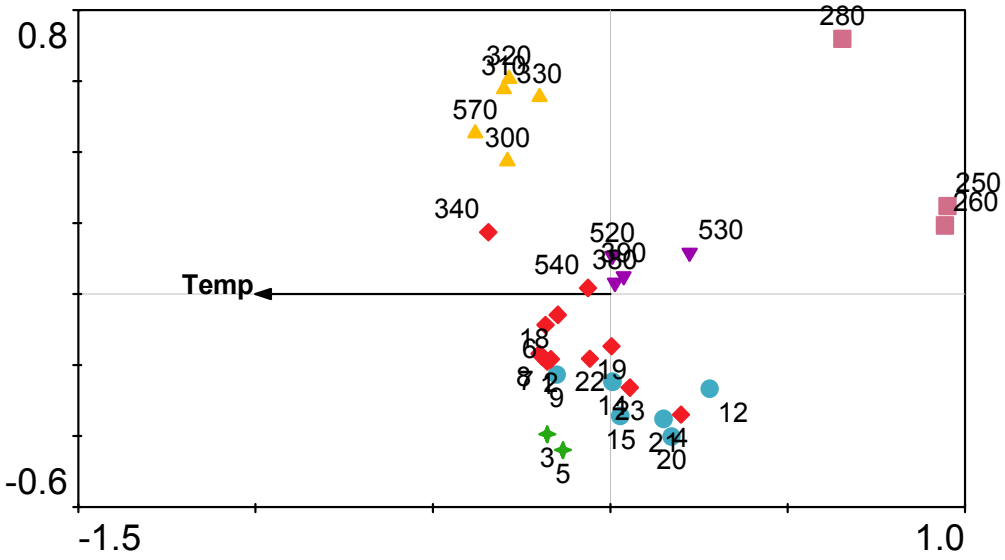

Figure 4.13 CCA biplot showing sample scores with temperature constrained to the first canonical axis

The preliminary transfer-function models indicate a close matching between predicted and observed temperature values. However, a number of caveats exist for the current transfer-function models. Perhaps most importantly, the current model contains only 32 samples beneath the surface layer. Summer bottom-water temperatures between 1.8°C and 4°C influence the majority of samples, while only five samples span the interval between -1.2°C and 1.8°C. There exists a need to extend the current database of foraminiferal samples, particularly those influenced by cooler waters. Taphonomic processes affect preservation of both agglutinated and calcareous foraminifera in fossil cores on the West Greenland shelf (Lloyd *et al.*, 2007). This presents a major problem for palaecological reconstructions. The TA model appears to be more statistically robust, though cannot be applied to fossil intervals characterised by calcareous dissolution. Furthermore, the low agglutinated fauna presence in samples influenced by colder Polar Water and the warmest WGC water suggests that applying the AA model to parts of the core where the calcareous assemblage has been significantly modified or lost by dissolution will result in reconstruction estimates biased to a "middle" temperature (i.e. predicting cool rather than cold or warm temperatures).

4.5 Chapter summary

The available modern foraminifera data do not span a wide enough environmental gradient, nor are there sufficient samples, to produce a robust transfer function that can be applied to fossil assemblages. The strong relationship between temperature and foraminifera suggests that it may be feasible to develop more robust transfer function models with improved predictive power in the future. However, these results highlight the strength of interpreting fossil assemblages in this study primarily based on foraminifera ecology for the purposes of this study.

Chapter 5

RAPID DEGLACIATION OF THE CENTRAL WEST GREENLAND SHELF IN THE DISKO BUGT AREA

XRF and magnetic susceptibility core scanning data was undertaken aboard the R/V "Maria S. Merian" shortly after core retrieval. Kerstin Perner and Matthias Moros (Leibniz-Institut für Ostseeforschung Warnemünde - IOW) provided digital X-ray radiographs of core MSM-343340_G.

Chapter 5

Rapid deglaciation of the central West Greenland shelf in the Disko Bugt area

5.1 Introduction

Funder and Hansen (1996) proposed a two-stage deglacial model with relatively early and rapid disintegration of marine-based ice, between *ca.* 15 and 10 ka cal. BP, driven by eustatic sea level rise and warmer air temperatures, followed by slower melting of the land-based ice-sheet due to atmospheric warming. Others (e.g. Ingólfsson *et al.*, 1990; Weidick, 1996) suggest deglaciation began later (13-10 ka BP), and that deglaciation was episodic (alternating between rapid retreat and relative stability during deglaciation), with high topographic 'pinning' slowing ice margin retreat (e.g. Warren and Hulton, 1990; Weidick, 1996). A synchronous ice margin response would be expected if external factors such as atmospheric warming or eustatic sea level rise drove shelf deglaciation, whereas ice dynamic and topographic controls are likely to result in asynchronous deglaciation, with some parts of the ice margin retreating whilst other parts were stable (Long and Roberts, 2003; Roberts and Long, 2005).

In order to address these shortcomings in our present understanding, this chapter aims to provide a minimum age for the retreat of marine-based ice from the shelf west of Disko Bugt. A further aim is to reconstruct oceanographic conditions and ice stream-ocean interactions during initial deglaciation and the subsequent ice retreat off the continental shelf using sedimentological and proxy evidence in a marine sediment core, MSM-343340_G, located in outer Egedesminde Dyb, west of Disko Bugt. A particular focus is to identify the potential influence of relatively warm and saline West Greenland Current (WGC) on ice sheet retreat. Marine archives potentially provide high resolution and uninterrupted records detailing environmental conditions during deglaciation, and allow us to constrain the timing and nature of deglaciation. New data from marine sediment cores is used to establish the timing and nature of marine-based deglaciation in the Disko Bugt area, and test Funder and Hansen's (1996) two-phase deglacial model proposed for Greenland.

5.2 Results

5.2.1 Chronology and sedimentation rates

The age-depth model (*Fig. 5.1*) for this core uses linear interpolation between six radiocarbon dates obtained from intact bivalves (see *Table 5.1*). The lowermost date of 12,325 yrs. BP (12.6-12.1 ka BP) from 902 cm core depth provides a minimum age for deglaciation at this site. This is a minimum age for deglaciation because it is the oldest date obtained from core MSM-343340, and was retrieved from immediately above ice-proximal glacimarine sediments. The absence of sufficient dateable material between 902 and 1074 cm in the core prevents a closer estimate of the age of the base of the core. However, the basal age of the core (hence a more accurate estimate of the age of deglaciation) can be estimated based on the sedimentation rate of the lower section of the core. If the sedimentation rate from up-core (approximately 450-900 cm) were assumed to remain constant for this lower interval, the basal age for the core would be *ca*. 13 ka BP. A relatively high sedimentation rate between 2.4 and 3 mm a^{-1} characterised the interval 12.3 to 11.2 ka BP. The sedimentation rate then slowed to between 1.47 and 2.29 mm a^{-1} during the next *ca.* 600 years, before a reduction by more than an order of magnitude to less than 0.25 mm a^{-1} from 8.8 ka BP until present, indicating a dramatic decline in sediment supply.

Core depth (cm)	Lab. code	Material	^{14}C age ± 1σ (yr BP)	Calibrated age (yr BP)	Age range 2σ (yr BP)
53 - 58	Poz-22361	Bivalve	2,555 ± 30	2,230	2,315-2,135
129	Poz-30988	Bivalve	8,240 ± 50	8,773	8,951-8,604
276	SUERC-26760	Bivalve	8,730 ± 39	9,414	9,490-9,300
456 - 457	Poz-30989	Bivalve *Nuculana* sp.	9,790 ± 50	10,646	10,876-10,533
632 - 634	Poz-30990	Bivalve	10,260 ± 60	11,240	11,545-11,128
901 - 902.5	Poz-30991	Bivalve *Portlandia arctica*	10,840 ± 60	12,325	12,562-12,100

Table 5.1 Radiocarbon dates for core MSM-343340-2-1_G. ^{14}C ages (uncorrected) calibrated using Oxcal v.4.1 (Bronk Ramsey, 2009) using the Marine09 curve (Reimer *et al.*, 2009), with ΔR=0±0.

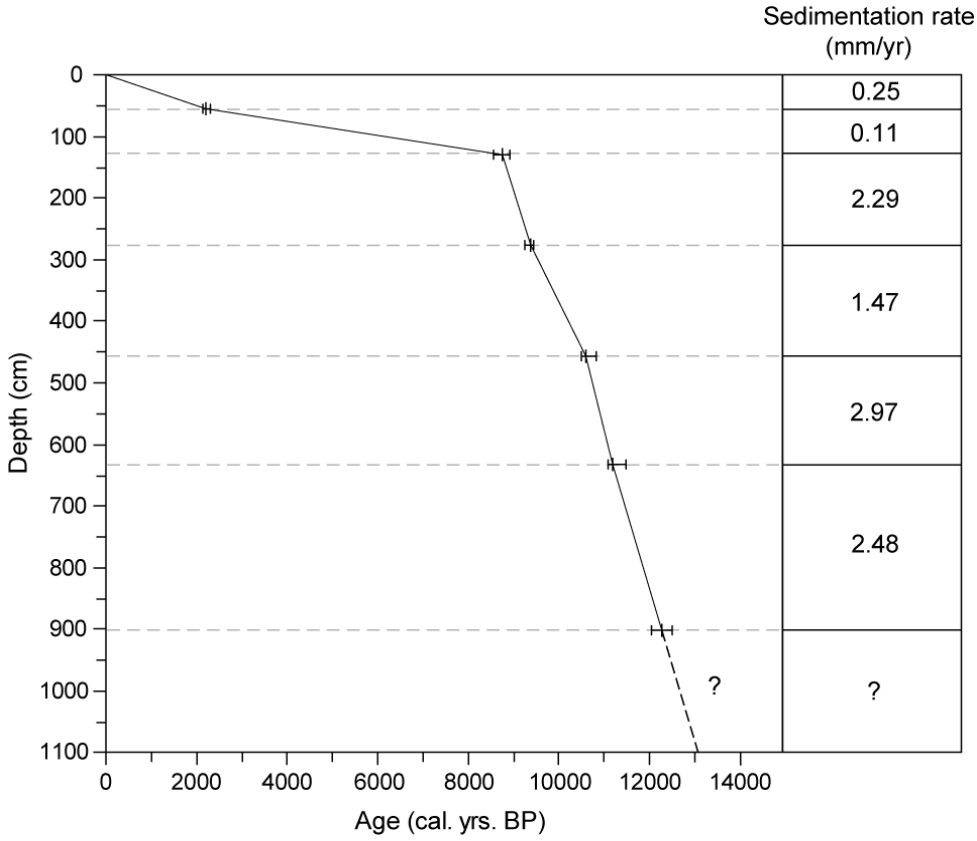

Figure 5.1 Age-depth model for core MSM-343340-2-1_G, with 2 s.d. age range, and sedimentation rates (mm/yr) based on linear interpolation between mean calibrated ages.

5.2.2 Core sedimentology

Sedimentological characteristics and sediment geochemistry are briefly described below according to four distinct sedimentological zones.

Zone 1: 1075-880 cm

Visual core logging and analysis of X-ray radiographs indicates that the base of core MSM-343340 (1074-950 cm) is composed of interbedded laminated or massive mud (Fl/Fm) and stratified clast-rich or clast-poor diamicton (Dms), with primarily gradational or conformable contacts between sedimentary units (*Fig. 5.2* and *5.3A*). These fine-grained grey muds are predominantly composed of clay with fine silt, and are typically parallel laminated (Fl), though occasionally massive (Fm), and range in thickness from a few millimetres to 8 cm. Dropstones (Fld) are rare or absent in the laminated muds, though larger clasts are common in the stratified diamicton (*Fig. 5.3A*). Macrobenthos are also uncommon or absent, and there is no evidence of

bioturbation. A thin layer of fine sand at 945 cm overlies the diamicton. There is an upcore shift to weakly stratified sediments containing networks of small branching tubes, interpreted as pyrite-infilled chondrites (*Fig. 5.3B*). Biogenic trace fossils disappear above 920 cm, where there is a gradual transition back to laminated sediments between 910-880 cm.

Sediment water content is initially low (32.6 %) in the laminated mud facies, though increases to *ca*. 40% in the overlying sediments, before peaking at 47.4 % at 753 cm. Percentage loss-on-ignition is low at the base of the core (1.1 %), though increases to 2.4 % just above the laminated mud at 977 cm. Loss-on-ignition is *ca*. 2.1 % throughout most of the lower sediments There are high frequency fluctuations between very low and very high magnetic susceptibility throughout the laminated mud lithofacies, though the magnitude of these variations falls in the overlying lithofacies (Fmd). XRF integral ratios for [Si/Al] and [S/Al] are low (*ca*. 10 and 0 respectively) for the lower 300 cm of the core.

Zone 2: 880-525 cm

Above 880 cm, there is increasing evidence of biogenic activity in the weakly stratified/massive muds. The sedimentology between 880 and 575 cm is characterised by preservation of numerous chondrite networks, as well as much larger subhorizontal to subvertical and slightly sinuous shafts (e.g. 5.3D), particularly at *ca.* 750 cm, and 665-675 cm. The interval 575-525 cm is characterised by a high occurrence of long (each up to *ca*. 4 cm) vertical burrows, interpreted to be escape structures through weakly laminated sediments (*Fig. 5.3C*). The fine-grained sediments between 750 cm and 560 cm are characterised by declining water content, reaching a minimum of 27.1 % at 561 cm, and increasing magnetic susceptibility, which also peaks at 560 cm core depth. Loss-on-ignition is relatively low in this zone (1.3-2.1 %), though begins a gradual increasing trend up core. The [S/Al] integral ratio remains low, but there is a stepped increase in the [Si/Al] ratio to *ca*. 12 at 750 cm, which stays relatively constant up core through the overlying zone 3.

Zone 3: 525-130 cm

A variety of burrow structures are present in sedimentological zone 3, particularly between 500 and 400 cm. Zone 3 is characterised by gradual increases in LOI, from *ca.* 1% to 3% and [S/Al] from an integral ratio of near 0 to 1. There is a gradual decline in magnetic susceptibility throughout this zone (from *ca.* 250 to 50 SI), coincident with increasing water content from *ca.* 30% to 45% (reaching a maximum at 300 cm core depth), and a reduction in dry bulk density, from *ca.* 1.4 g cm^{-3} to 0.8 g cm^{-3}.

Zone 4: 130-0 cm

Zone 4 begins at 130 cm core depth, and is marked by a sudden and significant decline in the sedimentation rate. While there is evidence of increasing bioturbation from 400 cm, sediments in the upper 40 cm of core MSM-343340 are heavily bioturbated (*Fig. 5.3D*). The clayey mud lithofacies (from 270 cm in zone 3 to the top of the core) is characterised by high water content (*ca*. 40-45%) and the lowest magnetic susceptibility (*ca*. 50 K) throughout the core, though this begins to increase above 50 cm core depth. Percentage loss-on-ignition continues to gradually increase up core, reaching at a maximum value of 4.9 % at the top of the core. There is a significant rise and peak (to an integral ratio just above 2) in [S/Al] at ~50 cm, before a decline towards the top of the core. The [Si/Al] data shows a similar increase to ~50 cm in zone 4, followed by a decline to the top of the core. These peaks correspond to an interval of stratified or laminated sediments (between 50-41 cm).

5.2.3 Foraminiferal analysis

Microscopic analysis identified 25 agglutinated and 19 calcareous species. There is a significant variation in foraminiferal abundance in core MSM-343340; some parts of the core, particularly below 880 cm, have very foraminiferal abundance (i.e. the total number of specimens counted), while foraminifera abundance is generally higher above 700 cm core depth. Relative abundances of species greater than 5% in at least one sample are shown in *Figure 5.4* (full foraminiferal counts in *appendix 1*). Core MSM-343340 can be divided into four distinct foraminiferal assemblage zones (FAZs) based on major faunal changes, which are described in turn below:

FAZ 1 (Before 12.3 ka BP, 1074-880 cm)

Well-preserved calcareous fauna dominate FAZ 1 from 12.4 ka BP to *ca*. 13 ka BP. Agglutinated species are common in the lower samples, decreasing significantly through this zone. The ice-proximal species *Cassidulina reniforme* (60-75%) dominates samples from the base of the core until *ca*. 12.4 ka BP. *Spiroplectammina biformis* also occurs in high percentage abundance at the base of the core (> 40%), before briefly disappearing by 12.5 ka BP. There are smaller occurrences of *Reophax gracilis* (up to 8 %), *Elphidium excavatum* f. *clavata* (up to 10 %) and *Islandiella norcrossi* (up to 15 %). Very low foraminifera concentrations (0-100 specimens/ml) characterise the lower part of the core. Some samples were devoid of foraminifera, including at the base of the core, while a statistically significant count of 300 specimens was only possible for one sample at 950 cm depth in FAZ 1.

FAZ 2 (12.3-11 ka BP, 880-560 cm)

The opportunistic Arctic species *Stainforthia feylingi* (=*S. fusiformis, F. fusiformis*) dominates (65-100%) all samples between 12 and 11 ka BP (and an earlier sample at *ca.* 12.6 ka BP). During this interval, *C. reniforme* is common in a number of samples (up to 13 %), though shows a steady decline to the top of this zone. *Islandiella norcrossi*, *E. excavatum* f. *clavata*, and *S. biformis* are generally less abundant between 12.5 and 11 ka BP, though constitute up to 15 % of assemblages.

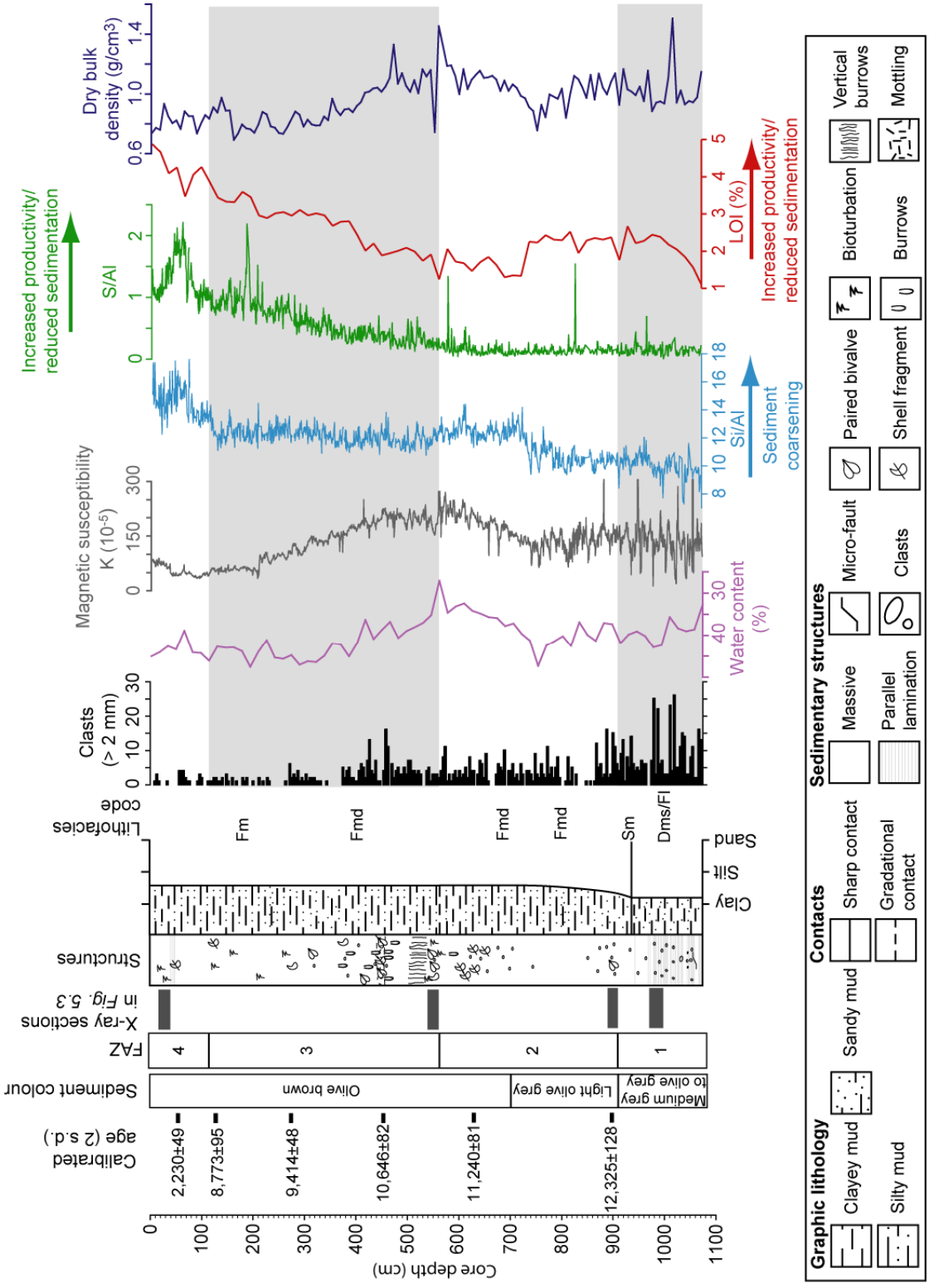

Figure 5.2 Sedimentology and geochemistry for core MSM-343340_G. Foraminifer assemblage zones (FAZ) are shown on left, and indicated by grey shading. The positions of X-ray radiograph example sections are also marked in order, from (**A**) at the base to (**D**) at the top. Lithofacies codes follow Eyles *et al.* (1992); Dms, diamicton (matrix supported, stratified); Fl, laminated mud; Fm, mud (massive); Fmd, mud (massive with dropstones; Sm, sand (massive). Note that sediment water content is on a reversed axis.

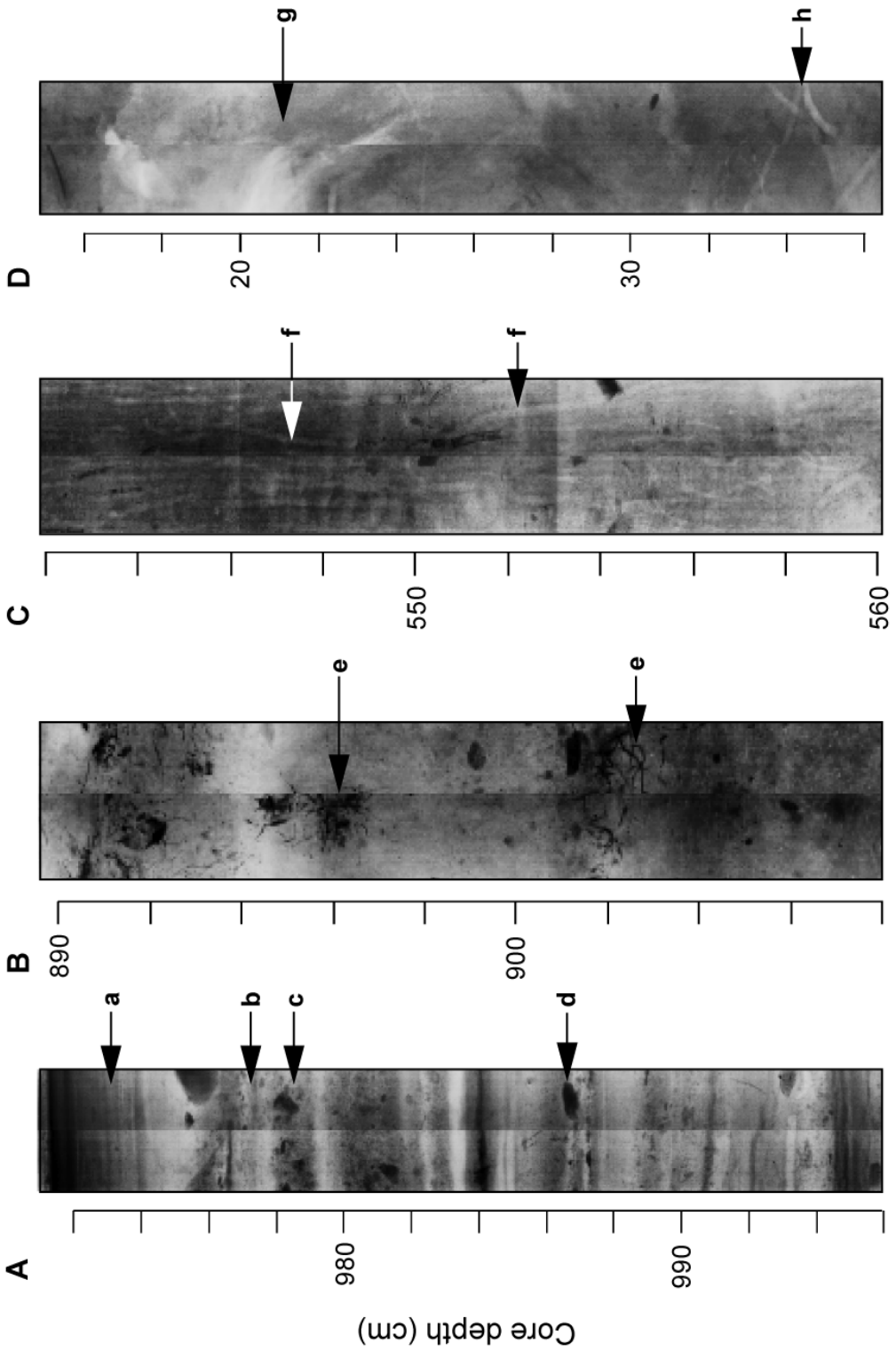

Figure 5.3 Representative X-ray radiograph sections of lithofacies from core MSM-343340_G (see *Fig. 5.2* for location of core sections (**A**) to (**D**). Arrows indicate examples of; (**a**) rhymically laminated mud, (**b**) clast-poor diamicton, (**c**) clast-rich diamicton, (**d**) ice-rafted clast, (**e**) chondrite burrowing networks, (**f**) rapid escape structures (polychaetes), (**g**) intensive bioturbation, (**h**) sub-horizontal burrows. Note the small differences in scale between images.

FAZ 4 (8.8 ka BP-present, 110-0 cm)

FAZ 4, spanning the past *ca*. 8.8 ka BP, is sampled at a coarse temporal resolution. This zone is characterised by an agglutinated only faunal assemblage, dominated by *C.arctica* with an increasing abundance of *Adercotryma glomerata* in the mid- to late-Holocene and *R. gracilis* is common. The initial appearance of *Reophax pilulifer* and *Saccammina difflugiformis* occurs shortly after 8.8 ka BP, with the latter species being particularly dominant during the mid-Holocene. Higher organic test lining counts in FAZ 4, suggesting increased dissolution of calcareous specimens, may partly contribute to the reduced foraminifera concentration in FAZ 4 (<220 specimens/ml).

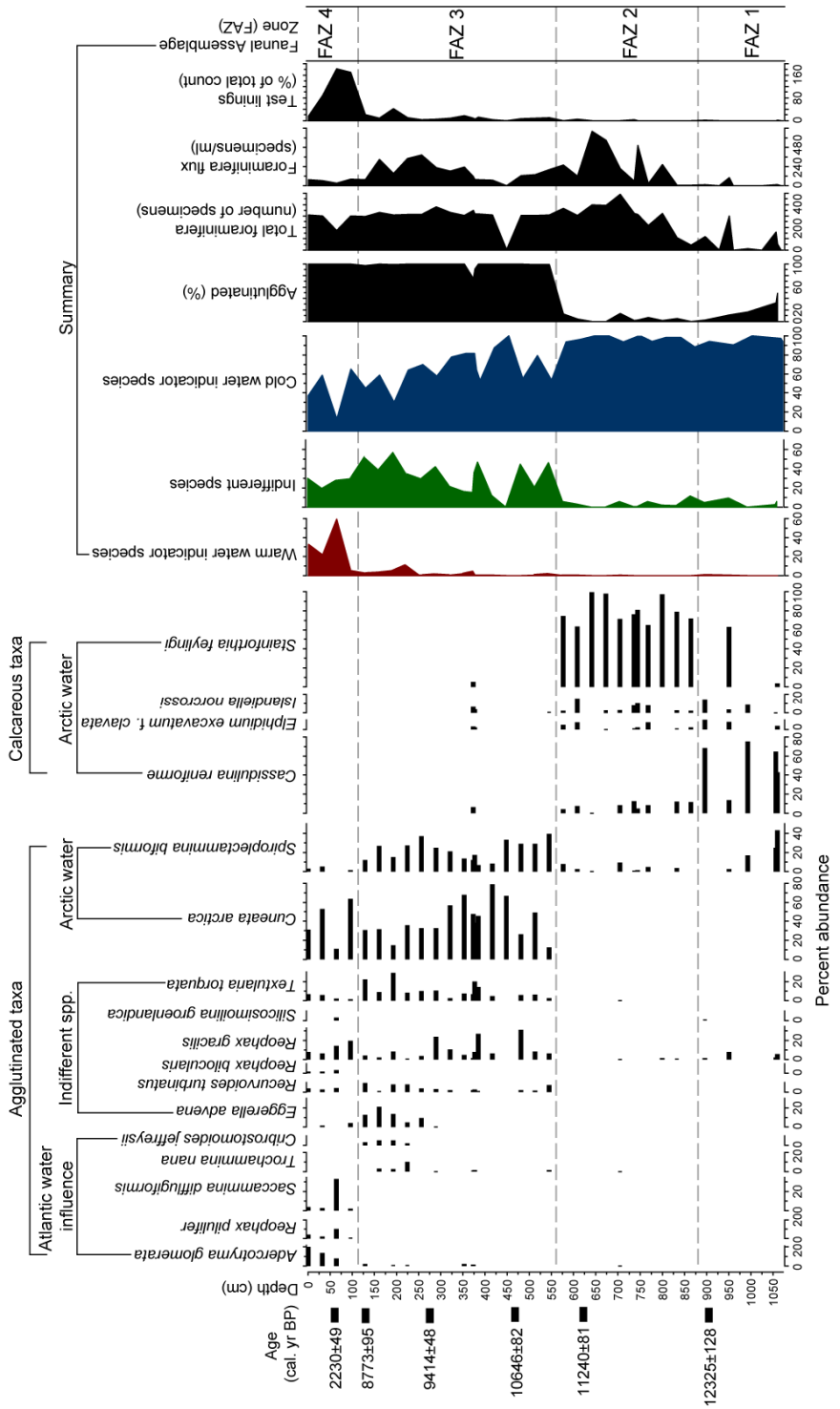

Figure 5.4 Foraminiferal assemblage from core MSM-343340_G. Foraminifera frequencies are shown as relative abundance of the total count, only species ≥ 5% of the total assemblage are shown. Faunal assemblage zone (FAZ) boundaries area based on major biostratigraphical changes. Summary graphs show the total sum (% relative abundance) of warm water and cold water indicator species. Test linings are calculated as a percentage of the total count of 'preserved' calcareous foraminifera.

5.3 Palaeoceanographic interpretation

An assessment of the core sedimentology indicated that the core was not significantly influenced by reworking processes. The sediment core is generally composed of clayey or silty mud with no hiatuses in the record. The upper *ca.* 9 m of the core MSM-343340_G comprises massive, occasionally bioturbated, hemipelagic mud with abundant foraminifera, indicating deposition under relatively quiescent conditions. The foraminiferal and sedimentological data provide information concerning changes in bottom water conditions and the relative proximity of the former ice margin to the core location. The close correspondence between sedimentological and foraminiferal changes allows palaeoceanographic interpretations to be made in turn according to foraminiferal assemblage zones.

5.3.1 FAZ 1 (Before 12.3 ka BP, 1074-890 cm)

The benthic foraminifera and sedimentological data support the interpretation of an ice-proximal glacimarine environment for the lower part of core MSM-343340 (*Fig. 5.2* and *5.4*). Sediments in the lower 200 cm of the core are dominantly clays, typically laminated, interbedded with stratified diamicton, with gradational, conformable, or occasionally sharp boundaries between sediment units. Foraminifera are rare or absent, indicating low benthic productivity and/or dilution due to rapid sedimentation. These features are consistent with sediments deposited through suspension settling from meltwater plumes in an ice-proximal depositional environment (Mackiewicz *et al.,* 1984; Dowdeswell *et al.*, 2000; Ó Cofaigh and Dowdeswell, 2001). Variations in the abundance of IRD throughout this zone may correspond to changes in fine-grained sedimentation ejected from the outlet glacier terminus, with intervals characterised by lower IRD possibly linked to greater suspension settling of fine-grained sediments. Despite the lack of chronological control, these sediments were presumably deposited extremely rapidly and in close proximity to the calving margin. Eitherway, this indicates that meltwater and calf-ice from fast-flowing ice exited Disko Bugt via outer Egedesminde Dyb during at least part of the Younger Dryas Stadial (GS-1), dated to *ca.* 12.8-11.7 ka BP (Rasmussen *et al.*, 2006; Lowe *et al.*, 2008) (12,896±138 to 11,703±99 yr. b2k on the GICC05 timescale, from NGRIP ice core).

The dominant foraminifera species in FAZ 1; *C. reniforme, S. feylingi* and the agglutinating *S. biformis*, are commonly found in glacimarine environments influenced by relatively cold water, extreme variations in salinity, and high sedimentation rates (Schafer and Cole, 1982; 1986). The dominance of *C. reniforme* indicates conditions at the seafloor most likely fluctuated between salinity extremes, presumably due to seasonally variable meltwater fluxes. Turbid meltwater hampers primary productivity in surface waters (which is supported by low LOI values), thereby reducing delivery of food to the sea floor (Korsun and Hald, 1998). This favours opportunistic species such as *C. reniforme*, which tolerate extreme seasonal variations in freshwater and sediment delivery, conditions usually found in close proximity to glacier calving margins (Korsun and Hald, 1998). Other well-preserved fragile species (i.e. *S. feylingi* and *S. biformis*) found in sediments deposited before 12.3 ka BP are consistent with ice-proximal conditions and high sedimentation rates (e.g. Lloyd *et al.*, 2005; Ullrich *et al.*, 2009; Jennings *et al.*, 2010). The excellent preservation of small, fragile Arctic calcareous fauna and the absence of organic test linings in the lower part of core MSM-343340 may be linked to rapid sediment accumulation before 12.3 ka BP, since the high dissolved CO_2 content in Arctic water causes dissolution of dead calcareous fauna (e.g. Aksu, 1983; Hald and Steinsund, 1992; de Vernal *et al.*, 1994; Jennings and Helgadottir, 1994).

5.3.2 FAZ 2 (12.3-11 ka BP, 890-575 cm)

The foraminifera and sedimentological data indicate the ice stream terminus retreated from close to the site of MSM-343340 after 12.3 ka BP, and ice-distal glacimarine conditions dominated outer Egedesminde Dyb between *ca.* 12.3 and 11 ka BP. The transition from ice-proximal to hemipelagic sedimentation in FAZ 2 marks a clear reduction in glacier influence compared to FAZ 1, with reduced sediment deposition from turbid meltwater plumes. However, the ice stream in inner Egedesminde Dyb continued to exert a strong influence on environmental conditions in outer Egedesminde Dyb. The distal-glacimarine indicator *S. feylingi* dominates FAZ 2, with smaller occurrences of the glacimarine species *E. excavatum* f. *clavata* and *C. reniforme* (Hald and Korsun, 1997; Jennings *et al.*, 2001). While these species are particularly dominant in unstable environments subject to large salinity fluctuations (e.g. Vilks, 1969; Knudsen and Seidenkrantz, 1994), *S. feylingi* may have a narrower temperature and

salinity tolerance (e.g. Alve, 1995), suggesting higher and more stable bottom water temperatures and salinities prevailed during this period. Indeed, in central West Greenland, *S. feylingi* has a weaker association to cold and relatively fresh water than *C. reniforme* and *E. excavatum* f. *clavata* (See Chapter 4).

However, a strong meltwater influence may have created a highly stratified and stressed environment favouring glacimarine species. *Stainforthia feylingi* colonises new habitats, and can survive with a low availability of food and oxygen (Gooday, 1993; Alve, 1995; 1999; Gooday and Alve, 2001), making it particularly suited to living in stratified waters. Chondrites networks, the trace fossils of burrowing polychaetes searching for food, are often associated with low oxygen conditions (Eyles *et al.*, 1992) and are indicative of pioneering colonisation by macrofauna (Rosenberg, 1979); interpretations consistent with foraminiferal evidence. Since *S. feylingi* undergoes rapid population growth in response to fresh phytodetritus inputs (Alve, 1994; Gustafsson and Nordberg, 2001), extremely high concentrations in the upper part of FAZ 2 may reflect bloom events following the break up of seasonal sea-ice, or reduced glacier influence.

5.3.3 FAZ 3 (11-8.8 ka BP, 575-125 cm)

The transition between FAZ 2 and FAZ 3 at *ca.* 10.9 ka BP marks a major shift in oceanographic conditions on the shelf outside Disko Bugt. This is most clearly indicated by a switch from dominantly calcareous to agglutinated-only foraminiferal assemblages dominated by *C. arctica* and *S. biformis* in the early Holocene, suggesting increasingly ice-distal conditions prevailed outside Disko Bugt, but still relatively cold water conditions. High abundances of *C. arctica* are indicative of a well-mixed water column typical of open-marine conditions. The high concentration of vertical escape structures suggests rapid sedimentation between 575 and 525 cm, possibly reflecting a brief interval of enhanced meltwater plume influence, increasing sediment delivery to the core site at 11 ka BP. In general, however, faunal changes are indicative of a less glacially-influenced environment, with a much weaker meltwater influence. Indeed, enhanced biological activity, revealed by increases in the [S/Al] ratio and percentage LOI, support a general reduction in glacier influence at this site, as does the enhanced bioturbation in the upper 400 cm of the core. The increase in *E. advena* and *C. jeffreysii*

between 9.4 ka BP and 8.8 ka BP may reflect increased nutrient levels in diluted Atlantic Water (a 'weak' WGC) outside Disko Bugt.

5.3.4 FAZ 4 (8.8 ka BP to present, 125-0 cm)

The sedimentation rate falls by more than an order of magnitude shortly after 8.8 ka BP, from around 2.2 mm a^{-1} for the preceding 3.5 ka, to 0.2 mm a^{-1} for the upper part of the core indicates a dramatic decline in sediment supply. The change in sedimentation rate is likely to occur at the boundary between FAZ 3 and FAZ 4, coincident with a change in the foraminifera species. This shift is marked by a large, abrupt increase in organic test linings, and the continued absence of preserved calcareous foraminifera in FAZ 4; a trend identified in POR 18 and DA00-06 in inner Disko Bugt by Lloyd *et al.* (2005). To some extent, the data supports a link between dissolution of calcareous foraminifera and low sedimentation rates, as identified by Lloyd *et al* (2005), who conclude that reduced sedimentation exposes dead calcareous foraminifera to corrosive bottom waters. Detailed discussions of the causes of calcium carbonate dissolution in Baffin Bay have been made elsewhere (e.g. de Vernal, *et al.*, 1992). De Vernal *et al.* (1992) identify increasing calcium carbonate dissolution in the Davis Strait beginning during, or shortly before, the Early Holocene, indicated by an increasing ratio of organic test linings to calcareous foraminifera. This pattern is similar to that identified in core MSM-343340. However, the results from this study do not support their suggestion that cold, poorly oxygenated subsurface, Arctic-sourced, waters contribute to increased dissolution during the Holocene, since this interval is characterised by an increased abundance of species associated with Atlantic Water influence on the West Greenland shelf. The initial shift to dominantly agglutinated fauna in FAZ 3 is not characterised by a coincident large increase in organic test linings, suggesting, in FAZ 3 at least, the faunal shift was due to environmental conditions and independent of changes in sedimentation rate.

Foraminifera assemblages (characterised by *A. glomerata*, *R. pilulifer*, and *S. difflugiformis*) in FAZ 4 are indicative of warmer subsurface water temperatures (i.e. an increase in the strength of the WGC influence) at the core site of MSM-343340 over the past *ca*. 8.7 ka cal. BP. These species are found under the influence of Atlantic Water in Disko Bugt (Lloyd, 2006a; see

Chapter 4). *Adercotryma glomerata* is found under the influence of "Transformed" Atlantic Water in the outer parts of Svalbard's fjords (Hald and Korsun, 1997), while *S difflugiformis* is common under Atlantic Water influence in outer Kangerdlugssuaq Fjord, East Greeenland (Jennings, and Helgadottir, 1994), and on the continental slope north of Svalbard (Scott and Vilks, 1991). Sporadic occurrences of *A. glomerata* in core MSM-343340 from *ca.* 10 ka BP may reflect a weak Atlantic water influence outside Disko Bugt during intervals of reduced deglacial meltwater. Prolonged sub-surface warming may also be marked by the appearance of *E. advena* at *ca*. 9.4 ka BP. Many studies have linked *E. advena* to higher nutrient levels from pollutant outfalls, for example in Clam Bay, Nova Scotia (Clark, 1971), and Chaleur Bay, Canada (Schafer and Cole, 1974, Schafer, 1982). High nutrient levels in West Greenland waters suggest enhanced entrainment of nutrient-rich Atlantic Water in the WGC, though to some extent may reflect greater surface water productivity and subsequent export of organic matter to the seafloor. The highest LOI and [S/Al] values throughout the core, suggestive of increased primary productivity, support this interpretation.

5.4 Discussion

5.4.1 Timing and nature of marine-based deglaciation from the mid-shelf through Disko Bugt

Figure 5.5 provides a conceptual representation of the retreat of the ice from the shelf through to the eastern margins of Disko Bugt and into Jakobshavn Isfjord based on new data and published information from Disko Bugt. The retreat of ice is based on dates from a transect of marine sediment cores between outer Egedesminde Dyb and eastern Disko Bugt (cores MSM-343340, MSM-343300, POR 18, and DA00-06, see *Fig. 5.6*) that provide minimum ages for deglaciation. These offshore dates provide the most reliable data constraining the retreat of the marine-based ice sheet in Disko Bugt.

The earliest date of 12.3 ka BP (12.6-12.1 ka BP, *Table 5.1*), obtained from a paired bivalve towards the top of the laminated lithofacies in core MSM-343340, provides a minimum age for deglaciation in Outer Egedesminde Dyb. Sedimentation in FAZ 1 of MSM-343340 was likely to be rapid and short-lived owing to the close proximity of the ice front. The high abundance of

ice-rafted material (*Fig. 5.2*) in Outer Egedesminde Dyb supports a nearby active calving margin during the YD and early Holocene. With ice filling Disko Bugt during this period, icebergs must have exited to the east through Outer Egedesminde Dyb (e.g. Brett and Zarudzki, 1979), before flowing northwards into Baffin Bay.

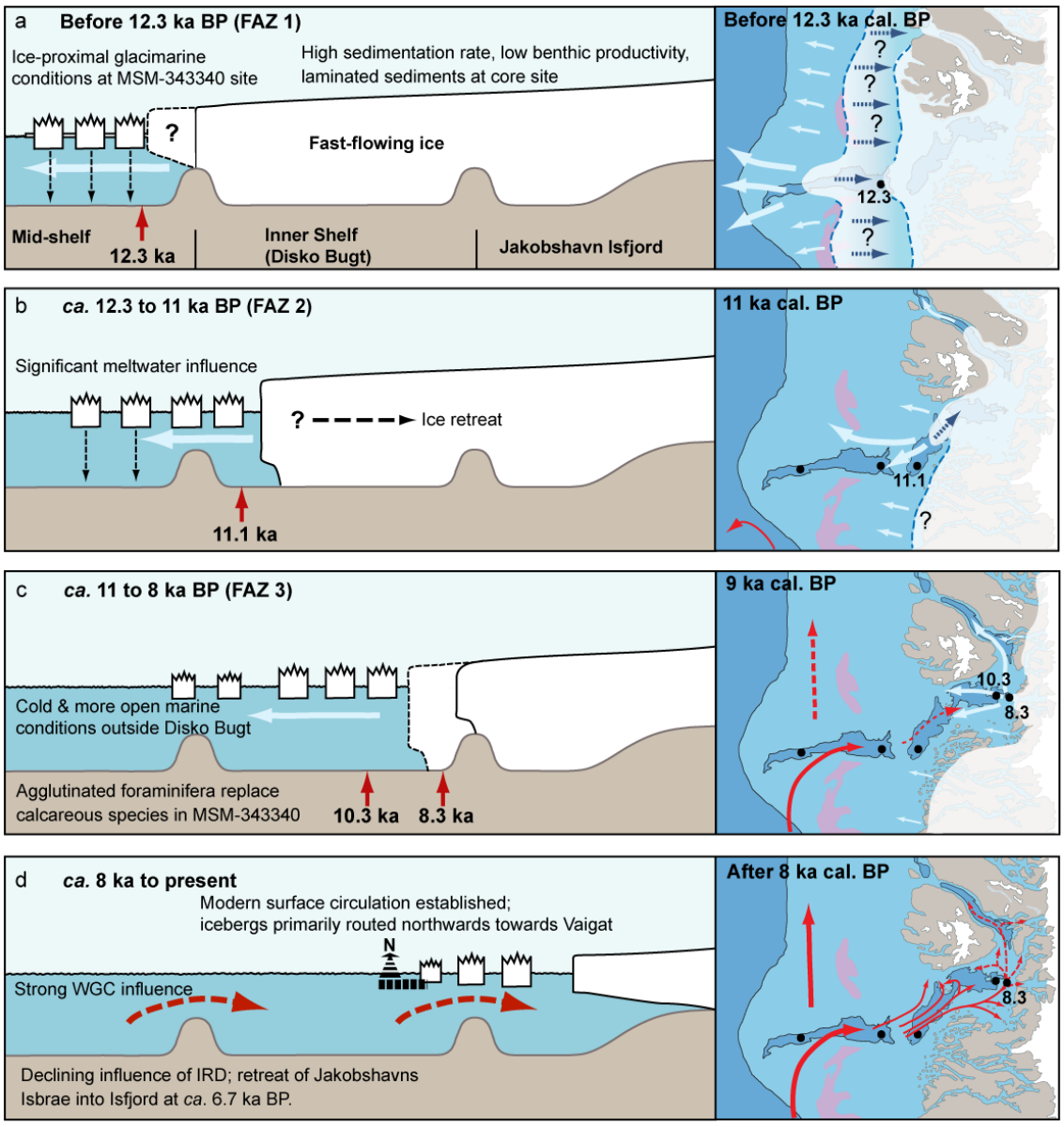

Figure 5.5 Conceptual cartoons of ice retreat from the outer shelf and across Disko Bugt. Cartoons in left panels show interpretations of major trends in data. A plausible retreat scenario based on presently available data is illustrated in the right panel. Red arrows (red panels) indicated the penetration of warm (solid) and 'diluted' (dashed) Atlantic-sourced water in the WGC. Light blue arrows show meltwater and iceberg loss and trajectories, while dark blue arrows indicate phases of ice retreat. Dashed blue lines highlight uncertainty in ice margin position.

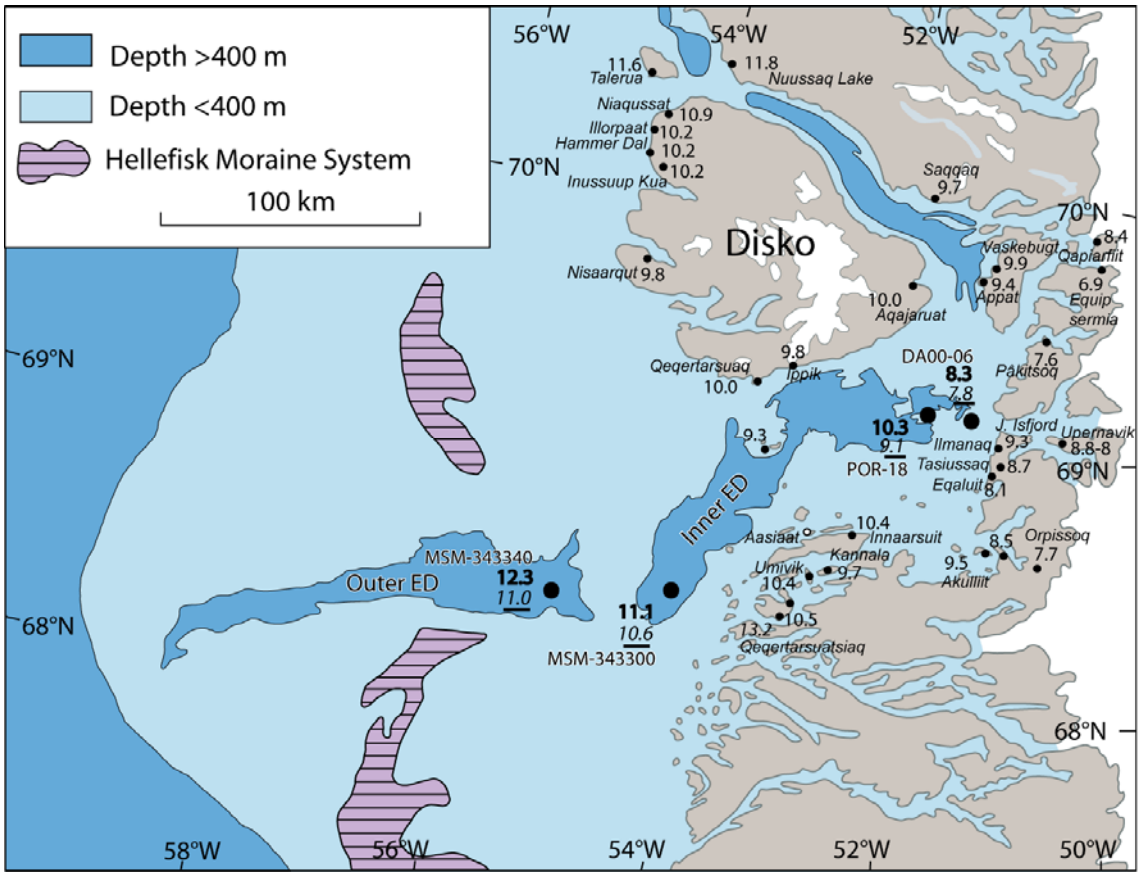

Figure 5.6 Minimum ages for deglaciation in the Disko Bugt area, updated from Long *et al.* (2003) and Long *et al.* (2006). The bold, marine-based dates are, west to east, from MSM-343340, MSM-343300 (Jennings *et al.*, 2010), POR 18, and DA00-06 (Lloyd *et al.*, 2005). The underlined calibrated dates indicate the approximate timing of the transition from glacimarine to more hemipelagic conditions. Inner/Outer ED refers to the inner and outer parts of Egedesminde Dyb, the trough that runs from inner Disko Bugt to the outer shelf.

The basal date from core MSM-343300 of 11.1 ka BP suggests deglaciation paused or slowed for *ca*. 1000 years (between MSM-343340 and MSM-343300, *Fig. 5.5a* and *Fig. 5.6*), perhaps linked to ice retreat into shallow waters between outer and inner Egedesminde Dyb. While glacial marine conditions persisted for *ca.* 1,300 years until 11 ka BP at MSM-343340, these conditions only lasted for approximately 500 years until 10.6 ka BP at core MSM-343300 (*Fig. 5.6* and *5.7*). The longer glacial marine influence at MSM-343340 is most easily explained if deglaciation slowed, or there was a still stand, as ice retreated across the relatively shallow bank bisecting inner and outer Egedesminde Dyb. Subsequent ice retreat towards, and into, Disko Bugt (*Fig. 5.5b*) appears to have taken place relatively quickly as suggested by Long and Roberts (2003), albeit slower than deglaciation of the outer shelf. As ice retreated landwards of

core MSM-343340 and into Disko Bugt (*Fig. 5.5.b*), there was amelioration to more open-marine conditions outside Disko Bugt at *ca.* 11.1 ka BP, possibly reflecting a decline in meltwater influence.

Deglaciation slowed as ice retreated into shallower waters in eastern Disko Bugt at *ca.* 10.3 ka BP at POR 18 (Lloyd *et al.*, 2005). This period was marked by relative ice stream stability for *ca.* 1000 years before ice retreated into Jakobshavn Isfjord. These correlations suggest glacial marine influence persisted at station MSM-343300 until *ca.* 10.6 ka BP. Rasch (2000) interprets a sudden fall in the marine limit at Aasiaat (southern margin of outer Disko Bugt, *Fig. 5.6*) as evidence for a stillstand or advance of the main ice sheet at *ca.* 11 ka BP. It is possible that the bedrock high between Aasiaat and Qeqertarsuaq reduced the speed of retreat of the ice into Disko Bugt. The escape structures in core MSM-343340 at *ca.* 11 ka BP suggest an interval of relatively high sedimentation, perhaps suggesting a period of relative ice stream stability in the early Holocene.

In southern Disko Bugt, the outer coast became ice free at, or just before, 10.5 ka BP at Qeqertarsuatsiaq based on bulk sediment dating of the onset of organic accumulation in coastal lakes (9330±99 ^{14}C yr BP, AA-38842, Long and Roberts, 2003) and 10.4 ka BP (9185±62 ^{14}C yr BP, Long and Roberts, 2003) at Umivik and Innaarsuit, respectively (*Fig. 5.6*). Deglaciation of the inner coast at Akulliit was complete by *ca.* 9.5 ka BP (8585±86 ^{14}C yr BP, Long and Roberts, 2002). These dates suggest ice retreated from the outer coast towards the eastern margin of Disko Bugt in approximately 1000 years. The decline in IRD at *ca.* 10 ka BP in MSM-343340 (*Fig. 5.*2; between 10.6 and 9.4 ka BP) appears to support these data. If ice had retreated to the eastern coast of Disko Bugt by 10 ka BP, and ice had vacated the Vaigat, then modern surface circulation patterns may have been established in Disko Bugt, with the result that calf-ice would be predominantly routed northwards, exiting Disko Bugt through the Vaigat, and not southwest through Disko Bugt (*Fig. 5.5c*; Andersen, 1981a).

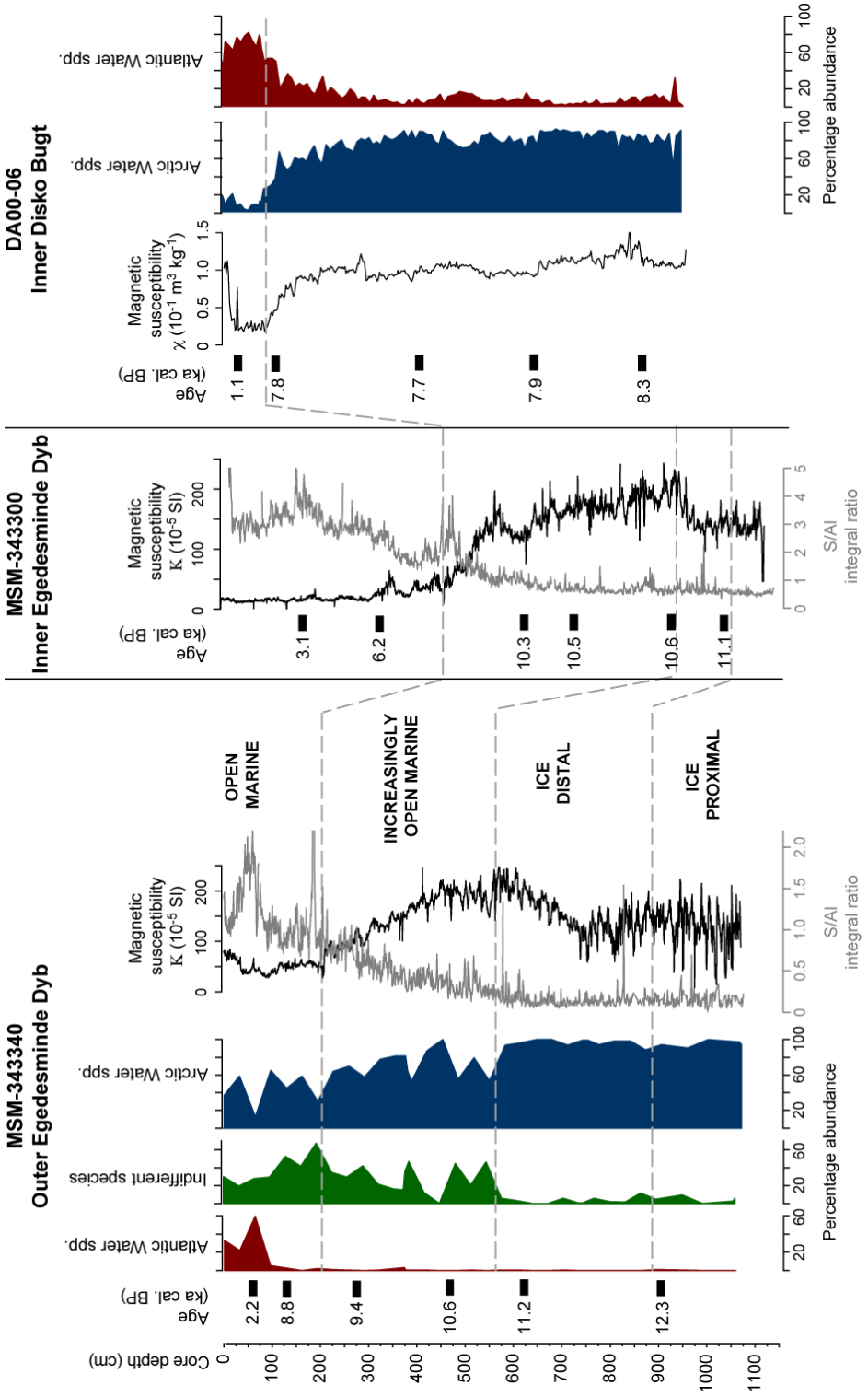

Figure 5.7 Summary data from three cores (MSM-343340, MSM-343300, DA00-06) along a transect between outer Egedesminde Dyb and inner Disko Bugt. Core scanning magnetic susceptibility (MS) data is shown for cores MSM-343340 and MSM-343300 and volumetric MS for core DA000-06. Broad environmental descriptions (ice-proximal glacimarine to open marine) are shown for MSM-343340 and DA00-06, and suggested environment descriptions for MSM-343300 based on MS and [S/Al] trends.

The southern coast of Disko Island appears to have been deglaciated later, with dates of 10 ka BP obtained from Qeqertarsuaq (shells, 9240±250 ^{14}C yr BP, Ingólfsson *et al.*, 1990) and Aqajaruat (gytjja, 8950±125 ^{14}C yr BP, Ingólfsson *et al.*, 1990) to the east, which suggest ice retreated rapidly across the bay. Indeed, dates from the outer coast of Arveprinsen Ejland, northeastern Disko Bugt, became deglaciated before 9.9-9.4 ka BP (8820±100 ^{14}C yr BP, Long *et al.*, 1999, and 8760±125 ^{14}C yr BP, Ingólfsson *et al.*, 1990, respectively, *Fig. 5.6*). These dates may more closely mirror the behaviour and retreat of the ice stream in Disko Bugt, retreating even faster than surrounding ice to the eastern coast of Disko Bugt (*Fig. 5.7c*).

Deglaciation of Jakobshavn Isbræ paused for at least 1000 years at the eastern margin of Disko Bugt. Ice retreated landwards of core POR 18 by 10.3 ka BP. The dominance of glacimarine foraminifera species in POR 18 suggest the ice margin was relatively stable, and stayed close to the core site until *ca.* 9.2 ka BP (Lloyd *et al.*, 2005). After 9.2 ka BP, there is a shift to warmer Atlantic Water species, suggesting ice retreated further landwards. This is supported by evidence from core DA00-06 (*Fig 5.6*), which indicates that the ice margin was located east of this site by *ca.* 8.3 ka BP, and was presumably grounded on Isfjeldbanken, a shallow sill with depths of 50-200 m at the mouth of Jakobshavn Isfjord (Lloyd *et al.*, 2005). A significant reduction in fine grained sedimentation (*Fig. 6* in Lloyd *et al.*, 2005) and an associated decline in sedimentation rate (13.81 mm a^{-1} to 0.24 mm a^{-1}), indicating a marked reduction in fine grained sedimentation produced at the ice terminus, records the withdrawal of ice from a grounded position on Isfjeldbanken into Jakobshavn Isfjord (Lloyd *et al.*, 2005). The timing of ice retreat into the Isfjord has been dated to 6.7 ka BP based on a new date from DA00-06, in addition to those presented by Lloyd *et al.* (2005) (J.M. Lloyd, personal communication).

As the Greenland Ice Sheet became land-based in Disko Bugt and areas to the south during the early Holocene, Jakobshavn Isbræ probably remained as the only significant contributor to sediment supply to the southwest of Disko Bugt. Thus, the sudden drop in sedimentation rate in core MSM-343340 shortly after 8.7 ka BP may be best explained by the retreat of Jakobshavn Isbræ into Jakobshavn Isfjord at 6.7 ka BP, identified by Lloyd *et al.* (2005). This would have permitted the establishment of modern Holocene oceanographic conditions (*Fig. 5.5d*) with

relatively warm and saline sub-surface waters penetrating into Disko Bugt (see increase in Atlantic water foraminifera species in MSM-343340 and DA00-06, *Fig. 5. 6*).

5.4.2 Driving mechanisms of deglaciation

These results indicate that different mechanisms controlled Jakobshavn Isbrae's mode of deglaciation across the central West Greenland shelf at various stages. Below, the relative importance of atmospheric warming, the influence of bedrock topography, relative sea-level change and oceanic warming in determining the timing and nature of ice retreat across the shelf are discussed.

Deglaciation of outer to mid-shelf outside Disko Bugt

Recent observations of rapid melting of floating ice shelves in Greenland and Antarctica (e.g. Rignot and Jacobs, 2002; Thomas, 2004; Payne *et al.*, 2004; Walker *et al.*, 2007; Holland *et al.*, 2008) has raised the possibility that marine forcing (by warmer ocean temperatures increasing melt rates at the marine-based ice sheet margin) as a driving mechanism for marine-based ice sheet collapse may be more important that previously thought. High-resolution foraminiferal evidence through the deglacial sequence in core MSM-343340 does not show any evidence for warming of sub-surface waters during initial deglaciation. The first evidence of a weak and sporadic Atlantic Water influence may be indicated by the low abundance of *R. turbinatus* from *ca*.11 ka BP. A significant Atlantic Water influence is not identified until after 8.7 ka BP, by which time ice had retreated onto land in Disko Bugt (e.g. Long and Roberts, 2001; Long *et al.*, 2006; Briner *et al.*, 2010).

Roberts *et al.* (2009; 2010) identify significant ice sheet surface lowering of more than 400 m in the Sisimiut area (*ca.* 200 km south of Disko Bugt; *Fig. 1.2*), beginning *ca.* 21 ka BP, before thinning rapidly until *ca.* 13.6 ka. This pattern of ice thinning is partly driven by increasing air temperatures and surface ablation into and during the Bølling-Allerød interstadial (GI-1e to GI-1a; Björck *et al.*, 1998) at *ca.* 14.7-12.65 ka BP (Roberts *et al.*, 2009; 2010). It is likely that surface melting of the neighbouring Jakobshavn Isbræ ice stream complex also took place at this time.

Roberts *et al.* (2009; 2010) find that rising RSL and ice sheet thinning combined to drive marine-based ice sheet retreat in the Sisimiut region. Modelling by Simpson *et al.* (2009) predicts a late and rapid deglaciation in Disko Bugt and the adjacent shelf, initiated by rising relative sea level between 12 and 11 ka BP. This corresponds very closely to the pattern of deglaciation identified in this study. To the east of site MSM-343340, the RSL highstand at Qeqertarsuatsiaq (116.07 ± 1.8 m a.s.l.), southwestern Disko Bugt (*Fig. 5.5*), was reached at *ca.* 11-10.2 ka BP (Long and Roberts, 2003). It is likely that fast-flowing ice extended onto the outer shelf at the LGM. The marine-based outlet glacier occupying outer Egedesminde Dyb would have been more susceptible to collapse by rising RSL than the ice grounded on the shallow banks at either side of Egedesminde Dyb. The style of retreat is likely to resemble that of a calving bay re-entrant (e.g. Hughes, 2002; Leventer *et al.*, 2006). This model for deglaciation is favoured by the bathymetry in the Disko Bugt area, with shallow banks either side of the deep water trough. Indeed, the morphology of the Hellefiske moraines either side of outer Egedesminde Dyb, which are orientated in a landward direction adjacent to the trough (*Fig. 5.6*), appear to support a calving bay.

Continued increasing RSL and surface lowering of ice occupying the trough from Disko Bugt to the outer shelf is likely to have destabilised and floated marine-based ice at the grounding line, reducing the friction between ice stream and bedrock, enabling higher flow velocities and subsequent ice retreat. Thinning of tidewater ice streams reduces the effective bed pressure at the marine terminus, increasing buoyancy of the ice front, and resulting in accelerated ice flow. The reduction in backforce/stresses is propagated 'upstream' in a process termed the "Jakobshavn effect" (Hughes, 1986). This would have resulted in increased fracturing (crevassing) and thinning during deglaciation, enabling greater delivery of meltwater to the base of the ice stream. This would have perpetuated the so-called "Zwally effect", in which increased surface ablation and meltwater penetration to the ice sheet bed facilitate higher ice flow velocities through increased basal lubrication and subsequent ice/bed decoupling (Zwally *et al.*, 2002). The geometry of Outer Egedesminde Dyb (straighter than inner Egedesminde Dyb, with no shallow topography) is likely to have facilitated a rapid deglaciation (Warren, 1991). The

retreat of the grounding line downslope into deeper water would have further increased the drawdown of interior ice, hastening ice retreat (Hughes, 1992).

Terrestrial geomorphological evidence in eastern Disko Bugt supports higher ice flow velocities and ice/bedrock decoupling (Roberts and Long, 2005). Roberts and Long (2005) suggest the high density of short bedforms (particularly whaleback bedforms modified by plucking) adjacent to Jakobshavn Isfjord resulted from increased ice velocities, which promoted greater basal erosion rates, and subsequent plucking. Plucking of bedforms may also have been promoted by basal pressure and freeze-thaw fluctuations linked to greater meltwater penetration to the base of the ice stream. Indeed, RSL investigations by Long and Roberts (2003) identify rapid and synchronous glacio-isostatic uplift across Disko Bugt, suggesting rapid ice thinning caused by atmospheric warming was responsible for initial deglaciation. The absence of evidence for a punctuated deglaciation from RSL curves outside Disko Bugt may not be surprising if these pauses were short-lived or the isostatic response of the shelf was "dampened" by seawater replacing ice on the shelf.

Deglaciation of the mid-shelf to inner-Disko Bugt

The role of topographic controls on ice stream dynamics has been widely debated, particularly for central West Greenland (e.g. Warren and Hulton, 1990; Warren, 1991; Weidick, 1996; Roberts and Long, 2005). Understanding the deglaciation of Jakobshavn Isbrae is an interesting case. The geometry of the outer shelf is dominated by a typically wide, deep, and straight, glacially-abraded trough (outer Egedesminde Dyb, *Fig. 5.5*), while the inner shelf consists of deeper (greater than 900 m, and shoaling to *ca.* 400 m in eastern Disko Bugt), narrower, and atypically non-linear/curvilinear channels. This trough is bisected by two notable bedrock highs; one dividing Egedesminde Dyb into an outer and inner trough on the shelf west of Disko Bugt, and a second between Qeqertarsuaq and Aasiaat at the entrance to Disko Bugt (*Fig. 5.5*) (Long and Roberts, 2003). The fjords in Disko Bugt are over-deepened, with Jakobshavn Isfjord exceeding 1,500 m in depth (Clarke and Echelmeyer, 1996), and have further 'pinning' points. Ice streams were topographically routed in Disko Bugt, and probably converged leading to a massive drawdown of ice from Disko Bugt and north of Nordre

Strømfjord to form a large coalesced ice stream on the outer shelf (Roberts and Long, 2005). On the outer shelf, the glacial Jakobshavn Isbrae probably exceeded 50 km in width and *ca.* 800-1000 m in thickness (Long and Roberts, 2003).

Since it is likely that the outer shelf deglaciated rapidly, it is possible that the *ca.* 1000 year difference in minimum ages for deglaciation between core MSM-343340 (*ca.* 12.3 ka BP) and MSM-343300 (*ca.* 11.1 ka BP; *Fig. 5.5*) suggests a slow-down or pause in deglaciation outside Disko Bugt. A slow down in ice retreat is most easily explained by topographic 'pinning' of the ice stream terminus as the grounding line retreated into the shallower waters between outer and inner Egedesminde Dyb. The bank bisecting this trough is at least *ca.* 160 m shallower than outer Egedesminde Dyb and *ca.* 550-700 m shallower than water depths in parts of inner Egedesminde Dyb (e.g. Harff, 2007). This would have resulted in a loss of basal buoyancy and increased ice-bedrock coupling, thereby reducing ice drawdown and increasing ice stream stability (Hughes, 1986; Warren and Hulton, 1990; Hughes, 1992; Warren, 1992).

5.4.3 Initiation of West Greenland Current in Disko Bugt

The WGC was the dominant influence on Baffin Bay oceanography before the last deglaciation because extensive ice cover in northern Baffin Bay prevented inflow of cold, relatively fresh, Arctic water through Nares Strait and other northern Arctic Channels (Aksu and Piper, 1979; Aksu and Mudie, 1986). However, this regime changed as these channels opened up during deglaciation, with increasing influence of cold, low-salinity waters from the Arctic Ocean.

The majority of relatively warm, saline WGC water is deflected in westward gyres at Davis Strait and west of Disko Bugt. However, the WGC water that penetrates into northern Baffin Bay provides a good indication of the strength (relative temperature) of the northwards-flowing current. Early Holocene penetration of Atlantic Water along West Greenland and into northern Baffin Bay, and subsequent changes in the relative strength of the WGC, is well documented (Donner and Jungner, 1975; Kelly, 1979, 1985; Osterman and Nelson, 1989; Feyling-Hanssen and Funder, 1990; Ingólfsson *et al.*, 1990; Funder and Weidick, 1991; Bennike *et al.*, 1994; Dyke *et al.*, 1996; Kelly *et al.*, 1999; Bennike *et al.*, 2000; Levac *et al.*, 2001; Bennike, 2004;

Knudsen *et al.*, 2008b). In central East Greenland, Hjort and Funder (1974) found that the subarctic bivalves *Mytilus edulis* and *Chlamys islandica* had expanded into areas no longer habitable between *ca.* 9 and 5.9 ka BP (8400-5500 ^{14}C yr BP). They suggest larvae must have been transported here in the West Spitsbergen Current, implying a greater influx of Atlantic Water along East Greenland, and therefore contributing to a relatively warmer, more saline, WGC. Knudsen *et al.* (2008b) suggest increasing WGC influence resulted in changes in the position of the sea-ice limit in northern Baffin Bay after *ca.* 10.9 ka BP, as indicated by increasing planktonic foraminifera flux, and supported by heavier benthic foraminifera δ^{18}O values. The initial increase in the flux of dinoflagellate cyst after *ca.* 10.4 ka BP (9275±110 ^{14}C yr. BP, Ua-4448) indicates continued amelioration of surface waters (Levac *et al.*, 2001). Radiocarbon dating of the earliest Subarctic mollusc species (e.g. *Mytilus edulis* Linné, *Chlamys islandica* Møller, *Balanus crenatus* Bruguière*, Balanus hammeri* (Ascanius)) indicate the WGC penetrated into the Thule area of northern Baffin Bay by *ca.* 10 ka BP (9,150±95 ^{14}C yr. BP, K-4781, Mörner and Funder, 1990; Kelly *et al.*, 1999). However, the relative strength of the WGC fluctuated during the Early Holocene, with cooling episodes around 10 ka BP and 8.8 to 8.2 ka BP (Knudsen *et al.*, 2008b).

Benthic foraminiferal assemblages in core MSM-343340 indicate relatively warm Atlantic-sourced water impinged on the shelf outside Disko Bugt (in outer Egedesminde Dyb) after *ca*. 8.7 ka BP (FAZ 4 in *Fig. 4*). However, there may have been a weak WGC influence from *ca.* 10 ka BP, with brief incursions likely facilitated by reduced meltwater flux from the retreating ice sheet, followed by gradual sub-surface warming after *ca.* 9.4 ka BP. Lloyd *et al.* (2005) identify warming of bottom waters in eastern Disko Bugt after 9.2 ka BP (core POR18). However, the major faunal shift, which is similar to that identified in MSM-343340, takes place further up-core, between PORZ2 and PORZ3, for which there is no chronological control. The penetration of warm Atlantic water into Disko Bugt at, or after, 8.7 ka BP may, therefore, be reasonable. Warming indicated by foraminiferal assemblages in core MSM-343340 corresponds well to the earliest occurrence of boreal molluscs in central West Greenland, which is dated to *ca.* 8.9 ka BP (8,360±120 ^{14}C yr. BP, K-5144, Funder and Weidick, 1991).

These data suggest a warming of the WGC penetrating to northern Baffin Bay (i.e. greater Atlantic Water entrainment) began at least a few hundred years before major warming in the Disko Bugt area (at sites MSM-343340 and POR-18). Warm Atlantic water incursions to inner shelf areas north of Disko Bugt suggest a weakening in Polar water influence at this time (e.g. Dyke *et al.*, 1996). However, the absence of an Atlantic Water signal on the shelf in the Disko Bugt area at this time suggests the northwards-flowing WGC was diluted (i.e. meltwater mixed with, and lowered, WGC bottom water temperatures) or re-routed off the shelf by glacial meltwater exiting Disko Bugt from the retreating ice margin, thereby restricting access into Disko Bugt. Indeed, the lag between increased calcareous dissolution (here assumed to be due to reduced sedimentation, *Fig. 5.4*) and a significant increase in Atlantic Water-indicator species suggests reduced glacimarine influence was followed later by increasing Atlantic Water inflow. However, the absence of a clear Atlantic signal in close proximity to the ice margin during deglaciation does not preclude an oceanic influence on ice retreat. Motyka *et al.* (2003) point out that warmer, saline ocean water would be cooled and diluted as it mixes with subglacial meltwater flux at the ice terminus. It may not, therefore, be possible to identify a true Atlantic Water influence on ice margin stability during initial deglaciation due to the dilution from meltwater flux.

The withdrawal of ice into Jakobshavn Isfjord appears to have had a major impact on Disko Bugt, reducing the sediment flux derived from meltwater plumes and ice-rafting, as well as substantially reducing the influence of meltwater discharged from Jakobshavn Isbræ. Consequently, in the absence of a substantial volume of meltwater to deflect surface and subsurface currents, the modern circulation pattern of water masses in Disko Bugt was established. Instead of meltwater and icebergs exiting Disko Bugt to the west, the modern regime is characterised by a counter-clockwise surface circulation, with waters entering from south-western Disko Bugt, and exiting to the north through the Vaigat, which became the main conduit for icebergs and meltwater leaving Disko Bugt (Andersen, 1981a).

5.5 Chapter summary

In total, fast-flowing ice on the West Greenland shelf retreated some 180 km to eastern Disko Bugt between 12.3 and 6.7 ka cal. BP, averaging roughly 30 m a^{-1}. Initial deglaciation appears to have been conditioned by lowering of the ice sheet surface due to atmospheric warming and/or dynamic thinning. As RSL increased, thinner ice resting on shallow banks would have been readily destabilised (due to lower basal buoyancy) and collapsed. Greater ice thicknesses and drawdown of interior ice (due to the removal of adjacent 'butressing' ice) probably maintained ice flow out of Disko Bugt through Egedesminde Dyb after the initial collapse of adjacent (inter-ice stream) marine-based ice. The subsequent deglaciation of the mid-shelf to the modern coastline in Disko Bugt is characterised by a slower and episodic marine-based ice retreat, suggested to be mainly the result of topographic pinning as the ice retreated between shallower and deeper waters.

Chapter 6

DEGLACIAL AND HOLOCENE PALAEOCEANOGRAPHIC RECORD FROM UUMMANNAQ FJORD, WEST GREENLAND

Kerstin Perner provided loss-on-ignition and moisture content data from core MSM-343520. XRF and magnetic susceptibility core scanning data was undertaken aboard the R/V "Maria S. Merian" shortly after core retrieval. Kerstin Perner and Matthias Moros (IOW) provided digital X-ray radiographs of core MSM-343520_G and grain size data obtained by sieving of coarse grain size fractions. Noortje Dijkstra (University of Amsterdam) provided grain size data analysed by laser diffraction. David H. Roberts provided unpublished cosmogenic radionuclide ages obtained from inner Uummannaq Fjord which permits a greater understanding the deglacial chronology from the mid- to inner-shelf.

Chapter 6

Deglacial and Holocene palaeoceanographic record from Uummannaq trough, West Greenland

6.1 Introduction

Few studies have investigated the palaeoenvironmental and glacial history of the onshore and offshore Uummannaq area. Our current understanding of the timing of deglaciation in this part of central West Greenland is limited. Following on from this, our understanding of the driving mechanisms behind ice sheet retreat in this area is also limited.

This chapter aims to assess the timing of deglaciation of the continental shelf in the Uummannaq area and compare deglaciation here to Disko Bugt and the south. The chapter will also investigate the interaction between ocean circulation and the ice sheet in Uummannaq, specifically identification of the meltwater influence from the Greenland Ice Sheet and initiation of the WGC. High resolution analysis of the full Holocene record will also allow investigation of the variability of the WGC flow (particularly temperature and salinity) that may be linked to ice margin response. Investigating ice margin reponse to short-lived climate events and changes in ocean temperature during the Holocene provides an opportunity to assess ice-ocean interactions in central West Greenland.

6.2 Results

6.2.1 Chronology and sedimentation rates

The age model for core MSM-343520 is based on ten AMS radiocarbon dates from a combination of benthic foraminifera (six dates) and intact shells (four dates) for the gravity core (*Table 6.1*), and ^{210}Pb and ^{137}Cs dating for the multicore.

Linear sedimentation rates between radiocarbon-dated horizons are used to produce the age-depth model for core MSM-343520_G. Sedimentation rates are relatively consistent, varying between 0.52 to 1.11 mm a^{-1} (*Fig.6.1*), though are generally higher in the lower part of the core,

and show a slight decline at *c*a. 5 ka BP. An AMS radiocarbon date of 10.9 ka BP (11,158-10,630 cal. yr BP) at 9.01 m core depth provides a minimum date on deglaciation from the Uummannaq shelf. The absence of sufficient calcareous material below 9 m prevents greater age control. All radiocarbon dates lie in stratigraphical order (*Table 6.*1) and the sedimentation rate remains relatively high and constant throughout the core (*Fig. 6.1*). While there is evidence of reworking in the gravity core, intense bioturbation is limited to the upper 50 cm of the core (see 6.2.2 below). Each 2 cm sample represents an 18 to 38.5 year time slice, before accounting for the effects of bioturbation.

The 'Simple' (CF:CS) model was used to construct the ^{210}Pb age-depth model (*Fig. 6.2c*). The decrease in $^{210}Pb_{excess}$ closely resembles a near-ideal exponential decrease in ^{210}Pb activity, and supports the use of the 'Simple' model (Robbins, 1978; Appleby and Oldfield, 1978) (*Fig. 6.2a*). Since there is very little variability in grain size distribution throughout the core (samples typically contain *ca.* 33.1% clay, 62.9% silt, and 4% sand) (Krauβ, 2009), there should not be any grain size-related variations in ^{210}Pb activity. ^{137}Cs activity counts were very low (typically less than 1.8 mBq g^{-1}), though nonetheless supports the ^{210}Pb chronology shown in *Fig. 6.2c*. Variability in ^{137}Cs counts between samples may suggest that the sediment has not been significantly reworked (e.g. by bioturbation) following deposition.

Both the multicore and gravity core of MSM-343520 therefore provide a reliable, high-resolution record of ice-marginal activity and oceanographic conditions since deglaciation. Multicore (MSM-343520_MC) and gravity core (MSM-343520_G) data are presented seperately because there was insufficient calcareous (dateable) material for tie-in dates that could be used to create a reliable composite record (spice records together) for station MSM-343520.

Core depth (cm)	Lab. code	Material	14C age ± 1σ (yr BP)	Mean calibrated age (yr BP)	Age range 2σ (yr BP)
41	Poz 22364	Shell	1205 ± 30	744	831-666
161	Poz 22365	Shell	2260 ± 30	1867	1963-1780
216 – 218	LuS 8601	Benthic foraminifera	3055 ± 60	2836	2980-2714
328 – 330	Lus 8550	Benthic foraminifera	4730 ± 70	4995	5220-4821
452 – 456	Lus 8549	Benthic foraminifera	6125 ± 65	6555	6713-6400
480	AAR 11700	Bivalve	6326 ± 43	6790	6906-6668
556 – 560	Lus 8548	Benthic foraminifera	7065 ± 70	7547	7666-7424
640 – 642	Poz 30962	Bivalve	7900 ± 40	8364	8457-8279
692 – 694	Lus 8547	Benthic foraminifera	8340 ± 70	8896	9106-8655
896 – 906	Lus 7707	Benthic foraminifera	9970 ± 100	10908	11158-10630

Table 6.1 Radiocarbon dates from core MSM-343520_G. All dates have been calibrated in Oxcal v4.1 (Bronk Ramsey, 2009) using the Marine09 calibration curve (Reimer *et al.*, 2009), with ΔR=0±0.

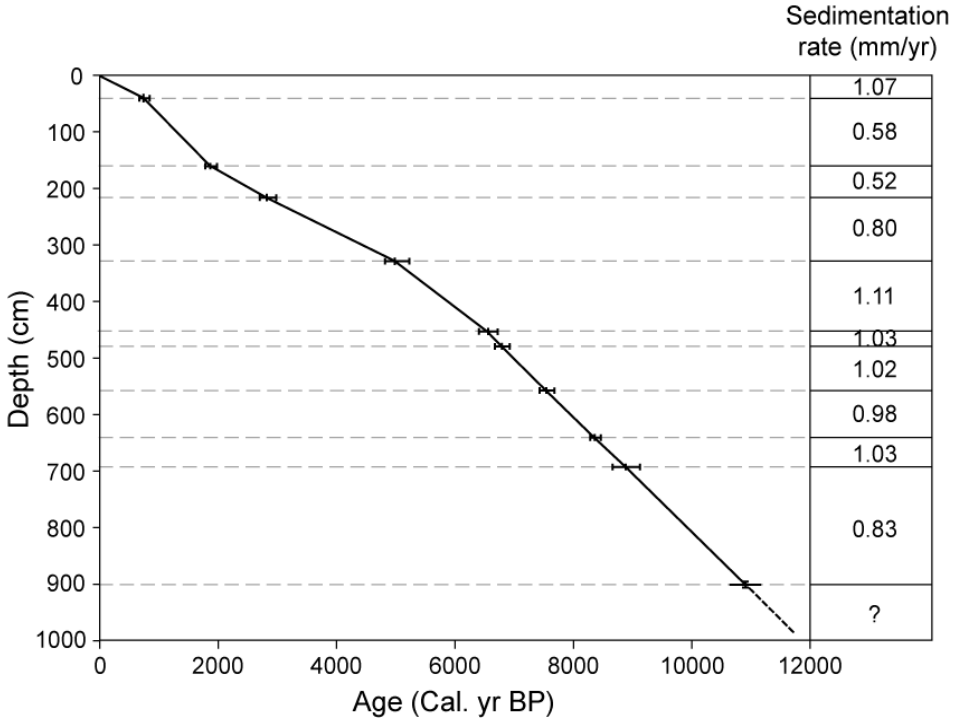

Figure 6.1 Age-depth model for core MSM-343520_G. Age-depth model for MSM-343520_G is based on linear interpolation between mean calibrated radiocarbon ages. Grey error bars indicate the two standard deviation age range.

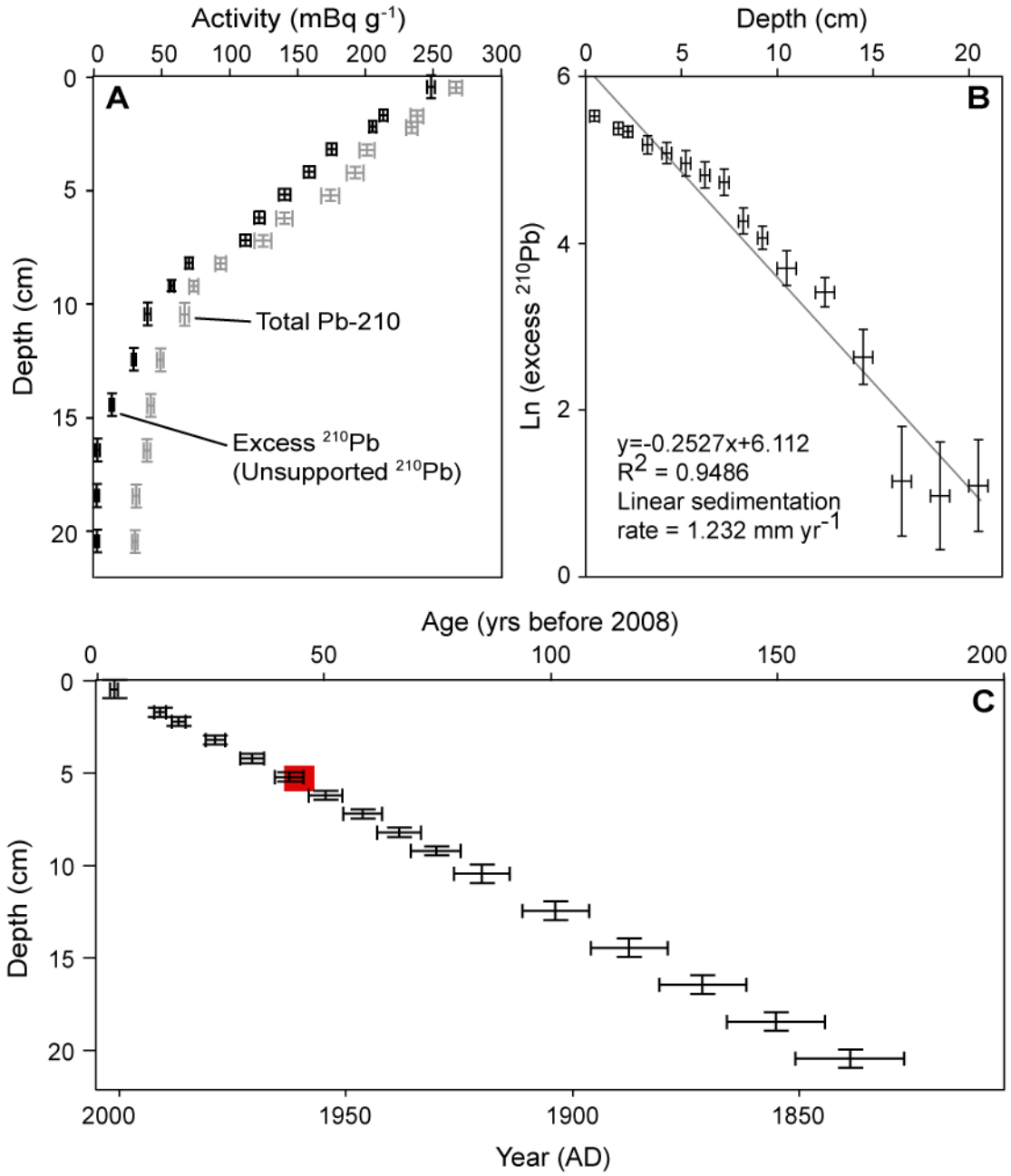

Figure 6.2 ^{210}Pb age-depth model for multicore MSM-343520_MC; (**A**), Total ^{210}Pb (mBq g^{-1}; grey marks) and excess ^{210}Pb (unsupported ^{210}Pb; black marks) with 1σ error bars, plotted versus core depth. (**B**), Calculation of linear sedimentation rate. (**C**), Age-depth model based on the 'Simple' (CF:CS) model with 1σ x-axis error bars. The red square marks the estimated position of the A.D. 1963 ^{137}Cs bomb spike. The usefulness of ^{210}Pb dating of sediments extends to just before A.D. 1900. A linear approximation for the sedimentation rate (**B**) appears to be robust for this interval, and in the absence of other dating evidence, is extended throughout core MSM-343520_MC.

6.2.2 Core sedimentology and geochemistry

In the following section, descriptions of core sedimentology are based on visual core logging, analysis of X-ray radiographs and grain size analyses, complemented by geochemical analyses including magnetic susceptibility and major elemental analyses by scanning XRF. The close correspondence between silt/sand (>4 μm) content and the [Si/Al] XRF ratio throughout core MSM-343520_G, shown in *Fig. 6.3*, suggests [Si/Al] may provide a reasonable high-resolution record of changes in clay content. This ratio varies depending on the relative abundance of quartz (SiO_2; coarse grain fractions) to aluminosilicates, which form a major component of clay minerals (e.g. Feniak, 1944). Higher [Si/Al] XRF ratios should therefore be linked to greater silt/sand content and lower clay content.

FAZ 1a (Before ca. 11 ka BP, 989-915 cm)

Sediments in FAZ 1a (989-922 cm, except 967-962 cm) are classified as clay (55.1-79.5 % clay content) according to analyses by laser diffraction, and have a high water content (typically >40%, *Fig. 6.4*). X-ray radiographs show parallel laminated mud from 989 to 969 cm (*Fig. 6.5H*). Visual core descriptions indicate these are alternating layers of clay and clay/silt with fine sand, possibly rhythmically deposited cyclopels. Coarse sediment particles (defined as particles > 63 um and > 2 mm) are abundant from 989 to 953 cm (11.8-11.4 ka BP) and 936 to 922 cm (11.3-11.1 ka BP) (see *Fig 6.4*). The laminated sediments grade into weakly stratified, matrix-supported diamict (978-968 cm), which is overlain by clast-poor clays. X-rays suggest there may be loading structures beneath a large (>3.5 cm) clast at the lower boundary of this unit, though visual inspection suggests this is a void that opened as the sediments dried during core analyses and sampling. The very dark greyscale X-ray radiograph for this area indicates high density (see shaded region, *Fig. 6.4*), confirmed by the high dry bulk density (1.37 g cm^{-3}). Other characteristics include low water content (30.1%), higher coarse-grained sediment content, high magnetic susceptibility (*ca.150* SI), and low LOI (*ca.* 4.6%). The C/N ratio for the top of this interval is very high (31.8). A small number (17) of benthic foraminifera were identified in the centre of this unit.

The sediments from 962-957 cm are clay with weakly developed diffuse and wispy laminations. Coarse sediments (clasts > 2 mm in *Fig. 6.3* and % sand > 63 µm in *Fig. 6.4*) are absent from this unit, though can be identified between 954-957 cm. Coarse particles are generally absent from the clay sediments in the interval 954-936 cm, apart from a brief section where there is a clustering of denser material (*Fig. 6.5f*) indicating turbidity (possibly traction current activity), with a possible rip-up from the underlying unit.

Coarse sediment particles are common from 936 cm to 922 cm. This interval contains textural variations where higher concentrations of coarse sediment can be identified. Cross-bedded ripples become more distinct upcore in this section (lower part of *Fig. 6.5h*), and correspond to an upward coarsening in sediments from clay to fine sandy mud. A continuous upcore presence of foraminifera begins from 928 cm. The boundary between this unit and the overlying diamict (FAZ 1b) at 922 cm appears sharp.

FAZ 1b (ca. 10.7-11 ka BP, 915-879 cm)

Sediments from 922 cm (the upper 7cm of FAZ 1a) to 881 cm (*Fig. 6.3* and *6.*4) are primarily massive, with abundant coarse-grained clasts. These sediments are similar to the unit between 967 cm and 962 cm, with low water content (typically 35-38%), high MS (*ca.* 250 SI), higher DBD (*ca.* 1 g cm^{-3}), which is further suggested by low greyscale values from the X-ray radiograph (*Fig. 6.4*). The [K/Ti] XRF integral ratio is low (< 2), as is the LOI (< 6%), while the C/N ratio for this interval decreases. The sediments (< 2 mm fraction) in this zone are predominantly mud, typically containing 50-60% clay. Benthic foraminifera increase in abundance, and are present throughout this zone.

FAZ 2 (10.7-7.3 ka BP, 879-531 cm)

There is a gradual transition in the lower part of FAZ 2 (879-867 cm) to less dense sediments (higher water content, lower DBD) with declining coarse grain content. Sediments above 867 cm are composed of predominantly poorly or very poorly sorted clayey mud. Mean grain size (and sorting) generally increases from the base of the core to 700 cm, from which there are small, but less distinct, changes in mean grain size trends in the sediments less than 2 mm in

size. There are chondrites (pyrite-infilled burrows) identifiable in X-ray radiographs between 850 cm and 750 cm (*Fig. 6.5c*). Above this, there is little evidence of bioturbation until 570 cm, where there are some sub-vertical burrows between 570 cm and 550 cm (*Fig. 6.5b*), followed by a small occurrence of pyrite-infilled burrows between 545 cm and 520 cm.

FAZ 3 (7.3-3.5 ka BP, 531-251 cm)

There is a slight upward coarsening in mean grain size (not shown) through FAZ 3, with sediments grading from clayey mud (below 450 cm) to coarse silt (*Fig. 6.3*). There is evidence of burrowing in this zone, though this does not appear as intense as in preceding or following sediments. Loss-on-ignition values are *ca.* 6.5%, and XRF integral ratios for [S/Al] increase from *ca.* 10 to 12, while [K/Ti] decreases slightly from *ca.* 1.5 to 1. Magnetic susceptibility is relatively high, and increases further, from 250 SI to 300 SI coincident with changes in XRF ratios at *ca.* 370 cm.

FAZ 4 (3.5 ka BP to present, 251-0 cm)

Silty mud sediments continue throughout most of FAZ 4, with sandy mud present in the upper 20 cm of the core (*Fig. 6.3*). Above 60 cm core depth, bioturbation becomes more intense, particularly between 43 cm and 20 cm (see *Fig. 6.5a*). While there is less bioturbation in the upper 20 cm of the core, these sediments contain a high percentage (up to 33 %) of sand. Sediments in FAZ 4 are also characterised by gradually decreasing C/N ratios (from *ca.* 11 to 9.9), generally increasing [S/Al] and [Si/Al] XRF ratios, and a generally decreasing [K/Ti] XRF ratio. Magnetic susceptibility initially declines slightly, before stabilising at *ca.* 220 SI, while LOI values increase from 6.1% to 8% between 250 cm and 180 cm, before steadily declining to *ca.* 6.4% at the top of the core. Dropstones (clasts > 2 mm) in FAZ 4 are rare, and are significantly less abundant compared to lower sediments. Foraminiferal abundance in FAZ 4 is generally high, particularly in the upper 120 cm.

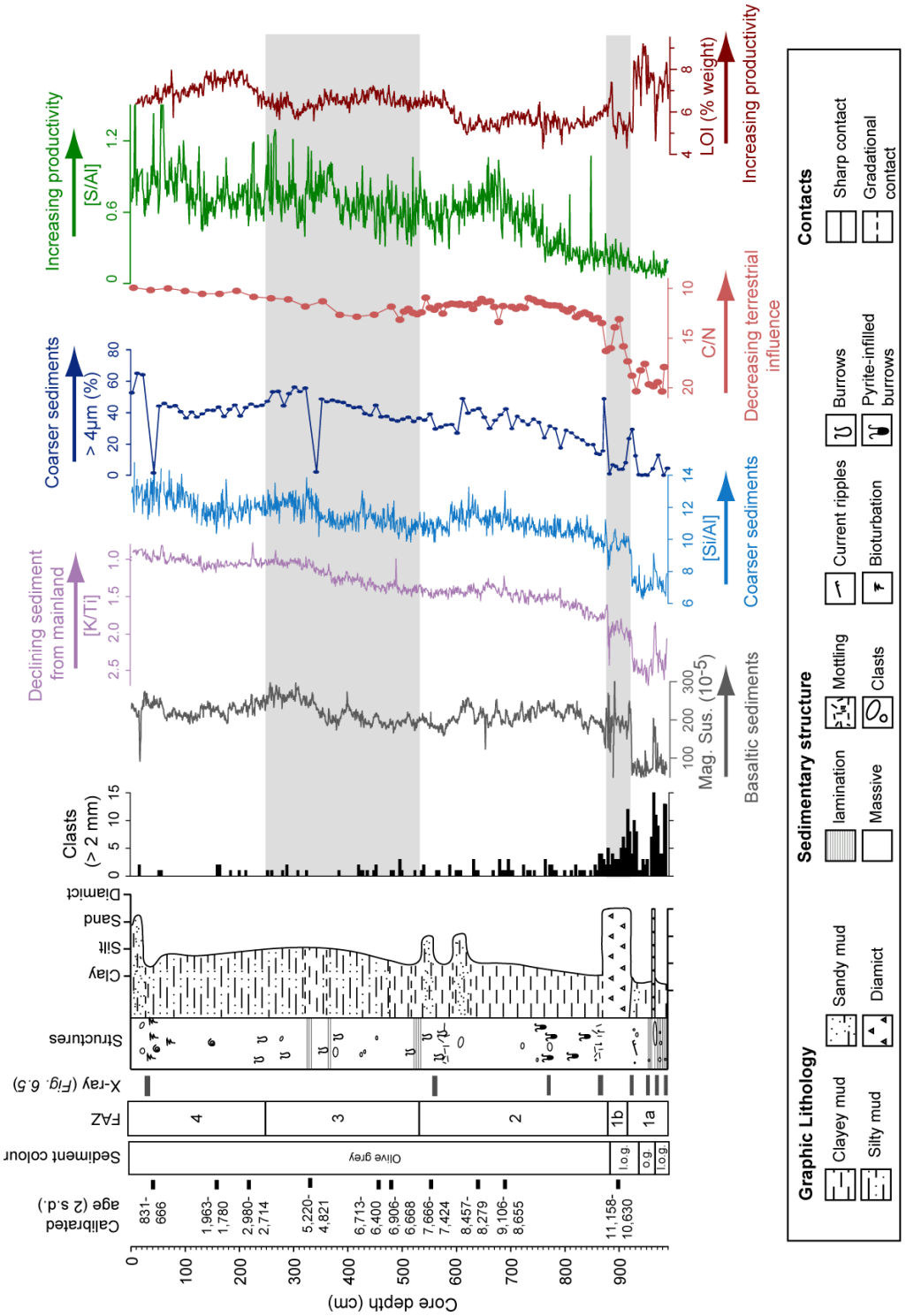

Figure 6.3 Stratigraphy of core MSM-343520_G, with graphs showing sedimentological and geochemical data. Grey shading highlights the position of foraminiferal assemblage zones. The position of example X-ray radiographs are marked, and are shown in order, from A at the top of the core, to H at the base of the core. Sediment colour abbreviations are; o.g., olive grey; l.o.g., light olive grey.

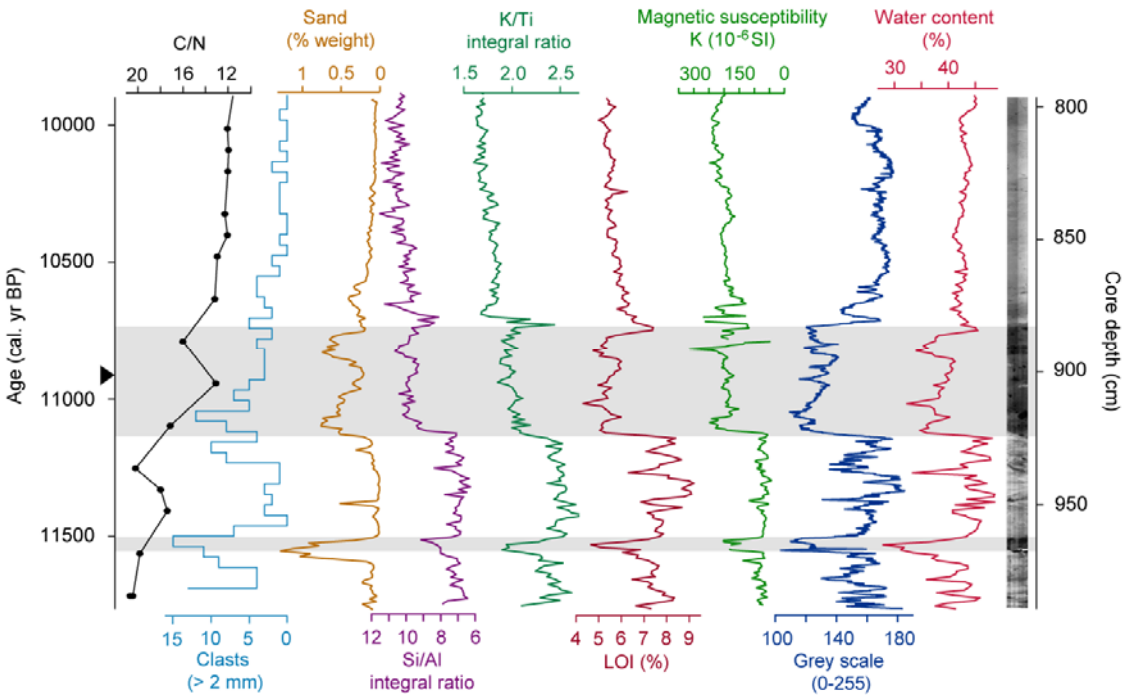

Figure 6.4 Sedimentology and geochemistry for the lower 2 metres of core MSM-343520_G, with X-ray radiographs shown on the right. Data is shown against extrapolated age-depth model and core depth. Grey shading shows the position of diamict core sections (dark intervals on the X-ray radiograph). The unshaded intervals below 900 cm are characterised by laminated sediments, while sediments in the upper unshaded interval is characterised by more hemipelagic sedimentation,

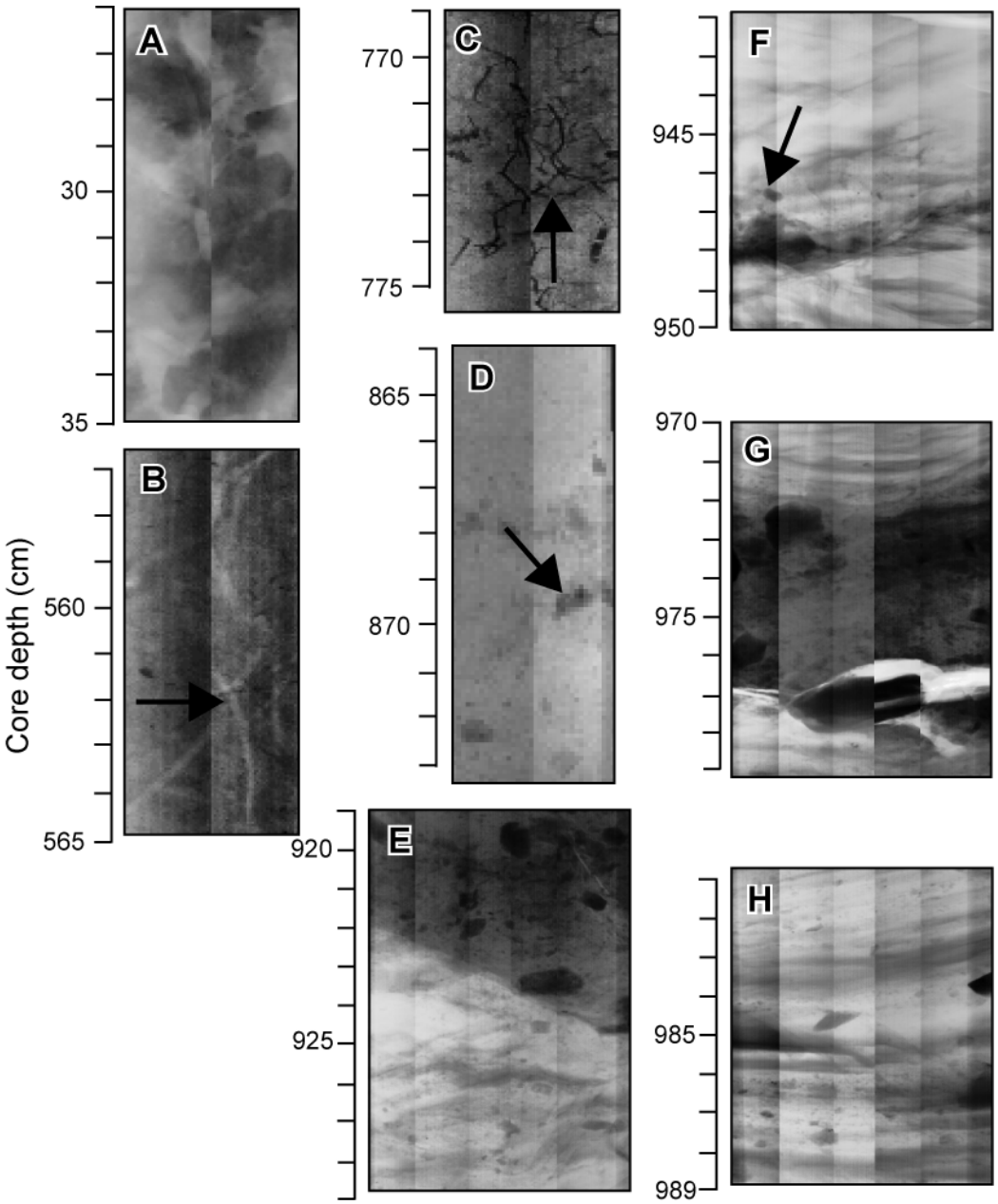

Figure 6.5 Example X-ray radiographs of sections of core facies in core MSM-343520_G (Positions of example sections are marked on *Fig. 6.3*): (**A**), intense bioturbation; (**B**), sub-vertical burrows; (**C**), pyrite-filled ichnofossils; (**D**), hemipelagic sedimentation with ice-rafted dropstone indicated by arrow; (**E**), transition from ripple, cross-laminated sediment to overlying diamict; (**F**), weakly laminated muds (predominantly clay) with wispy laminae and evidence of turbidty and possible rip-up (indicated by arrow); (**G**), diamict overlain by parallel laminated clayey mud; (**H**), laminated cyclopels with interspersed coarse grained clasts (> 2 mm), interpreted to be IRD deposited as sediment is released from melting icebergs.

6.2.3 Foraminiferal biostratigraphy

Forty-one species (23 agglutinated and 18 calcareous) were recorded from the sediment core. The total assemblage (TA; relative abundance of combined agglutinated and calcareous faunal counts) of core MSM-343520_G is shown in *Fig. 6.6*. Of the 226 samples containing benthic foraminifera, 172 samples have statistically robust counts exceeding 250 specimens, 31 samples contain 100-249 specimens (samples below the grey dashed line through 'total count' data in *Fig. 6.6*), and 23 samples contain less than 100 specimens (omitted from *Fig. 6.6*). *Post mortem* dissolution of calcareous fauna appears to be a major issue affecting assemblages in core MSM-343520_G, particularly between 6 ka BP and 2 ka BP (*Fig. 6.6*). For this reason, relative frequencies of agglutinated (AA) (*Fig. 6.7*) and calcareous assemblages (CA) (*Fig. 6.8*) have also been calculated separately. The AA data consists of 186 samples containing more than 100 specimens (of which 93 samples contain more than 250 specimens), while the CA data consists of only 74 samples containing more than 100 specimens, and only 7 containing more than 250 specimens. Since calcareous foraminifera in multicore MSM-343520_MC (*Fig. 6.9*) are also poorly preserved, and foraminifera counts are generally low throughout the majority of the multicore, only the agglutinated fauna are presented here. Results discussed in Chapter 4 indicate that reliable interpretations of sub-surface water conditions can indeed be made using solely agglutinated fauna.

Constrained cluster analysis of the TA of MSM-343520_G in CONISS (Grimm, 1987) identifies four key foraminiferal assemblage zones in core MSM-343520_G (FAZ 1 to 4). A barren zone at the base of the core, termed FAZ 1a, is also described in the following analysis. Cluster analysis of the AA data in MSM-343520_MC identifies three assemblage zones (FAZ 5 to 7). These foraminiferal assemblage zones are used to describe faunal changes in MSM-343520_G and MSM-343520_MC in turn below.

FAZ 1a (Before ca. 11 ka BP, 989-915 cm)

Benthic foraminifera are absent or in low abundance in FAZ 1a, while no foraminifera were found in the lower 20 cm of the core. *Miliolinella subrotunda* (37% of TA) and *Cassidulina*

reniforme (18% of TA) occur in isolated samples at the base of the core. Fragile calcareous foraminifera specimens are well preserved in FAZ 1a.

FAZ 1b (ca. 10.7-11 ka BP, 915-879 cm)

FAZ 1b is characterised by the presence of foraminifera throughout the zone, and higher foraminiferal concentrations (3-124 specimens per cm^3). *Spiroplectammina biformis* (8-23%), *C. reniforme* (8-40%), *Elphidium excavatum* f. *clavata* (6-41%), and *Stainforthia feylingi* (up to 27%) are abundant in the TA of this zone; species often found in glacimarine environments (e.g. Schafer and Cole, 1986; 1988). *Trochammina nana* (up to 47% of TA) and *Recurvoides turbinatus* are also present and are linked to Atlantic water influence (e.g. Jennings and Helgadóttir, 1994; Hald and Korsun, 1997; Lloyd, 2006a).

FAZ 2 (10.7-7.3 ka BP, 879-531 cm)

Foraminifera concentration increases from *ca.* 50 specimens per cm^3 at 10.7 ka BP to *ca.* 300-600 specimens per by 9.7 ka BP. Apart from very high concentrations at *ca.* 8.7 ka BP and 8.2 ka BP (up to 3000 specimens per cm^3), foraminiferal concentrations remain fairly stable until the start of FAZ 4. Low counts of organic test linings from calcareous foraminifera suggest preservation throughout FAZ 2 is good, particularly before 8 ka BP. Agglutinating foraminifera are particularly dominant before 9 ka BP, followed by an increasing abundance of calcareous fauna. *Cuneata arctica* and *S. biformis* are abundant (both 20-50% of TA) in FAZ 2, although the latter declines steadily after *ca.* 9 ka BP. *Cassidulina reniforme* occurs frequently (typically 10-20% of TA), with occasional *E. excavatum* f. *clavata* (generally <10%). A notable feature of this zone are the two abundance spikes of *Stainforthia feylingi* at *ca.* 9 to 8.7 ka BP (up to 72% of TA) and at *ca.* 8.4 ka BP (up to 56% of TA), coincident with decreases in *C. arctica* and *S. biformis*. *Eggerella advena* appears from 9.7 ka BP, and is common (10-23% of TA) from 9 ka BP to 8.4 ka BP, before maintaining low abundances through overlying sediments (typically <5%). There are rare occurrences of species linked to Atlantic water influence throughout this interval, including *R. turbinatus, T. nana, Bolivina pseudopunctata, Bucella frigida,* and *Nonionellina labradorica* (all <5% of TA). *Adercotryma glomerata* (up to 11% of TA) appears

after *ca.* 8 ka BP, together with *Saccammina difflugiformis* (<4% of TA). This is followed, at *ca.* 7.7 ka BP, by an increase in *N. labradorica* (up to 11% of TA).

FAZ 3 (7.3-3.5 ka BP, 531-251 cm)

FAZ 3 is characterised by poor carbonate preservation indicated by high test lining counts and patchy calcareous fauna. Faunal trends are therefore described using AA and CA data to avoid problems associated with *post mortem* losses of foraminiferal tests. The dominant feature of FAZ 3 is the gradual rise and fall in abundance of *Reophax gracilis* between *ca.* 7.4 ka BP and 4.8 ka BP, constituting up to 66% of the AA (62% of TA) during the mid-Holocene. *Textularia torquata* is found throughout the core and varies from 5 to 25 % (AA) through FAZ 3.

Reophax gracilis and *T. torquata* are grouped as 'indifferent' since they do not show a strong relationship with water mass characteristics, although *R. gracilis* may be opportunistic in nature. The abundance of *T. torquata* remains relatively constant throughout the core, while *R. gracilis* is present throughout the core and in particularly high abundance in FAZ 3

There is a persistent abundance of species associated with Atlantic water influence in both the AA and CA through FAZ 3. Examples from the AA include *A. glomerata*, *Ammoscalaria pseudospiralis*, and *R. turbinatus*. Atlantic water-associated species in the CA assemblage include *N. labradorica* (up to 27%), with lower abundances of *B. frigida* and *B. pseudopunctata*. The decline of *C. reniforme* (<20% of CA) is replaced by increasing abundances of *E. excavatum* f. *clavata* through the lower part of FAZ 3, with abundances typically *ca.* 55% between 6.5 ka BP and 4.7 ka BP. The interval 5.3 ka BP to 4.3 ka BP is typified by high test lining counts (*Fig. 6.6*). *Stainforthia feylingi* is abundant or dominant (19-67% of CA) from 7.3 ka to 6.3 ka BP, and rare or absent in the upper part of FAZ 3.

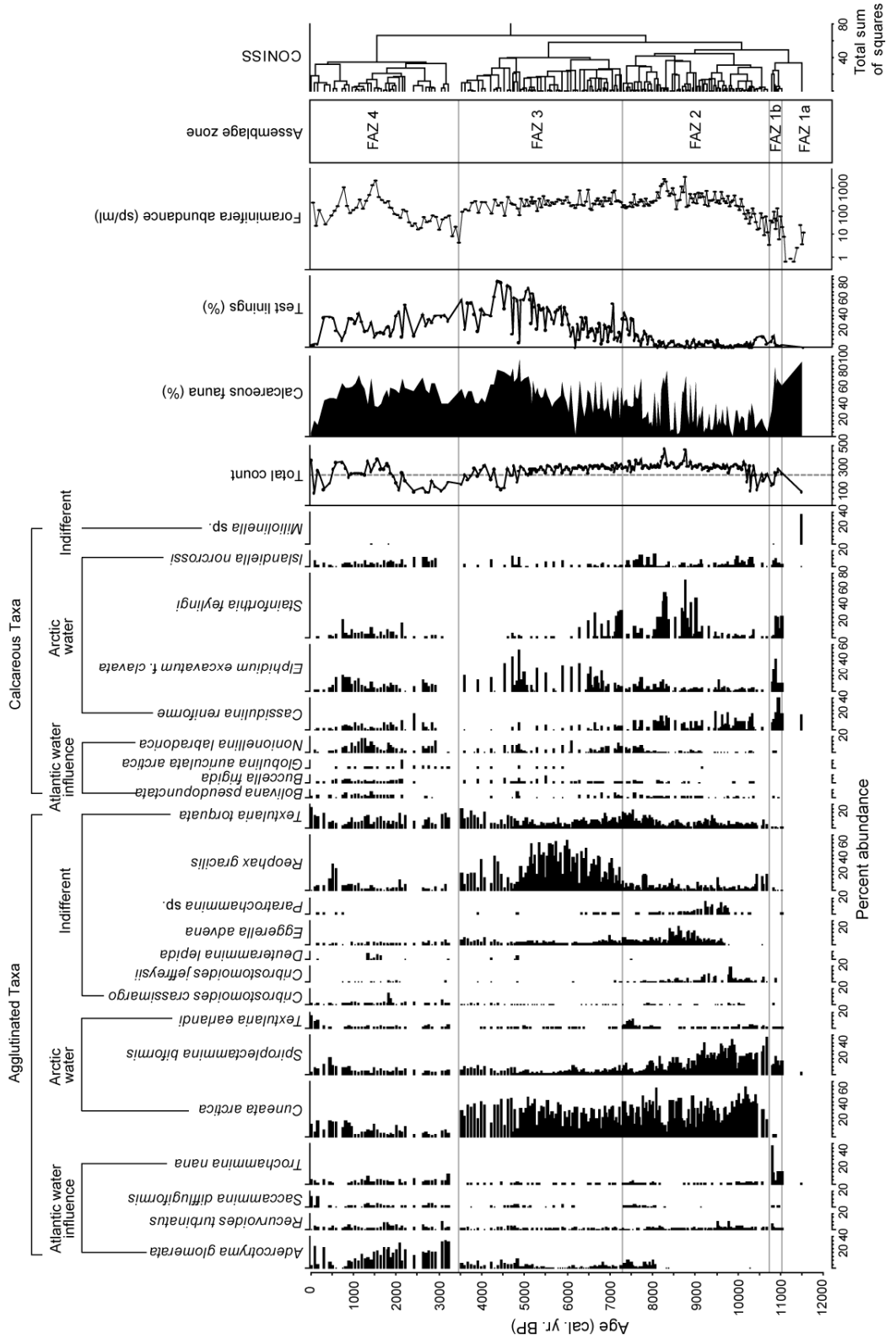

Figure 6.6 Benthic foraminifera with abundances ≥ 2.5% in the total assemblages (in samples with at least 100 specimens) of core MSM-343520_G. Species are grouped according to their affiliation to different basal water masses in West Greenland. The dashed line through the total count highlights samples where foraminifera counts exceed 250 specimens.

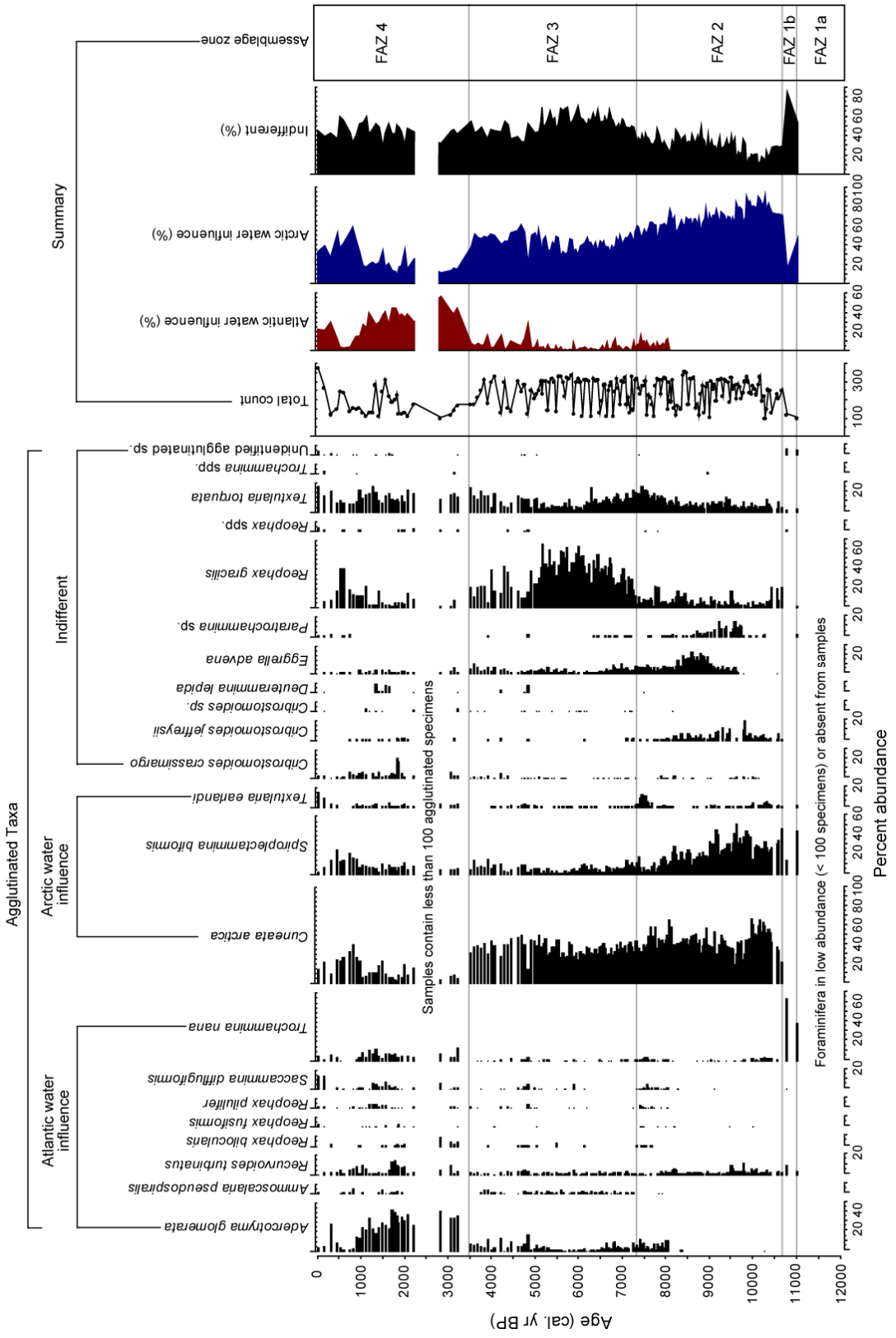

Figure 6.7 Benthic foraminifera with abundances ≥ 5% in the agglutinated assemblages of core MSM-343520_G. Summary diagrams show the total abundance of species in their faunal groupings. Only samples with at least 100 specimens in are shown.

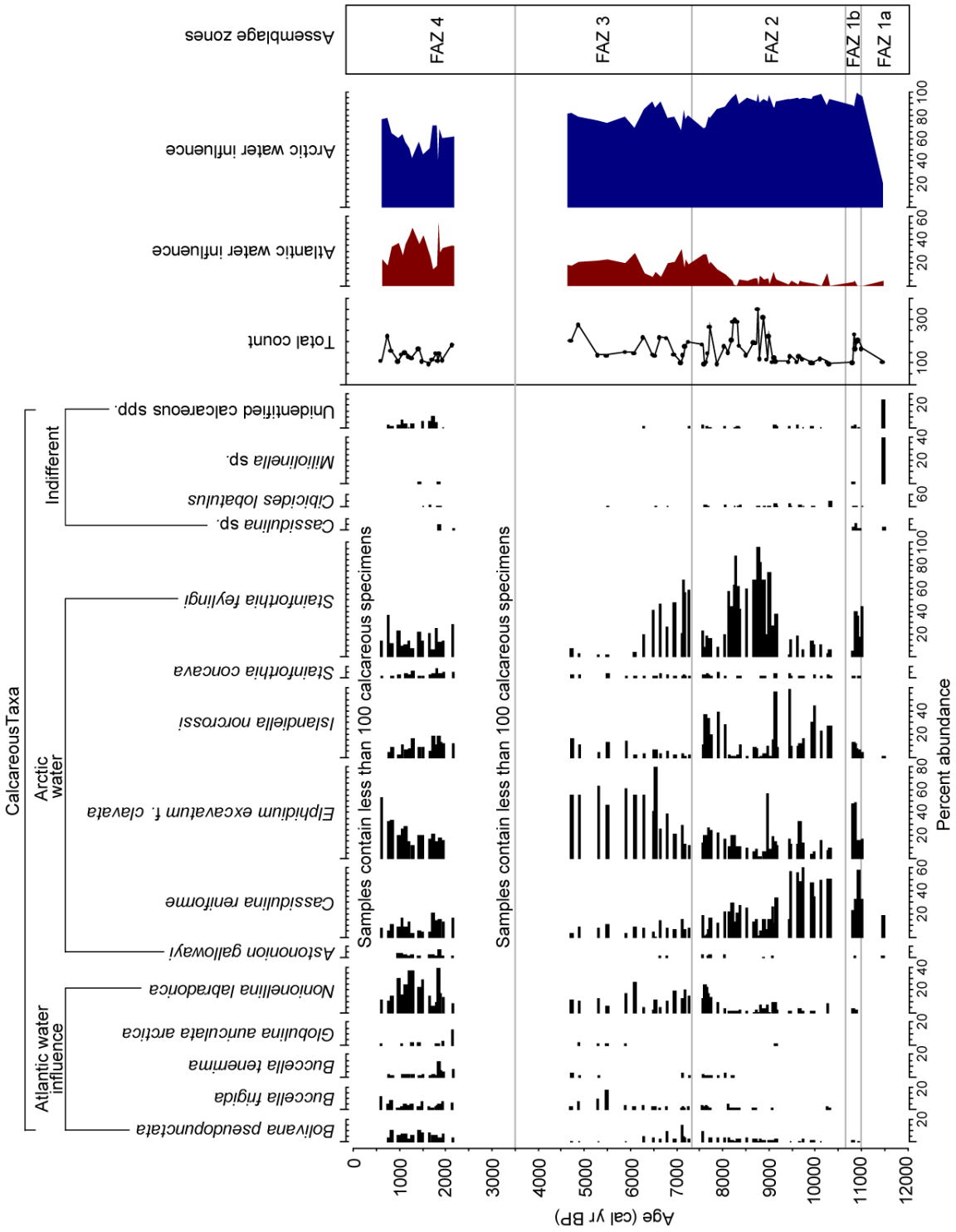

Figure 6.8 Foraminiferal stratigraphy for species occurring in abundances ≥ 5% in the calcareous assemblages of core MSM-343520_G. Only samples with at least 100 specimens are included.

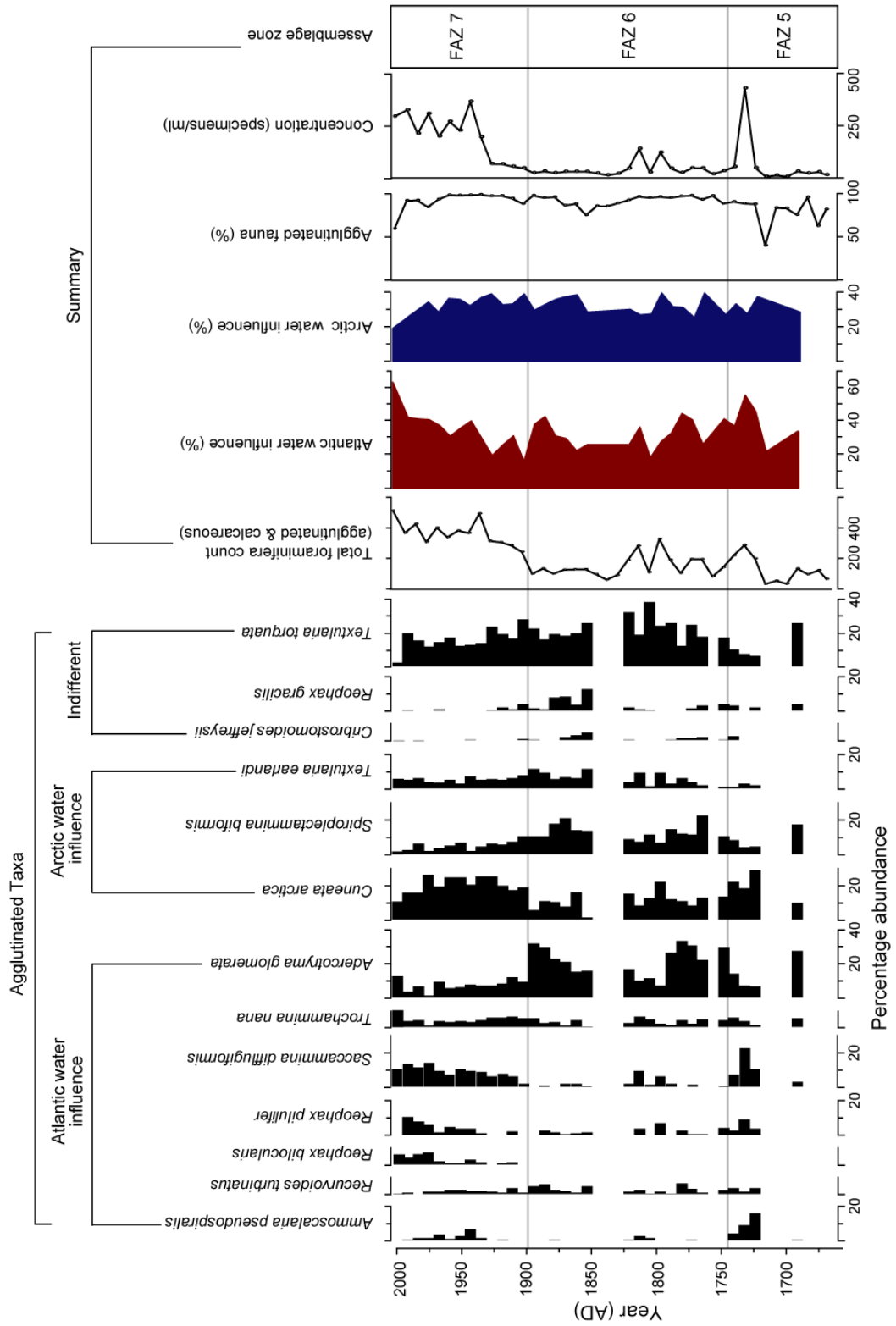

Figure 6.9 Agglutinated fauna (of assemblages containing at least 100 specimens) from multicore MSM-343520_MC. Species occurring with abundances of ≥ 5% are shown. The foraminiferal concentration (summary diagram) is based on agglutinated and calcareous foraminifera.

FAZ 4 (3.5 ka BP to present, 251-0 cm).

FAZ 4 is characterised by an abrupt and significant shift in the dominant taxa, with a decline in *C. arctica* coincident with a dramatic rise in *A. glomerata* at *ca.* 3.5 ka BP, which is abundant (*ca.* 30-40% of AA) until 1.5 ka BP. There are low foraminiferal concentrations from 3.5 ka BP to 1.9 ka BP. A reduction in test lining counts indicates this is an interval of increasing carbonate preservation, particularly in comparison to the upper part of FAZ 3. Several ancillary species occur in low abundances in FAZ 4, including *T. torquata* (*ca.* 10-20% of AA), *S. biformis* (typically 5-15%), and *C. arctica* (typically 10-20%). There is a notable increase in *R. turbinatus* (up to 14.3%) and *T. nana (*ca. *7%)* at 2 ka BP, succeeded by small increases in Atlantic water influenced species *Reophax pilulifer* and *S. difflugiformis*. In the calcareous fauna, *N. labradorica* is abundant, peaking at 36% of the CA at approximately 1.2 ka BP, while *B. pseudopunctata* and *B. frigida* have a greater presence. Abundance peaks of species linked to Atlantic water influence are followed by increased *E. excavatum* f. *clavata* (*ca*. 15–20% of TA between 1.1–0.6 ka BP), *C. arctica* (14-20% of TA), and *S. biformis* (*ca*. 10%, peaking at 21.5% of TA at 0.5 ka BP). Calcareous fauna constitute more than 60% of the TA at *ca.* 0.7 ka BP, before a significant decline in abundance in the upper 32 cm of the core. *Adercotryma glomerata* (28% of TA), *S. difflugiformis* (13%), *T. earlandi* (15%) and *T. torquata* (26%) are all important species towards the top of the core.

FAZ 5 (AD 1666-1724, 42.5-35 cm, MSM-343520_MC)

FAZ 5 in multicore MSM-343520_MC (*Fig. 6.9*) is typified by low foraminifera concentration (< 50 specimens per cm^3), particularly before AD 1720, and higher occurrences of calcareous fauna compared to upcore. Six samples have been omitted from FAZ 5 in *Fig. 6.9* because a representative count of foraminifera was not achieved. The samples that achieved quota have a high abundance of species associated with relatively warm water influence in the WGC. *Adercotryma glomerata*, associated with a warmer mixed WGC influence, is abundant (25%) towards the base of the core, though declines in the upper part of FAZ 5, and is replaced by other 'Atlantic water-influenced' species, including *S. difflugiformis* and *A. pseudospiralis.* From AD 1700, the cold, open water taxon, *C. arctica*, falls in abundance. The higher abundance of

calcareous fauna and a brief spike in foraminiferal concentration coincides with a higher abundance of agglutinated species associated with warmer water influence.

FAZ 6 (AD 1724-1895, 35-14 cm)

FAZ 6 is characterised by the peak in *A. glomerata* at the base of the zone, followed by a decline in abundance between AD 1780 and AD 1860, and an increase towards the top of the zone at AD 1895. *Textularia torquata*, a taxon with no obvious relationship to water mass characteristics, increases in abundance to *ca.* 20 % through this zone. *Cuneata arctica* occurs in its lowest abundance throughout the multicore in FAZ 6, while small increases in the abundance of *S. biformis* can be distinguished before the twin peaks of *A. glomerata.* The Atlantic water species are generally low in abundance, particularly compared to FAZ 5 and 7.

FAZ 7 (AD 1895-2007, 14-0 cm)

FAZ 7 is characterised by an abrupt switch from *A. glomerata* to higher abundances of *C. arctica.* There is also a gradual rise in the abundance of other Atlantic water species, with *S. difflugiformis* increasing throughout FAZ 7, and *R. pilulifer* from AD 1930 and *R. bilocularis* from *ca.* AD 1970. There is a concordant decline in the Arctic water species *S. biformis* and *T. earlandi* from, or just before, AD 1900. There is also a noticeable decline in *C. arctica* from *ca.* AD 1975. There is a dramatic increase in foraminiferal concentration from 25 specimens per cm^3 at AD 1890 to between 250 and 300 specimens per cm^3 from AD 1925.

6.2.4 Transfer function reconstruction of bottom water temperatures

The transfer functions developed in Chapter 4 were applied to cores MSM-343520_MC and MSM-343520_G. The 'agglutinated assemblage' (AA) transfer function was applied to core MSM-343520_G and MSM-343520_MC because of the high agglutinated foraminifera content and *post mortem* losses of calcareous foraminifera, which may significantly alter the calcareous foraminifera assemblage. To avoid a disproportionate influence of *R. gracilis*, which occurs in low numbers in modern assemblage but far higher abundances in fossil assemblages, this taxon was removed from the transfer function.

The high minimum dissimilarity coefficient (minDC) values throughout most of core MSM-343520_G (see *Fig. 6.10d*) suggest there are large differences between modern and fossil assemblages, and that modern assemblages may not provide good predictive power for reconstructing fossil assemblages. Despite this, there is clearly a good correspondence between trends in reconstructed bottom water temperatures and changes in $\delta^{18}O$ (*N. labradorica*), total Arctic water taxa (%), and LOI (%) changes (*Fig. 6.11*). This suggests that the transfer function reconstructions may provide a reasonable indication of warming and cooling trends in core MSM-343520_G. However, omitting calcareous foraminifera from the transfer function reduces the potential temperature range in reconstructions, since the warmest and coldest water species in West Greenland are calcareous foraminifera, whereas agglutinated foraminifera generally appear to occupy mid-range water temperatures (see Chapter 4).

The temperature reconstruction (*Fig. 6.10c*) suggests initially warm bottom waters were present in outer Uummannaq trough after deglaciation, followed by a significant cooling in basal water temperatures. However, the high MinDC values for the lower three assemblages at the base of the core suggest that there are no close modern analogues to these fossil assemblages in this part of the core, and that the temperature reconstruction here is inaccurate. This interpretation is supported by the high abundance of calcareous benthic foraminifera characteristic of a strong Arctic water influence (*Fig. 6.8*).

Generally cool bottom-waters are reconstructed for between *ca.*10.3 ka BP and 8 ka BP, followed by gradually warming bottom waters until 5.5 ka BP. Low MinDC values around 10 ka BP, including some fossil assemblages below the 10% threshold that identifies ‘good’ or ‘close’ modern analogues from ‘poor’ modern analogues, suggest that the transfer function provides more reliable temperature estimates for this part of the core. However, the gradually increasing MinDC values going upcore, corresponding with bottom water warming between 8 ka BP and 5.5 ka BP, suggests that there are no close modern analogues for this part of the core. This is perhaps not surprising, given the high abundance of *R. gracilis* found in these samples, which is a rare species in modern foraminifera samples.

The temperature reconstruction (characterised by poor modern analogues) suggests cooling from 5.5 ka BP to 3.5 ka BP, followed by warming from *ca.* 3.5 ka BP to 1 ka BP. This warming interval, towards the top of the gravity core, is characterised by generally closer and often 'good' modern analogues, suggesting the transfer function provides a more accurate reconstruction. The brief cooling and then warming trend in the past 1000 years are again characterised by poorer modern analogues.

The lack of modern analogues may reflect the poor preservation of fossil assemblages, or perhaps suggests that the full range of marine shelf environments recorded in the fossil core has not yet been sampled in the modern environment. It is, of course, possible that past characteristics of sub-surface WGC waters are beyond the range of modern extremes, precluding the possibility of further expanding the database of modern foraminifera surface samples from West Greenland.

6.2.5 Oxygen isotope data

A $\delta^{18}O$ (vs. PDB) record for core MSM-343520_G was produced using the species *N. labradorica*. While *N. labradorica* is an infaunal benthic foraminifera, and is not as ideally suited to reconstructing bottow water $\delta^{18}O$ changes as epifaunal species such as *Cibicides wuellerstorfi* and *C. lobatulus* (e.g. Hillaire-Marcel *et al.*, 2001), it is the only foraminifera species that occurs throughout core MSM-343520_G and in sufficient abundance for isotope analysis. Other studies in Nares Strait (Mudie *et al.*, 2006) and the Chuckchi Sea (Keigwin *et al.*, 2006) have used *N. labradorica* to reconstruct changes in water mass characteristics. Isotope studies by Ivanova *et al.* (2008) in the western Barents Sea indicate that *N. labradorica* has an estimated $\delta^{18}O$ disequilibrium effect of 0.28‰, compared to -0.76‰ for epifaunal *C. lobatulus.* The $\delta^{18}O$ recorded by *N. labradorica* was at least 0.4‰ higher than values recorded by other investigated species (*C. lobatulus*, *C. reniforme*, E*. excavatum* f. *clavata*, *M. barleeanus*). Additionally, $\delta^{13}C$ values for *N. labradorica* were depleted by 1.2-1.7‰ compared to epifaunal taxon *C. lobatulus* (Ivanova *et al.*, 2008).

Deviations in isotopic composition of biogenic calcite from equilibrium are commonly due to microhabitat and/or vital effects (Urey *et al.*, 1951; Wilson-Finelli *et al.*, 1998). The influence of microhabitat and metabolic vital effects is evident in isotopes of benthic foraminifera living at different sediment depths. The $\delta^{13}C$ values of epifaunal species are commonly less negative and more closely reflect $\delta^{13}C_{seawater}$ values than deep-infaunal species, which typically have lighter $\delta^{13}C$ values. This is because respired ^{13}C-depleted CO_2 in sediment porewaters may be incorporated into calcifying foraminifera tests (McCorkle *et al.*, 1990; 1997). Infaunal taxa may, therefore, be good palaeoproductivity indicators since high concentrations of organic matter in sediments (due to high surface water primary productivity or greater influx of nutrient-rich water carrying labile organic matter) may further decrease porewater $\delta^{13}C$ values (Mackensen *et al.*, 1993; Katz *et al.*, 2003).

The $\delta^{18}O$ curve reflects a combination of changes in global ice volume, temperature, salinity, and foraminifera species vital effects. The trends in $\delta^{18}O$ are interpreted to reflect long-term temperature and salinity changes in the waters transported by the WGC onto the West Greenland shelf. Isotopic values range from 3.356‰ to 4.458‰.

The temporal resolution of isotope samples is poor in the lower part of core MSM-343520, with only three samples before *ca.* 10.9 ka BP. Relatively light $\delta^{18}O$ values are found at 10.9 ka BP (3.880‰), followed by isotopic enrichment to 4.458‰ at *ca.* 10.3 ka BP. After 9 ka BP, there are two significant light isotopic excursions from 9.0 ka BP to 8.8 ka BP (spanning *ca.* 220 years; 3.842‰ at 8.8 ka BP) and 8.2 ka BP to 7.9 ka BP (spanning *ca.* 335 years; 3.848‰ at 8.2 ka BP) of approximately 0.42‰ and 0.50‰, respectively. Both events appear to begin abruptly, though this is perhaps more true for the second spike, where the initial shift to lighter isotope values is larger in magnitude. The close correspondence between the light isotope peaks at 8.9 ka BP and 8.2 ka BP, and blooming of *S. feylingi* (*Fig. 6.11a*), suggest these are indeed two discrete 'events'.

From 7.8 ka BP (4.3‰), the general isotopic trend is one of gradual depletion to *ca.* 3.5‰ at 5.6 ka BP, before a plateau until *ca.* 2.7 ka BP, and a trend of isotopic enrichment until 1.7 ka BP.

The past 1.7 ka BP is characterised by fluctuations with an amplitude of approximately 0.3‰, but with no long-term trend. These trends are overprinted with a number of heavy spikes at 4.7 ka BP, 2.8 ka BP, 2.7 ka BP, 2.2 ka BP, and 0.9 ka BP. While these may reflect temperature/salinity fluctuations, the magnitude and abruptness of these spikes suggest that foraminifera vital effects or analytical errors are the cause.

The $\delta^{13}C$ (PDB) is initially heavy (*ca.* -1‰) from 10.9 ka BP to 9.2 ka BP, before a significant depletion to -5.253‰ at 8.7 ka BP, followed by a brief enrichment to -1.72‰, and then a greater depletion to -5.932‰ at 8.3 ka BP (*Fig. 6.10*). After 7.9 ka BP, $\delta^{13}C$ becomes more positive (*ca.* -0.9‰ at 7.5 ka BP). There is a gradual depletion of *ca* 1.6‰ to 6.2 ka BP, followed by enrichment to 4.6 ka BP. From 4.6 ka BP to 2.8 ka BP, isotope values are *ca.* -0.9‰, followed by a stepped enrichment of *ca.* 0.4‰ until 0.9 ka BP. There is a brief negative trend of $\delta^{13}C$ values, reaching -2.3‰ at 0.6 ka BP, before a return to heavier values in the past *ca.* 400 years (*Fig. 6.10*).

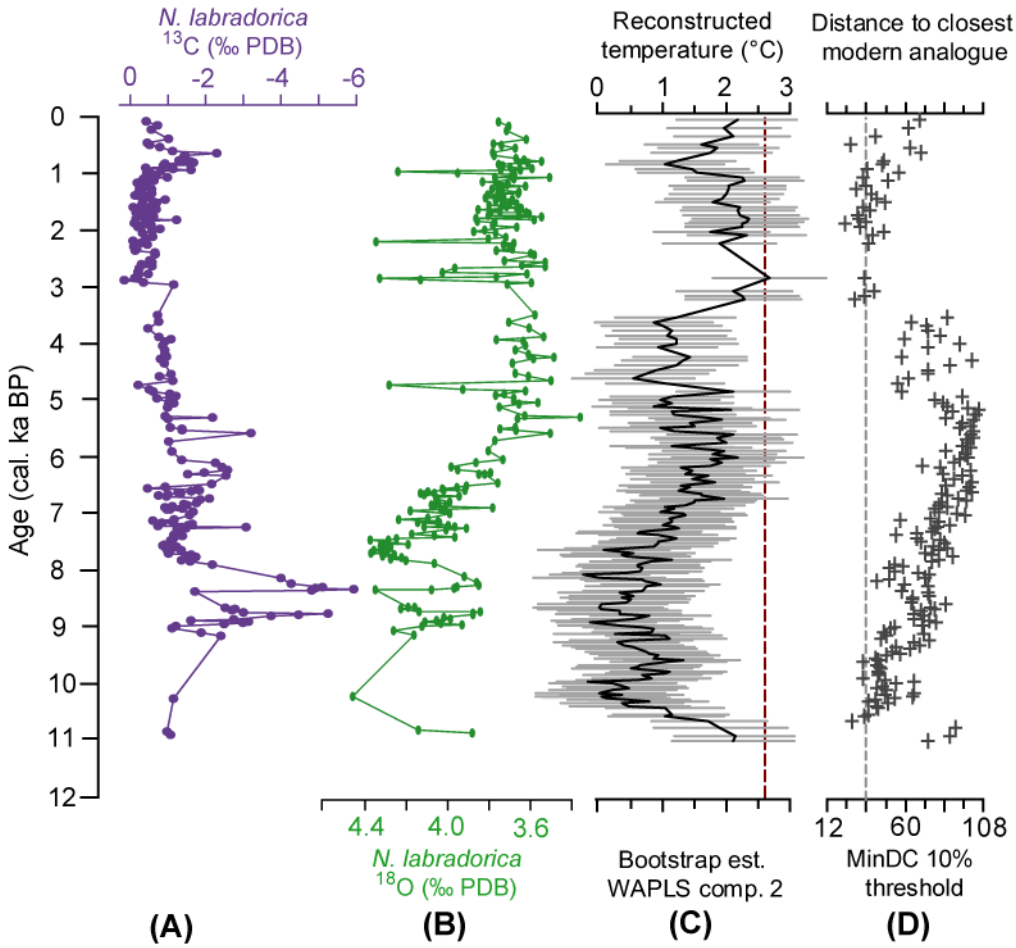

Figure 6.10 Comparison of foraminifera isotope data and foraminifera-based bottom-water temperature reconstruction from core MSM-343520_G, showing; (a) $\delta^{13}C$ (*N. labradorica*), (b) $\delta^{18}O$ (*N. labradorica*), (c) transfer function temperature reconstruction, with red dashed line indicating the modern (June 2007) temperature at the core station, (d) minimum dissimilarity coefficient values (MinDC).

6.3 Palaeoceanographic interpretation

There is no evidence that core MSM-343520_G has been significantly affected by downslope remobilization of sediments by debris flow processes. Above *ca.* 9 m, the core sedimentology is generally composed of massive clayey mud or silty mud with abundant foraminifera. This is interpreted to reflect continuous hemipelagic sedimentation, and indicates that proxy-evidence in the sediment core may be analysed for reliable palaeoceanographic reconstructions. There is evidence that the core sedimentology has been influenced by turbidity which may be linked to debris flow processes (e.g. cross-bedded ripples, possible rip-up). However, this does not significantly influence the palaeoenvironmental interpretation, since this probably took place in an ice-proximal setting when sediment accumulation due to the nearby ice front was rapid.

Relatively warm Atlantic-sourced water, a key component of the modern WGC, impinges on the seafloor of the outer Uummannaq Shelf below approximately 200-300 m depth at the present day (NOAA WOD05, Accessed September 2010), and may potentially penetrate into the fjords in the Uummannaq area, and directly influence ice dynamics. Core MSM-343520 is located within Uummannaq Trough, which provides a natural pathway for warmer subsurface waters to inner shelf areas, and as such, is ideally situated for understanding changes in relative water temperature. Benthic foraminiferal assemblages, which show a close correspondence with basal water temperatures in central West Greenland, provide a means of assessing the influence of ocean forcing on the Greenland Ice Sheet in the Uummannaq area.

6.3.1 FAZ 1a (Before *ca*. 11 ka BP, 989-915 cm)

The 'light' coloured, less dense, sediments identified in X-ray radiographs (*Fig. 6.4*; 989-967 cm, 962-922 cm) appear to be of a different origin compared to other sediments in core MSM-343520_G, as indicated by distinctly lower magnetic susceptibility, high LOI, and a high [K/Ti] ratio, suggestive of terrestrial sediment influence from the mainland (*Fig. 6.4*). The high LOI values for sediments in FAZ 1a may reflect organic rich sediments being released from formerly subglacial areas as the ice retreated. Zone 1 sediments are interpreted to be ice-proximal glacimarine in origin. In FAZ 1a, this is supported by an absence of foraminifera at the base of the core (989-969 cm), and low concentrations of well-preserved fragile foraminifera specimens in overlying sediments. Only two species, *C. reniforme* and *Miliolinella* (*subrotunda*?) sp., are found in relatively high numbers in FAZ 1a. *Cassidulina reniforme* is often an early colonising species where glacial influence is waning (e.g. Korsun and Hald, 2000), and suggests cold, reduced salinity waters were influential at the core station. While *Miliolinella* (*subrotunda*?) sp. is not abundant in high-latitude deep-sea and fjord studies, Korsun and Hald (2000) identified this species within 2 km of a calving margin in a Svalbard Fjord. Since it only occurs in FAZ 1a, this species is believed to reflect glacimarine conditions. However, low foraminiferal concentrations suggest reduced productivity and/or dilution of foraminiferal numbers by rapid accumulation though the sedimentation rate cannot be directly assessed because of a lack of dateable material in FAZ 1a. One explanation for excellent preservation of calcareous

foraminifera during this interval may be high sedimentation, with rapidly buried dead foraminifera being 'protected' from overlying cold, low salinity waters with high dissolved CO_2 content, which likely influences dissolution in the dead foraminifera assemblage (e.g. Lloyd *et al.*, 2005).

The dominance of clay suggests a close proximity to a calving margin ejecting fine-grained sediments in turbid meltwater plumes. The relatively high water content of these sediments (*Fig. 6.4*) suggests clay particles were laid down rapidly, therefore preventing dewatering, and supporting this interpretation. Planar parallel laminations (see *Fig. 6.5H*), corresponding exactly to the barren interval, with interspersed ice-rafted detritus (IRD) is characteristic of ice-proximal glacimarine sedimentation from meltwater plumes with a high suspended load (Dowdeswell *et al.*, 1994; Cowan *et al.*, 1997; Ó Cofaigh and Dowdeswell, 2001). The presence of granules and larger clasts in these sediments suggests ice-rafting was also taking place at this time. There is a general absence of coarser sediments fractions in the clay sediments between 953 and 936 cm, which may reflect suspension settling from turbid plumes while iceberg rafting was surpressed (e.g. Dowdeswell *et al.*, 2000).

The sediment facies that have been termed diamicts are believed to be ice-rafted in origin. The base of the upper diamict is composed of very poorly sorted, fine sandy mud (14.8% sand), similar in composition to underlying sediments. There is an upcore fining to mud with dropstones. The gradational contacts at the top of these units support an interpretation that the coarse fraction was deposited by iceberg rainout (Cowan *et al.*, 1997). The more hemipelagic sediments that overlie the upper diamicton (above 879 cm, *Fig. 6.4*) have similar magnetic susceptibility properties to the diamicton, and slightly decreased [K/Ti], which may be indicative of a common origin of terrestrial sediments in these facies.

6.3.2 FAZ 1b (*ca*. 11-10.7 ka BP, 915-879 cm)

The data from the core taken as a whole suggest that cold, low-salinity waters, influenced largely by meltwater from local deglaciation, were dominant in the Uummannaq trough and, most likely, across the shelf west of Uummannaq fjord during the early Holocene (*Fig. 6.11i*). This is indicated by abundant Arctic Water benthic foraminifera species (*Fig. 6.8 and 6.11i*) occupying the shelf at this time. The high abundance of opportunistic calcareous taxa, especially *S. feylingi, C. reniforme,* and *E. excavatum* f. *clavata*, are diagnostic of ice-proximal glacimarine conditions from 11 to 10.7 ka BP (e.g. Schröder-Adams *et al.*, 1990a, 1990b). These species tolerate large and abrupt salinity shifts associated with variability in meltwater flux at the terminus of marine-terminating glaciers (e.g. Korsun and Hald, 1998). Together, the low [S/Al] integral ratio, percentage LOI, and foraminiferal concentration during this interval suggest low marine productivity. Turbid waters caused by a high-suspended load associated with waters ejected close to the ice margin would have hampered surface water productivity and consequently reduced food supply to the benthos (Korsun and Hald, 1998). This would have created an environment inhospitable to many foraminifera species, with the limited food availability in glacimarine environments favouring opportunistic calcareous fauna (Schröder-Adams *et al.*, 1990a, 1990b; Korsun and Hald, 1998). The high abundance of *S. feylingi* at *ca.* 10.9 ka BP suggests this taxon initially colonised the formerly inhospitable environment (e.g. Alve, 1999; Alve, 2003).

Deglacial meltwater ejected from the glacier terminus in Uummannaq Fjord would have presumably been a major influence on the isotopic composition of bottom waters on the Uummanaq shelf. Isotopically-light benthic foraminifera $\delta^{18}O$ values (*Fig. 6.11c*) at *ca.* 10.9 ka BP therefore support the ice-proximal glacimarine environment in FAZ 1b suggested by the foraminifera data, and are interpreted to primarily reflect meltwater inputs from local deglaciation causing a freshening of the water column. The upcore increase in $\delta^{18}O$ values (*Fig. 6.11c*) and the overall decline in the C/N ratio (*Fig. 6.3*) through FAZ 1b suggest a reduction in glacimarine influence from 11 ka BP to 10.7 ka BP. The change in C/N ratio suggests a reduction in terrestrially-derived sediment and a relative increase in marine productivity, while the $\delta^{18}O$ enrichment probably reflects a reduction in meltwater influence. The large and abrupt shift in

magnetic susceptibility values and the [K/Ti] XRF ratio (*Fig. 6.3*) suggest that ice may have rapidly retreated from the core site, withdrawing into the inner Uummannaq shelf.

6.3.3 FAZ 2 (10.7-7.3 ka BP, 879-531 cm)

In general, benthic foraminifera and oxygen isotopes suggest relatively cold, low salinity waters occupied the Uummannaq trough during FAZ 2. Abundant *C. arctica* and *S. biformis*, and common *C. reniforme* before 9 ka BP indicates Arctic waters strongly influenced benthic foraminifera assemblages at this time (*Fig. 6.6-6.8*). *Cuneata arctica* and *S. biformis* are found together in Baffin Island and Svalbard fjords under the influence of Polar water and glacimarine conditions (Schafer and Cole, 1988; Korsun and Hald, 1997), and on the Labrador shelf under cooler water conditions (Vilks *et al.*, 1982). *Spiroplectammina biformis* is found under the influence of cold (≤ 0°C) Arctic waters in Baffin Island fjords (Schafer and Cole, 1986) and the Amerasian Basin of the Arctic Ocean (Ishman and Foley, 1996). The gradual decline in this species after 9 ka BP may, therefore, reflect a slight warming in waters impinging on the Greenland shelf or perhaps a reduction in glacimarine influence. A decline in glacial influence is suggested by increasing foraminiferal concentrations between 10.7 ka BP and 9.5 ka BP, which reflect either reduced sedimentation or increased benthic productivity at core station MSM-343520. Calcareous fauna, with *C. reniforme* (>50%) dominant from 11 ka BP to 9.5 ka BP, support colder conditions during the early part of FAZ 2.

The most notable features in this zone are the two distinct high abundance peaks of *S. feylingi* (*Fig. 6.11a, b*), a common opportunistic Arctic taxon that dominates foraminifera assemblages influenced by rapidly changing environmental conditions (Alve, 2003), and is a coloniser of recently established habitats (Alve, 1999). *Stainforthia feylingi* is widely associated with low oxygen conditions, often dominating assemblages in dysoxic/anoxic sediments of silled Norwegian fjords (e.g. Alve, 1990; 1994; 1995; Bernhard and Alve, 1996; Alve, 2003). However, it is also widely found as a dominant species under well-oxygenated shelf waters (Alve, 2003). Palaeoecological interpretations are further complicated by the feeding strategy of *S. feylingi,* since it feeds on a variety of food sources. *Stainforthia feylingi* blooms are linked to high phytodetritus fluxes to the seafloor (e.g. Bernhard and Bowser, 1999; Gustafsson and

Nordberg, 2000; 2001), particularly at hydrographic fronts (Alve, 2003). However, this taxon also feeds on degraded organic matter and bacterial sources (e.g. Alve and Bernhard, 1995, Alve, 2003). Mudie *et al.* (2006) have used *S. feylingi* as an indicator of low oxygen conditions in geological sediments from Nares Strait, northern Baffin Bay, linking higher abundances to increased primary productivity or increased sea-ice, which would have slowed bottom water circulation (hence reducing air-sea gas exchanges and vertical mixing).

On the Uummannaq shelf, the very high foraminifera concentration and dominance of *S. feylingi* at *ca.* 8.9-8.7 ka BP and *ca.* 8.3-8.1 ka BP, coinciding with depleted $\delta^{18}O$ and $\delta^{13}C$ values (*Fig. 6.11a-d*), may be a rapid, opportunistic response to increased fluxes of organic matter to the seafloor. Since *S. feylingi* feeds on a variety of food sources (e.g. Alve and Bernhard, 1995, Alve, 2003), the high abundance may be linked to a greater influx of labile organic matter transported in the nutrient-rich Atlantic Water (e.g. Jennings *et al.,* 2004; Lloyd, 2006a). However, the foraminifera are suggestive of a colder water influence impinging on the shelf at this time, perhaps suggesting a response to fresh phytodetritus inputs from surface water primary productivity linked to a more stable, seasonally stratified water column (e.g. Alve, 2003). This interpretation may be supported by relatively high [S/Al] during this interval, and the lower $\delta^{13}C$ (*N. labradorica*) values. Respired ^{13}C-depleted CO_2 in sediment porewaters (produced during the decay of organic matter) may be incorporated into calcifying foraminifera tests (McCorkle *et al.*, 1990; 1997). Enhanced fluxes of organic matter may further decrease porewater $\delta^{13}C$ values of infaunal taxa (Mackensen *et al.*, 1993; Katz *et al.*, 2003). Water column stratification has a limiting influence on primary production in surface waters because access to replenishing inorganic nutrients is restricted (Andersen, 1981b; Nielsen and Hansen, 1999; Nielsen *et al.*, 2010), which may favour the opportunistic life style (rapid growth and reproduction) of *S. feylingi*. In estuarine and shallow near-shore environments, *E. advena* is considered an opportunistic taxon and primary pioneer colonizer, found in high abundance near pollutant outfalls (e.g. Schafer and Young, 1977; Schafer, 1982; Alve, 1995). While the Uummannaq shelf is a much deeper location, similar ecological preferences may indicate that the high abundance of *E. advena* between 9 and 8.2 ka BP could be an opportunistic response to episodic nutrient enrichment.

There is a noticeable increase in species associated with increased Atlantic water influence on the West Greenland shelf, including *A. glomerata* and smaller occurrences of *Reophax* spp. from 8.1 ka BP, followed by an increase in *N. labradorica* (Lloyd, 2006a). Maximum abundances of *N. labradorica* are found under relatively warm and saline waters in the modern environment (where the mean temperature at sites where *N. labradorica* is dominant is 3.86°C), which has been linked to influxes of nutrient-rich Atlantic water into the Disko Bugt-Uummannaq area (Lloyd, 2006a). These assemblages appear most similar to modern assemblages under the influence of mixed-WGC water, with temperatures typically 1.5°C to 3°C (cf. Chapter 4). In light of this, the first significant influence of relatively warm and saline waters transported by the WGC to the central West Greenland shelf probably follows subsurface freshening at 8.2 ka BP.

6.3.4 FAZ 3 (7.3-3.5 ka BP, 531-251 cm)

FAZ 3 is characterised by both a reduction in agglutinated benthic foraminifera species associated with Polar water influence (*Fig. 6.7*), and an increase in calcareous fauna associated with Atlantic water influence (*Fig. 6.8*). A decline in $\delta^{18}O$ through this interval may further support a gradual warming in basal water mass characteristics. The increase in abundance of *N. labradorica* (*Fig. 6.8*) is diagnostic of warmer Atlantic waters impinging on the Uummannaq shelf between 7.7 and 6 ka BP. *Nonionellina labradorica* benefits from fresh phytodetritus inputs under hydrographic fronts and other high productivity areas in the northern North Atlantic and Arctic Ocean (e.g. Hald and Steinsund, 1992; Polyak *et al.,* 2002; Rytter *et al.*, 2002). On the West Greenland shelf, the presence of *N. labradorica* reflects an increase in fresh phytodetritus linked to the influx of Atlantic Water (e.g. Jennings *et al.*, 2004; Lloyd, 2006a). The relative decline in C*. arctica* and S*. biformis*, characteristic of cold waters (e.g. Schafer and Cole, 1986; 1988; Ishman and Foley, 1996), supports a slight warming in waters impinging on the Uummannaq shelf. The slightly lower $\delta^{13}C$ in the benthic foraminifera record (*Fig. 6.10*) and high percentage LOI (*Fig. 6.11*) on the Uummannaq shelf from between 7.6 and 5.4 ka BP may suggest a greater deposition of organic material during this interval, which may be linked to the greater influx of warmer Atlantic-sourced waters.

High abundances of *S. feylingi* from 7.3 and 6.4 ka BP, albeit at much lower concentrations than in FAZ 2, are succeeded by higher abundances of *E. excavatum* f. *clavata* between 6.4 and 4.5 ka BP (*Fig. 6.8*). This may reflect continued summer stratification of the water column, perhaps with more regular fluxes of organic matter to the seafloor (Murray, 1992, Jennings *et al.,* 2001; Alve, 2003). *Elphidium excavatum* f. *clavata* is often considered opportunistic in nature, dominating low diversity assemblages where environmental conditions are extremely variable, particularly close to glacier calving margins where there are extreme fluctuations in salinity and sediment supply (e.g. Hald and Korsun, 1997). However, *E. excavatum* f. *clavata* has also been found as a dominant species under stable Atlantic Water-influenced sites (stable bottom water temperatures and salinities of *ca.* 5°C and 34.7 ‰) in Isafjardardjúp, on the North Iceland shelf (Jennings *et al.*, 2004).

Reophax gracilis is a major component of foraminifera assemblages in FAZ 3, increasing in abundance from the base of the core, and peaking at *ca.* 5.5 ka BP. The ecology of *R. gracilis* is poorly understood in West Greenland shelf environments because of its low abundance in contemporary surface samples. However, *R. gracilis* (=*Leptohalysis gracilis, Leptohalysis catella*) is believed to have an opportunistic life strategy (Alve, 2010). This species is a common or dominant feature of Canadian (Blais-Stevens and Patterson, 1998; Patterson *et al.*, 2000) and Scandinavian fjords (Alve and Nagy, 1986; Alve, 2000; Gustafsson and Nordberg, 2000; 2001), where it has been linked to nutrient enrichment by anthropogenic sources such as terrestrial plant material and aquaculture. Gooday (1996) suggest larger populations of *R. gracilis* are associated with a feeding strategy dependent on degraded phytodetritus or associated bacteria (in shallow-water and deep-sea species; Goldstein and Corliss, 1994), rather than fresh organic inputs (e.g. Alve, 2010). In West Greenland waters, labile organic matter is supplied by nutrient-rich Atlantic Water transported in the WGC. This suggests that *R. gracilis* may be linked to an increase in relatively warm and saline Atlantic Water influence on the West Greenland shelf from 7.3 to 5 ka BP.

6.3.5 FAZ 4 (3.5 ka BP to present, 251-0 cm)

The boundary between FAZ 3 and FAZ 4 marks an abrupt faunal shift at 3.5 ka BP, which is interpreted to reflect a shift from Arctic water influence on the shelf to enhanced Atlantic-sourced water, characterised by abundant *A. glomerata* from 3.5 ka BP to 1 ka BP. In central West Greenland, the mean bottom water temperature above modern surface samples where *A. glomerata* is the dominant taxon is relatively warm at 3.11°C. A positive correlation with temperature and salinity has also been found for this taxon in Svalbard Fjords (Hald and Korsun, 1997). The decline in *C. arctica* and taxa with opportunistic life styles supports this interpretation. However, lower foraminiferal numbers, particularly calcareous specimens, mark the first *ca.* 1.5 ka during this interval. It is possible that the benthic environment would be inhospitable to calcareous foraminifera if decay of organic matter (due to higher primary productivity fluxes to seafloor) produces high concentrations of CO_2 (e.g. Jennings and Helgadóttir, 1994). Nethertheless, the increase in agglutinated taxa such as *Reophax* spp. and *S. difflugiformis* (*Fig. 6.7*) and calcareous taxa, particularly *N. labradorica* (*Fig. 6.8*), support an increase in Atlantic Water influence on the Uummannaq shelf between 3.5 ka BP and 1 ka BP. This increase in basal water temperature is clearly indicated by an increase in Atlantic fauna and a decrease in Arctic taxa, as well as the transfer function reconstruction (*Fig. 6.11*). The upper *ca.* 1 ka in core MSM-343520_G are marked by significant cooling in basal water temperatures. This is particularly indicated by decreases in Atlantic Water-influenced taxa such as *A. glomerata, R. pilulifer,* and *S. difflugiformis,* and relative increases in taxa associated with Arctic Water influence, such as *C. arctica, S. biformis, T. earlandi* and *E. excavatum* f. *clavata* (*Fig. 6.7* and *6.8*).

6.3.6 FAZ 5 (A.D. 1666-1740)

The high abundance of *A. glomerata* at the base of core MSM-343520_MC, with lower abundance of Arctic taxa *C. arctica* and *S. biformis* is interpreted to reflect the influence of mixed-WGC waters in the Uummannaq trough at *ca.* A.D. 1700. The dominance of Atlantic Water taxa (particularly *A. pseudospiralis, R. pilulifer,* and *S. difflugiformis*) indicates relatively warm, saline Atlantic Waters were present in Uummannaq trough between A.D. 1720 and 1740.

6.3.7 FAZ 6 (A.D. 1740-1895)

The interval A.D. 1740 to 1790 is characterised by a slight cooling, as indicated by a decline in the Atlantic Water taxa, *A. pseudospiralis, R. pilulifer,* and *S. difflugiformis,* and an increase in *A. glomerata*, which suggests mixed-WGC waters (i.e. mixed Atlantic and Polar Water influence) were present on the Uummannaq shelf. This is supported by an increased presence of Arctic Water taxa, *S. biformis* and *T. earlandi*. From A.D. 1790 to 1860, a further decline in Atlantic Water fauna marks cooling of sub-surface waters on the Uummannaq shelf, followed by increasing *A. glomerata* from A.D. 1860, marking the start of a warming trend through the upper part of FAZ 6.

6.3.8 FAZ 7 (A.D. 1895-2007)

The high abundance of *C. arctica* in FAZ 7 suggests well-mixed marine conditions and the influence of Arctic Water during the 20th Century. However, the increase in Atlantic fauna (particularly *S. difflugiformis*) between A.D. 1895 and 2007 mark the continuation of the warming trend that began at *ca.* A.D. 1860. The decline in *S. biformis* and small increase in abundance of *A. pseudospiralis, S. difflugiformis* and *R. bilocularis* between A.D. 1930 and 1940 suggest warming of sub-surface waters during this interval, followed by increased warming from *ca.* A.D. 1980, as marked by a further increase in *S. difflugiformis,* together with increases in *R. bilocularis* and *R. pilulifer.* The increase in foraminiferal concentration may also suggest greater transport of Atlantic Water in the WGC from *ca.* A.D. 1925.

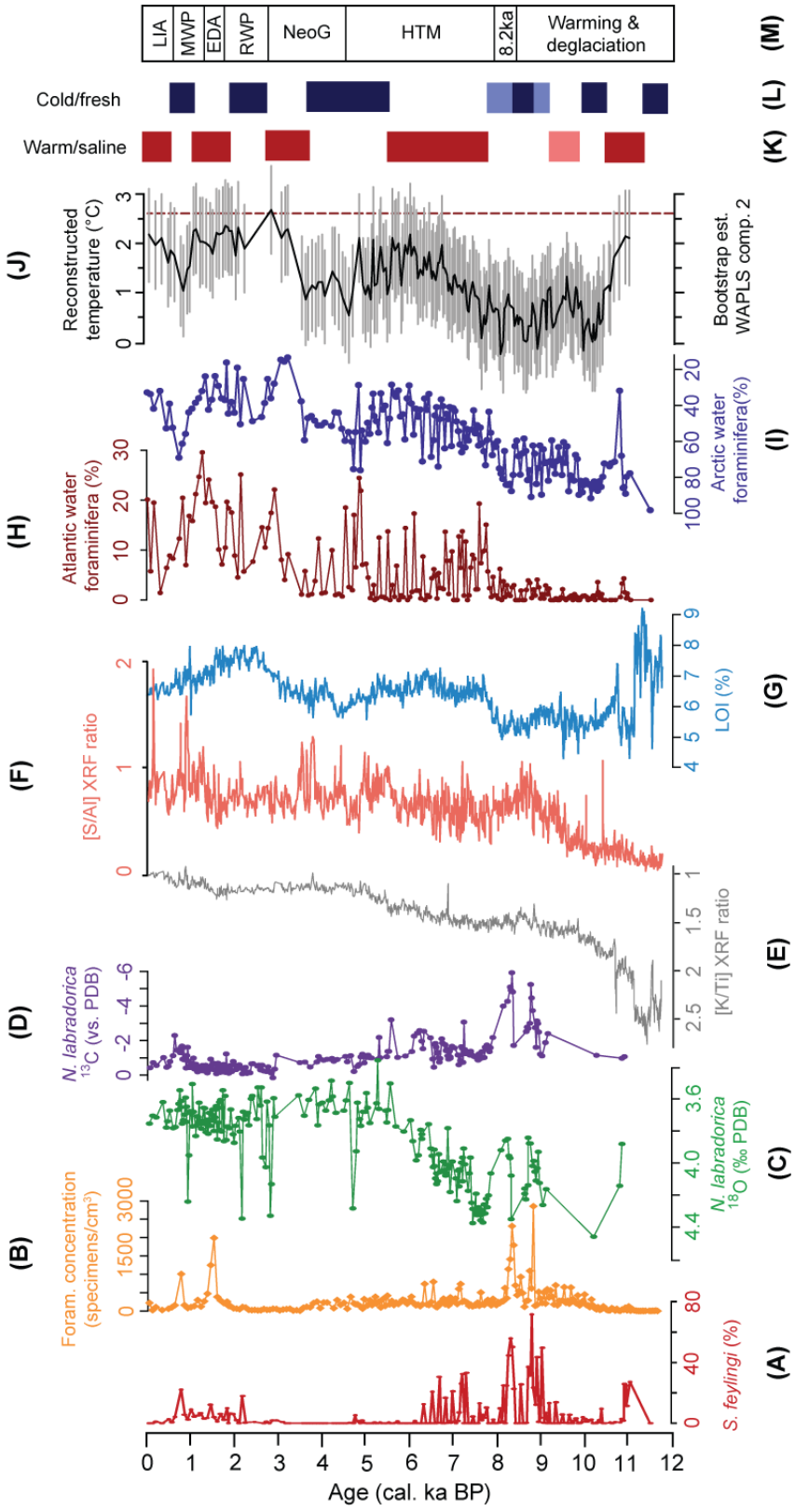

Figure 6.11 Foraminifera and sediment geochemistry data from core MSM-343520_G: (**a**) total abundance of *S. feyling* (TA); (**b**) foraminifera concentration; (**c**) $\delta^{18}O$ and (**d**) $\delta^{13}C$ (*N. labradorica*) data; (**e**) [K/Ti] and (**f**) [S/Al] XRF data; (**g**) Loss-on-ignition (550°C); (**h**) total Atlantic Water, and (**i**) total Arctic Water benthic foraminifera; (**j**) bottom water temperature

reconstruction using AA data; (**k**) warm/saline and (**l**) cold/fresh intervals in core MSM-343520_G; (**m**) Climate "events" in the North Atlantic region: Early Holocene warming and continued deglaciation of Northern Hemisphere ice sheets, the 8.2 ka event, the Holocene thermal maximum (**HTM**), Neoglaciation ice expansion (**NeoG**), Roman Warm Period (**RWP**), European Dark Ages (**EDA**), Medieval Warm Period (**MWP**), and the Little Ice Age (**LIA**).

6.4 Discussion

The following discussion of deglaciation and palaeoceanographic evolution in central West Greenland is illustrated with time-slice cartoons of the main changes in ice margin position and ocean temperature on the Uummanaq shelf (see below). Each cross section is accompanied by a map of central West Greenland to illustrate the evolution of sub-surface current patterns and relative temperature changes in these shelf waters, constrained (and hypothesized) changes in ice sheet margin position, and relative changes in Greenland Ice Sheet meltwater/iceberg flux based on core data from this study.

6.4.1 Deglaciation of the Uummannaq shelf

The Holocene deglacial chronology for the Uummannaq Fjord complex is poorly resolved, primarily because of the lack of dateable material in the area. There are no dates from the offshore realm accurately constraining deglaciation in this area. To the north of the Uummannaq area, a date from a shell in raised marine deposits on Svartenhuk Halvø places deglaciation of the inner shelf before 10.6 ka BP (10,764-10,467 cal. yr BP; 9730±60 ^{14}C yrs BP, Bennike, 2000, *Fig. 6.12*). In the southern part of the Uummannaq area, Símonarson (1981) obtained a date of 10.4 ka BP (10,705-9953 cal. yr BP; 9510±150 ^{14}C yrs BP) on a bivalve (*Hiatella arctica*) found in raised marine deposits (45 m a.s.l.) at Sarfâqfîk, half way along Nuussuaq peninsula (see *Fig. 6.12*). New cosmogenic surface exposure ages (*Fig. 6.12*) help further constrain the pattern of early Holocene deglaciation in the inner Uummannaq shelf area (D.H. Roberts, personal communication).

Material from a marine-terminating glacier in Uummannaq Fjord (clasts deposited from icebergs calving at the glacier termini and fine-grained glacial flour ejected in subglacial/englacial meltwater deposited from suspension) is interpreted to have been the major influence on sedimentation in core MSM-343520_G before *ca.* 10.7 ka BP (as illustrated in *Fig. 6.13a*). The

presence of glacimarine sediments at the base of core MSM-343520_G suggests that an extensive, rather than reduced, ice sheet configuration existed on the Uummannaq shelf during the early Holocene. The lowermost date obtained from ice-proximal glacimarine sediments near the base of core MSM-343520_G indicates deglaciation took place before *ca.* 10.9 ka BP (11,158-10,630 yr. BP) on the mid-Uummannaq shelf.

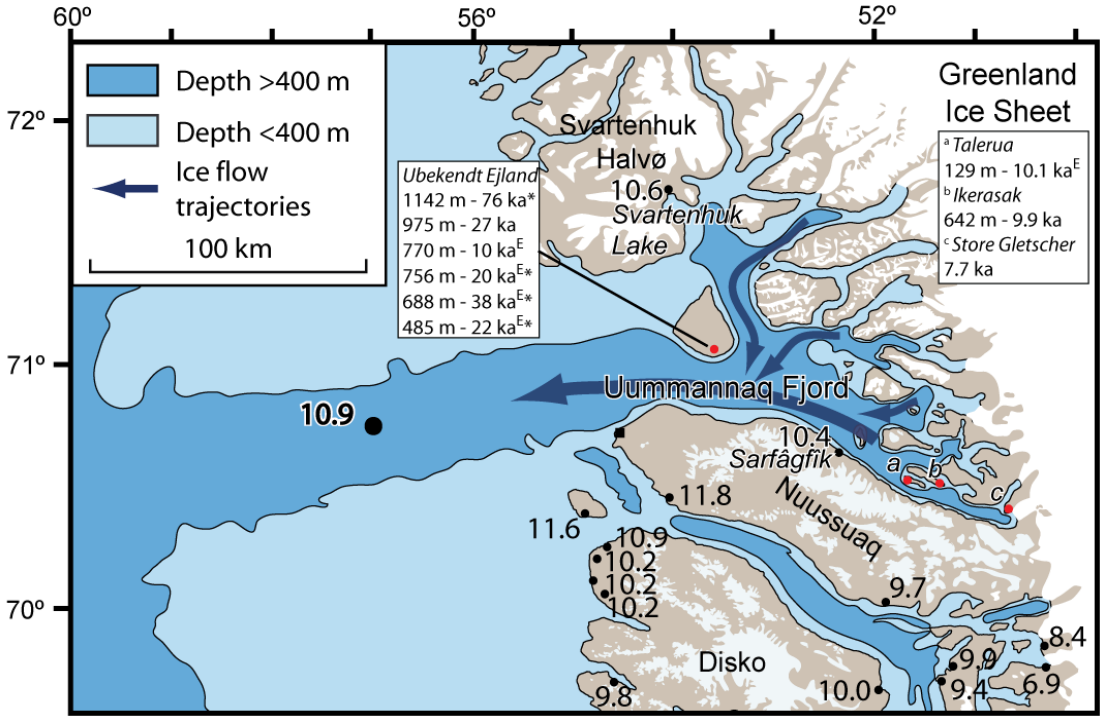

Figure 6.12 Minimum ages for deglaciation in the Uummannaq area. The date obtained from the lower part of core MSM-343520 is shown in bold (with larger filled circle). Dates from Ubekendt Ejland, Talerua (a), Ikerasak (b), and Store Gletscher (c) (all marked as filled red circles), are unpublished cosmogenic radionuclide exposure ages (D.H. Roberts, personal communication). Quoted altitudes for ages are metres a.s.l., ^{E} denotes dates obtained from erratic boulders (all others are taken from bedrock), and asterixes (*) denotes samples with isotopic inheritance from earlier surface exposure (i.e. sample age is too old). Black square marks the position of a raised delta complex at the western tip of Nuusuuaq peninsula discussed in the text. Arrows mark ice flow trajectories in the Uummannaq ice stream system onset zone (D.H. Roberts, personal communication).

A date of 10 ka on an erratic deposited on Ubekendt Ejland (770 m a.s.l.) by glacier ice in Uummannaq Fjord indicates ice was thinning at this time (D.H. Roberts, personal communication). A similar age of 9.9 ka at a slightly lower altitude (642 m a.s.l.) on glacially-abraded bedrock on Ikerasak further supports surface thinning of the ice sheet, while an age of 9.9 ka retrieved from an erratic on Talerua at a much lower altitude of 129 m a.s.l. suggests ice

must have retreated landwards of this location at *ca.* 10 ka (*Fig. 6.12*) (D.H. Roberts, personal communication). The two-sigma age range (10,705-9953 cal. yr BP) of the radiocarbon dated shell from Sarfâgfík encompasses these surface exposure ages indicating a slightly later deglaciation of the inner shelf area than the mean age (10.4 ka BP) suggests. While ice must have retreated in the order of 200 km in approximately 600-1200 years (*ca.* 170-330 m yr^{-1}) during the rapid clearance of the mid- to inner-Uummannaq shelf, ice retreat subsequently slowed dramatically, retreating only *ca.* 25 km between *ca.* 10 and 7.7 ka BP (< 11 m yr^{-1}) based on the exposure date obtained from Store Gletscher (*Fig. 6.12*) (D.H. Roberts, personal communication). Islands in the inner shelf and higher terrain along the modern coastline probably acted as topographic 'pinning points' to slow or halt ice recession during the latter stages of deglaciation (*sensu stricto* Warren and Hulton, 1990).

The fast nature of ice withdrawal into inner Uummannaq Fjord suggests that rapid calving, facilitated by a straight and relatively unobstructed glacial trough that deepens landwards, drove deglaciation. Calving velocity would have increased since the basal buoyancy of marine-based ice would have increased as it retreated into deeper waters where grounded ice would have been positioned relatively lower in the water. The foraminiferal data show no clear evidence for a significant oceanic influence during initial deglaciation. However, this is not unexpected, since the dominance of glacimarine sedimentation and meltwater injections during initial deglaciation provide inhospitable conditions for species commonly associated with relatively warm Atlantic water influence, and instead favour opportunistic species (e.g. Korsun and Hald, 1997). It is further possible that the preceding collapse of ice cover in Disko Bugt would have had a cooling influence on ocean temperatures by deflecting relatively warm Atlantic-sourced water off the shelf, though there is no evidence of a northwards penetration of Atlantic water into Baffin Bay at this time.

The apparently fast retreat across the Uummannaq shelf is similar in nature to deglaciation across the outer- to mid-shelf west of Disko Bugt, albeit more than 1000 years later. One possible explanation for this could be that the grounded ice sheet in Uummannaq Fjord was thicker than ice in Disko Bugt, and therefore more resistant to rising eustatic sea-level. The

glacial limit was located at *ca.* 770 m a.s.l. on Ubekendt Ejland during the early Holocene (D.H. Roberts, personal communication), suggesting ice thicknesses in excess of *ca.* 1500 m in Uummannaq Fjord (i.e. a 'thick' ice sheet configuration in Uummannaq fjord prior to deglaciation). A submarine escarpment, composed of Tertiary basalts which are harder and more resistant than the Cretaceous-Paleocene sediments to the east, crosses Karrats Fjord between Ubekendt Ejland and Svartenhuk Halvø. Ice streams feeding from the northern part of the Uummannaq ice stream system would have been routed southwards past the east side of Ubekendt Ejland by this escarpment (see *Fig. 6.*12; D.H. Roberts, personal communication). The confluence of ice streams from the north would have contributed to maintaining thicker ice in Uummannak Fjord. This combined with the buttressing effect of Nuussuaq peninsula against the southern side of the ice stream would have contributed to maintaining ice stream stability in the Uummannaq area later than to the south in Disko Bugt.

A raised delta/alluvial fan complex at the westernmost tip of Nuussuaq peninsula (black square in *Fig. 6.12*) must have formed when extensive outlet glaciers occupying Vaigat and Uummannaq Fjords coalesced under full glacial conditions (Bennike *et al.*, 1994). However, the youngest dates (based on amino acid racemisation) obtained from *in situ* shell material (at 48 m a.s.l.) found just below the local marine limit (60 m a.s.l.) suggests these sediments were deposited during the Svartenhuk marine event during the last interglacial, or perhaps even earlier (Bennike *et al.*, 1994). While the old age of these dates does not fit in the new deglacial chronology presented here, there is also no apparent geomorphological evidence in aerial photographs to suggest this area was glaciated. Instead, this small enclave may have remained unglaciated, bounded by a valley glacier to the east, and ice streams in Uummannaq Fjord and the Vaigat to the north and south, respectively, preserving this feature from an earlier glaciation.

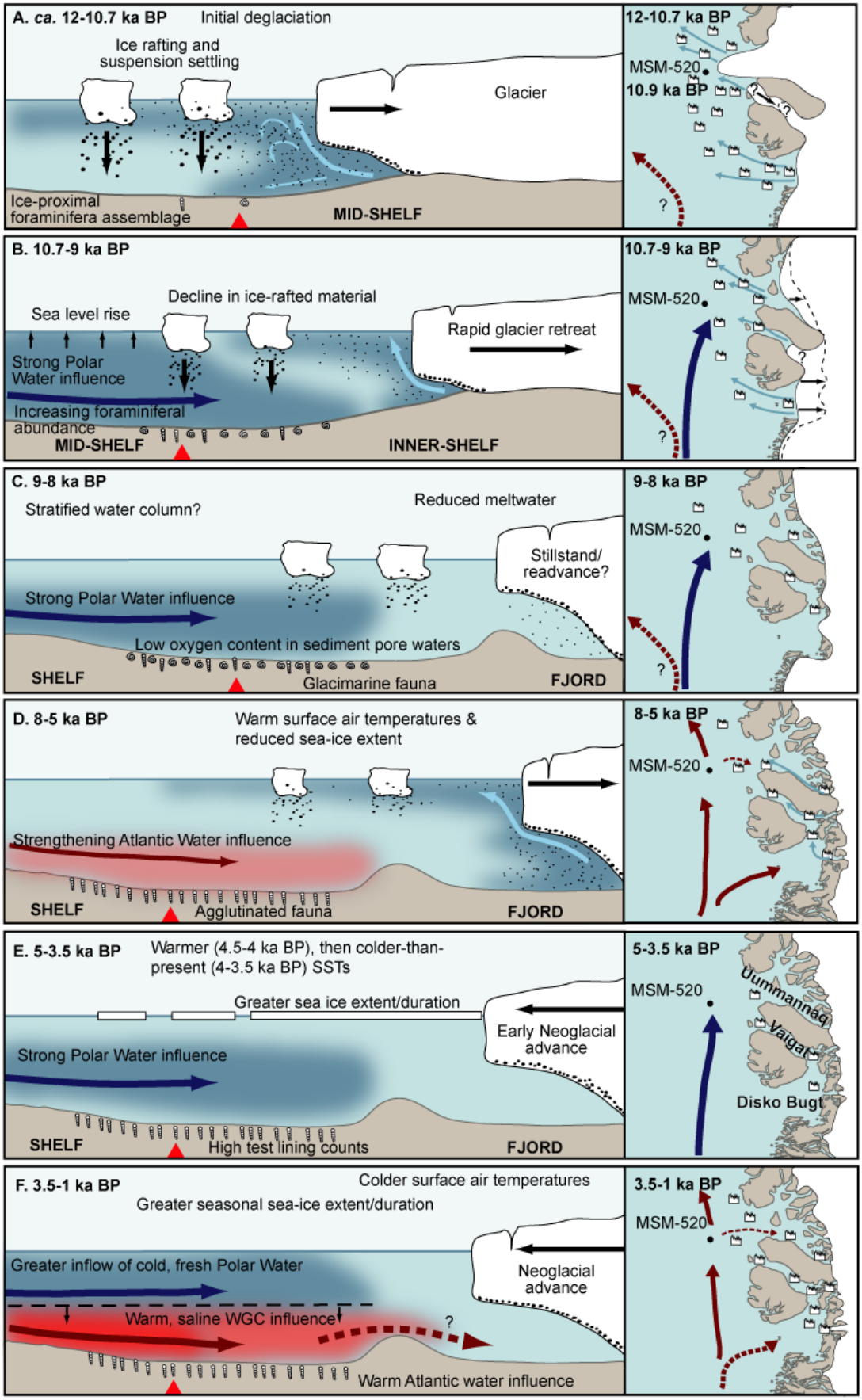

Figure 6.13 (continued below).

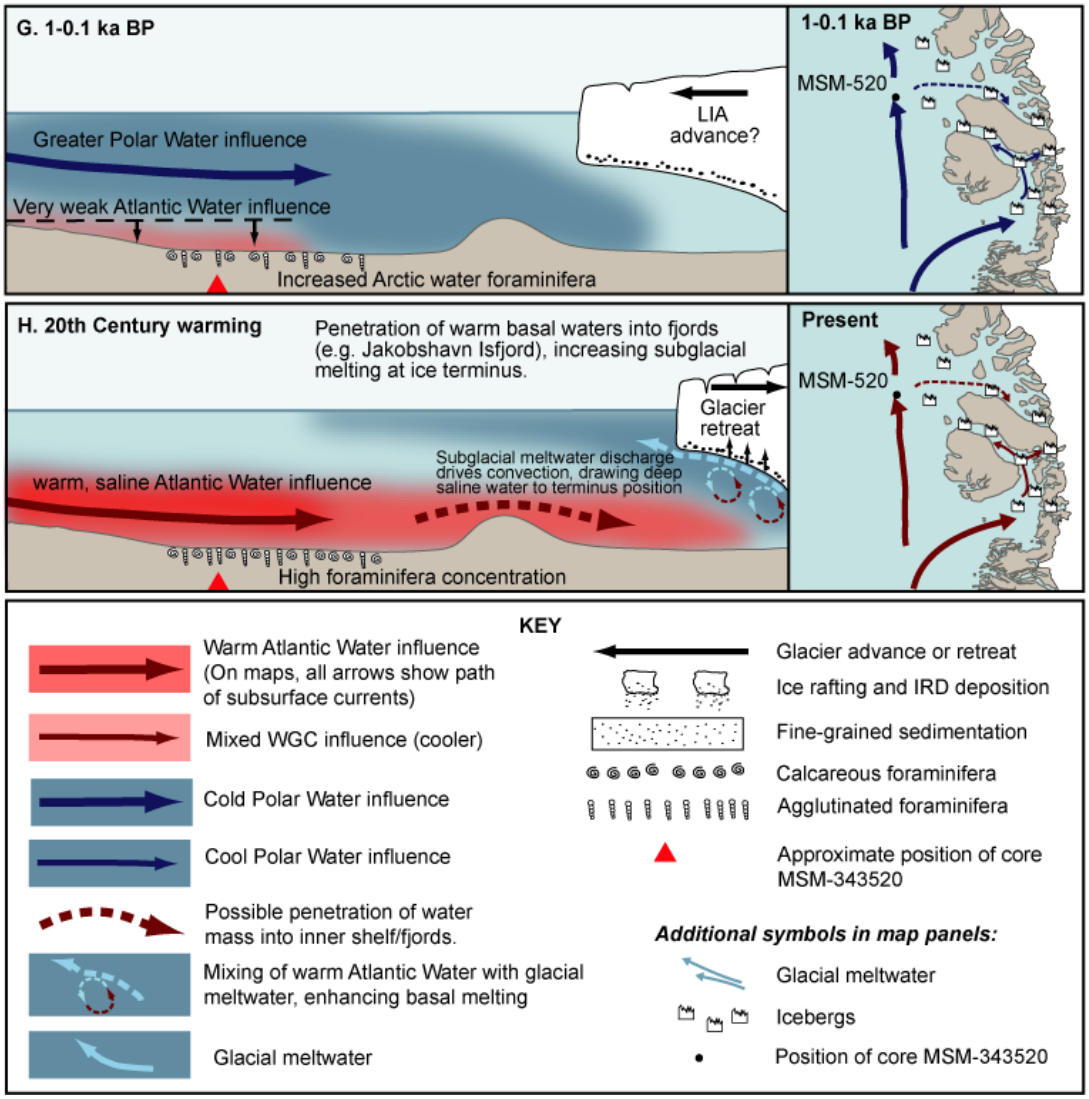

Figure 6.13 Time-slice conceptual cartoons identifying the main changes in water mass characteristics on the Uummannaq shelf and corresponding changes in ice margin position. The left panel shows a cartoon cross-section across the shelf, illustrating the main ocean and glacier changes. The right panel shows the evolution of sub-surface currents in the West Greenland area based on foraminiferal data from core MSM-343520_G and MSM-343520_MC, together with a new model for ice margin retreat for the Uummannaq shelf.

6.4.2 Links between climate change and ice-ocean interactions

As ice retreated into Uummannaq fjord during deglaciation and glacimarine influences at site MSM-343520 declined, the foraminifera assemblages in core MSM-343520_G record more regional palaeoceanographic changes in sub-surface water mass characteristics (compare *Fig. 6.13a and c*). As a result, foraminiferal data from core MSM-343520_G record Holocene changes in the relative temperature of basal waters impinging on the shelf in the Uummannaq trough. The following section addresses linkages between changes in ocean temperature and ice margin position.

The Holocene is an ideal period in which to assess the relative contribution of climatic versus oceanic temperature changes on ice margin stability because there are several well-established brief climate oscillations, including, for example, the Medieval Warm Period and the Little Ice Age, and the so-called 8.2 ka event. Identifying Holocene warming trends in marine records is critical to understanding the possible role of ocean forcing on ice front stability linked to changes in the sub-surface water temperature of the WGC. Despite generally poor constraints on Holocene glacial history in the Uummanaq area, the subsurface temperature records from core MSM-343520_G and MSM-343520_MC presumably provide a good indication of subsurface temperatures of water masses that may also penetrate into Disko Bugt, where glacial history is more tightly constrained. Foraminifera-based temperature estimates for basal waters on the Uummannaq shelf probably underestimate temperatures of sub-surface waters entering Disko Bugt, since further cooling takes place as Atlantic and Polar water components of the WGC continue to mix as they move northwards (e.g. Chapman and Beardsley, 1989).

The text in parentheses at the end of the following sub-titles identifies the relevant time-slice in *Fig. 6.13* discussed in each section.

A record of the 8.2 ka BP event in West Greenland waters (Stage C)

The drainage of glacial lakes Agassiz and Ojibway through Hudson Strait during the final stages of Laurentide ice sheet collapse at *ca.* 8.2 ka (e.g. Barber *et al.*, 1999; Teller *et al.*, 2002; Nesje *et al.*, 2004; Flesche Kleiven *et al.*, 2008) added an estimated 183,000 km^3 of meltwater to the

Labrador Sea (Clark *et al.*, 2001). However, the response of the North Atlantic current system to large meltwater injections and how these impact on climate are still poorly understood. The so-called 8.2 ka event (the most extreme Holocene climate oscillation), is identified in Greenland ice cores as a 4-8°C cooling spanning *ca.* 160 years (Alley *et al.*, 1997; Rasmussen *et al.*, 2007; Thomas *et al.*, 2007; Lowe *et al.*, 2008). The climate anomaly is thought to have been caused by a slow down in thermohaline circulation due to freshening of North Atlantic surface waters by glacial meltwater (e.g. Alley *et al.*, 1997; Barber *et al.*, 1999; Nesje *et al.*, 2004; Alley and Agústsdóttir, 2005; Ellison *et al.*, 2006; Flesche Kleiven *et al.*, 2008). The 8.2 ka event occurred during a period of broader climate cooling, particularly in the North Atlantic region, from *ca.* 8.6 to 7.9 ka BP (Alley and Agústsdóttir, 2005; Rohling and Pälike, 2005).

Two significant and abrupt spikes in S *feylingi* abundance, coeval with decreased benthic foraminifera $\delta^{13}C$, can be recognised in core MSM-343520_G (*Fig. 6.11*) at *ca.* 9.0-8.8 ka BP and *ca.* 8.2-7.9 ka BP. Since the West Greenland Ice Sheet margin was situated within fjords at the present terrestrial margin after 9 ka BP (*Fig. 6.12* and *6.13c*), these distinctive features most likely reflect a more regional palaeoceanographic influence. There are no major changes in MSM-343520_G core sedimentology that may accompany an event of local origin, and furthermore, it is unlikely that freshwater flux from a distal West Greenland Ice Sheet margin would directly influence bottom-water oxygen isotope composition on the Uummannaq shelf. There is a remarkable similarity in timing and nature of the two spikes in core MSM-343520_G spike to other North Atlantic Ocean records that suggest two major stages of proglacial lake drainage during the collapse of the Laurentide ice sheet (e.g. Keigwin *et al.*, 2005; Ellison *et al.*, 2006; Hillaire-Marcel *et al.*, 2007; Flesche Kleiven *et al.*, 2008). The first *S. feylingi* and isotope spike (9-8.8 ka BP) occurs earlier than in these North Atlantic records, although the precise timing of these features are subject to constraints of the age-depth model, including dating errors and uncertainties in the local reservoir age. Nevertheless, these data provide the first evidence that a low-salinity anomaly linked to glacial outburst floods propagated into Baffin Bay along the West Greenland shelf.

Ice sheet response to 8.2 ka event

The possibility of an ice sheet response the 8.2 ka event in central West Greenland was raised by Long and Roberts (2002), who identified a deviation from the steep falling RSL trend in southwestern Disko Bugt at this time indicative of crustal reloading due to ice sheet expansion. More recent investigations by Young *et al. (2011)* found evidence for an advance of Jakobshavn Isbræ just before 8.0±0.2 ka, corresponding to the deposition of the Tasisussaq moraine (the younger of the 'Fjord Stade' moraines). The coincidence of this brief ice sheet advance and the 8.2 ka event may represent a rapid ice-margin response to a short-lived climate event (Young *et al.*, 2011). However, Long *et al.* (2006) suggest that the 8.2 ka event was too short to have a significant impact on ice dynamics in Disko Bugt, and was unlikely to reverse the trend of rapid Early Holocene ice retreat. Instead, Long *et al.* (2006) suggest the Fjord Stade moraines fringing the eastern coast of Disko Bugt represent diachronous ice margin retreat at *ca.* 10-8 ka BP, due to the varying influence of topography and ice sheet/ice stream dynamics on regional deglaciation.

The increase in magnetic susceptibility and [Si/Al] at *ca.* 8.3-8 ka BP may be interpreted as a reduced mainland terrestrial influence (particularly a decline in fine-grained sedimentation from suspension) during this interval, resulting in a relative increase in magnetite-bearing basaltic sediments derived from Disko Island and Nuussuaq peninsula. These changes may reflect an ice sheet response to the 8.2 ka cooling event, possibly linked to atmospheric cooling over Greenland, a reduction in surface ablation, and a subsequent decline in fine-grained sediments ejected at glacier termini. The $\delta^{18}O$ (*N. labradorica*) minima may be indicative of bottom water freshening. However, it is possible that the $\delta^{18}O$ values from the infaunal *N. labradorica* reflect microhabitat changes and pH and carbonate sediment porewaters, perhaps linked to changes in the depth habitat of *N. labradorica* (e.g. Ravello and Hillaire-Marcel, 2007).

The Fjord Stade has been divided into two phases of moraine formation; an older Marrait moraine system (9.9-9.3 ka BP) deposited due to decreasing ablation and calf ice production, partly because of reduced marine influence at the ice margin and due to complex climate interactions, and the younger Tasisussaq Moraine system (8.7-7.7 ka BP). The deposition of

the Marrait moraine appears to have preceded the first interval of freshening, which more closely corresponds to the glacier expansion on Disko Island at *ca.* 9 ka BP identified by Ingólfsson *et al.* (1990). These glacier advances suggest a link with cooler surface waters, which probably had a cooling influence on regional air temperatures during these intervals.

Initiation of the West Greenland Current on the Uummannaq shelf

A number of studies from along West Greenland (e.g. Donner and Jungner, 1975; Funder and Weidick, 1991; Dyke *et al.*, 1996; Lloyd *et al.*, 2005) and northern Baffin Bay (e.g. Mörner and Funder, 1990; Kelly *et al.*, 1999; Levac *et al.*, 2001; Knudsen *et al.*, 2008b) document an early re-establishment of Atlantic water intrusion into Baffin Bay following deglaciation. A warmer WGC influence has been identified from as early as 10.9 ka BP (9275±110 ^{14}C yr. BP, Ua-4448) in northern Baffin Bay (Knudsen *et al.*, 2008b) based on increased planktonic foraminifera flux. In central West Greenland, however, foraminifera and mollusc data suggest warming did not take place until after 9.2 ka BP (Funder and Weidick, 1991; Lloyd *et al.*, 2005), and probably not until after 8.7 ka BP (see Chapter 5).

Foraminiferal evidence indicates that the initiation of WGC warming in central West Greenland began at *ca.* 8 ka BP (*Fig. 6.11h,i; Fig. 6.13d*); much later than in northwest Greenland (Dyke *et al.*, 1996), northern Baffin Bay (Levac *et al.*, 2001; Knudsen *et al.*, 2008b), and the Baffin Island shelf (Osterman and Nelson, 1989). This can be partly explained by the significant meltwater flux produced during the retreat of the central west sector of the Greenland Ice Sheet from an extensive mid- to outer-shelf position to the inner shelf. This would have diluted the north-flowing WGC (and thereby lowering the temperature of the basal water mass) or deflected warmer WGC waters off the shelf (as illustrated by the dashed red line in the right panel of *Fig. 6.13a*).

Palaeoenvironmental conditions from 8-5 ka BP (Holocene thermal optimum, Stage D)

This is the first high-resolution marine record with a robust dating framework that captures the pattern and timing of early Holocene warming on the shelf in central West Greenland. Lloyd *et al.* (2005) constrained the initiation of subsurface warming (and the establishment of the modern

pattern of circulation) inside Disko Bugt to sometime after 9.2 ka BP. Data from core MSM-343340_G (Chapter 5) further constrains the initiation of warming to shortly after 8.7 ka BP. However, the foraminifera record (*Fig. 6.11h* and *i*) in core MSM-343520_G suggest warming of subsurface waters impinging on the seafloor in the Uummannaq trough did not begin until *ca.* 8 ka BP, and lasted until 5.2 ka BP, with peak warmth (indicated by higher abundances of *N. labradorica*) occurring between 7.7 and 6 ka BP (*Fig. 6.*8). The cartoon in *Fig. 6.13d* shows the reconstructed warming in sub-surface waters during this interval as an intrusion of warmer mixed-WGC waters on to the Uummannaq shelf (i.e. mix of Atlantic and Polar water, characterised by dominance of agglutinated fauna), rather than a dominant warm Atlantic influence. This is because sub-surface water temperatures probably remained below modern values (see *Fig. 6.11j*), with optimal marine conditions not occurring until the late Holocene.

Cosmogenic surface exposure dates from the adjacent to Store Gletsher (*Fig. 6.12*) suggest the ice sheet retreated onto land at *ca.* 7.7 ka BP (D.H. Roberts, personal communication), though marine-terminating glaciers would have continued to occupy fjords at this time. In the more widely studied Disko Bugt area, ice retreated behind its present extent before 6.1 ka BP and advanced after 3.5 ka BP based on reworked shells and bone material found in moraine adjacent to Jakobshavn Isfjord (Weidick *et al.*, 1990; Weidick, 1992; Weidick and Bennike, 2007). Marine-terminating glaciers in Disko Bugt (Jakobshavn Isbræ, Alángordliup sermia, and glaciers terminating in Pâkitsoq, *ca.* 35 km north of Jakobshavn Isfjord) are estimated to have retreated 15-20 km during the HTM Data from subsurface radar mapping of fjords in Disko Bugt. By identifying the likely origin of morainal material from radar mapping, Weidick (1992) estimates that Jakobshavn Isbræ retreated more than 20 km behind the present margin during the HTM. Young *et al.* (2011) use ^{10}Be surface exposure dating of bedrock and erratic boulders, combined with radiocarbon dating of proglacial/threshold lakes (conceptual approach described in detail in Briner *et al.*, 2010) at locations within a few kilometres either side of Jakobshavn Isfjord to demonstrate that ice retreated rapidly at *ca.* 100 m yr^{-1} between 8 ka and 7.5 ka. Additional ^{10}Be ages from bedrock approximately 10-15 km north of Jakobshavn Isfjord indicate that land-based ice retreated synchronously with that of marine-based ice in the Isfjord

(Young *et al.*, 2011), suggesting atmospheric warming was the dominant driving mechanism for ice retreat during the early- to mid-Holocene.

In Disko Bugt (e.g. Weidick *et al.*, 1990; 1992) and southerly areas such as Holsteinborg (e.g. Roberts *et al.*, 2009), surface ablation due to warmer air temperatures has been suggested as the main mechanism by which the ice sheet lost mass after the initial marine-based deglaciation.

The timing of the HTM varies spatially across the Arctic region (Kaufman *et al.*, 2004). In central West Greenland, a HTM of *ca.* 7-4 ka BP has been identified in terrestrial records (Fredskild, 1983, 2000; Willemse and Törnqvist, 1999; Bennike, 2000; McGowan *et al.*, 2003; Axford *et al.*, 2010; Young *et al.*, 2011). Chironomid reconstructions from a proglacial lake on the northern flank of Jakobshavn Isfjord, Disko Bugt, suggest summer air temperatures were approximately 2°C warmer than present between *ca.* 6 and 4.5 ka BP (Axford *et al.*, 2010; Young *et al.*, 2011). This corresponds closely to Bennike's (2000) interpretation for the terrestrial HTM in central West Greenland occurring between 6.5 and 4 ka BP based on the presence of *Betula nana* (Dwarf Birch) pollen in lacustrine sediments from Nuussuaq peninsula. The period of sub-surface WGC warming recorded in core MSM-343520_G closely corresponds to the occurrence of warmth-demanding boreal molluscs along West Greenland (from Holsteinborg to Orpigsôq, southeastern Disko Bugt) between 8.9 ka BP (8360±120 ^{14}C yr. BP) and 5.2 ka BP (4870±110 ^{14}C yr. BP). These thermophilous molluscs suggest water temperatures were 1-3°C warmer than present during this interval (Weidick, 1972a; Funder and Weidick, 1991). The initiation of ocean warming on the Uummannaq shelf precedes the terrestrial Holocene thermal maximum (HTM) in West Greenland by 1.5-2 ka.

The reduction in meltwater flux as the Greenland Ice Sheet approached its modern limit in the Uummannaq area shortly after *ca.* 8 ka BP may have permitted the intrusion of relatively warm and saline deep waters into inner fjord areas, possibly influencing ice stream dynamics by increasing basal melt of marine terminating ice streams. However, since foraminiferal reconstructions suggest slightly cooler subsurface water conditions than at present, and there is

no significant WGC influence in the modern Uummannaq fjord, at least close to the calving margin, any ocean warming may have only had a minor direct influence on ice dynamics. However, it is likely that the early Holocene warming in WGC temperatures played an important role in the development of a warmer Baffin Bay climate, driving land-based deglaciation. The interval of initial warming in core MSM-343520_G from *ca.* 8 ka BP corresponds with reconstructions of maximum August sea-surface temperatures (Solignac *et al.*, 2006) and open water conditions (<0.5 months where sea-ice cover is greater than 50%) between 8 and 6 ka BP in HU90-013-013P from the southwest Greenland Rise (de Vernal and Hillaire-Marcel, 2006).

Palaeoenvironmental conditions from 5-3.5 ka BP (Neoglaciation, Stage E)

The HTM was followed by the Neoglacial, a period of cooling and ice sheet expansion in Greenland spanning the past *ca.* 4 ka BP and culminating in the Little Ice Age (e.g. Weidick, 1993; 1996; Kaplan *et al.*, 2002). The dominance of *C. arctica* and the relative increase in abundance of *S. biformis* in the agglutinated foraminifera assemblages indicates that this period of ice sheet expansion was characterised by a dominance of cold Arctic Waters on the Uummannaq shelf (*Fig. 6.13E*). The pre-Historical moraines on Nuussuaq peninsula may be linked to the Drygalski moraines (Weidick, 1972; Kelly, 1980). While the age of the Drygalski moraines are unknown, they are thought to have been deposited during the Neoglaciation between *ca.* 5-2.5 ka BP (Weidick, 1996), and are associated with a glaciation limit 200-500 m lower than the modern limit (Weidick, 1968; Kelly and Lowell, 2009). The cooling in sub-surface ocean temperatures is associated with a deterioration in climatic conditions from *ca.* 5-4 ka BP documented in West Greenland lacustrine pollen and chironomid records (Fredskild, 1984; Young *et al.*, 2011). This interval of cold atmospheric and oceanic temperatures corresponds to the gradual advance of Jakobshavn Isbræ from 5-4 ka BP (Weidick, 1992; Weidick *et al.*, 1990; 2004).

Palaeoenvironmental conditions from 3.5-1 ka BP (Stage F)

The major shift in foraminifera assemblage composition at 3.5 ka BP, from fauna dominated by *C. arctica* to one dominated by *A. glomerata*, is indicative of amelioration in subsurface waters

impinging on the Uummannaq shelf. This is followed by further warming of subsurface waters between 1.5 and 1 ka BP, suggested by higher abundances of species associated with Atlantic Water influence. However, in inner Disko Bugt, Lloyd *et al.* (2007) identify the period 3.5 ka BP to 2 ka BP as an interval of cooling in bottom waters, with particularly cold bottom waters at 2.7-2.2 ka BP. Surface water cooling is also identified from diatom and dinoflaggellate cyst assemblages in Disko Bugt from 3.5 ka BP to 2 ka BP (Moros *et al.*, 2006; Seidenkrantz *et al.*, 2008), and suggested by a reduction in sea salts from the Devon Ice Cap ice core on Baffin Island, suggesting greater sea-ice cover in Baffin Bay from 3.5 ka BP (Fisher, 1976). Lloyd (2006b) find a link between warmer sub-surface waters in inner Disko Bugt between *ca.* 1650-500 cal. yr BP and recession of the Jakobshavn Isbræ ice front.

Palaeoenvironmental conditions from 1-0.1 ka BP (Little Ice Age, Stage G)

The interval 1-0.1 ka BP is characterised by Arctic Water influence on the Uummannaq shelf (*Fig. 6.13 G*). A chironomid-based temperature reconstruction from Disko Bugt suggests that July air temperatures were close to modern values at *ca.* 2.5 ka BP, and approximately 1°C cooler than present at 500 cal. yr BP (Young *et al.*, 2011). The dominance of Arctic Water along central West Greenland at this time may be linked to changes in the NAO. A proxy-based reconstruction by Trouet *et al.* (2009) suggests the Medieval Warm Period from 900 to 500 cal. yr BP was characteterised by a persistent positive NAO phase. At present, a positive NAO phase is linked with increased westerly wind stress and a strengthening and narrowing of the North Atlantic Current. Under these conditions, there is less westward branching of warm, saline Atlantic Water, and therefore a reduced contribution of Irminger Current water to the WGC. In Disko Bugt, the cold atmospheric and marine conditions are associated with the continued advance of Jakobshavn Isbrae towards the mouth of Jakobshavn Isfjord, reaching its maximum extent sometime around AD 1800 (Briner *et al.*, 2010).

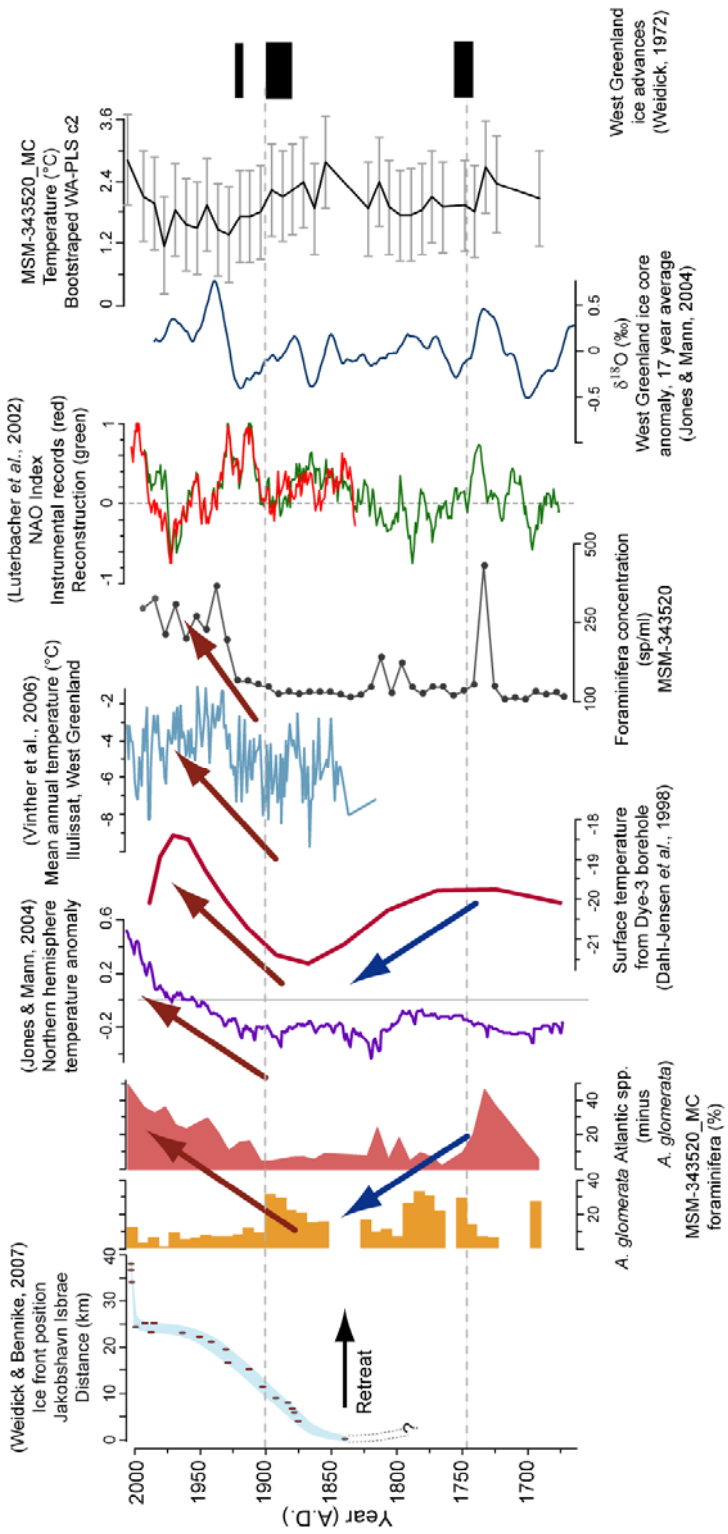

Figure 6.14 Summary data and transfer function reconstruction for core MSM-343520_MC, with climate reconstructions and instrumental data, and periods of ice advance in West Greenland, and the observed retreat of Jakobshavn Isbrae.

20th Century warming (Stage H)

The foraminiferal record illustrated in *Fig. 6.14* clearly shows a period of cooling in sub-surface WGC temperatures between *ca.* A.D. 1750 and A.D. 1850, as indicated by a minima in the Atlantic group of agglutinated foraminifera. Briner et al. (2010) and Young et al. (2011) suggest that Jakobshavn Isbræ, and presumably other tidewater glaciers in Disko Bugt and Uummannaq District, reached its LIA maximum extent coeval with cool ocean temperatures. While cooler atmospheric temperatures permitted ice sheet expansion at this time, the absence of warmer waters penetrating into the inner fjords would have allowed marine-based ice to advance. After A.D. 1850, there is a gradual warming in sub-surface water temperatures, indicated by an increase in *A. glomerata* up to the start of the 20th Century, and followed by increases in Atlantic Water species and foraminifera concentration (*Fig. 6.14*) that indicate higher sub-surface water temperatures in central West Greenland. The increase in Atlantic Water influence on the Uummannaq shelf coincides with the gradual retreat of Jakobshavn Isbræ (with more frequent observations of ice margin position from A.D. 1875) (Weidick and Bennike, 2007).

Chapter 7

MID- TO LATE-HOLOCENE PALAEOCEANOGRAPHY IN THE VAIGAT, WEST GREENLAND

Camilla S. Andresen (GEUS) provided sedimentological (sieving of coarse grain size fractions and clast counts), petrological, and magnetic susceptibility core scanning data from core DA06-139G. This data is presented in Andresen et al. (2011).

Chapter 7

Mid- to late-Holocene palaeoceanography in central West Greenland: Ice sheet history and ocean forcing

7.1 Introduction

The Vaigat (*Fig. 2.1*), located between Disko Island and Nuussuaq peninsula, is an important location for understanding late Holocene changes in ice stream activity because at present the majority of calf ice produced in Disko Bugt is routed northwards through this fjord by the dominant surface currents (see *Fig. 2.6*). The modern water mass structure of the Vaigat is characterised by a three-layer structure, with surface waters (0-50m), Polar water (50-100/200m), underlain by Atlantic water (>100/200m). Surface waters (<50m depth) are cooled and freshened by melting of icebergs and seasonal sea ice. A cold and low-salinity Polar water layer sits between 50 to 100m depth. During boreal summer months, inflow of surface-heated waters from Disko Bugt raise temperatures in this layer, and deepen the temperature minima from *ca.* 100m to *ca*. 200m. Atlantic-sourced waters lie beneath the Polar water layer, generally at depths exceeding 150m. The warm core of Atlantic water outside Disko Bugt is located at 300-400m depth (2.5-3.5°C), and enters the main part of the bay by crossing a threshold depth of 305m (*Fig. 2.2*). Relatively warm, saline Atlantic water in Disko Bugt is located at depths exceeding 250m. However, in order to enter the Vaigat, Atlantic water must cross a shallow threshold (*ca. 245 m*) in northeast Disko Bugt (between Disko Island and Arveprinsens Ejland) (*Fig. 2.2*).

Core DA06-139 was collected midway along the Vaigat (see Chapter 3 for core details, and *Fig. 3.1* for core location). In this chapter, a combination of benthic foraminifera and sedimentological data are used to investigate the linkages between ocean circulation and ice margin stability. The benthic foraminifera are used to reconstruct changes in the influence of relative warm and saline Atlantic Water transported by the WGC into Disko Bugt and the Vaigat. Since warm Atlantic Water must overtop the shallow sill at the southeastern entrance to the Vaigat, the foraminifera in core DA06-139G presumably allow intervals influenced by generally

warmer intermediate waters in Disko Bugt to be identified. Foraminifera data are supplemented by sedimentological data (grain size, basalt versus non-basalt clasts > 500 μm) provided by C.A. Andresen (see Andresen *et al.*, 2011). Sedimentological data provide information on the calving activity of marine-terminating glaciers in Torssukátak, as well as Jakobshavn Isbræ to the south, which would also presumably exert a significant influence on sedimentation via ice-rafting.

7.2 Results

7.2.1 Chronology and sedimentation rates

The age model for core DA06-139G (*Fig. 7.1*) is based on 9 AMS ^{14}C dates from shells, benthic foraminifera and plant remains measured at the AMS ^{14}C Dating Centre, University of Aarhus. A general low abundance of calcareous foraminifera necessitated the use of these other materials for dating. OxCal v4.1 (Bronk Ramsey, 2000) was used to calibrate radiocarbon dates using the Reimer *et al.* (2009) marine radiocarbon curve (ΔR 0±0) (*Table* 7.*1*). A near-basal date (at 435cm) of 4933±80 cal. yr BP indicates that this core provides a record of mid- to late-Holocene palaeoceanographic changes. The age model is based on linear interpolation between calibrated radiocarbon dates. The uppermost date (AAR 10953, *Table* 7.1) of 652-597 cal. yrs BP has been removed from the age model. This has been done for two main reasons. Firstly, the calibrated age of AAR 10952 (*Table* 7.*1*) is similar in age to sample AAR 10953, though is situated approximately 50 cm lower in the stratigraphical record, and, together with an additional calibrated date in the upper part of the core (AAR 13060, *Table* 7.*1*) lies close to a straight line between the underlying calibrated radiocarbon date and the top of the core. Secondly, the age of the top of the core is believed to be close to modern since the 125 mm diameter gravity corer causes relatively little disturbance of surface sediments (A. Kuijpers, personal communication, 2009). However, since the age-depth model is based on dates obtained from shells (which are more mobile in near-surface sediments) and plant material (which have been transported into the area) the age model is susceptible to dating areas. Not withstanding these possible errors, the age model appears to be robust (*Fig. 7.1*). These dates in general lie in stratigraphical order; there are no major changes in sedimentation rates, and no evidence of hiatuses in the record.

The age model indicates that the sedimentation rate has gradually increased over the past 5 ka BP, from 0.44 mm yr^{-1} at the base to more than 1 mm yr^{-1} in the upper part of the core DA06-139G (*Fig. 7.1*). This includes an interval of apparently rapid sedimentation (3.87 mm yr^{-1}) at 1.4 ka BP, although this may be a result of an erroneous date at 134 cm depth. Assuming constant sedimentation and without taking into account sediment reworking, each 2 cm foraminifera sample represents approximately 20 to 50 years of sediment accumulation.

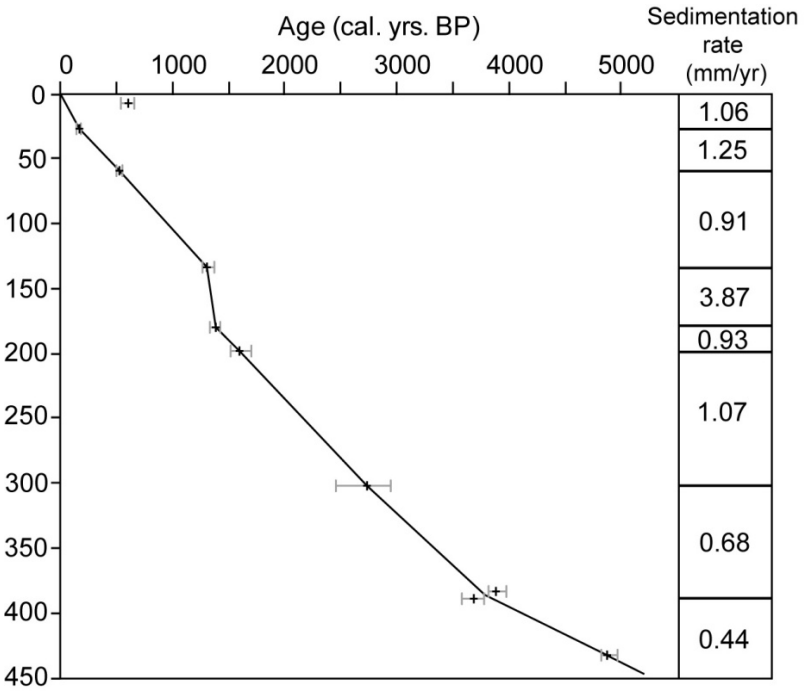

Figure 7.*1* Age-depth model for core DA06-139G, based on linear interpolation between mean calibrated radiocarbon ages. Grey error bars indicate the two standard deviation age range.

Core depth (cm)	Lab. Code	Material	14C age ± 1σ (yr BP)	Calibrated age (yr BP)	Age range 2σ (yr BP)
7 – 8	AAR 10953*	Gastropod	1013 ± 35	590	652 - 527
27 – 28	AAR13060	Gastropod	607 ± 22	250	302 - 145
58 – 60	AAR 10952	Gastropod	903 ± 35	515	598 - 457
132 – 136	AAR 10951	Plant remains	1797 ± 40	1342	1440 - 1260
180	AAR13059	Plant remains	1913 ± 27	1456	1535 - 1373
199 – 200	AAR 10950	Plant remains	2090 ± 42	1666	1792 - 1547
302 – 304	AAR 13061	Benthic forams.	3030 ± 90	2822	3070 - 2604
385	AAR 10949**	Gastropod	3976 ± 38	3977	4093 - 3849
390 – 393	AAR 10948**	Plant remains	3833 ± 43	3783	3913 - 3783
435	AAR 10947	Shell	4709 ± 40	4939	5059 - 4825

Table 7.1 Radiocarbon dates from core DA06-139G. The calibrated using the Marine09 curve, with ∆R=0±0, (Reimer *et al.*, 2009) in Oxcal v.4.1 (Bronk Ramsey, 2009).

* Date considered too old and removed from age-model.

**Dates are within 2σ range and considered coeval. The mean of these calibrated dates is used in the age model.

7.2.2 Sediment properties

Particle size data show several peaks in the >150µm (% weight) and >500µm (grain frequency) fraction interspersed throughout core DA06-139G (*Fig.* 7.*2*). There is a steady decline in sediment >150µm (% weight) between 5-4 ka BP, followed by very little coarse-grained sedimentation until after 3 ka BP, with the exception of an isolated peak at 3.6 cal. ka BP. Between 3 and 1.7 ka BP, there is an increase in coarse sediment content, which matches a greater delivery of clasts > 2 mm, as identified in X-ray radiographs (*Fig.* 7.*2*). Coarse-grained sedimentation is greatest from 1.7 to 0.4 ka BP, as indicated by an increase in the number of clasts > 2 mm and percentage weight of sediment >150µm. After 4.7 ka BP, 80-90% of coarse sediments are non-basaltic in origin, indicating sediment sourced from the mainland rather than Disko Island and Nuussuaq peninsula. The upper part of the core (upper *ca.* 400 cal. yrs.) is marked by a decline in coarser sedimentation, with the exception of one significant spike at 0.3 ka BP. Basaltic material, sourced from Disko Island and/or Nuussuaq Peninsula, consistently comprises 10–20% of grains >500µm, with the exception of the base of the core (4.7-5.1 ka BP), where 40–60% of grains are basaltic. There are further peaks of basaltic grains (>500µm)

at 2.1 and 3.6 ka BP. However, there is greater low frequency inputs of basaltic material in the past 2.0 ka BP compared to the interval 5.1-2.0 ka BP.

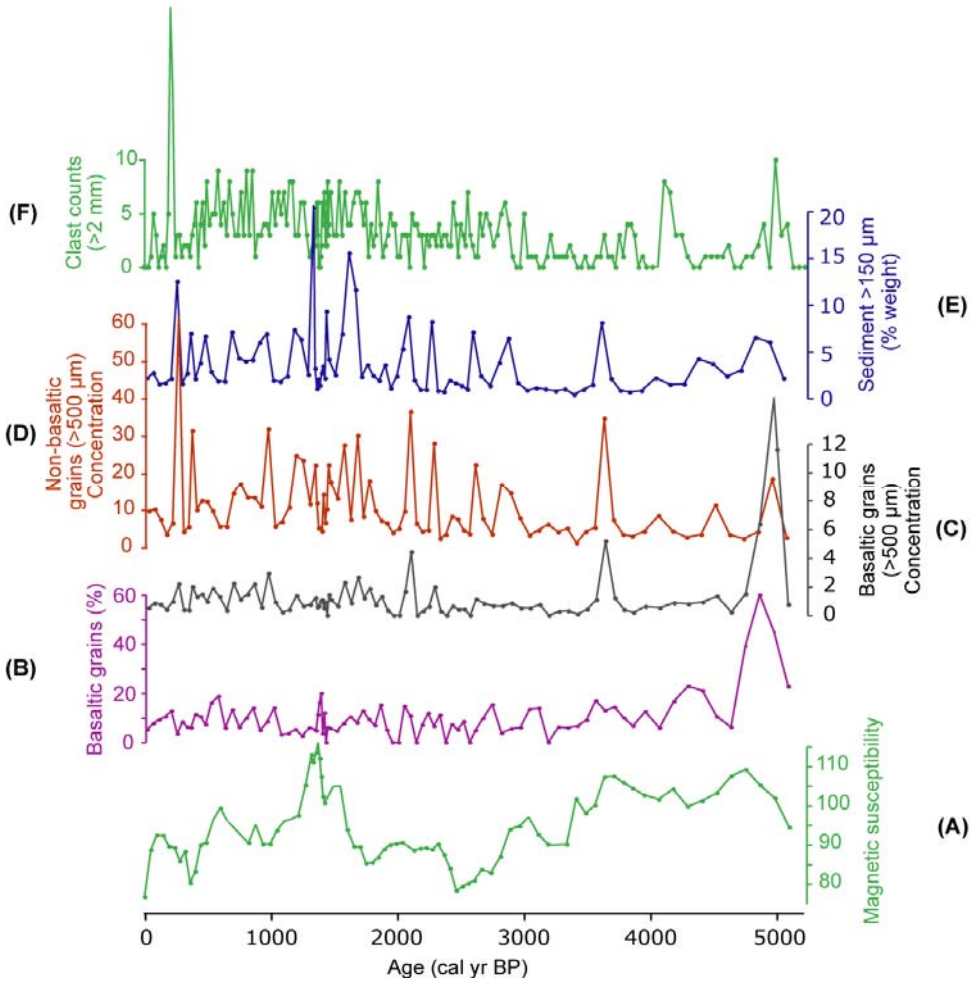

Figure 7.2 Sedimentological data for core DA06-139G (provided by C.S. Andresen); (**A**) magnetic susceptibility (SI x10^{-5}), (**B**) percentage basalt grains, concentration of (**C**) basaltic grains and (**D**) non-basaltic grains calculated as the number of grains/weight of sample, (**E**), percentage weight of dry sediment fraction > 150 µm, (**F**) number of clasts > 2 mm in diameter identified in X-ray radiographs, and used as an indicator of ice-rafting.

7.2.3 Foraminiferal biostratigraphy

Forty-one species (23 agglutinated and 18 calcareous) were recorded from the sediment core. The morphologically similar species of *Islandiella helenae* and *Islandiella norcrossi* are presented together as *I. norcrossi.* Test lining counts provide an indication of calcareous dissolution, and are presented as a proportion of total preserved calcareous foraminifera and test linings. However, not all calcareous foraminifera have organic test linings, so the impact of dissolution may be underestimated, while samples with low calcareous counts must also be

interpreted with caution using this method. Dominantly agglutinated foraminifera samples are probably the result of calcareous dissolution. These data suggest dissolution of calcareous foraminifera has significantly modified fossil assemblages, especially in FAZ 2 and 3, becoming extreme from 900 cal. yrs. BP.

The greater abundance of the robust *C. arctica* in the fossil record (Lloyd *et al.*, 2007; this study) compared to modern samples (occasionally >10%, e.g. Korsun and Hald, 2000; Murray and Alve, 2000; Lloyd, 2006a) suggests either modern samples do not span the full range of environments and/or post-mortem changes have influenced foraminiferal assemblage composition. Since abundances of *C. arctica* are relatively high from the top of the core (compared to abundance in modern samples), this suggests that any *post-mortem* changes occur immediately after burial, rather than increasing with sediment depth (i.e. due to increased sediment accumulation). However, the high abundance of the slender and fragile *R. gracilis* is found at the base of the core suggests that taphonomic processes do not significantly affect agglutinated foraminifera in core DA06-139G.

In light of these apparent preservation issues, agglutinated and calcareous species have been treated as separate components for percentage calculations. However, there is a significant variability in species abundance between these components; all agglutinated assemblages contain more than 100 specimens (two-thirds of samples have more than 250 specimens), while 29 of the 46 samples contained fewer than 50 calcareous specimens. Stratigraphically constrained cluster analysis (incremental sum of squares) of the combined agglutinated and calcareous assemblage (total %) in CONISS (Grimm, 1987) divided the foraminiferal assemblages into three distinct zones (*Fig.* 7.*3*). For simplicity, these faunal zones facilitate the description of both foraminiferal and sedimentological data. Descriptions of faunal trends pertain to total agglutinated or calcareous foraminifera unless otherwise stated.

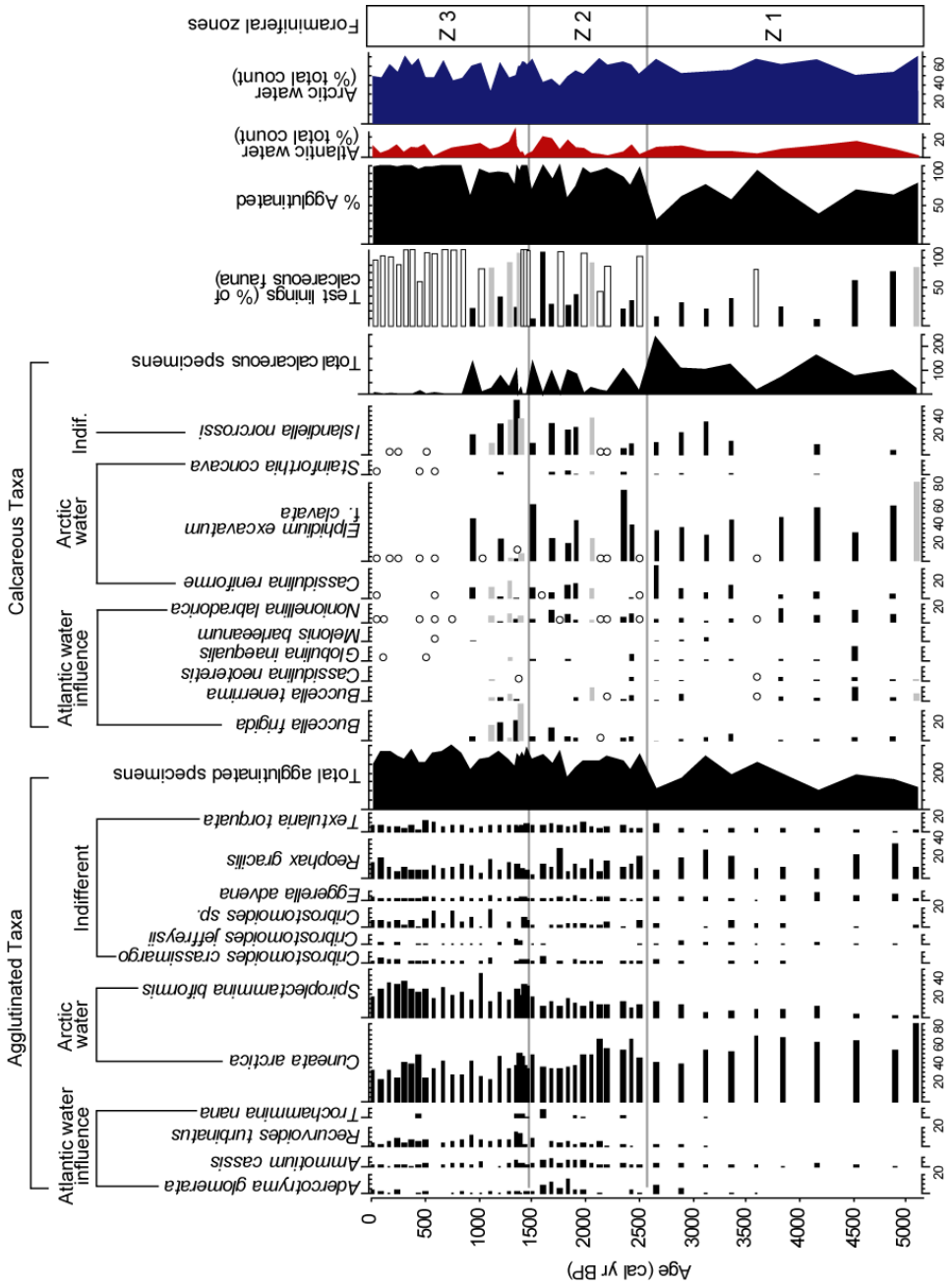

Figure 7.3. Foraminiferal assemblages from DA06-139G. Foraminiferal counts are expressed as percentages of total agglutinated or total calcareous specimens counted. Only taxa >5% in samples containing a minimum of 50 agglutinated or calcareous specimens are included in the diagram. Samples containing ≥50 specimens are identified by solid black bars, 20-49 specimens have solid grey bars. Species presence in samples with <20 specimens is indicated by hollow circles. The core has been divided into foraminiferal zones based on stratigraphically constrained cluster analysis of the total assemblage data in CONISS (Grimm, 1987). Species associations with Atlantic and Arctic water masses are based on ecological studies in West Greenland and other high-latitude shelf locations.

FAZ 1 (5.1-2.6 ka BP, 443-297 cm)

FAZ 1 is characterised by the greatest proportion of calcareous fauna throughout the core, making up to 70% of the total assemblage. The dominant *Elphidium excavatum* f*. clavata* (30–60%) gradually declines in abundance to 3.0 ka BP. *Elphidium excavatum* f*. clavata* is found in ice-proximal glaciomarine conditions (e.g. Feyling-Hanssen, 1964; Hansen and Knudsen, 1995; Hald and Korsun, 1997; Korsun and Hald, 2000), as well as ice-distal shelf environments dominated by relatively cold, low salinity Arctic waters (Korsun and Hald, 1998; Hald and Steinsund, 1996). *Elphidium excavatum* f*. clavata* thrives under a variable hydrographic regime, often under the influence of turbid meltwater plumes with high suspension settling of sediment (Korsun and Hald, 1998, 2000; Jennings *et al.*, 2001). At *ca.* 4.5 ka BP the calcareous assemblage is composed of *Nonionella labradorica* (10-15%)*, Cassidulina neoteretis* (5-10%)*, Bucella* spp. (5-15%), and an isolated peak in *Globulina inaequalis* (15%), which are considered diagnostic foraminifera for Atlantic Water influence in central West Greenland (Lloyd, 2006a). On the Labrador Shelf, *N. labradorica* is found under the influence of Labrador Sea Water, with a temperature of 3°C and a salinity of 34‰ (Bilodeau *et al.*, 1994). Many investigators suggest increasing abundances of *N. labradorica* reflect higher nutrient levels (e.g. Jennings *et al.*, 2004). In West Greenland waters, increases in *N. labradorica* are positively correlated with temperature and salinity (Lloyd, 2006a), and likely reflect influxes of warm Atlantic water with relatively high nutrient concentrations compared to Arctic water (Stefánsson and Ólafsson, 1991**;** Jennings *et al.*, 2004).

The dominance of *Cuneata arctica* (50 to 80%) in the agglutinated fauna, particularly between 5.1 and 3.6 ka BP, indicates the presence of cold Arctic waters in the Vaigat. *Cuneata arctica* is thought to reflect annually well-mixed open marine conditions (e.g. Hald and Steinsund, 1992; 1996; Korsun *et al.*, 1994; Murray and Alve, 2000; Jennings *et al.*, 2001). However, the low diversity (see *Fig.* 7.3) of samples where *C. arctica* abundance is greatest (especially at 5.1 and 3.6 ka BP) suggests unstable and severe environment conditions prevailed (Feyling-Hanssen and Funder, 1990). The abundance of *C. arctica* begins to decline towards the top of FAZ 1. Peaks in *R. gracilis* (up to 35%) at 4.8 and 3.1 ka BP correspond to the reduced abundance of *C. arctica*. While *R. gracilis* is considered opportunistic, high abundances of the taxonomically-

similar *Leptohalysis catella* found in Canadian and Scandinavian fjords (e.g. Alve, 2000; Gustafsson and Nordberg, 2000; Blais-Stevens and Patterson, 1998; Patterson *et al.*, 2000) have been linked to high organic inputs from terrestrial plant debris and a fine-grained substrate (Schafer *et al.*, 1995; Blais-Stevens and Patterson, 1998). Peaks in *R. gracilis* (4.9 and 3.1 ka BP) follow low diversity samples dominated by *C. arctica*, possibly reflecting initial amelioration of bottom-water conditions. While *E. advena, Spiroplectammina biformis,* and *Textularia torquata* are present as accessory species throughout FAZ 1, diversity of the agglutinated fauna increases through this zone (mean of 9 species before 3.5 ka BP, compared to 13 species after 3.5 ka BP).

In general, there is a trend of cooler bottom waters in the Vaigat from 5.1 to 3.5 ka BP as suggested by the dominance of *C. arctica* and *E. excavatum* f. *clavata* and the low diversity, interrupted by a brief warm interval at *ca.* 4.5 ka BP. This is followed by a warming trend from 3.5 ka BP, indicated by a decline in *C. arctica* and *E. excavatum* f. *clavata*, and increased abundance of *A. glomerata, R. turbinatus* and *I. Norcrossi.* A minor increase in *A. glomerata* at 2.7 ka BP may be indicative of an increase in Atlantic Water influence at this time. However, the increase in *S. biformis* and *C. reniforme* suggests a cooling trend into FAZ 2.

FAZ 2 (2.6-1.5 ka BP; 297-189 cm)

FAZ 2 appears to be marked by enhanced calcareous dissolution. *Elphidium excavatum* f. *clavata* is abundant, though not as important as in FAZ 1. *Islandiella norcrossi, C. reniforme*, and *N. labradorica* are common species in FAZ 2, the latter increasing in abundance after 2.0 ka BP. Arctic water indicators *C. arctica* (typically *ca.* 40%) and *S. biformis* (*ca.* 15%) are abundant, though generally less important compared to FAZ 1. The exception is a brief interval *ca.* 2.5-2.2 ka BP where the abundance of *C. arctica* increased (*ca.* 65%), representing conditions colder similar to those shortly before 4.0 ka BP. *Adercotryma glomerata, Ammotium cassis, Recurvoides turbinatus* occur in increasing abundance throughout FAZ 2. Hald and Korsun (1997) found these species correlate well with temperature and salinity, and are common under the influence of transformed Atlantic water in Svalbard Fjords. These species

indicate a greater influence of Atlantic water (weak WGC) compared to FAZ 1, particularly between 2.0 and 1.5 ka BP.

FAZ 3 (1.5 ka BP to present; 189-0 cm)

FAZ 3 is characterised by the gradually increasing dominance of *S. biformis* (from *ca.* 15 to 35% at 200 cal. yrs BP), and the absence of calcareous fauna after 1.0 ka BP. Dominantly agglutinated assemblages have been interpreted as indicating cold, low salinity bottom waters (e.g. Vilks *et al.*, 1982). There is a continued decline in the abundance of *C. arctica*, although it is still the dominant species typically comprising *ca.* 25% of assemblages in FAZ 3. *Spiroplectammina biformis* is a dominant species in fjords of Baffin Island and Svalbard where it is found under the influence of Arctic waters and glaciomarine conditions (Schafer and Cole, 1986; Korsun and Hald, 2000). Despite wide temperature and salinity tolerances (Alve, 1990), *S. biformis* often dominates in low salinity (<30 psu) and low oxygen (<1 ml l^{-1}) waters (Alve, 1991), suggesting a greater influence of Polar water and reduced overturning/bottom water renewal in the Vaigat. The opportunistic *R. gracilis* shows a slight decrease in abundance compared to FAZ 1 and 2, suggesting more stable environmental conditions persisted. *Reophax turbinatus, T. torquata,* and *Cribrostomoides* sp. are common in FAZ 3, while there are smaller occurrences of *A. glomerata, A. cassis, Cribrostomoides crassimargo,* and *E. advena.* Ishman and Foley (1996) identify a biozone dominated by the agglutinated foraminifera *T. torquata* and *S. biformis* as indicating cold Arctic waters in the Amerasian basin of the Arctic Ocean. The uppermost significant calcareous assemblage at 900 cal. yrs BP consists of *E. excavatum* f. *clavata* (45%), *I. norcrossi* (25%), and *C. reniforme* (12%) indicating strong Polar water influence with occasional weak WGC incursions.

7.3 Discussion

The benthic foraminifera and sedimentological data provide a record of changes in the oceanographic regime and glacier calving activity during the mid- to late-Holocene. Benthic foraminifera have been found to respond primarily to changes in the temperature and salinity of subsurface waters impinging on the West Greenland shelf, which are linked to variations in the influence of the WGC (Lloyd, 2006a; Chapter 4). The foraminiferal data from DA06-139G

reflects interactions between the regional scale influence of the WGC and Arctic waters from Baffin Bay entering Disko Bugt, and meltwater fluxes from local tidewater glaciers. The primary sources of sediments deposited in the Vaigat include suspension settling of fine-grained sediments from meltwater plumes, sediment rafting by icebergs and sea-ice, and mass transport by turbidity currents and debris flows. Because subsurface WGC water must cross a *ca.* 245 m-deep threshold (*Fig. 2.2*) to enter the Vaigat (Andersen, 1981a), DA06-139G may provide a reasonable analogue for the penetration of Atlantic water into Disko Bugt fjords with sills located at similar depths.

7.3.1 Preservation of benthic foraminifera

Fossil foraminiferal assemblages represent the time-averaged accumulation of specimens and the combined effects of *post mortem* alterations, which include transport and destruction of foraminifera tests (Murray, 1991; Murray and Alve, 1999a, 1999b). Water mass characteristics (particularly temperature and salinity) exert a significant control on the composition of modern benthic foraminiferal assemblages on the West Greenland shelf (see Chapter 4), indicating these should provide suitable proxies for reconstructing past bottom-water temperature and salinity changes. However, palaeocological interpretations may be influenced if taphonomic processes in fossil sediments are not identified. It is possible that significant differences between the composition of modern total (living + dead) and fossil assemblages will be because assemblages spanning the full environmental gradient have not yet been sampled. However, taphonomic processes may also have a major influence on the composition of foraminiferal assemblages.

Test lining counts are high throughout core DA06-139G, indicating dissolution of calcareous foraminifera plays a significant role in altering the death assemblage, particularly over the past 2.5 ca. ka BP. The causes of calcium carbonate dissolution in high-latitude benthic marine environments are widely debated, and various processes have been proposed (e.g. Schröder-Adams *et al.*, 1990a, 1990b; Hald and Steinsund, 1992; Hunt and Corliss, 1993; Jennings and Helgadottir, 1994; Steinsund and Hald, 1994; Alve, 1996; Murray *et al.*, 2003; Lloyd *et al.*, 2007). Furthermore, there is debate as to whether dissolution takes place at the sediment-

water interface or within the sediment pore waters, since this has implications for the processes involved. Enhanced primary production leads to greater organic fluxes to the seafloor and subsequent decomposition helps create anoxic and acidic pore waters in the top few centimetres below the sediment-water interface, resulting in dissolution of infaunal calcareous foraminifera (Reaves, 1986; Walton and Burton, 1990; Freiwald, 1995; Steinsund and Hald, 1996). Since foraminifera primarily live below the sediment-water interface, acidic pore waters may be more likely to cause calcareous foraminifera dissolution, rather than highly oxygenated bottom waters. This suggests better preservation is linked to reduced organic accumulation (Reaves, 1986). Higher sedimentation rates may further dilute organic matter influxes and help preserve calcareous foraminifera (e.g. Korsun and Hald, 2000). However, the increased sedimentation rate in the upper part of the core has no influence on calcareous preservation, in contrast to better preservation identified by Lloyd *et al.* (2005) in Disko Bugt during periods of increased sedimentation rate. This is perhaps not surprising as sedimentation rates through this core are an order of magnitude less than intervals of good calcareous preservation identified by Lloyd *et al.* (2005).

The role of sea ice in calcareous preservation has been widely debated (e.g. Anderson, 1975; Osterman and Kellogg, 1979; Scott *et al.*, 1989; Schröder-Adams *et al.*, 1990a, 1990b; de Vernal *et al.*, 1992; Steinsund and Hald, 1996). Schröder-Adams *et al.* (1990a; 1990b) suggest agglutinated fauna dominate in the Canadian Arctic during extended periods of seasonal ice-free conditions where highly oxygenated meltwater influence enhances dissolution of calcareous fauna. Glacier advances, greater iceberg transport and associated melting, and seasonal melting of greater sea ice cover may have contributed to enhancing meltwater delivery to the Vaigat during the past 2.5 ka BP. However, it is difficult to envisage how meltwater alone would affect calcareous preservation, especially since greater meltwater delivery from surface ablation would presumably be more pronounced under warmer atmospheric conditions (i.e. prior to 2.5 ka BP).

Water mass characteristics are likely to be an important factor controlling calcareous preservation. Purely agglutinated assemblages altered by calcareous dissolution have been

found under the influence of cold, low salinity Polar waters in the Arctic Ocean and on the East Greenland shelf (Hald and Steinsund, 1992; Steinsund and Hald, 1994; Jennings and Helgadottir, 1994). Agglutinated foraminiferal assemblages not altered by taphonomic processes have also been reported in the Canadian Arctic under Polar water influence, whereas increasing numbers of calcareous specimens are found under the influence of Atlantic water (Vilks, 1969; Hunt and Corliss, 1993). Calcareous foraminifera under the influence of warm Atlantic water are likely to be better preserved than fauna under cold, highly oxygenated Arctic waters (de Vernal *et al.*, 1992; Jennings and Helgadottir, 1994). Greater calcareous content before 2.5 ka BP may therefore suggest a greater influence of Atlantic water, whereas increasing test lining counts and agglutinated foraminifera up core suggest a greater Polar water influence, particularly during the past 900 cal. yrs BP. In the Vaigat, stronger stratification caused by a greater meltwater influence may reduce bottom water renewal, and further contribute to dissolution of calcareous foraminifera (e.g. Osterman *et al.*, 1999).

7.3.2 Palaeoceanographic interpretation

Sediment logging indicated that core DA06-139G is comprised of hemipelagic muds with interspersed IRD. There is no evidence that this core has been significantly disturbed by instantaneous mass wasting. The sequential order of radiocarbon dates and absence of sharp erosive contacts supports an interpretation of continuous sedimentation during the past *ca.* 5 ka. The results from DA06-139G are used to interpret the palaeoceanographic evolution of the Vaigat over the last *ca.* 5 ka and are illustrated schematically using the five scenarios shown in *Fig. 7.4.*

Palaeoenvironmental conditions from ca. 5.1 to 4.7 ka BP (Stage A)

The foraminiferal record from DA06-139G indicates colder than present Arctic bottom-waters were present in the Vaigat before 4.7 ka BP (*Fig. 7.4a*) as suggested by high abundances of *C. arctica* and *E. excavatum* f. *clavata*. Lloyd *et al.* (2007) also found foraminiferal evidence of bottom-water cooling in Kangersuneq Fjord, southeast Disko Bugt, at this time. This cooling can be traced to upstream changes in oceanic source regions for the WGC. There is evidence for reduced advection of Atlantic water (sea-surface cooling) to the North Atlantic region after

ca. 5.7 ka BP based on diatom records from the Reykjanes Ridge, the Vøring Plateau (west of Norway), and the North Iceland Shelf (Andersen *et al.*, 2004a; 2004b). Castañeda *et al.* (2004) also identify a weaker Atlantic influence (compared to the early Holocene) on the North Iceland shelf between 6.2 and 4.5 ka BP based on benthic and planktic foraminifera $\delta^{18}O$ isotopes. Sea-surface temperature reconstructions from the East Greenland shelf are less clear for this period. Jennings *et al.* (2002) and Bennike *et al.* (2002) identify a marked cooling between 5.0-4.7 ka BP off East Greenland, while other studies suggest relatively stable sea-surface temperatures, or a slight warming of winter sea-surface temperatures at this time (Andersen *et al.*, 2004b; Solignac *et al.*, 2006). The reduced Atlantic influence at this time favours a greater entrainment of Arctic water sourced from the East Greenland Current in the WGC. Meltwater inputs from the Greenland Ice Sheet would further cool and freshen the WGC as it flows northwards.

The concentration of sand-sized basalt grains sourced locally from the Tertiary basalts of Disko Island and Nuussuaq peninsula are markedly higher between *ca.* 5.1 and 4.7 ka BP compared to after 4.7 ka BP (*Fig.* 7.*2*). Since there are no calving glaciers on Disko Island and Nuussuaq Peninsula that could transport and deposit sand-sized basalt grains, these deposits reflect either enhanced wind-blown deposition or greater sea-ice rafting of terrestrial basaltic sediments. Eisner *et al.* (1995) identify high pollen and minerogenic accumulation rates from a lacustrine record in the Kangerlussuaq region of West Greenland indicating greater aeolian activity during the mid-Holocene, followed by a dramatic decline at 4.7 ka BP. It is possible that the retreat of ice caps on Disko Island and Nuussuaq peninsula during the mid-Holocene may have increased the availability of basalt sediment for aeolian transport (e.g. Eisner *et al.*, 1995). The interpretation of greater sea-ice rafting of sediment is supported by diatom records from Kangersuneq Fjord, southwest Disko Bugt, which records higher abundances of sea-ice associated diatoms (especially *Fragilariopsis cylindrus, Fragilariopsis oceanica*) during this interval (Moros *et al.*, 2006). In addition, there is strong evidence to support an interpretation of greater wind activity before 4.7 ka BP. O'Brien *et al.* (1995) linked enhanced sea-salt and terrestrial dust concentrations in the GISP2 ice core record to an expansion of the north polar vortex or increased meridional air flow between 6.1 and 5.0 ka BP. Furthermore, Fredskild

(1983) suggests strengthening south-westerlies along West Greenland brought exotic pollen from North America during the mid-Holocene. These atmospheric conditions would strengthen surface current circulation in Disko Bugt and the Vaigat, promoting sea-ice export and rafting of terrestrial sediments as the main dispersal mechanism.

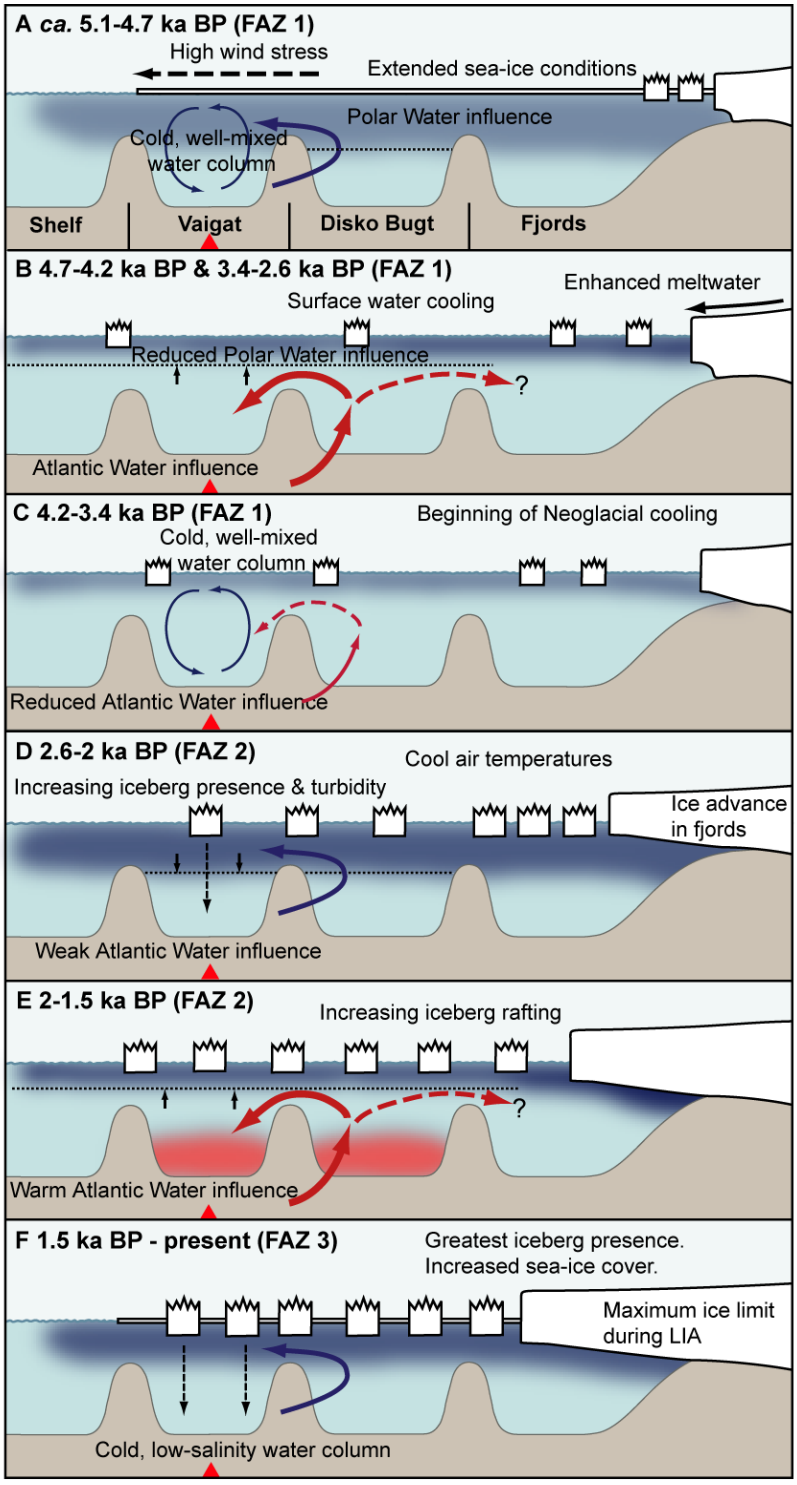

Figure 7.4 Cartoons of hydrographic conditions and glacier activity in Disko Bugt and the Vaigat during the past *ca.* 5.1 ka. Intermediate waters enter the Vaigat via Disko Bugt, and exit into the

mid-shelf area to the west. Red arrows indicate influxes of Atlantic Water, and thicker arrows represent greater Atlantic Water influence. Red shading highlights the presence of relatively warm Atlantic Water in the Vaigat and Disko Bugt in (E). Blue arrows represent the dominance of Polar Water, and a thicker Polar Water layer (shown by dark blue shading) preventing penetration of Atlantic-sourced water into the Vaigat.

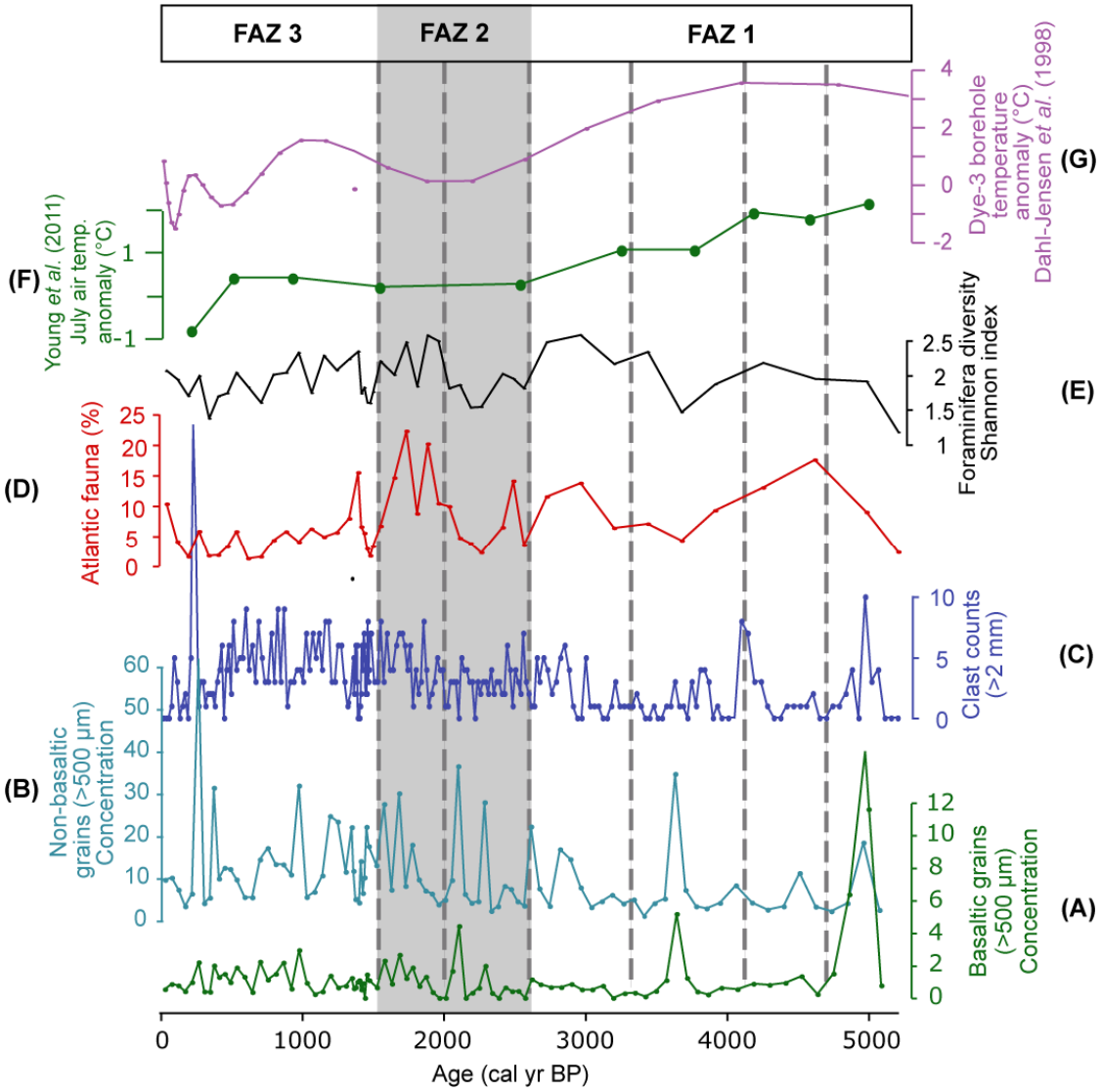

Figure 7.5 Selected sedimentological (**A-C**) and summary foraminifera (**D-E**) data, compared against air temperature reconstructions; (**F**), chironomid-based July air temperature reconstruction from North Lake, near Ilulissat (Young *et al.*, 2011), and (**D**), Dye-3 borehole temperature anomaly (Dahl-Jensen *et al.*, 1998). Grey shading identifies boundaries between FAZs, and dashed lines separate stages A to F schematically illustrated in *Fig. 7.4.*

Palaeoenvironmental conditions from ca. 4.7 to 4.3 ka BP (Stage B)

The warmest calcareous assemblages in the core replace Arctic water fauna at *ca.* 4.5 ka BP, possibly reflecting warmer than present subsurface waters. This brief warming spell indicates a

greater entrainment of warm and saline Atlantic water in the WGC (*Fig. 7.4b*). A reduced Polar water influence is also required to allow Atlantic water to cross a threshold and penetrate into the Vaigat. This scenario is corroborated by Moros *et al.* (2006), who identify an abrupt decline in sea-ice associated diatoms indicating maximum sea-surface temperatures peaking at *ca.* 4.5 ka BP and persisting until shortly after 4 ka BP (Moros *et al.*, 2006).

After 4.5 ka BP there is a clear increase in preservation of the calcareous fauna (*Fig. 7.3*). This can be explained by a strengthening in Atlantic water influence (i.e. lower dissolved CO_2), and/or less acidic sediment pore waters, linked to lower surface productivity and decay of organic matter at the seafloor (e.g. Reaves, 1986). If the latter explanation is responsible, this may be linked to a well-developed turbid meltwater plume hampering primary productivity in the photic zone. Indeed, the low coarse sediment content at this time suggests sedimentation was primarily by suspension settling from meltwater plumes, rather than ice-rafting. The presence of laminated sediments identified in core X-ray radiographs supports an interpretation of strong turbid meltwater plume influence at this time due to enhanced melting of local tidewater glaciers in northern Disko Bugt (see *Fig. 2.1*).

Weidick *et al.* (1990) found evidence for a gradual recession of the Greenland Ice Sheet margin and outlet glaciers around Jakobshavn Isbræ in Disko Bugt during the HTM based on radiocarbon dating of reworked biogenic material found in moraines. Borehole temperature reconstructions suggest continued atmospheric warming characterised this interval (Dahl-Jensen *et al.*, 1998), and this corresponds to thinning near the Greenland Ice Sheet margin (Vinther *et al.*, 2009). At the end of the HTM, Weidick *et al.* (1990) estimate Jakobshavn Isbræ was located more than 15 km behind its present position. The low sedimentation rate before 3.8 ka BP in core DA06-139G is consistent with a more distal position of marine-terminating outlet glaciers in northeast Disko Bugt. Warmer air temperatures during the HTM are suggested to have contributed to driving ice sheet recession primarily through calving rather than ablation (Weidick *et al.,* 1990; Weidick, 1992). However, there is no record of increased calving activity during the mid-Holocene from sedimentary evidence in core DA06-139G as might be expected from a Vaigat location along which icebergs exiting Disko Bugt pass over. If

ice loss was primarily through calving, warmer air and sea surface temperatures combined with a choking of icebergs behind the shallow sill of Isfjeldbanken at the mouth of Jakobshavn Isfjord, and in Torssukátak, northeast Disko Bugt, could result in melting and dumping of IRD within close proximity of calving fronts.

Palaeoenvironmental conditions from ca. 4.3 to 3.4 ka BP (Stage C)

Increased abundances of Arctic-associated species, particularly *C. arctica* and *E. excavatum* f. *clavata*, and reduced abundances of warmer water species between 4.3 and 3.4 ka BP indicate a greater influence of Polar waters in the Vaigat. This is supported by an increase in test lining counts and a high percentage abundance of agglutinated specimens (*Fig. 7.3*). In general, this period is characterised by low inputs of coarse sediment, reflecting reduced iceberg rafting in the Vaigat.

A decline in bottom-water temperatures in the Vaigat between 4.3 and 3.4 ka BP may mark the beginning of Neoglacial cooling. This suggests that the warmest part of the WGC was unable to penetrate into the Vaigat at this time. High sediment accumulation rates and more brackish diatom assemblages in Ameralik Fjord have been interpreted to reflect greater melting of outlet glaciers producing sediment-laden surface plumes in the interval 4.4-3.2 ka BP (Møller *et al.*, 2006; Seidenkrantz *et al.*, 2007). Greater meltwater additions and mixing of the WGC as it flows northwards would deepen the cool and low salinity Polar water mass that enters Disko Bugt and prevent warm Atlantic incursions to the Vaigat. However, reconstructions indicate a continued cooling of Atlantic-sourced surface waters during this period linked to declining insolation (Andersen *et al.*, 2004b).

Neoglacial cooling began *ca.* 4000 yrs. BP (Kelly, 1980; Weidick *et al.*, 1990; Weidick, 1992; 1993) following peak warming as indicated in the Dye-3 borehole temperature reconstruction (*Fig 7.5g*) and chironomid-based temperature reconstructions from Disko Bugt (*Fig. 7.5f*) (Axford *et al.*, 2010; Young *et al.*, 2011). Ice sheet and glaciers advances during the Neoglacial have been widely recorded in West Greenland, and more widely. This interval is characterised by low IRD, which may partly be linked to cooler sub-surface water temperatures in the fjords.

Palaeoenvironmental conditions from ca. 2 to 1.5 ka BP (Stage E)

The past 2,000 years are characterised by both an increase in the sedimentation rate (*Fig.* 7.*1*) and an increased abundance of IRD largely sourced from outlet glaciers draining the Greenland Ice Sheet (*Fig.* 7.*3*). Together, these data are indicative of a greater intensity of ice-rafting, presumably reflecting glacier advances in the fjords.

Palaeoenvironmental conditions from ca. 1.5 ka BP to present (Stage F)

Concentrations of coarse non-basalt grains provide a proxy for ice rafting originating from tidewater glaciers, primarily Jakobshavn Isbrae in Disko Bugt, and Sermeq kujatdleq and Sermeq avangnardleq draining into Torssukátak (*Fig. 1.2*). Distinct increases in IRD suggest either increased ice rafting, greater transport of icebergs through the Vaigat, or more rapid melting of icebergs due to warmer surface water and air temperatures.

Dominantly agglutinated foraminiferal fauna characterised by high abundances of *C. arctica* and increased abundances of *S. biformis* indicate cold Polar waters have been dominant in the Vaigat during the past 1500 yrs. BP. With the exception of isolated occurrences, there is a general absence of calcareous fauna. This most likely reflects high calcium carbonate dissolution because of the influence of cold Arctic waters with high concentrations of dissolved CO_2. Surface water proxies indicate cooling and greater sea-ice cover during this period in Disko Bugt (Moros *et al.*, 2006; Seidenkrantz *et al.*, 2008). This is consistent with greater iceberg rafting as indicated by a further increase in IRD clast counts shortly before 1.5 ka BP. Records of bottom water temperatures indicate relatively warm, saline WGC water was present in Ameralik Fjord and Igaliku Fjord, southewest Greenland (Lassen *et al.*, 2004; Seidenkrantz *et al.*, 2007). Lloyd *et al.* (2007) find that relatively warm subsurface waters were present in Kangersuneq Fjord, Disko Bugt, until 900 cal. yrs. BP. In Disko Bugt itself, warm, saline bottom waters were present west of Jakobshavn Isbrae until 500 cal. yrs. BP (Lloyd, 2006b). This differs from the record in Vaigat, where the influence of cooler waters is evident much earlier. This is perhaps not surprising since the greater iceberg flux during the summer and increasing sea-ice influence during the winter would further cool waters in the Vaigat. Greater meltwater

inputs into the Vaigat from these sources may partly be responsible for delivering highly oxygenated waters responsible for enhanced dissolution of calcareous foraminifera.

Chapter 8

DEGLACIAL AND HOLOCENE ICE-OCEAN INTERACTIONS IN CENTRAL WEST GREENLAND

Unpublished cosmogenic radionuclide ages from Uummannaq Fjord supplied by David H. Roberts (presented in Chapter 6) and clast count data for core DA06-139G (presented in Chapter 7) are further used in summary figures in this chapter.

Chapter 8
Deglacial and Holocene ice-ocean interactions in central West Greenland

8.1 Introduction

This chapter summarises the major findings from this thesis. These findings are discussed with respect to the main research aim of this thesis:

> *To investigate deglacial and Holocene changes in the activity of major West Greenland ice streams, and identify possible interactions between climate, ocean, and ice sheet dynamics.*

In order to address this aim, this chapter is divided into two main parts. The first part addresses the timing and nature of deglaciation of marine-based ice in the Disko Bugt and Uummannaq area. A discussion of the possible driving mechanisms for deglaciation in these two areas is presented by exploring linkages with ocean temperatures (based on foraminiferal records in cores MSM-343340 and MSM-343520_G), air temperatures, and changes in relative sea-level (RSL). The second part addresses Holocene palaeoceanographic changes in the relative warmth of the WGC (i.e. once the Greenland Ice Sheet had retreated landwards to an ice-distal location) on the central West Greenland shelf. Holocene ice-ocean interactions in central West Greenland are discussed based on changes in foraminifera assemblages in cores MSM-343520 (Uummannaq shelf) and DA06-139G (Vaigat), and, more broadly, from MSM-343340 (outside Disko Bugt), and by comparison to other regional climate and ocean records. This chapter is concluded by stating the key findings from this thesis.

8.2 Deglaciation in central West Greenland

8.2.1 Regional pattern of shelf deglaciation in West Greenland

Funder and Hansen's (1996) two-stage deglacial model proposed that for central West Greenland eustatic sea-level rise drove early deglaciation (*ca.* 16-15 ka BP) and synchronous marine-based ice retreat eastwards from close to the shelf edge to the modern coastline by *ca.* 10 ka BP. This was followed by slower land-based ice retreat driven by atmospheric warming. While a number of studies have helped further constrain relatively small-scale changes (i.e. ice advance or retreat) in Holocene ice margin position in the Disko Bugt area (e.g. Bennike, 2000; Long and Roberts, 2002; 2003; Long *et al.*, 2003; 2006; Lloyd *et al.*, 2005; Briner *et al.*, 2010; Young *et al.*, 2011), these have not demanded a major revision of Funder and Hansen's (1996) two-stage model for the culmination and decay of the Greenland Ice Sheet.

However, data presented in this thesis offers new insights concerning the timing, nature, and mechanisms of marine-based deglaciation of the shelf in central West Greenland indicating that the first stage of Funder and Hansen's (1996) model requires revising. Sedimentological and foraminiferal evidence indicate that the marine-based ice occupying the troughs outside Disko Bugt and Uummannaq Fjord (shown in *Fig. 8.1*) extended at least to the mid-shelf area in these two areas, and probably to the shelf edge. Basal radiocarbon dates (providing the first constraints on initial deglaciation) obtained from sediment cores collected from troughs on the mid-shelf west of the Disko Bugt (MSM-343520_G) and Uummannaq Fjord (MSM-343340_G), suggest that marine-based deglaciation in these two parts of the central west sector of the Greenland Ice Sheet took place much later than previously thought. Ice had retreated east of the MSM-343340_G core site by *ca.* 12.3 ka BP and east of the MSM-343520 core site by 10.9 ka BP (*Fig. 8.1*). Comparisons to existing and unpublished (e.g. Jennings *et al.*, 2010; D.H. Roberts, personal communication) dates on deglaciation provide strong evidence for the timing and nature of retreat (see *Fig. 8.1*). It is clear that ice retreated more than 1000 years earlier in the Disko Bugt area than in the Uummannaq area to the north and several 1000 years later than suggested in the Funder and Hansen (1996) model.

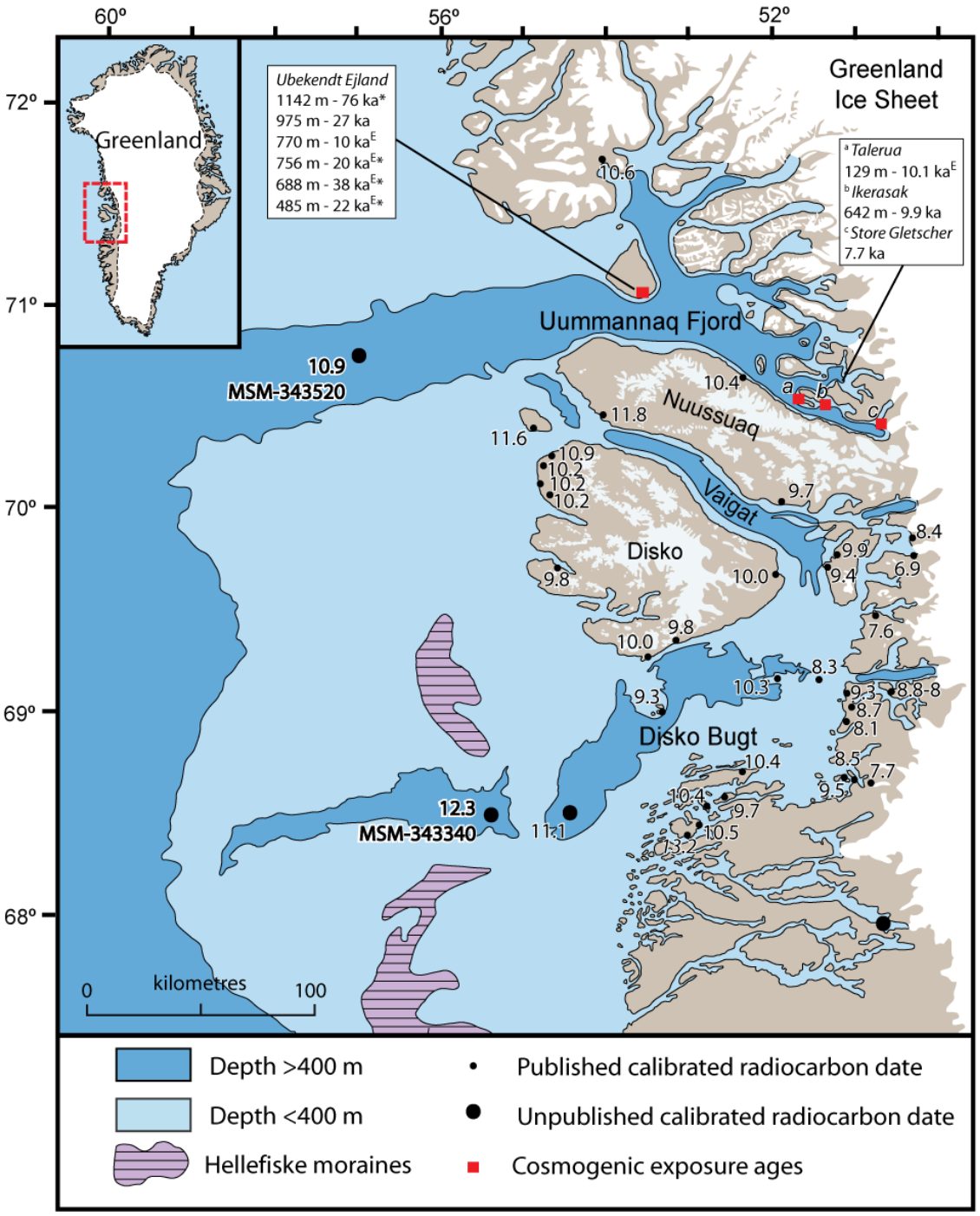

Figure 8.1 Compilation of calibrated radiocarbon ages and unpublished CRN ages (D.H. Roberts, personal communication) in central West Greenland that provide minimum ages for deglaciation.

8.2.2 Driving mechanisms for marine-based deglaciation

A number of authors have speculated about the potential role of marine forcing (ocean warming) on ice stream and ice shelf stability in Greenland (e.g. Bindschadler, 2006; Luckman *et al.*, 2006; Nick *et al.*, 2009), Antarctica (e.g. Rignot and Jacobs, 2002; Payne *et al.*, 2004; Walker *et al.*, 2007) and on other marine-terminating glaciers (e.g. Motkya *et al.*, 2003). Holland *et al*. (2008) recently demonstrated that the thinning of Jakobshavn Isbræ's floating ice tongue in 1997 (followed by acceleration and eventual collapse in 2003) coincided with the penetration of warmer Atlantic-sourced waters into Disko Bugt and into Jakobshavn Isfjord. More recent studies have speculated on the potential importance of ocean warming as a major driver of deglacial and Holocene ice dynamics (e.g. Roberts *et al.*, 2009; 2010).

The establishment of the WGC at 10 ka BP can be identified by the expansion of thermophilous molluscs to their modern limit along the West Greenland coast (Funder and Weidick, 1991; Dyke *et al.*, 1996; Kaufman *et al.*, 2004). In northern Baffin Bay, there is evidence of warmer surface waters from 10.9 ka BP, with surface waters reaching close to modern temperatures at *ca.* 9.6 ka BP (Levac *et al.*, 2001; Knudsen *et al.*, 2008b). However, there is no evidence of Atlantic Water influence in central West Greenland until *ca.* 9.2-8.7 ka BP (Lloyd *et al.*, 2005; Chapter 5), by which time the ice margin in Disko Bugt and Uummannaq had already retreated towards and onto the mainland. This suggests that ocean forcing was not a significant influence on the marine-based deglaciation in central West Greenland (see *Fig. 8.2*). The high glacial meltwater discharge from the Disko Bugt and Uummannaq ice stream systems would most likely have deflected warmer sub-surface waters off the West Greenland shelf, or mixing of Atlantic Water and glacial meltwater may have diluted the WGC influence.

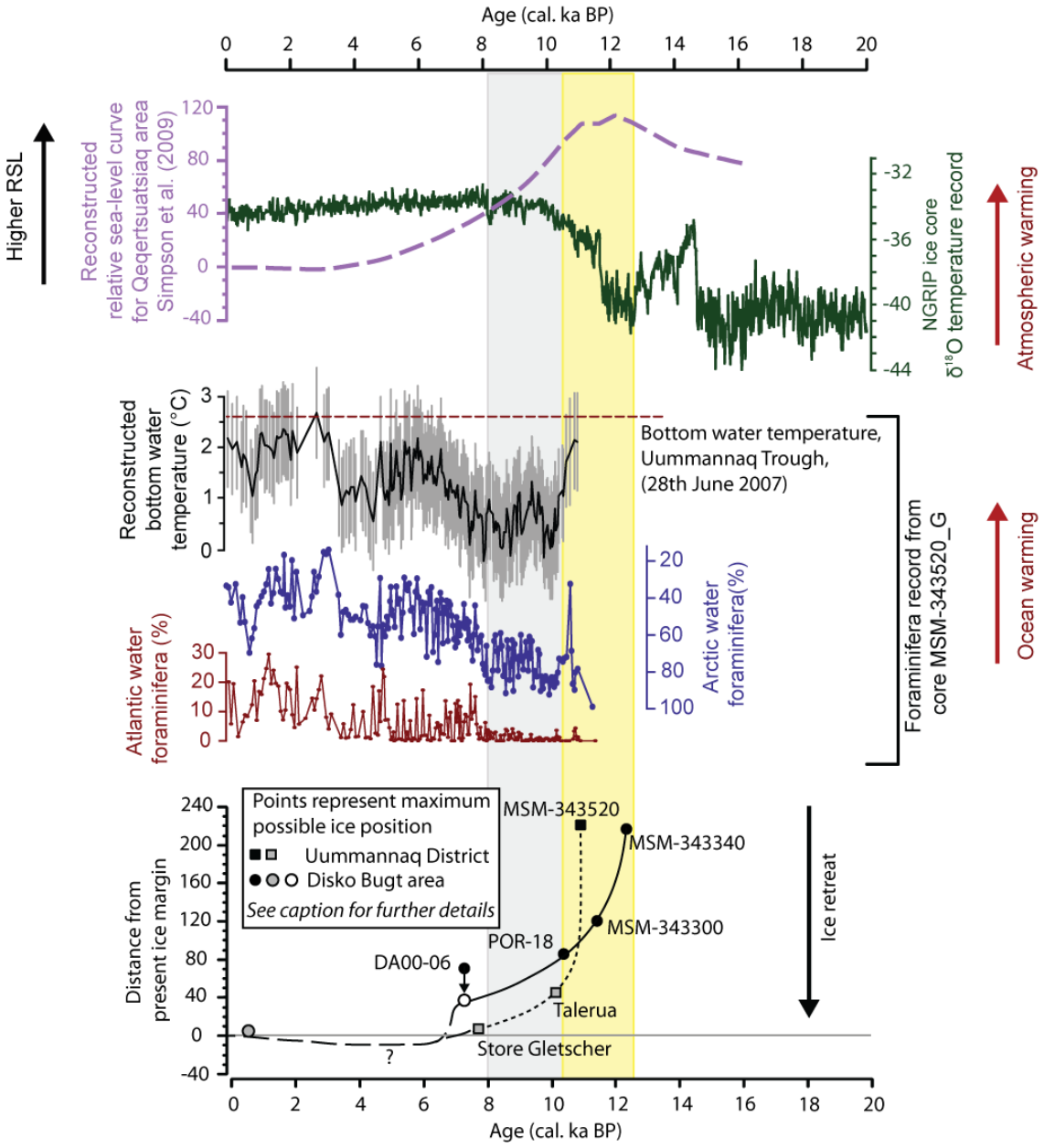

Figure 8.2 Cartoon illustrating the relative timing and speed of ice retreat in the Disko Bugt (solid line, circles) and Uummannaq (short dashed line, squares) area, and potential driving mechanisms (air/ocean temperatures, relative sea-level rise) for deglaciation. Approximate changes in ice margin position are based on minimum ages for deglaciation and the distance of the dated sample to the modern ice margin (taken as Jakobshavn Isbræ in Disko Bugt, Store Gletscher in Uummannaq Fjord). The curves illustrate the maximum extent of ice at each point. Solid black circles and squares indicate radiocarbon dates based on calcareous fauna from marine sediment cores (Lloyd *et al.*, 2005; Jennings *et al.*, 2010; Ó Cofaigh *et al.*, 2010; this thesis). Grey squares represent cosmogenic exposure ages (D.H. Roberts, personal communication). Grey circles represent a cluster of dates on Fjord Stade moraines, LIA moraine and ice retreat (advance) behind (in front) of present margin based on data from proglacial-threshold lakes (e.g. Long *et al.*, 2006; Weidick and Bennike, 2007; Briner *et al.*,

2010; Young *et al.*, 2011). An abrupt shift in foraminifera and sedimentary characteristics in core DA00-06 at *ca.* 8.3 ka BP is interpreted to reflect ice retreating into Jakobshavn Isfjord. The hollow circle therefore marks the position of Isfjeldbanken at the fjord mouth. Changes in air temperatures illustrated using NGRIP $\delta^{18}O$ record (Andersen *et al.*, 2006; Rasmussen *et al.*, 2006; Svensson *et al.*, 2006; Vinther *et al.*, 2006). RSL prediction for the best-fit Earth model of Huy2 for Qeqertsuatsiaq, southwest Disko Bugt (modified after Simpson *et al.*, 2009). Model prediction shows a close fit to RSL data (Long and Roberts, 2003). The Holocene marine limit at this site is at *ca.* 110-120 m a.s.l.

However, the opening of the Arctic Channels in northern Baffin Bay, and the initiation of the south-flowing Baffin Current are believed to be a key factor in strengthening gyre circulation in Baffin Bay and the Labrador Sea, and initiating the north-flowing WGC in Baffin Bay (e.g. de Vernal *et al.*, 1992). The retreat of ice between Ellesmere Island and Greenland in northern Baffin Bay opened Nares Strait between *ca.* 10 and 9 ka BP (Zreda *et al.*, 1999; England, 1999). This would have been accompanied by a significant change in oceanographic conditions, since around one-third of Polar Water export from the Arctic to Atlantic Ocean takes place through these channels into northern Baffin Bay (Aagaard and Carmack, 1989). The first evidence for WGC initiation in northern Baffin Bay at *ca.* 10.9 ka BP (Levac *et al.*, 2001; Knudsen *et al.*, 2008b) is coincident with the initiation of rapid ice collapse on the Uummannaq shelf. The evidence for a weak Atlantic Water influence in northern Baffin Bay (Levac *et al.*, 2001; Knudsen *et al.*, 2008b) before the deglaciation of Nares Strait suggests that warmer waters may still penetrate into Baffin Bay without a strong gyre circulation driven by Polar Water outflow in the Baffin Current. It may be possible that an extensive ice sheet configuration (possibly reaching the shelf edge) in central West Greenland may have acted to "block" (by acting as both a physical barrier, and due to a significant meltwater and cooling influence) and divert an early Holocene WGC southwards into the Labrador Sea.

The rapid collapse of marine-based ice across the shelf in both Disko Bugt and Uummannaq areas suggests that deglaciation was driven primarily by relative sea-level rise. The initial retreat of ice in both locations occurs during the interval *ca.* 12.5-11 ka BP, during which the RSL highstand in southwestern Disko Bugt is predicted to have occurred (*Fig. 8.2*) (Simpson *et al.*, 2009). The marine limit on Hareøen (island in outer Vaigat) has been dated to *ca.* 11.6 ka

BP (12,081-11,211 cal. yr BP, 10,470±130 ^{14}C yr) (Bennike *et al.*, 1994), suggesting that RSL highstands were obtained at similar times in these two areas. The differences in the timing of deglaciation between these two ice stream systems cannot be explained by climatic warming; the earlier deglaciation of ice in Disko Bugt took place during the colder conditions of the Younger Dryas. Instead, the diachronous nature of ice retreat (schematically illustrated in *Fig. 8.2*) suggests that differences in ice thickness in these adjacent parts of the Greenland Ice Sheet play an important role in conditioning the timing of ice retreat. Earlier deglaciation of marine-based ice in Disko Bugt may well be a result of reduced ice thickness in comparison to the Uummannaq area. A lower basal buoyancy of the thicker ice cover in the Uummannaq trough, maintained by the regional drawdown of ice into the southern part of the Uummannaq system, would have been less susceptible to collapse due to rising relative sea-level than thinner ice cover in Disko Bugt to the south. Such a mechanism has been proposed by Roberts *et al.* (2010) to explain the longevity of Holsteinborg Isbræ on the inner shelf during deglaciation.

New ^{10}Be cosmogenic surface exposure ages obtained from the inner Uummannaq Fjord area (*Fig. 8.1*), indicate that ice thinning (lowering of ice surface elevation), potentially due to warm early Holocene atmospheric temperatures, preceded ice retreat in the Uummannaq area (though dynamic thinning due to accelerated calving can't be completely ruled out). This suggests that climatically-driven ice thinning (resulting in a gradual increase in basal buoyancy at the ice terminus) helped lower ice thickness to a critical threshold, at which point the rising relative sea-level initiated the collapse of marine-based ice. Collapse and withdrawal of ice from the outer to mid-shelf probably took place rapidly. However, as the ice retreated east of core site MSM-343520, deglaciation began to slow. High bedrock features immediately outside and at the entrance into the Disko Bugt may have acted as topographic pinning points, causing a decline in the speed of ice retreat during the latter stages of marine-based deglaciation (see *Fig. 8.2*).

To summarise, the new deglacial chronology for marine-based deglaciation in central West Greenland began *ca.* 3 to 5 ka later than Funder and Hansen (1996) speculated. Ice retreat was primarily driven by rising relative sea-level (*Fig. 8.2*), but it seems most likely that regional differences in ice thickness were responsible for the later retreat of ice in Uummannaq Fjord. Ice in the Uummannaq area collapsed catastrophically, retreating from the mid-shelf to inner Uummannaq Fjord in less than 1000 years. Ice recession from the mid-shelf to inner Disko Bugt, on the other hand, probably took just over 2000 years, and may largely be attributed to topographic influences. It took more than *ca.* 2000 years for ice to retreat from the inner shelf into the coastal fjords in both Disko Bugt and Uummannaq Fjord (*Fig. 8.2*). As the outlet glaciers retreated into shallower waters, the role of topography would have become more important than relative sea-level changes in determining ice margin position. The final retreat of ice across shallow topography at the entrance to the inner fjords was likely facilitated by increasing atmospheric temperatures and continued thinning of the ice sheet periphery after *ca.* 10 ka BP (*Fig. 8.2*).

8.2.3 Deglaciation of the Vaigat

One part of the deglaciation jigsaw in central West Greenland that requires further attention is the extent of ice advance in the Vaigat, and the timing and nature of subsequent deglaciation. At the LGM, ice is likely to have extended out of the Vaigat, and merged with the adjacent Uummannaq ice stream to the north, though there is at present no direct evidence to support this. On Hareøen (Talerua), in the outer Vaigat (see *Fig. 8.3*), marine shells (*Mya truncata*) in postglacial deposits at 30-35 m a.s.l. have been dated to *ca.* 11.6 ka BP (12,077-11,211 cal. yrs. BP; 10,470±130 ^{14}C yrs. BP, Bennike *et al.*, 1994). Radiocarbon ages of 10.9 ka BP (northern Disko Bugt) and 11.8 ka BP (southwestern Nuussuaq) provide minimum ages of deglaciation at the mouth of the Vaigat, while further dates from shells on the southern margin of eastern Nuussuaq peninsula indicate ice had retreated landwards of this site by 10.1 ka BP (see *Fig. 8.1*). It is possible that the lower part of the sediment record in MSM-343520_G may, therefore, partly reflect sedimentation as ice filling the Vaigat broke up. Unbuttressing of ice in the Vaigat may have resulted in influxes of basaltic material from Disko Island and Nuussuaq peninsula.

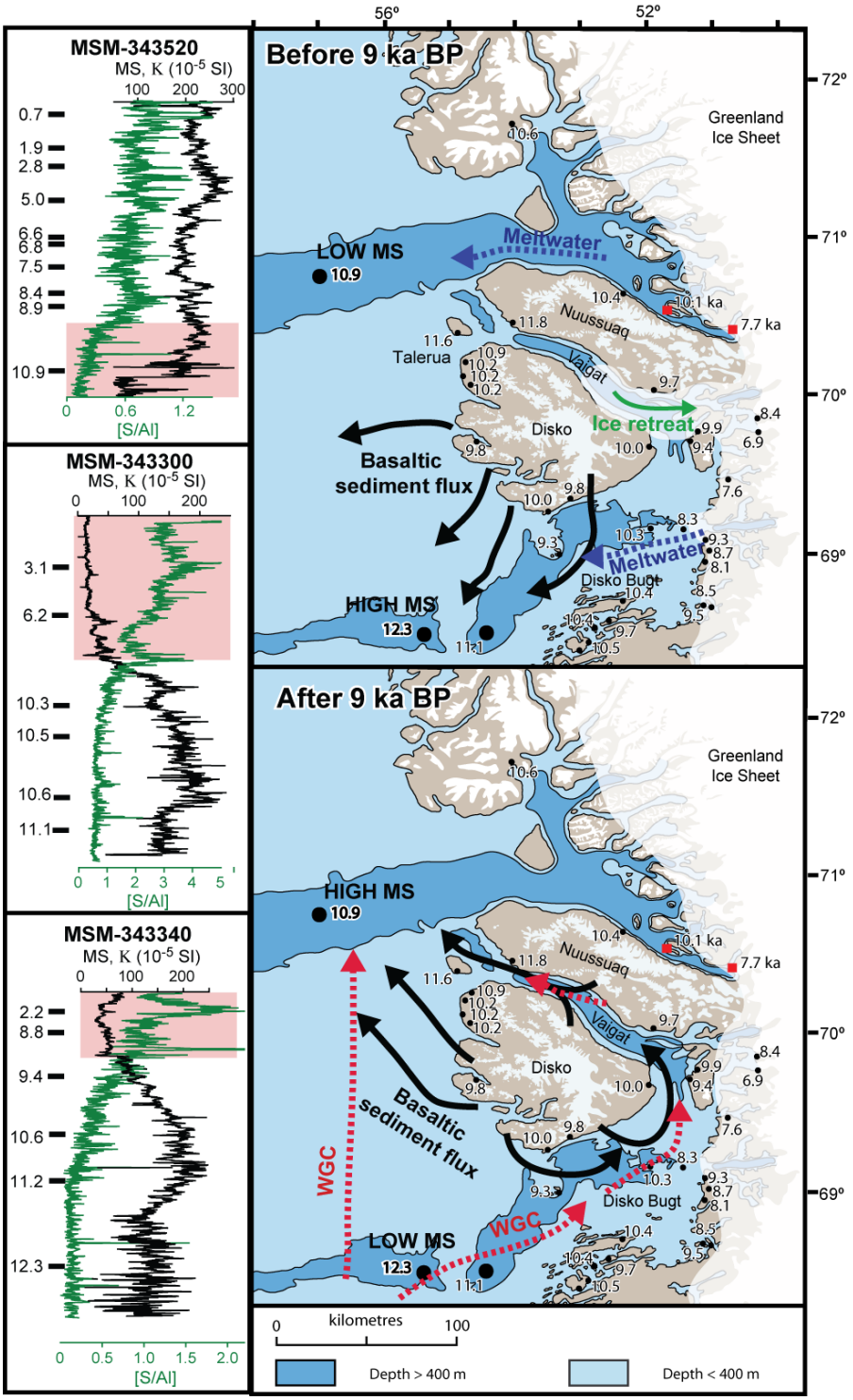

Figure 8.3 Hypothetical withdrawal of ice from the Vaigat. Left panels show magnetic susceptibility (MS) and [S/Al] XRF trends from (1) MSM-520, (2) MSM-343300 and (3) MSM-343340. Red shading highlights the period characterised by modern ocean circulation patterns in Disko Bugt and the Vaigat following final withdrawal of ice into inner fjords. Black bars show position of dated samples (mean ka BP) indicating approximate age. Right panels show conceptual maps in two time slices before (unshaded interval on left panels) and after (shaded interval) 9 ka BP.

The combination of low magnetic susceptibility and high [K/Ti] (suggesting a low concentration of magnetic minerals) in the fine-grained laminated facies at the base of core MSM-343520_G may reflect the low magnetite content of sediments sourced from Uummannaq Fjord. The up-core increase in magnetic susceptibility and decrease in [K/Ti] may consequently reflect a greater influence of basaltic sediments as ice vacated the Vaigat and retreated eastwards in Uummannaq Fjord.

8.3 Holocene palaeoceanography in central West Greenland

8.3.1 Holocene ice-ocean interactions in central West Greenland

Neoglacial and LIA ice sheet expansion destroyed geomorphological evidence for the minimum extent of the central West Greenland Ice Sheet during the HTM. However, reworked marine fauna in moraines in the Jakobshavn Isfjord area indicate that ice retreated landwards of the present ice sheet margin at *ca.* 6.1 ka BP, and readvanced to its modern limit after 3.5 ka BP (Weidick *et al.*, 1990; Weidick, 1992; Weidick and Bennike, 2007). The interval 8-5.2 ka BP was characterised by warming of sub-surface waters on the Uummannaq shelf, with a particularly warm interval between 7.7 and 6 ka BP, indicated by higher abundances of *N. labradorica* in the foraminiferal assemblages. This is similar to West Greenland records of thermophilous molluscs that indicate a warming in the WGC between *ca.* 9.2 and 5.6 ka BP (e.g. Weidick, 1972a; Kelly, 1980; Funder and Weidick, 1991; Kaufman *et al.*, 2004).

In the Jakobshavn Isfjord area, Young *et al.* (2011) show that both the marine-based ice in the Isfjord, and the terrestrial ice sheet margin rapidly retreated *ca.* 50 km between 8±0.2 ka BP and 7.5±0.2 ka BP (illustrated in *Fig. 8.4*). The synchronous response of marine and terrestrial-based ice suggests initial atmospheric warming was the key driver in these ice margin changes (Young *et al.*, 2011). However, this period coincides with initial warming of sub-surface waters identified in core MSM-343520_G on the Uummannaq shelf (*Fig. 8.4*). This suggests that the more southerly location of Disko Bugt may have experienced warmer oceanographic conditions at this time. It is possible that an incursion of warm Atlantic Water into Jakobshavn Isfjord (e.g. Holland *et al.*, 2008) may have increased melting at the glacier terminus, and further contributed to ice margin retreat at this time. Ice retreated up to 20 km behind the present ice sheet margin

between 7 and 5 ka BP (Funder, 1989; Weidick, 1992). Air temperatures in Disko Bugt were up to 2°C warmer than present between *ca.* 6 and 4.5 ka BP (*Fig. 8.4*) (Axford *et al.*, 2010; Young *et al.,* 2011), lagging the early HTM in sub-surface water temperatures by nearly 2000 years. Mid-Holocene warming in sub-surface waters, particularly pronounced between 7.7 and 6 ka BP based on foraminifera assemblages in core MSM-343520_G, may have influenced marine-based ice retreat in inner fjords at this time.

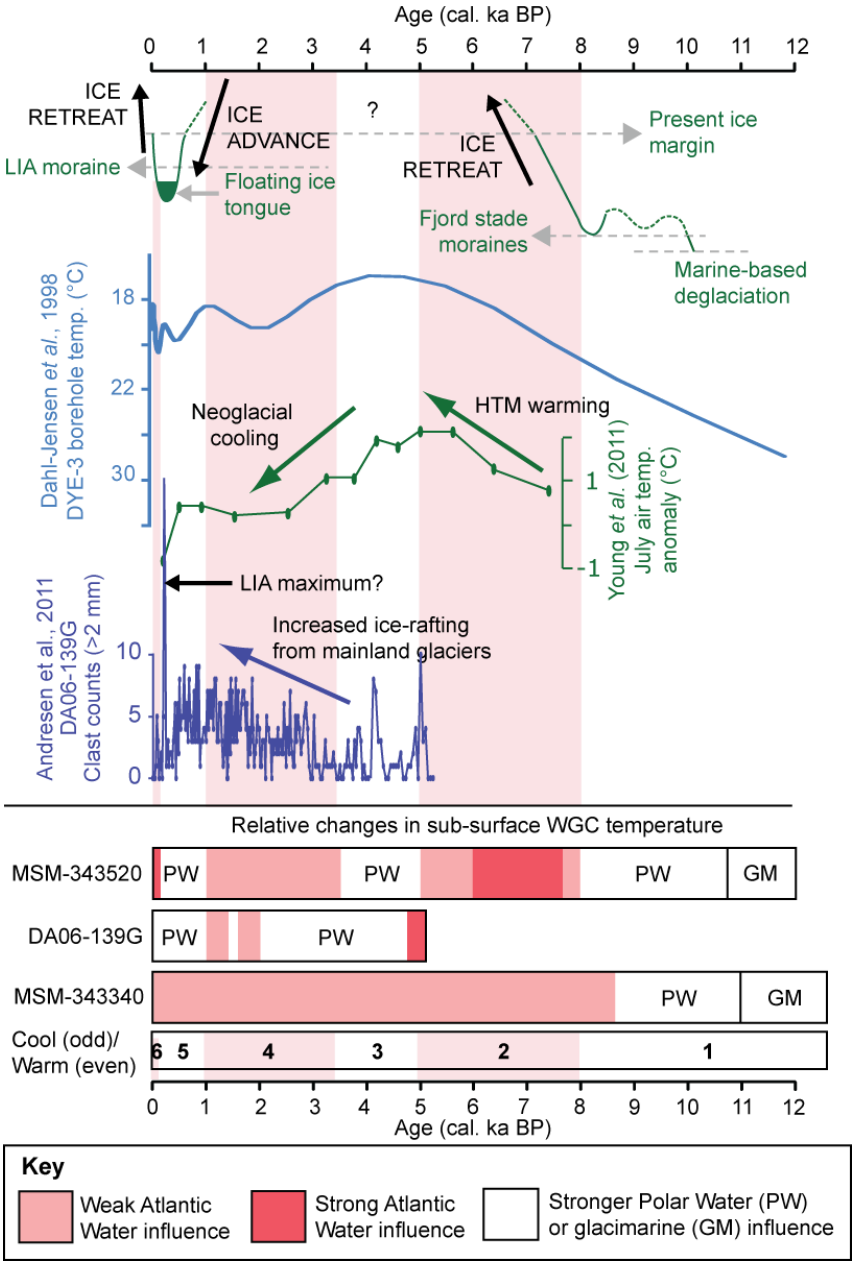

Figure 8.4 Comparison of main changes in foraminiferal assemblages in three cores (MSM-343340, DA06-139G, MSM-343520) investigated in this study, indicating periods of relatively warm or cool WGC influence in central West Greenland. Background shading indicates periods of generally warmer water conditions (2, 4, 6). Clast counts from the Vaigat core, DA06-139G (Andresen *et al.*, 2011), indicate the increase in ice rafting from calving glaciers in Disko Bugt

during the Neoglacial and LIA. Air temperature records are based on chironomid-based reconstruction from Disko Bugt (Young *et al.*, 2011) and Dye-3 borehole temperature reconstruction, from southern Greenland (Dahl-Jensen *et al.*, 1998). Conceptual changes in ice margin position (retreat and advance phases) for the Jakobshavn Isjord area is modified from Young *et al.* (2011). Dashed green lines indicate uncertainty in ice position.

Dinocyst assemblages in northwest Baffin Bay indicate that sea-surface temperatures were up to 3°C warmer than present, and surface waters were ice-free for 4-5 months per years, between 7.3 and 4 ka BP (Levac *et al.*, 2001). Indeed, the generally warmer WGC in eastern Baffin Bay (suggested by foraminiferal assemblages in core MSM-343520_G) at this time would have favoured milder climatic and reduced sea-ice (extent and duration) conditions in central West Greenland. The warm peak at the base of core DA06-139G suggests that there was a particularly strong Atlantic Water influence, and a relatively weaker Polar Water and/or meltwater influence at the entrance to the Vaigat (in northeastern Disko Bugt) at *ca.* 5-4.5 ka BP. In Kangersuneq Fjord, southwestern Disko Bugt, diatom evidence suggests amelioration of surface waters between *ca.* 4.8 and 3.5 ka BP (Moros *et al.*, 2006), while Lloyd *et al.* (2007) identify a warm WGC influence on sub-surface waters between *ca.* 6.2 and 4.3 ka BP. This period of warmth is similar to the pattern of warming on the Uummannaq shelf (MSM-34352_G) and at the base of the Vaigat record (DA06-139G). It is possible that a reduced glacial meltwater influence from marine-based glaciers in Disko Bugt provided suitable conditions for warmer waters to penetrate over shallow bedrock areas, such as at the entrance to Disko Bugt allowing warmer water penetration into the Vaigat. A thinner meltwater cap and a weaker Polar Water influence in surface waters may permit warmer Atlantic Water intrusion into fjord basins, potentially influencing the dynamics of tidewater glaciers (e.g. Motkya *et al.*, 2003).

Foraminiferal evidence suggests a cooling in sub-surface waters on the Uummannaq shelf between 5 and 3.5 ka BP (and 4.5 to 2 ka in the Vaigat). This predates atmospheric cooling by *ca.* 800 years (Fredskild, 1983). The Greenland Ice Sheet expanded between *ca.* 4 ka BP and A.D. 1850 during the Neoglacial (e.g. Kelly, 1980; Weidick *et al.*, 1990; Weidick, 1992; 1993; Long *et al.*, 2003). The increase in clast counts (*Fig. 8.4*) from DA06-139G in the Vaigat, suggests ice rafting was particularly pronounced after *ca.* 3 ka BP (Andresen *et al.*, 2011). Submarine melting at tidewater glacier termini in Disko Bugt may have influenced ice margin

dynamics at this time. In the Vaigat, two "ice rafting intervals" appear to correspond with the intrusion of warmer WGC waters into the Vaigat (*Fig. 8.4*), suggesting there may be a direct link between ocean forcing and Holocene ice dynamics. However, the subsequent period (time interval '5' in *Fig. 8.4*) characterised by increased ice rafting occurs during an interval of cooler sub-surface water temperatures in the Vaigat. The trend of 20th Century warming is clearly identified in the multicore from the Uummannaq shelf (MSM-343520_MC).

8.4 Summary

Using benthic foraminifera, sedimentological, geochemical, and dating evidence from three marine sediment cores, the deglacial history and Holocene palaeoceanographic history in central West Greenland has been reconstructed and compared to other marine, terrestrial, and ice core records. The major findings from this thesis are briefly summarised below.

Basal ages from sediment cores MSM-343340_G and MSM-343520_G provide minimum ages for deglaciation of the mid-continental shelf. In Disko Bugt, a suite of radiocarbon dates collected from cores between outer Egedesminde Dyb and Isfjeldbanken provide constraints on the minimum ages for deglaciation, and the timing of ice retreat into Jakobshavn Isfjord (Lloyd *et al.*, 2005; Jennings *et al.*, 2010). The mid-shelf outside Disko Bugt was ice free by *ca.* 12.3 ka BP, and was subsequently followed by episodic ice retreat into Disko Bugt. The calving margin retreated landwards rapidly within the deep water of Egedesminde Dyb as a calving bay re-entrant, though appears to have slowed as the grounding line retreated across the shallow topography. This is most noticeable between outer and inner Egedesminde Dyb and, later, as ice retreated into the shallower waters of inner Disko Bugt and towards the present coastline. It took *ca.* 5.6 ka for ice to retreat from the mid-shelf and into Jakobshavn Isfjord at 6.7 ka BP (J.M. Lloyd, personal communication).

The basal age in core MSM-343520_G of 10.9 ka BP suggests deglaciation began more than 1000 years later in the Uummannaq area than Disko Bugt to the south. While the timing of deglaciation is more poorly constrained in the Uummannaq area, new CRN ages from inner Uummannaq Fjord (D.H. Roberts, personal communication) suggest that marine-based

deglaciation took place much more rapidly than in Disko Bugt, retreating from the mid-shelf in and into the coastal fjords in around 3.2 ka. The much faster deglaciation in the Uummannaq area may in part be attributed to the the morphology of the deep Uummannaq trough; topographic pinning of the ice stream would not have influenced ice dynamics until ice retreated into inner Uummannaq Fjord.

Foraminiferal data from cores MSM-343340_G and MSM-343520_G do not show any evidence that ocean forcing (due to warmer sub-surface waters) influenced the timing of initial marine-based deglaciation. Instead, climatically-driven ice thinning and high relative sea-level were key driving mechanisms for the rapid collapse of ice in these two areas. The diachronous nature of ice retreat is interpreted to be due to regional differences in ice thickness. Thicker ice cover in Uummannaq Fjord would have been more resistant to changes in relative sea-level and maintained a position on the outer shelf for longer compared to thinner ice cover in Disko Bugt.

There is evidence of longer-timescale changes in the relative temperature of the sub-surface WGC that impinges on the West Greenland shelf, linked to wider-scale climatic and oceanographic changes. There appears to be a clearer link between changes in ice margin position and changes in sub-surface ocean temperatures once ice had retreated into the coastal fjords. In particular, the warming in the WGC during the HTM corresponds to an interval of ice recession, while Polar Water occupied the central West Greenland shelf during the LIA ice advance. Changes in the temperature of sub-surface waters that penetrate into coastal fjords may therefore have apotentially significantly impact on sub-marine melt rates at the calving margin and on floating ice tongues.

REFERENCES

9 References

Aagaard, K., Carmack, E.C. (1989) The Role of Sea Ice and Other Fresh Water in the Arctic Circulation. *Journal of Geophysical Research* 94: 14485. doi: 10.1029/JC094iC10p14485.

Abdalati, W., Krabill, W.B. (1999) Calculation of ice velocities in the Jakobshavns Isbrae area using airborne laser altimetry. *Remote Sensing Environments* **67**: 194-204.

Abdalati, W., Krabill W., Frederick, E., Manizade, S., Martin, C., Sonntag, J., Swift, R., Thomas, R., Wright, W., Yungel, J. (2001) Outlet glacier and margin elevation changes: Near-coastal thinning of the Greenland ice sheet. *Journal of Geophysical Research-Atmospheres* **106**: 33729-33741.

Aksu, A.E. (1985) Climatic and oceanographic changes over the past 400,000 years: evidence from deep-sea cores in Baffin Bay and Davis Strait. In: Andrews, J.T. (ed.), *Quaternary environments, Eastern Canadian Arctic, Baffin Bay and Western Greenland* Boston: Allen and Unwin, pp. 181-209.

Aksu, A.E. (1983) Holocene and Pleistocene dissolution cycles in deep-sea cores of Baffin Bay and Davis Strait: Palaeocenaographic implications. *Marine Geology* **53**: 331-348.

Aksu, A.E., Piper, D.J.W. (1979) Baffin Bay in the past 100,000 yr. *Geology* **7**: 245-248.

Aksu, A.E., Mudie, P.J. (1985) Late Quaternary stratigraphy and paleoecology of northwest Labrador Sea. *Marine Micropaleontology* **9**: 537-557.

Aksu, A.E., Mudie, P.J. (1986) Late Quaternary stratigraphy of Davis Strait. *Marine Micropaleontology* **9**: 537-557.

Alley, R.B., Ágústsdóttir, A.M. (2005) The 8k event: cause and consequences of a major Holocene abrupt climate change. *Quaternary Science Reviews* **24**: 1123-1149.

Alley, R.B., Mayewski, P.A., Sowers, T., Stuiver, M., Taylor, K.C., Clark, P.U. (1997) Holocene climatic instability: A prominent widespread event 8,200 yr ago. *Geology* **25**: 483-486.

Alley, R.B., Clark, P.U., Huybrechts, P., Joughin, I. (2005) Ice-Sheet and Sea-Level Changes. *Science* **310**: 456-460.

Alve, E. (1990) Variations in estuarine foraminiferal biofacies with diminishing oxygen conditions in Drammesfjord, southeast Norway. In: Hemleben, C., Scott, D.B., Kaminski, M., Kuhnt, W. (eds.), *Palaeoecology, biostratigraphy, palaeoceanography, and taxonomy of agglutinated foraminifera.* Dordrecht/Boston/London: Kluwer Academic Publishers, pp. 661-694.

Alve, E. (1991) Foraminifera, climatic change and pollution: A study of Late Holocene sediments in Drammensfjord, SE Norway. *The Holocene* **1**: 243-261.

Alve, E. (1994) Opportunistic features of the foraminifer Stainforthia fusiformis (Williamson): evidence from Frierfjord. *Norway: Journal of Micropalaeontology* **13**: 24.

Alve, E. (1995) Benthic foraminiferal distribution and recolonization of formerly anoxic environments in Drammensfjord, southern Norway. *Marine Micropaleontology* **25**: 169-186.

Alve, E. (1996) Benthic foraminiferal evidence of environmental change in the Skagerrak over the past six decades. *Norske Geologiske Undersoknung Bulletin* **430**: 85-93.

Alve, E. (1999) Colonization of new habitats by benthic foraminifera: a review. *Earth-Science Reviews* **46**: 167-185.

Alve, E. (2000) Environmental stratigraphy: A case study reconstructing bottom water oxygen conditions in Frierfjord, Norway, over the past five centuries. In: Martin, R. (ed.) *Environmental Micropaleontology.* New York: Kluwer Academic/Plenum Publishers, pp. 323-350.

Alve, E. (2003) A common opportunistic foraminiferal species as an indicator of rapidly changing conditions in a range of environments. *Estuarine, Coastal and Shelf Science* **57**: 501-514.

Alve, E. (2010) Benthic foraminiferal responses to absence of fresh phytodetritus: A two-year experiment. *Marine Micropaleontology* **76**: 67-75.

Alve, E., Nagy, (1986) Estuarine foraminiferal distribution in Sandebukta, a branch of the Oslo Fjord. *Journal of Foraminiferal Research* **16**: 261-284.

Alve, E., Bernhard, J.M. (1995) Vertical migratory response of benthic foraminifera to controlled oxygen concentrations in an experimental mesocosm. *Marine Ecology Progress Series* **116**: 137-151.

Ambaum, M.H.P., Hoskins, B.J., Stephenson, D.B. (2001) Arctic Oscillation or North Atlantic Oscillation? *Journal of Climate* **14**: 3495-3507.

Andersen, O.G.N. (1981a) The annual cycle of temperature, salinity, currents and water masses in Disko Bugt and adjacent waters, West Greenland. *Meddelelser om Grønland, Bioscience* **5**: 33 pp.

Andersen, O.G.N. (1981b) The annual cycle of phytoplankton, primary production, and hydrography in the Disko Bugt area, West Greenland. *Meddelelser om Grønland, Bioscience* **6**: 65 pp.

Andersen, K.K., Svensson, A., Johnsen, S.J., Rasmussen, S.O., Bigler, M., Röthlisberger, R., Ruth, U., Siggaard-Andersen, M.-L., Steffensen, J.P., Dahl-Jensen, D., Vinther, B.M., Clausen, H.B. (2006) The Greenland Ice Core Chronology 2005, 15-42 ka. Part 1: Constructing the time scale. *Quaternary Science Reviews* **25**: 3246-3257.

Anderson, N.J., Leng, M.J. (2004) Increased aridity during the early Holocene in West Greenland inferred from stable isotopes in laminated-lake sediments. *Quaternary Science Reviews* **23**: 841-849.

Andresen, C.S., McCarthy, D.J., Dylmer, C.V., Seidenkrantz, M.-S., Kuijpers, A., Lloyd, J.M. (2011) Interaction between subsurface ocean waters and calving of the Jakobshavn Isbræ during the late Holocene. *The Holocene* **21**: 211-224.

Andrews, J.T., Tedesco, K. (1992) Detrital carbonate-rich sediments, northwestern Labrador Sea: Implications for ice-sheet dynamics and iceberg rafting (Heinrich) events in the North Atlantic. *Geology* **20**: 1087-1090.

Andrews, J.T., Keigwin, L., Hall, F., Jennings, A.E. (1999) Abrupt deglaciation events and Holocene palaeoceanography from high-resolution cores, Cartwright Saddle, Labrador Shelf, Canada. *Journal of Quaternary Science* **14**: 383-397.

Andrews, J.T. (2000) Icebergs and iceberg rafted detritus (IRD) in the North Atlantic: facts and assumptions. *Oceanography* **13**: 100-108.

Andrews, J.T., Principato, S.M. (2002) Grain-size characteristics and provenance of ice-proximal glacial marine sediments. In: Dowdeswell, J.A., and Ó Cofaigh, C. (eds.)

Glacier-Influenced Sedimentation on High-Latitude Continental Margins. Geological Society, London, Special Publications **203**: 305-324.

Appleby, P.G., Oldfield, F. (1978) The calculation of ^{210}Pb dates assuming a constant rate of supply of unsupported ^{210}Pb to the sediment. *Catena* **5**: 1-8.

Appleby, P.G., Oldfield, F. (1992) *Application of lead-210 to sedimentation studies*. In: Ivanovich, M., and Harmon, S. (Eds.) Uranium Series Disequilibrium: Applications to Earth, Marine, and Environmental Sciences. Oxford: Oxford University Press, p. 731-778.

Ascough, P.L., Cook, G.T., Dugmore, A.J., Scott, E.M. (2007) The North Atlantic marine reservoir effect in the Early Holocene: Implications for defining and understanding MRE values. *Nuclear Instruments and Methods in Physics Research Section B: Beam Interactions with Materials and Atoms* **259**: 438-447.

Austin, W.E.N., Kroon, D. (1996) Late glacial sedimentology, foraminifera and stable isotope stratigraphy of the Hebridean Continental Shelf, northwest Scotland. In: Andrews, J.T., Austin, W.E.N., Bergsten, H., *et al.* (eds.) *Late Quaternary Paleoceanography of North Atlantic Margins*. London: Geological Society Special Publication **111**: 187-213.

Axford, Y., Briner, J., Young, N., Francis, D., Darko, O. (2010) New constraints on Greenland's Holocene climate history: Chironomid-based temperature reconstructions from two West Greenland lakes. *40th International Arctic Workshop*, Winter Park, Colorado, 10-12th March 2010. INSTAAR, University of Boulder at Colorado.

Bamber, J.L, Alley, R.A., Joughin, I. (2007) Rapid response of modern day ice sheets to external forcing. *Earth and Planetary Science Letters* **257**: 1-13.

Barber, D.C., Dyke, A., Hillaire-Marcel, C., Jennings, A.E., Andrews, J.T., Kerwin, M.W., Bilodeau, G., McNeely, R., Southon, J., Morehead, M.D., Gagnon, J.-M. (1999) Forcing of the Cold Event of 8,200 years ago by catastrophic drainage of Laurentide lakes. *Nature* **400**: 344-348.

Bard, E., Arnold, M., Mangerud, J., Paterne, M., Labeyrie, L., Duprat, J., Mélières, M.-A., Sønstegaard, E., Duplessy, J.-C. (1994) The North Atlantic atmosphere-sea surface ^{14}C gradient during the Younger Dryas climatic event. *Earth and Planetary Science Letters* **126**: 275-287.

Bauer, A., Baussart, M., Carbonnell, M., Kasser, P., Perroud, P., Renaud, A. (1968) Missions aériennes de reconnaissance au Groenland 1957-1958. Observations aériennes et terrestres, exploitation des photographies aériennes, détermination des vitesses des glaciers vêlant dans Disko Bugt et Umanak Fjord. *Meddelelser om Grønland* **173**: 116 pp.

Belkin, I.M., Levitus, S., Antonov, J., Malmberg, S.-A. (1998) "Great Salinity Anomalies" in the North Atlantic. *Progress in Oceanography* **41**: 1-68.

Belkin, I.M. (2004) Propagation of the “Great Salinity Anomaly” of the 1990s around the northern North Atlantic. *Geophysical Research Letters* **31**: L08306, doi: 10.1029/2003GL019334

Bennike, O. (2000) Palaeoecological studies of Holocene lake sediments from West Greenland. *Palaeoecology, Palaeoclimatology, Palaeogeography* **155**: 285-304.

Bennike, O. (2004) Holocene sea-ice variations in Greenland: onshore evidence *Holocene* **14**: 607-613.

Bennike, O., Björck, S. (2002) Chronology of the last recession of the Greenland Ice Sheet.

Journal of Quaternary Science **17**: 211-219

Bennike, O., Björck, S., Böcher, J., Walker, I.R. (2000) Quaternary arthropods from Greenland: A review with new data. *Bulletin of the Geological Society of Denmark* **47**: 111-134.

Bennike, O., Hanses, K.B. Knudsen, K.L., Penney, D.N., Rasmussen, K.L. (1994) Quaternary marine stratigraphy and geochronology in central West Greenland. *Boreas* **23**: 194-215.

Berger, A., Loutre, M.F. (1991) Insolation values for the climate of the last 10 million years. *Quaternary Science Reviews* **10**: 297-317.

Bernhard, J.M., Alve, E. (1996) Survival, ATP pool, and ultrastructural characterization of benthic foraminifera from Drammensfjord (Norway) - response to anoxia. *Marine Micropaleontology* **28**: 5-17.

Bernhard, J.M., Bowser, S.S. (1999) Benthic foraminifera of dysoxic sediments: Chloroplast sequestration and functional morphology, *Earth-Science Reviews* **46**: 149-165.

Bersch, M. (1995) On the circulation of the northeastern North Atlantic. *Deep-Sea Research* **42**: 1583-1607.

Bersch, M., Meincke, J., Sy, A. (1999) Interannual thermohaline changes in the northern North Atlantic 1991-1996. *Deep Sea Research Part II: Topical Studies in Oceanography* **46**: 55-75.

Bergsten, H. (1994) Recent benthic foraminifera of a transect from the North Pole to the Yermak Plateau, eastern central Arctic Ocean. *Marine Geology* **119**: 251-267.

Bianchi, G.G., McCave, I.N. (1999) Holocene periodicity in North Atlantic climate and deep-ocean flow south of Iceland. *Nature* **397**: 515-517.

Bigg, G.R. (1999) An estimate of the flux of iceberg calving from Greenland. *Arctic, Antarctic and Alpine Research* **31**: 174-178.

Bigg, G.R., Wadley, M.R. (2001) The origin and flux of icebergs released into the Last Glacial Maximum Northern Hemisphere oceans: the impact of ice-sheet topography. *Journal of Quaternary Science* **16**: 565-573.

Bilodeau, G., de Vernal, A., Hillaire-Marcel, C. (1994) Benthic foraminiferal assemblages in Labrador Sea sediments: relations with deep-water ass changes since deglaciation. *Canadian Journal of Earth Sciences* **31**: 128-138.

Bindschadler, R. (2006) Hitting the Ice Sheets Where It Hurts. *Science* **311**: 1720-1721.

Bindschadler, R.A. (1984) Jakobshavns Glacier drainage basin; a balance assessment. *Journal of Geophysical Research. C. Oceans and Atmospheres* **89**: 2066-2072.

Birks, H.J.B. (1995) Quantitative palaeoenvironmental reconstructions. In: Maddy, D., Brew, J.S. (eds.), *Statistical modelling of Quaternary science data, Technical Guide 5*. Cambridge: Quaternary Research Association, pp. 161-254.

Björck, S., Bennike, O., Rosén, P., Andresen, C.S., Bohncke, S., Kaas, E., Conley, D. (2002) Anomalously mild Younger Dryas summer conditions in southern Greenland. *Geology* **30**: 427-430.

Blais-Stevens, A., Patterson, R.T. (1998) Environmental indicator potential of Foraminifera from Saanich Inlet Vancouver Island, British Columbia, Canada. *Journal of Foraminiferal Research* **28**: 201-219.

Blake, W., Jr. (1970) Studies of glacial history in arctic Canada. I. Pumice, radiocarbon dates, and differential postglacial uplift in the eastern Queen Elizabeth Islands. *Canadian Journal of EarthSciences* **7**: 634-664.

Blindheim, J.R., Toresen, R., Loeng, H. (2001) Fremtidige klimatiske endringer og betydningen for fiskeressuresene: Havets miljo. *Fisken og Havet*, **2**: 73-78.

Bond, G.C., Lotti, R. (1995) Iceberg discharges into the North Atlantic on millennial timescales during the Last Glaciation. *Science* **267**: 1005-1009.

Bond, G., Heinrich, H., Broecker, W., Labeyrie, L., McManus, J., Andrews, J., Huon, S., Jantschik, R., Clasen, S., Simet, C., Tedesco, K., Klas, M., Bonani, G., Ivy, S. (1992) Evidence for massive discharges into the North-Atlantic Ocean during the last glacial period. *Nature* **360**: 245-249.

Bond, G., Broecker, W., Johnsen, S., McManus, J., Labeyrie, L., Jouzel, J., Bonani, G. (1993) Correlations between climate records from North Atlantic sediments and Greenland ice. *Nature* **365**: 143-147.

Bond, G., Showers, W., Cheseby, M., Lotti, R., Almasi, P., deMenocal, P., Priore, P., Cullen, H., Hajdas, I., Bonani, G. (1997) A Pervasive Millennial-Scale Cycle in North Atlantic Holocene and Glacial Climates. *Science* **278**: 1257-1266.

Bond, G.C., Showers, W., Elliot, M., Evans, M., Lotti, R., Hajdas, I., Bonani, G., Johnson, S. (1999) The North Atlantic's 1-2 kyr climate rhythm: Relation to Heinrich events, Dansgaard/Oeschger cycles and the little ice age. In: Clark, P.U., Webb, R.S., Keigwin, L.D. (eds.), *Mechanisms of Global Climate Change at Millennial Time Scales*. Washington D.C.: American Geophysical Union, pp. 35-68.

Bond, G., Kromer, B., Beer, J., Muscheler, R., Evans, M.N., Showers, W., Hoffmann, S., Lotti-Bond, R., Hajdas, I., Bonani, G. (2001) Persistent solar influence on North Atlantic climate during the Holocene. *Science* **294**: 2130-2136.

Bondevik, S., Mangerud, J., Birks, H.H., Gulliksen, S., Reimer, P. (2006) Changes in North Atlantic radiocarbon reservoir ages during the Allerød and Younger Dryas. *Science* **312**: 1514-1517.

Bonow, J.M. (2005) Re-exposed basement landforms in the Disko region, West Greenland-disregarded data for estimation of glacial erosion and uplift modelling. *Geomorphology* **72**: 106-127.

Bonow, J.M., Lidmar-Bergstrom, K., Japsen, P. (2006) Palaeosurfaces in central West Greenland as reference for identification of tectonic movements and estimation of erosion. *Global and Planetary Change* **50**: 161-183.

Borcard, D., Legendre, P., Drapeau, P. (1992) Partialling out the spatial component of ecological variation. *Ecology* **73**: 1045-1055.

Box, J.E. (2002) Survey of Greenland instrumental temperature records: 1873-2001. *International Journal of Climatology* **22**: 1829-1847.

Brett, C.P., Zarudzki, E.F.K. (1979) Project Westmar. A shallow marine geophysical survey on the West Greenland continental shelf. *Rapport Grønlands Geologiske Undersøgelse* **87**: 27pp.

Briner, J.P., Stewart, H.A.M., Young, N.E., Philipps, W., Losee, S. (2010) Using proglacial-threshold lakes to constrain fluctuations of the Jakobshavn Isbræ ice margin, western Greenland, during the Holocene. *Quaternary Science Reviews* **29**: 3861-3874.

Broecker, W.S. (1991) The Great Ocean Conveyor. *Oceanography* **4**: 79-89.

Broecker, W.S. (1994) Massive iceberg discharges as triggers for global climate change. *Nature* **372**: 421-424.

Broecker, W.S. (2003) Does the trigger for abrupt climate change reside in the ocean or in the atmosphere? *Science* **300**: 1519-1522.

Broecker, W.S., Kennett, J.P., Flower, B.P., Teller, J.T., Trumbore, S., Bonani, G., Wolfli, W. (1989) Routing of meltwater from the Laurentide Ice Sheet during the Younger Dryas cold episode. *Nature* **341**: 318-321.

Broecker, W., Bond, G., Klas, M., Clark, E., McManus, J. (1992) Origin of the northern Atlantic's Heinrich events. *Climate Dynamics* **6**: 265-273.

Bronk Ramsey, C. (2009) Bayesian analysis of radiocarbon dates. *Radiocarbon* **51**: 337-360.

Buch, E. (1993) The North Atlantic water component of the West Greenland Current. *Contribution to ICES statutory meeting hydrographic committee*, pp. 17.

Buch, E., Stein, M. (1989) Environmental conditions off West Greenland, 1980-1985. *Journal of Northwest Atlantic Fishery Science* **9**: 81-89.

Buch, E., Nielsen, M.H. (2001) Oceanographic Investigations off West Greenland 2000. *NAFO Scientific Council Documents* **01/002**. pp. 17.

Buch, E., Nielsen, M.H. (2002) Oceanographic Investigations off West Greenland 2001. *NAFO Scientific Council Documents* **02/017**.

Calvert, S.E., Pedersen, T.F. (2007) Elemental proxies for palaeoclimatic and palaeoceanographic variability in marine sediments: interpretation and application. In: Hillaire-Marcel, C., de Vernal, A. (eds.), *Proxies in Late Cenozoic Paleoceanography*. Amsterdam: Elsevier Science, pp. 567–644.

Cao, L., Fairbanks, R.G., Mortlock, R.A*., et al.* (2007) Radiocarbon reservoir age of high latitude North Atlantic surface water during the last deglacial. *Quaternary Science Reviews* **26**: 732-742.

Caralp, M.H. (1989a) Abundance of *Bulimina exilis* and *Melonis barleeanum*: Relationship to the quality of marine organic matter. *Geo-Marine Letters* **8**: 37-43.

Caralp, M.H. (1989b) Size and morphology of the benthic foraminifer *Melonis barleeanun*: Relationships with marine organic matter. *Journal of Foraminiferal Research* **19**: 235-245.

Carbonell, M., Bauer, A. (1968) Exploitation des couvertures photographiques aériennes répétées du front des glaciers vélant dans Disko Bugt et Umanak Fjord, juin-juillet 1964. *Meddelelser om Grønland, Kommissionen for widenskabelige Undersøgelser i Grønland* **173**: 78 pp.

Carlson, A.E., Stoner, J.S., Donnelly, J.P*.,* Hillaire-Marcel, C. (2008) Response of the southern Greenland Ice Sheet during the last two deglaciations. *Geology* **36**: 359-362.

Carmack, E.C. (2007) The alpha/beta ocean distinction: a perspective on freshwater, fluxes convection, nutrients and productivity in high-latitude seas. . *Deep Sea Research Part II: Topical Studies in Oceanography* **54**: 2578-2598.

Cavalli-Sforza, L.L., Edwards, A.W.F. (1967) Phylogenetic analysis: models and estimation procedures. *American Journal of Human Genetics* **19**: 233-257.

Cedhagen, T. (1991) Retention of chloroplasts and bathymetric distribution in the sublittoral foraminiferan Nonionellina labradorica. *Ophelia* **33**: 17-30.

Chapman, D.C., Beardsley, R.C. (1989) On the origin of shelf water in the Middle Atlantic Bight. *Journal of Physical Oceanography.* **19**: 384-391.

Chapman, W.L., Walsh, J.E. (1993) Recent variations of sea ice and air temperature in high latitudes. *Bulletin of the American Meteorological Society* **74**: 33-47.

Chen, J.L., Wilson, C.R., Tapley, B.D. (2006) Satellite gravity measurements confirm accelerated melting of Greenland Ice Sheet. *Science* **313**: 1958-1960.

Clark, D.E. (1971) Effects of aquaculture outfall on benthonic foraminifera in Clam Bay, Nova Scotia. *Maritime Sediments* **2**: 76-84.

Clark, P.U., Marshall, S.J., Clarke, G.K.C., Hostetler, S.W., Licciardi, J.M., Teller, J.T. (2001) Freshwater forcing of abrupt climate change during the last glaciation. *Science* **293**: 283-287.

Clarke, T.S., Echelmeyer, K. (1996) Seismic-reflection evidence for a deep subglacial trough beneath Jakobshavns Isbrae, West Greenland. *Journal of Glaciology* **14**: 219-232.

Climatology/Meteorology Research Group, Institute of Geography, University of Bern (2004) *North Atlantic Oscillation (NAO) [online].* Available from*:* http://www.giub.unibe.ch/klimet/wanner/nao.html, Accessed October, 2010.

Corliss, B.H. (1985) Microhabitats of benthic foraminifera within deep-sea sediments. *Nature* **314**: 435-438.

Corliss, B.H. (1991) Morphology and microhabitat preferences of benthic foraminifera from the northwest Atlantic Ocean. *Marine Micropaleontology* **17**: 195-236.

Cowan, E.A., Cai, J., Powell, R.D., Clark, J.D., Pitcher, J.N. (1997) Temperate glacimarine varves: an example from Disenchantment Bay, southern Alaska. *Journal of Sedimentary Research* **67**: 536-549.

Croudace, I.W., Rindby, A., Rothwell, R.G. (2006) ITRAX: description and evaluation of a new multi-function X-ray core scanner. In: Rothwell, R.G. (ed.), *New Techniques in Sediment Core Analysis*. London: Geological Society, pp. 51-63.

Cuny, J., Rhines, P.B., Ron, K. (2005) Davis Strait volume, freshwater and heat fluxes. *Deep Sea Research Part I: Oceanographic Research Papers* **52**: 519-542.

Curry, R., Mauritzen,C. (2005) Dilution of the northern North Atlantic in recent decades. *Science* **308**: 1772-1774.

Curry, R., Dickson, B. Yashayaev, I. (2003) A change in the freshwater balance of the Atlantic Ocean over the past four decades. *Nature* **426**: 826-829.

Dadey, K.A., Janecek, T., Klaus, A. (1992) Dry-bulk density: its use and determination. *Proceedings of the Ocean Drilling Scientific Results* **126**: 551-554.

Dahl-Jensen, D., Mosegaard, K., Gundestrup, N., Clow, G.D., Johnsen, S.J., Hansen, A.W., Balling, N. (1998) Past temperatures directly from the Greenland ice sheet. *Science* **282**: 268-271.

Dansgaard, W., Johnsen, S., Clausen, H.B., Langway, C.C. (1971) Climatic Record Revealed by the Camp Century Ice Core. In: Turekian, *K.K*. (ed.) *The Late Cenozoic Glacial Ages,* New Haven, Connecticut: Yale University Press. pp. 37-56.

Dansgaard, W., Clausen, H.B., Gundestrup, N., Hammer, C.U., Johnsen, S.F., Kristinsdottir, P.M., Reeh, N. (1982) A New Greenland Deep Ice Core. *Science* **218**: 1273-1277.

Dansgaard, W., Johnsen, S.J., Clausen, H.B., Dahl-Jensen, D., Gundestrup, N.S., Hammer, C.U., Hvidberg, C.S., Steffensen, J.P., Sveinbjörnsdottir, A.E., Jouzel, J., Bond, G. (1993) Evidence for general instability of past climate from a 250-kyr ice-core record. *Nature* **364**: 218-220.

Dean, W.E.J. (1974) Determination of carbonate and organic matter in calcareous sediments and sedimentary rocks by loss on ignition: comparison with other methods. *Journal of Sedimentary Petrology* **44**: 242-248.

de Angelis, H., Skvarca, P. (2003) Glacier surge after ice shelf collapse. *Science* **299**: 1560-1562.

Dearing, J. (1999) Magnetic Susceptibility. In: Walder, J., Oldfield, F., Smith, J.P. (eds.) *Environmental Magnetism: a practical guide*. *Technical Guide, No. 6*. London: Quaternary Research Association, pp. 35-62.

Dennison, J.M., Hay, W.W. (1967) Estimating the needed sampling area for subaquatic ecological studies. *Journal of Paleontology* **41**: 706 -708

Denton, G.H., Broecker, W.S. (2008) Wobbly ocean conveyor during the Holocene? *Quaternary Science Reviews* **27**: 1939-1950.

Denton, G.H., Alley, R.B., Comer, G.C., Broecker, W.S. (2005) The role of seasonality in abrupt climate change. *Quaternary Science Reviews* **24**: 1159-1182.

Desloges, J.R., Gilbert, R., Nielsen, N., Christiansen, C., Rasch, M., Øhlenschläger, R. (2002) Holocene glacimarine sedimentary environments in fiords of Disko Bugt, West Greenland. *Quaternary Science Reviews* **21**: 947-963.

de Vernal, A., Hillaire-Marcel, C. (2000) Sea-ice, sea-surface salinity and the halo/thermocline structure in the northern North Atlantic: modern versus full glacial conditions. *Quaternary Science Reviews* **19**: 65-85.

de Vernal, A., Hillaire-Marcel, C. (2006) Provincialism in trends and high frequency changes in the northwest North Atlantic during the Holocene. *Global and Planetary Change* **54**: 263-290.

de Vernal, A., Bilodeau, G., Hillaire-Marcel, C., Kassou, N. (1992) Quantitative assessment of carbonate dissolution in marine sediments from foraminiferal test linings vs. shell ratios: Davis Strait, northwest North Atlantic. *Geology* **20**: 527-530.

de Vernal, A., Turon, J.-L., Guiot, J. (1994) Dinoflagellate cyst distribution in high-latitude marine environments and quantitative reconstruction of sea-surface salinity, temperature, and seasonality *Canadian Journal of Earth Sciences* **31**: 48-62.

de Vernal, A., Hillaire-Marcel, C., Bilodeau, G. (1996) Reduced meltwater outflow from the Laurentide ice margin during the Younger Dryas. *Nature* **381**: 774-777.

Dickson, R.R., Meincke, J., Malmberg, S.-A., Lee, A.J. (1988) The "Great Salinity Anomaly" in the northern North Atlantic, 1968-1982. *Progress in Oceanography* **20**: 103-151.

Dickson, R., Lazier, J., Meincke, Rhines, P., Swift, J. (1996) Long-term coordinated changes in the convective activity of the North Atlantic. *Progress in Oceanography* **38**: 241-295.

Dickson, B., Yashayaev, I., Meincke, J., Turrell, B., Dye, S., Holfort, J. (2002) Rapid freshening of the deep North Atlantic Ocean over the past four decades. *Nature* **416**: 832-837.

Donner, J. (1978) Holocene History of the West Coast of Disko, Central West Greenland. *Geografiska Annaler. Series A, Physical Geography* **60**: 63-72.

Donner, J., Jungner, H. (1975) Radiocarbon dating of shells from marine Holocene deposits in the Disko Bugt area, West Greenland. *Boreas* **4**: 25-45.

Dowdeswell, J.A., Whittington, R.J., Marienfeld, P. (1994) The origin of massive diamicton facies by iceberg rafting and scouring, Scoresby Sund, East Greenland. *Sedimentology* **41**: 21-35.

Dowdeswell, J.A., Maslin, M.A., Andrews, J.T., McCave, I.N. (1995) Iceberg production, debris rafting and extent and thickness of Heinrich layers (H-1, H-2) in North Atlantic sediments. *Geology* **23**: 301-304.

Dowdeswell, J.A., Whittington, R.J., Jennings, A.E., Andrews, J.T., Mackensen, A., Marienfield, P. (2000) An origin for laminated glacimarine sediments through sea-ice build-up and suppressed iceberg rafting. *Sedimentology* **47**: 557-576.

Drinkwater, K.F. (1996) Climate and oceanographic variability in the Northwest Atlantic during the 1980s and early-1990s. *Journal of Northwest Atlantic Fishery Science* **18**: 77-97.

Dyke, A.S., Dale, J.E., McNeely, R.N. (1996) Marine molluscs as indicators of environmental changes in glaciated North America and Greenland during the last 18 000 years. *Geographie Physique et Quaternaire* **50**: 125-184.

Dyke, A.S., Andrews, J.T., Clark, P.U., England, J.H., Miller, G.H., Shaw, J., Veillette, J.J. (2002) The Laurentide and Innuitian ice sheets during the last glacial maximum. *Quaternary Science Reviews* **21**: 9-31.

Echelmeyer, K., Clarke, T.S., Harrison, W.D. (1991) Surficial glaciology of Jakobshavns Isbræ, West Greenland. Part I: Surface morphology. *Journal of Glaciology* **37**: 368382.

Eiríksson, J., Knudsen, K.L., Haflidason, H., Henriksen, P. (2000) Late-glacial and Holocene palaeoceanography of the North Icelandic shelf. *Journal of Quaternary Science* **15**: 23-42.

Elverhøi, A., Liestøl, O., Nagy, J. (1980) Glacial erosion, sedimentation and microfauna in the inner part of Kongsfjorden, Spitsbergen. *Norsk Polarinstitute Skrifter* **132**: 33-61.

Emiliani, C. (1955) Pleistocene Temperatures. *Journal of Geology* **63**: 538-578.

England, J. (1976) Late Quaternary glaciation of the eastern Queen Elizabeth Islands, Northwest Territories, Canada: alternative models. *Quaternary Research* **6**: 185-202.

England, J. (1983) Isostatic adjustments in a full glacial sea. *Canadian Journal of Earth Sciences* **20**: 895-917.

England, J. (1999) Coalescent Greenland and Innuitian ice during the Last Glacial Maximum: revising the Quaternary of the Canadian High Arctic. *Quaternary Science Reviews* **18**: 421-456.

Eyles, N., Eyles, C.H., Miall, A.D. (1983) Lithofacies types and vertical profile models; an alternative approach to the description and environmental interpretation of glacial diamict and diamictite sequences. *Sedimentology* **30**: 393-410.

Eyles, N., Vossler, S.M., Lagoe, M.B. (1992) Ichnology of a glacially-influenced continental shelf and slope; the Late Cenozoic Gulf of Alaska (Yakataga Formation).pdf. *Palaeogeography, Palaeoclimatology, Palaeoecology* **94**: 193-221.

Fairbanks, R.G. (1989) A 17,000 year glacio-eustatic sea level record: influence of glacial melting rates on the Younger Dryas event and deep ocean circulation. *Nature* **342**: 637-642.

Fastook, J.L., Hughes, T.J. (1994) A plan to model iceberg outbursts from Greenland outlet glaciers in response to greenhouse warming. In: Rhee, N. (ed.), *Report on the Workshop on the Calving Rate of West Greenland Glaciers in Response to Climate Change*. Danish Polar Center: University of Copenhagen, pp. 21-36.

Fatela, F., Taborda, R. (2002) Confidence limits of species proportions in microfossil assemblages. *Marine Micropaleontology* **45**: 169-174.

Feyling-Hanssen, R.W., Funder, S. (1990) Fauna and flora: Late Quaternary stratigraphy and glaciology in the Thule area, Northwest Greenland. *Meddelelser om Grønland* **22**: 19-22.

Fisher, D.A. (1976) *A study of two O-18 records from Devon Ice cap, Canada, and comparison of them to Camp Century O-18 record, Greenland. Ph.D. thesis*, University of Copenhagen. 278 pp.

Flatau, M.K., Talley, L., Niler, P.P. (2003) The North Atlantic Oscillation, Surface Current Velocities, and SST Changes in the Subpolar North Atlantic. *Journal of Climate* **16**: 2355-2369.

Fleming, K., Lambeck, K. (2004) Constraints on the Greenland Ice Sheet since the Last Glacial Maximum from sea-level observations and glacial-rebound models. *Quaternary Science Reviews* **23**: 1053-1077.

Fredskild, B. (1984) Holocene palaeo- winds and climatic changes in West Greenland as indicated by long-distance transported and local pollen in lake sediments. In: Morner, N.-A. (ed.), *Climatic changes on a yearly to millennial basis.* Dordrecht; Boston: D. Reidel Publishing Company, pp. 163-171.

Frich, P., Ingólfsson, Ó. (1990) Det holocæne sedimentationsmiljö ved Igpik samt en model for den relative landhævning i Disko Bugt området, Vestgrönland. *Dansk Geologisk Forening Årsskrift* **1987-89**: 1-10.

Funder, S. (1989) Quaternary geology of the ice-free areas and adjacent shelves of Greenland. In: Fulton, R.J. (ed.), *Quaternary Geology of Canada and Greenland.* Geological Survey of Canada, pp. 741-792.

Funder, S., Weidick, A. (1991) Holocene boreal mollluscs in Greenland; palaeoceanographic implications *Palaeogeography, Palaeoclimatology, Palaeoecology* **85**: 123-135.

Funder, S., Hansen, L. (1996) The Greenland ice sheet-a model for its culmination and decay during and after the Last Glacial Maximum. *Bulletin of the Geological Society of Denmark* **42**: 137-152.

Funder, S., Hjort, C., Landvik, J., Nam, S.-I., Reeh, N., Stein, R. (1998) History of a stable ice margin – East Greenland during the middle and upper Pleistocene. *Quaternary Science Reviews* **17**: 77-123.

Furevik, T., and Nilsen, J.E.Ø. (2005) Large-scale atmospheric circulation variability and its impacts on the Nordic Seas ocean climate-A review. In Drange, H. *et al.* (eds.) The Nordic Seas: An integrated Perspective. Geophysical Monograph Series 158. American Geophysical Union, Washington D.C., pp 105-136.

Ganachaud, A., Wunsch, C. (2000) Improved estimates of global ocean circulation, heat transport and mixing from hydrographic data. *Nature* **408**: 453-457.

Garde, A.A., Steenfelt, A. (1999) Precambrian geology of Nuussuaq and the area north-east of Disko Bugt, West Greenland. In: Kalsbeek, F. (ed.), *Precambrian geology of the Disko Bugt region, West Greenland*. Copenhagen: GEUS, pp. 6-40.

Gilbert, R., Nielsen, N., Desloges, J.R., Rasch, M. (1998) Contrasting glacimarine sedimentary environments of two arctic fjords on Disko, West Greenland. *Marine Geology* **147**: 63-83.

Gilbert, R., Nielsen, N., Möller, H., Deslodges, J.R., Rasch, M. (2002) Glacimarine sedimentation in Kangerdluk (Disko Fjord), West Greenland, in response to a surging glacier. *Marine Geology* **191**: 1-18.

Gooday, A.J. (1993) Deep-sea benthic foraminiferal species which exploit phytodetritus: characteristic features and controls on distribution. *Marine Micropaleontology* **22**: 187-205.

Google (2009) *Google Earth* [online]. Version 5.2. Google Inc.: Mountain View, California, USA. Available from: http://earth.google.com, Accessed November 2010.

Gooday, A.J., Alve, E. (2001) Morphological and ecological parallels between sublittoral and abyssal foraminiferal species in the NE Atlantic: a comparison of Stainforthia fusiformis and Stainforthia sp. *Progress In Oceanography* **50**: 261-283.

Greatbach, R.J. (2000) The North Atlantic Oscillation. Stochastic Environmental Research and Risk Assessment, 14: 213-242.

Grimm, E.C. (1987) CONISS: a FORTRAN 77 program for stratigraphically constrained cluster analysis by the method of incremental sum of squares. *Computers & Geosciences* **13**: 13-35.

Grobe, H. (1987) A simple method for the determination of ice-rafted debris in sediment cores. *Polarforschung* **57**: 123-126.

Gustafsson, M., Nordberg, K., (2001) Living (stained) benthic foraminifera and their response to the seasonal hydrographic cycle, periodic hypoxia and to primary production in Havstens Fjord on the Swedish West Coast. *Estuarine, Coastal and Shelf Science* **51**: 743–761.

Gustafsson, M., Nordberg, K., (2001) Living (stained) benthic foraminiferal response to primary production and hydrography in the deepest part of the Gullmar Fjord, Swedish West coast, with comparisons to Hoglund's 1927 material. *Journal of Foraminiferal Research* **31**: 2-11.

Gutt, J. (2001) On the direct impact of ice on marine benthic communities, a review. *Polar Biology* **24**: 553-564.

Hakkinen, S., Rhines, P.B. (2004) Decline of subpolar North Atlantic circulation during the 1990s. *Science* **304**: 555-559.

Hald, M., Steinsund, P.I. (1996) Benthic foraminifera and carbonate dissolution in surface sediments of the Barents and Kara Seas. *Reports on Polar Research* **212**: 285-303. In: R. Stein, G.I. Ivanov, M.A. Levitan, K. Fahl (eds.) *Surface-sediment composition and sedimentary processes in the central Arctic Ocean and along the Eurasian Continental Margin.* Berichte zur Polarforschung **212**: p. 285-307.

Hald, M., Korsun, S. (1997) Distribution of modern benthic foraminifera from fjords of Svalbard, European Arctic. *Journal of Foraminiferal Research* **27**: 101-122.

Hald, M., Steinsund, P.I. (1992) Distribution of surface sediment benthic foraminifera in the southwestern Barents Sea. *Journal of Foraminiferal Research* **22**: 347-362

Hanna, E., Cappelen, X., Fettweis, P., Huybrechts, P., Luckman, A., Ribergaard, M.H. (2009) Hydrologic response of the Greenland ice sheet: the role of oceanographic warming. *Hydrological Processes* **23**: 7-30.

Hansen, A., Knudsen, K.L. (1995) Recent foraminiferal distribution in Freemansundet and Early Holocene stratigraphy on Edgeøya, Svalbard. *Polar Research* **14**: 215-238.

Hald, M., Steinsund, P.I., Dokken, T., Korsun, S., Polyak, L., Aspeli, R. (1994) Recent and Late Quaternary distribution of Elphidium excavatum f. clavatum in Arctic seas. *Cushman Foundation Special Publication* **32**: 141-153.

Hald, M., Steinsund, P.I. (1992) Distribution of surface sediment benthic foraminifera in the southwestern Barents Sea. *Journal of Foraminiferal Research* **22**: 347-362.

Hansen, B., Østerhus, S. (2000) North Atlantic-Nordic Seas exchanges. *Progress in Oceanography* **45**: 109–208.

Harff, J. (ed.) (2007) *Deglaciation history, coastal development, and environmental change during the Holocene in western Greenland*, Cruise Report R/V Maria S. Merian, Cruise MSM 05/03, pp. 169.

Hátún, H., Sandø, A.B., Drange, H., Hansen, B., Valdimarsson, H. (2005) Influence of the Atlantic Subpolar Gyre on the Thermohaline Circulation. *Science* **309**: 1841-1844.

Heinrich, H. (1988) Origin and consequences of cyclic ice rafting in the Northeast Atlantic Ocean during the past 130,000 years. *Quaternary Research* **29**: 142-152.

Helland, A. (1876) Om de isfyldte Fjorde og glaciale Dannelser i Nordgrönland. *Archiv for Matematik og Naturvidenskab* **1**: 69 pp. Cited in: Weidick, A., Bennike, O. (2007) *Quaternary glaciation history and glaciology of Jakobshavn Isbræ and the Disko Bugt region, West Greenland: a review.* Geological survey of Denmark and Greenland Bulletin **14**: 78 pp.

Henriksen, N., Higgins, A.K., Kalsbeek, F., Pulvertaft, T.C.R. (2000) *Greenland from Archaean to Quaternary Descriptive text to the Geological map of Greenland,1:2 500 000* Copenhagen: GEUS.

Herman, Y., O'Neil, J.R., Drake, C.L. (1972) Micropaleontology and paleotemperatures of postglacial SW Greenland fjord cores. In: Y. Vasari, H.H., S. Hicks (ed.), *Climatic Changes in Arctic Areas during the last ten thousand years*. Oulou: University of Oulou, pp. 357-407.

Hill, M.O. (1979) *TWINSPAN - a FORTRAN program for detrended correspondence analysis and reciprocal averaging*. Ithaca, New York: Section of Ecology and Systematics, Cornell University.

Hill, M.O., Gauch, H.G. (1980) Detrended correspondence analysis, an improved ordination technique. *Vegetatio* **42**: 47-58.

Hillaire-Marcel, C., de Vernal, A., Bilodeau, G., Weaver, A.J. (2001) Absence of deep-water formation in the Labrador Sea during the last interglacial period. *Nature* **410**: 1073-1077.

Hillaire-Marcel, C., de Vernal, A., Piper, D.J.W. (2007) Lake Agassiz final drainage event in the northwest North Atlantic. *Geophysical Research Letters* **34**: L15601, doi: 10.1029/2007GL030396.

Hjort, C., Funder, S. (1974) The subfossil occurrence of *Mytilus edulis* L. in central East Greenland. *Boreas* **3**: 23-33.

Hobbs III, C.H. (1983) A method for determining the dry bulk density of subaqueous sediments. *Journal of Sedimentary Research* **53**: 663-665.

Holland, D.M., Thomas, R.H., de Young, B., Ribergaard, M.H., Lybeth, B. (2008) Acceleration of Jakobshavn Isbræ triggered by warm subsurface ocean waters. *Nature Geoscience* **1**: 659-664.

Holliday, N.P., Hughes, S.L., Bacon, S., Beszczynska-Möller, A., Hansen, B., Lavín, A., Loeng, H., Mork, K.A., Østerhus, S., Sherwin, T., Walczowski, W. (2008) Reversal of the 1960s to 1990s freshening trend in the northeast North Atlantic and Nordic Seas. *Geophysical Research Letters* **35**: L03614, doi: 10.1029/2007GL032675

Howat, I.M., Joughin, I., Tulaczyk, S., Gogineni, S. (2005) Rapid retreat and acceleration of Helheim Glacier, east Greenland. *Geophysical Research Letters* **32**: L22502, doi: 10.1029/2005GL024737.

Howat, I.M., Joughin, I., Scambos, T.A. (2007) Rapid changes in ice discharge from Greenland outlet glaciers. *Science* **315**: 1559-1561.

Howat, I.M., Joughin, I., Fahnestock, M., Smith, B.E., Scambos, T.A. (2008) Synchronous retreat and acceleration of southeast Greenland glaciers 2000-06: ice dynamics and coupling to climate. *Journal of Glaciology* **54**: 646-660.

Hughes, T. (1986) The Jakobshavn Effect. *Geophysical Research Letters* **13**: 46-48.

Hughes, T.J. (1992) On the pulling power of ice streams. *Journal of Glaciology* **38**: 125-151.

Hughes, T. (2002) Calving bays. *Quaternary Science Reviews* **21**: 267-282.

Hulbe, C.L., Fahnestock, M.A. (2004) West Antarctic ice-stream discharge variability: mechanism, controls and pattern of grounding-line retreat *Journal of Glaciology* **50**: 471-484.

Hunt, A.S., Corliss, B.H. (1993) Distribution and microhabitats of living (stained) bethic foraminifera from the Canadian Arctic Archipelago. *Marine Micropaleontology* **20**: 321-345.

Huntingdon, H., Weller, G. (2004) An introduction to the Arctic Climate Impact Assessment. In: Corell, R. (ed.), *Impacts of a warming climate: Arctic Climate Impact Assessment*. New York, USA: Cambridge University Press, pp. 1-20.

Hurrell, J.W. (1996) Influence of variations in extratropical wintertime teleconnections on Northern Hemisphere temperature. *Geophysical Research Letters* **23**: 665-668.

Hurrell, J.W., van Loon, H. (1997) Decadal variations in climate associated with the North Atlantic Oscillation. *Climatic Change* **36**: 301–326.

Husum, K., Hald, M. (2004) Modern foraminiferal distribution in the subarctic Malangen Fjord and adjoining shelf, northern Norway. *Journal of Foraminiferal Research* **34**: 34-48.

Ingólfsson, O., Frich, P., Funder, S., Humlum, O. (1990) Paleoclimatic implications of an early Holocene glacier advance on Disko Island, West Greenland. *Boreas* **19**: 297–311.

Ingram, R.G., Prinsenberg, S. (1998) Coastal oceanography of Hudson Bay and surrounding eastern Canadian Arctic waters. In: Robinson, A.R., Brink, K.H. (eds.), *The Sea.* New York: John Wiley & Sons Inc., pp. 835-861.

Ishman, S.E., Foley, K.M. (1996) Modern benthic foraminifer distribution in the Amerasian Basin, Arctic Ocean. *Micropaleontology* **42**: 206-220.

Ivanova, E.V. (2006) The Global Thermohaline Paleocirculation. Moscow: Scientific World, 320 pp. (in Russian). Cited in: Ivanova, E.V., Ovsepyan, E.A., Risebrobakken, B., *et al.* (2008) Downcore distribution of living calcareous foraminifera and stable isotopes in the Western Barents Sea. *The Journal of Foraminiferal Research* **38**: 337-356.

Ivanova, E.V., Ovsepyan, E.A., Risebrobakken, B., Vetrov, A.A. (2008) Downcore distribution of living calcareous foraminifera and stable isotopes in the Western Barents Sea. *The Journal of Foraminiferal Research* **38**: 337-356.

Jenkins, A., Vaughan, D.G., Jacobs, S.S., Hellmer, H.H., Keys, J.R. (1997) Glaciological and oceanographic evidence of high melt rates beneath Pine Island Glacier, West Antarctica. *Journal of Glaciology* **43**: 114-121.

Jennings, A.E. (1993) The Quaternary history of Cumberland Sound, southeastern Baffin Island: The marine evidence. *Géographie physique et Quaternaire* **47**: 21-42.

Jennings, A.E., Helgadottir, G. (1994) Foraminiferal assemblages from the fjords and shelf of Eastern Greenland. *Journal of Foraminiferal Research* **24**: 123-144.

Jennings, A.E., Weiner, N.W. (1996) Environmental change in eastern Greenland during the last 1300 years: evidence from foraminifera and lithofacies in Nansen Fjord, 68°N. *The Holocene* **6**: 179-191.

Jennings, A.E., Vilks, G., Deonarine, B., Silis, A., Weiner, N. (2001) Foraminiferal biostratigraphy and paleoceanography. *Bulletin of the Geological Survey of Canada* **566**: 127-146.

Jennings, A.E., Knudsen, K.L., Hald, M., Hansen, C.V., Andrews, J.T. (2002) A mid-Holocene shift in Arctic sea-ice variability on the East Greenland shelf. *The Holocene* **12**: 48-59.

Jennings, A.E., Weiner, N.J., Helgadottir, G., Andrews, J.T. (2004) Modern foraminiferal faunas of the southwestern to northern Iceland Shelf: Oceanographic and environmental controls. *Journal of Foraminiferal Research* **34**: 180-207.

Jennings, A.E., Hald, M., Smith, M., Andrews, J.T. (2006) Freshwater forcing from the Greenland Ice Sheet during the Younger Dryas: evidence from southeastern Greenland shelf cores. *Quaternary Science Reviews* **25**: 282-298.

Jennings, A.E., Moros, M., Kilfeather, A.A., Perner, K., Andrews, J., Walton, M., Ó Cofaigh, C. (2010) Holocene deglaciation and marine paleoenvironments at the SW entrance to Disko Bugt, West Greenland. *40th International Arctic Workshop*, Winter Park, Colorado, 10-12th March 2010. INSTAAR, University of Boulder at Colorado.

Jennings, A.E., Vilks, G., Deonaire, B., Silis, A., Weiner, N. (2001) Foraminiferal biostratigraphy and paleoceanography. *Bulletin of the Geological Survey of Canada* **566**: 127-146.

Jorissen, F.J., de Stigter, H.C., Widmark, J.G.V. (1995) A conceptual model explaining benthic foraminiferal microhabits. *Marine Micropaleontology* **26**: 3-15.

Joughin, I., Abdalati, W., Fahnestock, M. (2004) Large fluctuations in speed on Greenland's Jakobshavn Isbræ glacier. *Nature* **432**: 608-610.

Joughin, I., Das, S.B., King, M.A., Smith, B.E., Howat, I.M., Moon, T. (2008) Seasonal speedup along the western flank of the Greenland Ice Sheet. *Science* **320**: 781-783.

Juggins, S. (2007) *C2 Version 1.5 User guide. Software for ecological and palaeoecological data analysis and visualisation.* Newcastle upon Tyne, UK: Newcastle University.

Kaplan, M.R., Wolfe, A.P., Miller, G.H. (2002) Holocene environmental variability in southern Greenland inferred from lake sediments. *Quaternary Research* **58**: 149-159.

Katz, M.E., Katz, D.R., Wright, J.D., Miller, K.G., Pak, D.K., Shackleton, N.J., Thomas, E. (2003) Early Cenozoic benthic foraminiferal isotopes: Species reliability and interspecies correction factors. *Paleoceanography* **18**: 1024-1035.

Kaufman, D.S., Ager, T.A., Anderson, N.J., Anderson, P.M., Andrews, J.T., Bartlein, P.J., Brubaker, L.B., Coats, L.L., Cwynar, L.C., Duvall, M.L., Dyke, A.S., Edwards, M.E., Eisner, W.R., Gajewski, K., Geirsdóttir, A., Hu, F.S., Jennings, A.E., Kaplan, M.R., Kerwin, M.W., Lozhkin, A.V., MacDonald, G.M., Miller, G.H., Mock, C.J., Oswald, W.W., Otto-Bliesner, B.L., Porinchu, D.F., Rühland, K., Smol, J.P., Steig, E.J., Wolfe, B.B. (2004) Holocene thermal maximum in the western Arctic (0-180°W). *Quaternary Science Reviews* **23**: 529-560.

Kaufman, D.S., and Arctic Lakes 2k Project Members (2009) Recent warming reverses long-term Arctic cooling. *Science* **325**: 1236-1239.

Keigwin, L.D., Lehman, S.J. (1994) Deep circulation change linked to HEINRICH event 1 and Younger Dryas in a middepth North Atlantic core *Paleoceanography* **9** 185-194.

Keigwin, L.D., Sachs, J.P., Rosenthal, Y., Boyle, E.A. (2005) The 8200 year B.P. event in the slope water system, western subpolar North Atlantic. *Paleoceanaography* **20**: PA2003, doi: 10.1029/2004PA001074

Kelly, M. (1979) Comments on the implications of new radiocarbon dates from the Holsteinsborg region, central West Greenland. *Rapport Grønlands Geologiske Undersøgelse* **95**: 35-42.

Kelly, M. (1980) The status of the Neoglacial in western Greenland. *Rapport Grønlands Geologiske Undersøgelse* **96**: 24 pp.

Kelly, M. (1985) A review of the Quaternary geology of western Greenland. In: Andrews, J.T. (ed.), *Quaternary environments, Eastern Canadian Arctic, Baffin Bay and Western Greenland.* Boston: Allen and Unwin, pp. 461-501.

Kelly, M., Bennike, O. (1992) Quaternary geology of western and central North Greenland. *Grønlands Geologiske Undersøgelse Rapport* **153**: 1-34.

Kelly, M., Funder, S., Houmark-Nielsen, M., Knudsen, K.L., Kronborg, C., Landvik, J., Sorby, L. (1999) Quaternary glacial and marine environmental history of northwest Greenland: a review and reappraisal. *Quaternary Science Reviews* **18**: 373-392.

Kelly, M.A., Lowell, T.V. (2009) Fluctuations of local glaciers in Greenland during latest Pleistocene and Holocene time. *Quaternary Science Reviews* **28**: 2088-2106.

Kjær, K., Korsgaard, N.J. (2009) Spatial changes of lakes on the Greenland ice sheet. *Third International Conference and Workshop Arctic Palaeoclimate and its Extremes (APEX) – beyond the frontier*, Copenhagen, Denmark, 31st March-3rd April 2009. The Natural History Museum, University of Copenhagen.

Knudsen, K.L., Seidenkrantz, M-S. (1994) *Stainforthia feylingi* new species from arctic to subarctic environments, previously recorded as *Stainforthia schreibersiana* (Czjek). *Cushman Foundation Special Publication* **32**: 5-13.

Knudsen, K.L., Jiang, H., Jansen, E., Eiríksson, J., Heinemeier, J., Seidenkrantz, M.-S. (2004) Environmental changes off North Iceland during the deglaciation and the Holocene: foraminifera, diatoms and stable isotopes. *Marine Micropaleontology* **50**: 273-305.

Knudsen, K.L**.,** Søndergaard, M.K.B., Eiríksson, J., Jiang, H. (2008a) Holocene thermal maximum off North Iceland: Evidence from benthic and planktonic foraminifera in the 8600-5200 cal. year BP time slice. *Marine Micropaleontology* **67**: 120-142.

Knudsen, K.L., Stabell, B., Seidenkrantz, M.-S., Eiríksson, J., Blake Jr., W. (2008b) Deglacial and Holocene conditions in northernmost Baffin Bay: sediments, foraminifera, diatoms and stable isotopes. *Boreas* **37**: 346-376.

Korsun, S.A., Polyak, L.V. (1989) Distribution of benthic foraminiferal morphogroups in the Barents Sea. *Oceanology* **29**: 838–844.

Korsun, S., Hald, M. (1998) Modern benthic foraminifera off Novaya Zemlya tidewater glaciers, Russian Arctic. *Arctic and Alpine Research* **30**: 61-77.

Korsun, S., Hald, M. (2000) Seasonal dynamics of benthic foraminifera in a glacially fed fjord of Svalbard, European Arctic. *Journal of Foraminiferal Research* **30**: 251-271.

Kovach, W.L. (1995) Multivariate data analysis. In: Maddy, D., Brew, J.S. (eds.), *Statistical modelling of Quaternary science data, Technical Guide 5*. Cambridge: Quaternary Research Association.

Krabill, W., Frederick, E., Manizade, S., *et al.* (1999) Rapid thinning of parts of the southern Greenland Ice Sheet. *Science* **283**: 1522-1524.

Krabill, W., Abdalati, W., Frederick, E., Manizade, S., Martin, C., Sonntag, J., Swift, R., Thomas, R., Wright, W., Yungel, J. (2000) Greenland ice sheet: high-elevation balance and peripheral thinning. *Science* **289**: 428-430.

Krabill, W., Hanna, E., Huybrechts, P., Abdalati, W., Cappelen, J., Csatho, B., Frederick, E., Manizade, S., Martin, C., Sonntag, J., Swift, R., Thomas, R., Yungel, J. (2004) Greenland Ice Sheet: Increased coastal thinning. *Geophysical Research Letters* **31**: L24402, doi: 10.1029/2004GL021533.

Krauβ, N. (2009) *Paleoceanographic indication from selected short sediment cores, Disko Bugt area, West Greenland*. University of Greifswald, Germany. Diploma thesis. 59 pp.

Krawczyk, D., Witkowski, A., Moros, M., Lloyd, J., Kuijpers, A., Kierzek, A. (2010) Late-Holocene diatom-inferred reconstruction of temperature variations of the West Greenland Current from Disko Bugt, central West Greenland. *The Holocene* **20**: 659-666.

Kuhlbrodt, T., Griesel, A., Montoya, M., Levermann, A., Hofmann, M., Rahmstorf, S. (2007) On the driving processes of the Atlantic meridional overturning circulation. *Reviews of Geophysics* **45**: RG2001, doi: 10.1029/2004RG000166.

Kuijpers, A. Werner, F. (2007) Extremely deep draft iceberg scouring in the glacial North Atlantic. *Geo-Marine Letters* **27**: 383-389.

Kuijpers, A., Lloyd, J.M., Jensen, J.B., Endler, R., Moros, M., Park, L.A., Schulz, B., Gutfelt, J., Laier, T. (2001) Late Quaternary circulation changes and sedimentation in Disko Bugt and adjacent fjords, central West Greenland. *Geology of Greenland Survey Bulletin* **189**: 41-47.

Kuijpers, A., Dalhoff, F., Brandt, M.P., Hümbs, P., Schott, T., Zotova, A. (2007) Giant iceberg plow marks at more than 1 km water depth offshore West Greenland. *Marine Geology* **246**: 60-64.

Krog H., Tauber H. (1974) C-14 chronology of late- and post-glacial marine deposits in north Jutland. *Danmarks geologiske Undersøgelse, Årbog* **1973**: 93-105.

Lagoe, M.B. (1979) Recent benthic foraminiferal biofacies in the Arctic Ocean. *Micropaleontology* **25**: 214-224.

Lassen, S.J., Kuijpers, A., Kunzendorf, H., Hoffmann-Wieck, G., Mikkelsen, N., Konradi, P. (2004) Late-Holocene Atlantic bottom-water variability in Igaliku Fjord, South Greenland, reconstructed from foraminifera faunas. *The Holocene* **14**: 165-171.

Lazerte, B.D. (1983) Stable carbon isotope ratios: implications for the source of sediment carbon and for phytoplankton carbon assimilation in Lake Memphremagaog, Quebec. *Canadian Journal of Fisheries and Aquatic Sciences* **40**: 1658-1666.

Lemke, P., Ren, J., Alley, R.B., Allison, I., Carrasco, J., Flato, G., Fujii, Y., Kaser, G., Mote, P., Thomas, R.H., Zhang, T. (2007) Observations: Changes in Snow, Ice and Frozen Ground. In: Solomon, S., Qin, D., Manning, M., Chen, Z., Marquis, M., Averyt, K.B., Tignor, M., Miller, H.L. (eds.), *Climate Change 2007: The Physical Science Basis. Contribution of Working Group I to the Fourth Assessment Report of the Intergovernmental Panel on Climate Change*. Cambridge, United Kingdom and New York, NY, USA: Cambridge University Press.

Lepš, J., Šmilauer, P. (2003) *Multivariate Analysis of Ecological Data Using CANOCO*. Cambridge: Cambridge University Press.

Levac, E., de Vernal, A., Blake, W.J. (2001) Sea-surface conditions in northernmost Baffin Bay during the Holocene: palynological evidence. *Journal of Quaternary Science* **16**: 353-363.

Leventer, A., Domack, E., Dunbar, R., Pike, J., Stickley, C. E., Maddison, E. J., Brachfeld, S.,Manley, P. and McClennen, C. (2006) Marine sediment record from the East Antarctic margin reveals reveals dynamics of ice sheet recession. *GSA Today* **16**: 4-10.

Lloyd, J. (2006a) Modern distribution of benthic foraminifera from Disko Bugt, West Greenland. *Journal of Foraminiferal Research* **36**: 315-331.

Lloyd, J.M. (2006b) Late Holocene environmental change in Disko Bugt, west Greenland: interaction between climate, ocean circulation and Jakobshavn Isbrae. *Boreas* **35**: 35-49.

Lloyd, J.M., Park, L.A., Kuijpers, A., Moros, M. (2005) Early Holocene palaeoceanography and deglacial chronology of Disko Bugt, West Greenland. *Quaternary Science Reviews* **24**: 1741-1755.

Lloyd, J.M., Kuijpers, A., Long, A., Moros, M., Park, L.A. (2007) Foraminiferal reconstruction of mid- to late-Holocene ocean circulation and climate variability in Disko Bugt, West Greenland. *The Holocene* **17**: 1079-1091.

Loizeau, J.L., Arbouille, D., Santiago, S., Vernet, J.-P. (2006) Evaluation of a wide range laser diffraction grain size analyser for use with sediments. *Sedimentology* **41**: 353-361.

Long, A.J., Roberts, D.H. (2002) A revised chronology for the 'Fjord Stade' moraine in Disko Bugt, west Greenland. *Journal of Quaternary Science* **17**: 561-579.

Long, A.J., Roberts, D.H. (2003) Late Weichselian deglacial history of Disko Bugt, West Greenland, and the dynamics of the Jakobshavns Isbrae ice stream. *Boreas* **32**: 208-226.

Long, A.J., Roberts, D.H., Dawson, S. (2006) Early Holocene history of the west Greenland Ice Sheet and the GH-8.2 event. *Quaternary Science Reviews* **25**: 904-922.

Long, A.J., Roberts, D.H., Rasch, M. (2003) New observations on the relative sea level and deglacial history of Greenland from Innaarsuit, Disko Bugt. *Quaternary Research* **60**: 162-171.

Long, A.J., Roberts, D.H., Wright, M.R. (1999) Isolation basin stratigraphy and Holocene relative sea-level change on Arveprinsen Ejland, Disko Bugt, West Greenland. *Journal of Quaternary Science* **14**: 323-345.

Lowe, J.J., Rasmussen, S.O., Björck, S., Hoek, W.Z., Steffensen, J.P., Walker, M.J.C., Yu, Z.C., and the INTIMATE group (2008) Synchronisation of palaeoenvironmental events in the North Atlantic region during the Last Termination: a revised protocol ecommended by the INTIMATE group. *Quaternary Science Reviews* **27**: 6-17.

Luckman, A., Murray, T., de Lange, R., Hanna, E. (2006) Rapid and synchronous ice-dynamic changes in East Greenland. *Geophysical Research Letters* **33**: L03503, doi: 10.1029/2005GL025428.

Luthcke, S.B., Zwally, H.J., Abdalati, W., Rowlands, D.D., Ray, R.D., Nerem, R.S., Lemoine, F.G., McCarthy, J.J., Chinn, D.S. (2006) Recent Greenland ice mass loss by drainage system from satellite gravity observations. *Science* **314**: 1286-1289.

MacEyeal, D.R. (1993) Binge/Purge Oscillations of the Laurentide Ice Sheet as a cause of the North Atlantic's Heinrich Events. *Paleoceanography* **8**: 775-784.

Macdonald, A.M., Wunsch, C. (1996) An estimate of global ocean circulation and heat fluxes. *Nature* **382**: 436-439.

Mackensen, A., Sejrup, H.P., Jansen, E. (1985) The distribution of living benthic foraminifera on the continental slope and rise off southwest Norway. *Marine Micropaleontology* **9**: 275-306.

Mackiewicz, N.E., Powell, R.D., Carlson, P.R., Molnia, B.F. (1984) Interlaminated ice-proximal glacimarine sediments at Muir Inlet, Alaska. *Marine Geology* **57**: 113-147.

Madsen, H.B., Knudsen, K.L. (1994) Recent foraminifera in shelf sediments of the Scoresby Sund fjord, East Greenland. *Boreas* **23**: 495-504.

McCorkle, D.C., Keigwin, L.D., Corliss, B.H., Emerson, S.R. (1990) The influence of microhabitats on the carbon isotopic composition of deep-sea benthic foraminifera. *Paleoceanography* **5**: 161-185.

McCorkle, D.C., Corliss, B.H., Farnham, C.A. (1997) Vertical distributions and stable isotopic compositions of live (stained) benthic foraminifera from the North Carolina and California continental margins. *Deep-Sea Research. Part 1. Oceanographic Research Papers* **44**: 983-1024.

Miller, G.H., Wolfe, A.P., Steig, E.J., Sauer, P.E., Kaplan, M.R., Briner, J.P. (2002) The Goldilocks dilemma: big ice, little ice, or “just-right” ice in the Eastern Canadian Arctic. *Quaternary Science Reviews* **21**: 33-48.

Moon, T., Joughin, I. (2008) Changes in ice front position on Greenland's outlet glaciers from 1992 to 2007. *Journal of Geophysical Research-Earth Surface* **113** F02022, doi: 10.1029/2007JF000927.

Moore Jr., T.C. (2005) The Younger Dryas: From whence the fresh water? *Paleoceanography* **20**: PA4021, doi: 10.1029/2005PA001170.

Mörner, N-A., Funder, S. (1990) C-14 dating of samples collected during the NORDQUA 86 expedition, and notes on the marine reservoir effect. In Funder, S. (Ed.) Late Quaternary stratigraphy and glaciology in the Thule area, Northwest Greenland. Meddelelser om Grønland, Geoscience **22**: 57-59.

Moros, M., Jensen, K.G., Kuijpers, A. (2006) Mid- to late-Holocene hydrological and climatic variability in Disko Bugt, central West Greenland. *The Holocene* **16**: 357-367.

Motyka, R.J., Hunter, L., Echelmeyer, K.A., Conner, C. (2003) Submarine melting at the terminus of a temperate tidewater glacier, LeConte Glacier, Alaska. *Annals of Glaciology* **36**:57-63.

Mudie, P.J., Aksu, A.E. (1984) Palaeoclimate of Baffin Bay from 300,000-year record of foraminifera, dinoflagellates and pollen. *Nature* **312**: 630-634.

Mudie, P.J., Keen, C.E., Hardy, I.A., Vilks, G. (1983) Multivariate analysis and quantitative paleoecology of benthic foraminifera in surface and Late Quaternary shelf sediments, northern Canada. *Marine Micropaleontology* **8**: 283-313.

Mudie, P.J., Rochon, A., Prins, M.A., Soenarjo, D., Troelstra, S.R., Levac, E., Scott, D.B., Roncaglia, L., Kuijpers, A. (2006) Late Pleistocene-Holocene marine geology of Nares Strait region: paleoceanography from foraminifera and dinoflagellate cysts, sedimentology and stable isotopes, *Polarforschung* **74**: 169-183.

Murray, J.W. (1991) *Ecology and Palaeoecology of Benthic Foraminifera*. Harlow: Longman Scientific and Technical, pp. 397.

Murray, J.W. (1992) Distribution and Population Dynamics of. Benthic Foraminifera from the Southern North Sea. *Journal of Foraminiferal Research* **22:** 114-128.

Murray, J.W., Alve, E. (1999a) Natural dissolution of modern shallow water benthic foraminifera: taphonomic effects on the palaeoecological record. *Palaeogeography, Palaeoclimatology, Palaeoecology* **146**: 195-209.

Murray, J.W., Alve, E. (1999b) Taphonomic experiments on marginal marine foraminiferal assemblages: how much ecological information is preserved? *Palaeogeography, Palaeoclimatology, Palaeoecology* **149**: 183-197.

Murray, J.W., Alve, E., Cundy, A. (2003) The origin of modern agglutinated foraminiferal assemblages: evidence from a stratified fjord. *Estuarine, Coastal and Shelf Science* **58**: 677-697.

Myers, P.G., Donnelly, C., Ribergaard, M.H. (2009) Structure and variability of the West Greenland Current in Summer derived from 6 repeat standard sections. *Progress in Oceanography* **80**: 93-112.

Mysak, L.A., Ingram, R.G., Wang, J., Van der Baaren, A. (1996) The anomalous sea-ice extent in Hudson Bay, Baffin Bay and the Labrador Sea during three simultaneous NAO and ENSO episodes. *Atmosphere and Ocean* **34**: 313-343.

Nagy, J. (1965) Foraminifera in some bottom samples from shallow waters in Vestspitsbergen. *Norsk Polarinstitut Arbok* **1963**: 109-125.

Nesje, A., Dahl, S.O., Bakke, J. (2004) Were abrupt Lateglacial and early-Holocene climatic changes in northwest Europe linked to freshwater outbursts to the North Atlantic and Arctic Oceans? *The Holocene* **14**: 299-310.

Nick, F.M., Vieli, A., Howat, I.M., Joughin, I. (2008) Large-scale changes in Greenland outlet glacier dynamics triggered at the terminus. *Nature Geoscience* **2**: 110-114.

Nielsen, T.G., Hansen, B.W. (1999) Plankton community structure and carbon cycling on the western coast of Greenland during the stratified summer situation. I. Hydrography, phytoplankton and bacterioplankton. *Aquatic Microbial Ecology* **16**: 205-216.

Nielsen, M.H., Erbs-Hansen, D.R., Knudsen, K.L. (2010) Water masses in Kangerlussuaq, a large fjord in West Greenland: the processes of formation and the associated foraminiferal fauna *Polar Research* **29***:* 159-175.

NorthGRIP Project Members (2004) High resolution climate record of the Northern Hemisphere into the last interglacial period. *Nature* **431**: 147-151.

O'Brien, S.R., Mayewski, P.A., Meeker, L.D., Meese, D.A., Twickler, M.S., Whitlow, S.I. (1995) Complexity of Holocene climate as reconstructed from a Greenland Ice Core. *Science* **270**: 1962-1964.

Ó Cofaigh, C., Dowdeswell, J.A. (2001) Laminated sediments in glacimarine environments: diagnostic criteria for their interpretation. *Quaternary Science Reviews* **20**: 1411-1436.

Ó Cofaigh, C., Taylor, J., Dowdeswell, J.A., Rosell-Melé, A., Kenyon, N.H., Evans, J., Mienert, J. (2002) Sediment reworking on high-latitude continental margins and its implications for palaeoceanographic studies: insights from the Norwegian-Greenland Sea. In: *Glacier-Influenced Sedimentation on High Latitude Continental Margins.* Dowdeswell, J.A. and Ó Cofaigh, C. (eds.) London: Geological Society, Special Publications **203**: 325-348.

Ó Cofaigh, C., Jennings, A.E., Moros, M., Andrews, J.T., Kilfeather, A., Dowdeswell, J.A., Richter, T. (2008) Long-term changes in the behaviour of Jakobshavns Isbrae, West Greenland during the late Quaternary-Holocene. [Abstract #C11B-0512]. *American Geophysical Union Fall Meeting*, San Francisco, USA, 15-19th December 2008.

Ó Cofaigh, C. (ed.) (2009) *Marine geophysical and geological investigations of past flow and stability and stability of a major Greenland ice stream in the late Quaternary*, RRS Cruise Report RRS James Clark Ross, Cruise JR175 West Greenland and Baffin Bay, pp. 26.

Oka, A., Hasumi, H., Okada, N., Sakamoto, T.T., Suzuki, T. (2006) Deep convection seesaw controlled by freshwater transport through the Denmark Strait. *Ocean modelling* **15**: 157-176.

Osterman, L.E., Nelson, A.R. (1989) Latest Quaternary and Holocene paleoceanography of the eastern Baffin island continental shelf, Canada: benthic foraminiferal evidence. *Canadian Journal of Earth Sciences* **26**: 2236-2248.

Overpeck, J.T., Otto-Bliesner, B.L., Miller, G.H.*,* Muhs, D.R., Alley, R.B., Kiehl, J.T. (2006) Paleoclimatic evidence for future ice-sheet instability and rapid sea-level rise. *Science* **311**: 1747-1750.

Park, L.A. (2003) *Late Quaternary Palaeoceanography in Disko Bugt, West Greenland. Unpublished PhD thesis,* University of Durham.

Parker, W.K., Jones, T.R. (1865) On some foraminifera from the North Atlantic and Arctic Oceans, including Davis Straits and Baffin's Bay. *Royal Society of London, Philosophical Transactions* **155**: 325-441.

Payne, A.J., Vieli, A., Shepherd, A.P., Wingham, D.J., Rignot, E. (2004) Recent dramatic thinning of largest West Antarctic ice stream triggered by oceans. *Geophysical Research Letters* **31**: L23401, doi: 10.1029/2004GL021284.

Pereira, C.P.G., Woodworth-Lynas, C.M.T., Barrie, J.V. (1988) Iceberg scour investigations and sedimentology of the southeast Baffin Island continental shelf. *Arctic* **41**: 221-230.

Peterson, B.J., McClelland, J., Curry, R., Holmes, R.M., Walsh, J.E., Aagaard, K. (2006) Trajectory shifts in the Arctic and Subarctic freshwater cycle. *Science* **313**: 1061-1066.

Phleger, F.B. (1960) Ecology and distribution of recent Foraminifera. Baltimore: John Hopkins Press. 297 pp.

Podlech, S., Weidick, A. (2004) A catastrophic break-up of the front of Jakobshavn Isbrae, West Greenland, 2002/03. *Journal of Glaciology* **50**: 153-154.

Polyak, L., Korsun, S., Febo, L.A., Stanovoy, V., Khusid, T., Hald, M., Paulsen, B.E., Lubinski, D.J. (2002) Benthic foraminiferal assemblages from the southern Kara Sea, a river-influenced arctic marine environment. *Journal of Foraminiferal Research* **32**: 252-273.

Prahl, F.G., Ertel, J.R., Goni, M.A., Sparrow, M.A., Eversmeyer, B. (1994) Terrestrial organic carbon contributions to sediments on the Washington margin. *Geochimica et Cosmochimica Acta* **58**: 3035-3048.

Rahmstorf, S. (2002) Ocean circulation and climate during the past 120,000 years. *Nature* **419**: 207-214.

Ramillien, G., Lombard, A., Cazenave, A., Ivins, E.R., Llubes, M., Remy, F., Biancale, R. (2006) Interannual variations of the mass balance of the Antarctica and Greenland ice sheets from GRACE. *Global and Planetary Change* **53**: 198-208.

Rasband, (2008) ImageJ, version 1.41 for Mac OSX. U.S. National Institutes for Health. Methesda, Maryland, U.S.: U.S. Department of Health and Human Sciences, Available from: http://rsb.info.nih.gov/ij

Rasch, M. (2000) Holocene relative sea level changes in Disko Bugt, West Greenland. *Journal of Coastal Research* **16**: 306-315.

Rasch, M., Jakobsen, B.H., Nielsen, N. (1997) Geomophology and sedimentary record of three cuspate forelands as indicators of late Holocene relative sea-level changes, Disko, West Greenland. *Geografisk Tidsskrift* **97**: 33-46.

Rasch, M., Jensen, J.F. (1997) Ancient Eskimo dwelling sites and Holocene relative sea-level changes in southern Disko Bugt, central West Greenland. *Polar Research* **16**: 101-115.

Rasch, M., Jensen, J. F. (1997) Ancient Eskimo dwelling sites and Holocene relative sea-level changes in southern Disko Bugt, central West Greenland. *Polar Research* **16**: 101-115.

Rasch, M., Nielsen, N. (1994) Holocene relative sea-level changes indicated by morphostratigraphic sequences; Sinigfik, Disko Island, West Greenland. *Danish Journal of Geography* **94**: 37-45.

Rasch, M., Nielsen, N. (1995) Coastal morpho-stratigraphy and Holocene relative sea level changes at Tuapaat, southeastern Disko Island, central West Greenland. *Polar Research* **14**: 277-289.

Rasmussen, S. O., Andersen, K.K., Svensson, A.M. *et al*. (2006) A new Greenland ice core chronology for the last glacial termination. *Journal of Geophysical Research* **111**: D06102, doi: 10.1029/2005JD006079.

Rasmussen, T.L., Thomsen, E., Slubowska, M.A., *et al.* (2007) Paleoceanographic evolution of the SW Svalbard margin (76°N) since 20 000 ^{14}C yr BP. *Quaternary Research* ***67***: 100-114.

Ravello, A.C., Hillaire-Marcel, C. (2007) The use of carbon and oxygen isotopes of foraminifera in paleoceanography. In: Hillaire-Marcel, C., de Vernal, A. (eds.) *Proxies in Late Cenozoic Paleoceanography*, Developments in Marine Geology 1. Amsterdam: Elsevier, pp. 735-764.

Reeh, N. (1985) Greenland ice sheet mass balance and sea level change. In: *Glaciers, Ice Sheets and Sea Level: Effect of a CO2-induced Climatic Change*. Washington D.C.: National Academy Press: U.S. Department of Energy Report, DOE/ER/60235-1, pp. 155-171.

Reeh, N. (1994) Calving from Greenland glaciers: observations, balance estimates of calving rates, calving laws. In: Reeh, N. (ed.), *Workshop on the Calving Rate of West Greenland Glaciers in Response to Climatic Change*. Copenhagen: Danish Polar Centre, pp. 85-102.

Reimer, P.J., Baillie, M.G.L., Bard, E., Bayliss, A., Beck, J.W., Blackwell, P.G., Ramsey, C.B., Buck, C.E., Burr, G.S., Edwards, R.L., Friedrich, M., Grootes, P.M., Guilderson, T.P., Hajdas, I., Heaton, T.J., Hogg, A.G., Hughen, K.A., Kaiser, K.F., Kromer, B., McCormac, F.G., Manning, S.W., Reimer, R.W., Richards, D.A., Southon, J.R., Talamo, S., Turney, C.S.M., van der Plicht, J., Weyhenmeyer, C.E. (2009) IntCal09 and Marine09 radiocarbon age calibration curves, 0-50,000 years cal BP. *Radiocarbon* **51**: 1111-1150.

Richter, T.O., Van der Gaast, S., Koster, B., Vaars, A., Gieles, R., de Stigter, H.C., De Haas, H., van Weering, T.C.E. (2006) The Avaatech XRF core scanner: technical description and applications to NE Atlantic sediments. In: Rothwell, R.G. (ed.), *New Techniques in Sediment Core Analysis.* London: Geological Society, pp. 39-50.

Rignot, E. (1998) Fast recession of a West Antarctic glacier. *Science* **281**: 549-551.

Rignot, E. (2001) Evidence for the rapid retreat and mass loss of Thwaites Glacier, West Antarctica. *Journal of Glaciology* **47**: 213-222.

Rignot, E., Jacobs, S.S. (2002) Rapid bottom melting widespread near Antarctic ice sheet grounding lines. *Science* **296**: 2020-2023.

Rignot, E., Kanagaratnam, P. (2006) Changes in the Velocity Structure of the Greenland Ice Sheet. *Science* **311**: 986-990.

Rignot, E., Vaughan, D.G., Schmeltz, M., Dupont, T., MacAyeal, D. (2002) Acceleration of Pine Island and Thwaites Glaciers, West Antarctica. *Annals of Glaciology* **34**: 189-194.

Rignot, E., Koppes, M., Velicogna, I. (2010) Rapid submarine melting of the calving faces of West Greenland glaciers. *Nature Geoscience* **3**: 187-191.

Rinterknecht, V., Gorokhovich, Y., Schaefer, J., Caffee, M. (2009) Preliminary ^{10}Be chronology for the last deglaciation of the western margin of the Greenland Ice Sheet. *Journal of Quaternary Science* **24**: 270-278.

Risum, J.B., Croxton, C.A., Rolle, F. (1980) Developments in petroleum exploration offshore West Greenland. *Rapport Grønlands Geologiske Undersøgelse* **100**: 55-58.

Robbins, J.A. (1978) Geochemical and geophysical applications of radioactive lead. In: *The Biogeochemistry of Lead in the Environment, Part A,* Nriagu, J.O. (ed.), Amsterdam; New York: Elsevier-North Holland Biomedical Press, pp. 285-393.

Roberts, D.H., Long, A.J. (2005) Streamlined bedrock terrain and fast ice flow, Jakobshavns Isbrae, West Greenland: implications for ice stream and ice sheet dynamics. *Boreas* **34**: 25-42.

Roberts, D.H., Long, A.J., Schnabel, C., Davies, B.J., Xu, S., Simpson, M.J.R., Huybrechts, P. (2009) Ice sheet extent and early deglacial history of the southwestern sector of the Greenland Ice Sheet. *Quaternary Science Reviews* **28**: 2760-2773.

Roberts, D.H., Long, A.J., Davies, B.J., Simpson, M.J.R., Schnabel, C. (2010) Ice stream influence on West Greenland Ice Sheet dynamics during the Last Glacial Maximum. *Journal of Quaternary Science* **25**: 850-864.

Rohling, E.J., Pälike, H. (2005) Centennial scale climate cooling with a sudden cold event around 8,200 years ago. *Nature* **434**: 975-979.

Rosenberg, R. (1979) Effect of oxygen deficiency on benthic macrofauna in fjords. In: Freeland, H.J., Farmer, D.M., Levings, C.D. (eds.), *Fjord Oceanography*. New York: Plenum Press, pp. 499-522.

Rothwell, R.G., Hoogakker, B., Thomson, J., Croudace, I.W., Frenz, M. (2006) Turbidite emplacement on the southern Balearic Abyssal Plain (western Mediterranean Sea) during Marine Isotope Stages 1-3: an application of ITRAX XRF scanning of sediment cores to lithostratigraphic analysis. In: Rothwell, R.G. (ed.), *New Techniques in Sediment Core Analysis*. London: Geological Society, pp. 79-98.

Ruddiman, W.F. (1977) Late Quaternary deposition of ice-rafted sand in the subpolar North Atlantic (lat 40° to 65°N). *Geological Society of America Bulletin* **88**: 1813-1827.

Rytter, F., Knudsen, K.L., Seidenkrantz, M.-S., Eiríksson, J. (2002) Modern distribution of benthic foraminifera on the north Icelandic shelf and slope. *Journal of Foraminiferal Research* **32**: 217-244.

Schafer, C.T. (1982) Foraminiferal colonization of an offshore dump site in Chaleur Bay, New Brunswick, Canada. *Journal of Foraminiferal Research* **12**: 317-326.

Schafer, C.T., Cole, F.E. (1974) Distribution of benthic foraminifera: Their use in delimiting local near shore environments. *Offshore geology of Canada, Eastern Canada. Geological Survey of Canada* **1**: 103-108.

Schafer, C.T., Cole, F.E. (1982) Living benthic foraminifera distributions on the continental slope and rise east of Newfoundland, Canada. *Geological Society of America* **93**: 207-217.

Schafer, C.T., Cole, F.E. (1986) Reconaissance survey of benthonic foraminifera from Baffin Fjord environments. *Arctic* **39**: 232-239.

Schafer, C.T., Cole, F.E. (1988) Environmental associations of Baffin Island Fjord agglutinated foraminifera. *Abhandlungen der Geologischen Bundesanstalt* **41**: 307-323. In: Rogl, F.,

Gradstein, F.M. (eds.) *Proceedings of a Workshop on Agglutinated Foraminifera*, Vienna, 1986.

Schlitzer, R. (2007) Ocean Data View, version 3.3.2. Bremerhaven, Germany: Alfred-Wegener-Institute for Polar and Marine Research (AWI). Available at: http://odv.awi.de.

Schröder-Adams, C.J., Cole, F.E., Medioli, F.S., Mudie, P.J., Scott, D.B., Dobbin, L. (1990a) Recent arctic shelf foraminifera: seasonally ice covered vs. perennially ice covered areas. *Journal of Foraminiferal Research* **20**: 8-36.

Schröder-Adams, C.J., Mudie, P.J., Cole, F.E., Medioli, F.S. (1990b) Late Holocene benthic foraminifera beneath perennial sea ice on an Arctic continental shelf. *Marine Geology* **93**: 225-242.

Scott, D.B., Vilks, G. (1991) Benthic foraminifera in the surface sediments of the deep-sea Arctic Ocean. *Journal of Foraminiferal Research* **21**: 20-38.

Scott, D.B., Mudie, P.J., Vilks, G., Younger, D.C. (1984) Latest Pleistocene-Holocene paleoceanographic trends on the continental margin of eastern Canada: foraminiferal, dinoflagellate, and pollen evidence. *Marine Micropaleontology* **8**: 181-218.

Scott, D.B., Mudie, P.J., de Vernal, A., Hillaire-Marcel, C., Baki, V., MacKinnon, K.D., Medioli, F.S., Mayer, L. (1989) *Lithostratigraphy, biostratigraphy and stable isotope stratigraphy of cores from ODP Leg 105 site surveys, Labrador Sea-Baffin Bay*. Initial Reports, ODP, **105** (Part B): 561-582.

Scourse, J.D., Hall, I.R., McCave, I.N., Young, J.R., Sugdon, C. (2000) The origin of Heinrich layers: Evidence from H2 for European precursor events. *Earth and Planetary Science Letters* **182**: 187-195.

Seidenkrantz, M.-S. (1995) *Cassidulina teretis* Tappan and *Cassidulina neoteretis* new species (Foraminifera): stratigraphic markers for deep sea and outer shelf areas. *Journal of Micropalaeontology* **14**: 145-157.

Seidenkrantz, M.-S., Roncaglia, L., Fischel, A., Heilmann-Clausen, C., Kuijpers, A., Moros, M. (2008) Variable North Atlantic climate seesaw patterns documented by a late Holocene marine record from Disko Bugt, West Greenland. *Marine Micropaleontology* **68**: 66-83.

Serreze, M.C., Francis, J.A. (2006) The Arctic amplification debate. *Climate Change* **76**: 241-264.

Severinghaus, J.P., Bender, M.L., Sowers, T., Brook, E.J., Alley, R.B. (1998) Timing of abrupt climate change at the end of the younger dryas interval from thermally fractionated gases in polar ice. *Nature* **391**: 141-146.

Shepherd, A., Wingham, D. (2007) Recent Sea-Level Contributions of the Antarctic and Greenland Ice Sheets. *Science* **315**: 1529-1532.

Shepherd, A., Wingham, D.J., Mansley, J.A.D., Corr, H.F.J. (2001) Inland thinning of Pine Island Glacier, West Antarctica. *Science* **291**: 862-864.

Shepherd, A., Wingham, D., Mansley, J.A. (2002) Inland thinning of the Amundsen Sea sector, West Antarctica. *Geophysical Research Letters* **29**: 1364, doi: 10.1029/2001GL014183.

Shepherd, A.P., Wingham, D.J., Rignot, E. (2004) Warm ocean is eroding West Antarctic Ice Sheet. *Geophysical Research Letters* **31**: L23402, doi: 10.1029/2004GL021106.

Shindell, D.T., Schmidt, G.A., Mann, M.E., Rind, D., Waple, A. (2001) Solar Forcing of Regional Climate Change During the Maunder Minimum. *Science* **294**: 2149-2152.

Símonarson, L.A. (1981) Upper Pleistocene and Holocene marine deposits and faunas on the north coast of Nûgssuaq, West Greenland. *Bulletin Grønlands Geologiske Undersøgelse* **140**: 107 pp.

Simpson, M.J.R., Milne, G.A., Huybrechts, P., Long, A.J. (2009) Calibrating a glaciological model of the Greenland ice sheet from the Last Glacial Maximum to present-day using field observations of relative sea level and ice extent. *Quaternary Science Reviews* **28**: 1631-1657.

Smith, E.H., Soule, F.M., Mosby, O. (1937) The "Marion" and "General Greene" Expeditions to Davis Strait and Labrador Sea; under the direction of the U.S. Coast Guard, 1928-1931-1933-1934-1935. Scientific results pt. 2: Physical Oceanography. *U.S. Treasury Department Coast Guard Bulletin* **19**. Cited in: Andersen, O.G.N. (1981a) The annual cycle of temperature, salinity, currents and water masses in Disko Bugt and adjacent waters, West Greenland. *Meddelelser om Grønland, Bioscience* **5**: 33 pp.

Sohn, H.G., Jezek, K.C., van der Veen, C.J. (1998) Jakobshavn Glacier, West Greenland: 30 years of space-borne observations. *Geophysical Research Letters* **25**: 2699-2702.

Sole, A., Payne, T., Bamber, J., Nienow, P., Krabill, W. (2008) Testing hypotheses of the cause of peripheral thinning of the Greenland Ice Sheet: is land-terminating ice thinning at anomalously high rates? *The Cryosphere* **2**: 205-218.

Solignac, S., Giraudeau, J., de Vernal, A. (2006) Holocene sea surface conditions in the western North Atlantic: Spatial and temporal heterogeneities. *Paleoceanography* **21**: PA2004, doi: 10.1029/2005PA001175.

Stefansson, U., Olafsson, J. (1991) Nutrients and fertility of Icelandic waters. *Rit Fiskideildar* **12**: 1-56.

Stein, M. (2005) North Atlantic Subpolar gyre warming-impacts on Greenland offshore waters. *Journal of Northwest Atlantic Fishery Science* **36**: 43-54.

Steinsund, P.I., Hald, M. (1994) Recent carbonate dissolution in the Barents Sea: Paleoceanographic applications. *Marine Geology* **117**: 303-316.

Stern, H.L., Heide-Jørgensen, M.P. (2003) Trends and variability of sea ice in Baffin Bay and Davis Strait, 1953–2001. *Polar Research* **22**: 11-18.

St-Onge, G., Mulder, T., Francus, P., Long, B. (2007) Continuous physical properties of cored marine sediments. In: Hillaire-Marcel, C., de Vernal, A. (eds.), *Proxies in Late Cenozoic Paleoceanography*. Amsterdam: Elsevier, pp. 63-98.

Straneo, F., Hamilton, G.S., Sutherland, D.A., Stearns, L.A., Davidson, F., Hammill, M.O., Stenson, G.B., Rosing-Asvid, A. (2010) Rapid circulation of warm subtropical waters in a major glacial fjord in East Greenland. *Nature Geoscience* **3**: 182-186.

Straneo, F. (2006) Heat and Freshwater Transport through the Central Labrador Sea. *Journal of Physical Oceanography* **36**: 606-620.

Sutherland, D., Pickart, R.S. (2008) The East Greenland Coastal Current: Structure, variability, and forcing. *Progress in Oceanography* **78**: 58-77.

Svensson, A., Andersen, K.K., Bigler, M., Clausen, H.B., Dahl-Jensen, D., Davies, S., Johnsen, S.J., Muscheler, R., Rasmussen, S.O., Röthlisberger, R., Steffensen, J.P., Vinther, B.M. (2006) The Greenland Ice Core Chronology 2005, 15-42 ka. Part 2: Comparison to other records. *Quaternary Science Reviews* **25**: 3258-3267.

Tang, C.C.L., Ross, C.K., Yao, T., Petrie, B., DeTracey, B.M., Dunlap, E. (2004) The circulation, water masses and sea-ice of Baffin Bay. *Progress in Oceanography* **63**: 183-228.

Tarasov, L., Peltier, W.R. (2002) Greenland glacial history and local geodynamic consequences. *Geophysical Journal International* **150**: 198-229.

Teller, J.T., Leverington, D.W., Mann, J.D. (2002) Freshwater outbursts to the oceans from glacial Lake Agassiz and their role in climate change during the last deglaciation. *Quaternary Science Reviews* **21**: 879-887.

Ten Brink, N.W. (1975) Holocene history of the Greenland Ice-Sheet based on radiocarbon-dated moraines in West-Greenland. *Grønlands Geologiske Undersøgelse Bulletin* **113**: 41-44.

Ten Brink, N.W., Weidick, A. (1974) Greenland Ice Sheet history since the last glaciation. *Quaternary Research* **4**: 429-440.

ter Braak, C.J.F. (1986) Canonical correspondence analysis: a new eigenvector technique for mulivariate direct gradient analysis. *Ecology* **67**: 1167-1179.

ter Braak, C.J.F. (1987) The analysis of vegetation-environment relationships by canonical correspondence analysis. *Vegetatio* **69**: 69-77.

ter Braak, C.J.F. (1988) Partial canonical correspondence analysis. In: Bock, H.H. (ed.), *Classification and related methods of data analysis*. Amsterdam: North-Holland, pp. 551-558.

ter Braak, C.J.F. (1990) Interpreting canonical correlation analysis through biplots of structural correlations and weights. *Psychometrika* **55**: 519-531.

ter Braak, C.J.F., Juggins, S. (1993) Weighted averaging partial least squares regression (WA-PLS): an improved method for reconstructing environmental variables from species assemblages. *Hydrobiologia* **269**: 485-502.

ter Braak, C.J.F., Juggins, S., Birks, H.J.B*., et al.* (1993) Weighted averaging partial least squares regression (WA-PLS): definition and comparison with other methods for species-environment calibration. In: Patil, G.P., Rao, C.R. (eds.), *Multivariate Environmental Statistics*. Amsterdam: North-Holland, pp. 525-560.

ter Braak, C.J.F., Šmilauer, P. (2002) *CANOCO Reference Manual and CanoDraw for Windows User's Guide: Software for Canonical Community Ordination (version 4.5)*. Ithaca, New York, USA: Microcomputer Power.

ter Braak, C.J.F., Verdonschot, P.F.M. (1995) Canonical correspondence analysis and related multivariate methods in aquatic ecology. *Aquatic Sciences* **57**: 256-289.

Thomas, E.R., Wolff, E.W., Mulvaney, R., Steffensen, J.P., Johnsen, S.J., Arrowsmith, C., White, J.W.C., Vaughan, B., Popp, T. (2007) The 8.2 ka event from Greenland ice cores. *Quaternary Science Reviews* **26**: 70-81.

Thomas, R.H. (2004) Force-perturbation analysis of recent thinning and acceleration of Jakobshavn Isbrae, Greenland. *Journal of Glaciology* **50**: 57-66.

Thomas, R.H., Abdalati, W., Akins, T.L., Csatho, B.M., Frederick, E.B., Gogineni, S.P., Krabill, W.B., Manizade, S.S., Rignot, E.J. (2000) Substantial thinning of a major east Greenland outlet glacier. *Geophysical Research Letters*. **27**: 1291-1294.

Thomas, R.H., Abdalati, W., Frederick, E., Krabill, W.B., Manizade, S., Steffen, K. (2003) Investigation of surface melting and dynamic thinning on Jakobshavn Isbrae, Greenland. *Journal of Glaciology* **49**: 231-239.

Thomas, R., Rignot, E., Casassa, G., Kanagaratnam, P., Acuna, C., Akins, T., Brecher, H., Frederick, E., Gogineni, P., Krabill, W., Manizade, S., Ramamoorthy, H., Rivera, A., Russell, R., Sonntag, J., Swift, R., Yungel, J., Zwally, J. (2004) Accelerated sea-level rise from West Antarctica. *Science* **306**: 255-258.

Thomas, R., Frederick, E., Krabill, W., Manizade, S., Martin, C. (2006) Progressive increase in ice loss from Greenland. *Geophysical Research Letters* **33**: L10503, doi: 10.1029/2006GL026075.

Thomas, R., Davis, C., Frederick, E., Krabill, W., Li, Y., Manizade, S., Martin, C. (2008) A comparison of Greenland ice-sheet volume changes derived from altimetry measurements. *Journal of glaciology* **54**: 203-212

Thomas, R., Frederick, E., Krabill, W., Manizade, S., Martin, C. (2009) Recent changes on Greenland outlet glaciers. *Journal of Glaciology* **55**: 147-162.

Thomson, R., Oldfield, F. (1986) *Environmental Magnetism*. London: Allen and Unwin, 227 pp.

Thornalley, D.J.R., Elderfield, H., McCave., I.N. (2009) Holocene oscillations in temperature and salinity of the surface subpolar North Atlantic. *Nature* **457**: 711-714.

Trenberth, K.E., Jones, P.D., *et al.* (2007) Observations: Surface and Atmospheric Climate Change. In: Solomon, S., D. Qin, M. Manning, Z., *et al.* (eds.), *Climate Change 2007: The Physical Science Basis. Contribution of Working Group I to the Fourth Assessment Report of the Intergovernmental Panel on Climate Change*. Cambridge: Cambridge University Press.

Trouet, V., Esper, J., Graham, N.E., Baker, A., Scourse, J.D., Frank, D.C. (2009) Persistent positive North Atlantic Oscillation Mode dominated the Medieval Climate Anomaly. *Science* **324**: 78-80.

Uehara, K., Scourse, J.D., Horsburgh, K.J., Lambeck, K., Purcell, A.P. (2006) Tidal evolution of the northwest European shelf seas from the Last Glacial Maximum to the present. *Journal of Geophysical Research* **111**: C09025, doi: 09010.01029/02006JC003531

Ullrich, A.D., Cowan, E.A., Zellers, S.D., Jaeger, J.M., Powell, R.D. (2009) Intra-annual variability inbenthic foraminiferal abundance in sediments of Disenchantment Bay, an Alaskan Glacial Fjord. *Arctic, Antarctic and Alpine Research* **41**: 257-271.

Urey, H.C. (1947) The thermodynamic properties of isotopic substances. *Journal of the Chemistry Society* **1947**: 562-581.

Valeur, H.H., Hansen, C., Hansen, K.Q., Rasmussen, L., Thingvad, N. (1996) *Weather, sea and ice conditions in eastern Baffin Bay, offshore Northwest Greenland. A review*. Copenhagen: DMI, 36 pp.

Valeur, H.H., Hansen, C., Hansen, K.Q., Rasmussen, L., Thingvad, N. (1998) *Physical environment of eastern David Stait and northeastern Labrador Sea, Parts 1 and 2*. Copenhagen, Denmark.

Van der Zwaan, G.J., Duijnstee, I.A.P., den Dulk, M., Ernst, S.R., Jannink, N.T., Kouwenhoven, T.J. (1999) Benthic foraminifers: proxies or problems? A review of paleoecological concepts. *Earth Science Reviews* **46**: 213-236.

Van Tatenhove, F.G.M., Van der Meer, J.J.M., Koster, E.A. (1996) Implications for deglaciation chronology from new AMS age determinations in central West Greenland. *Quaternary Research* **45**: 245-253.

Vaughan, D.G., Spouge, J.R. (2002) Risk estimation of collapse of the West Antarctica Ice Sheet. *Climatic Change* **52**: 65-91.

Velicogna, I., Wahr, J. (2005) Greenland mass balance from GRACE. *Geophysical Research Letters* **32**: L18505, doi: 10.1029/2005gl023955.

Velicogna, I., Wahr, J. (2006) Acceleration of Greenland ice mass loss in spring 2004. *Nature* **443**: 329-331.

Vilks, G. (1969) Recent foraminifera from the Canadian Arctic. *Micropaleontology* **15**: 35-60.

Vilks, G. (1980) Postglacial basin sedimentation on the Labrador Shelf. *Geological Society of Canada*, Paper 78**-**28.

Vilks, G. (1989) Ecology of recent Foraminifera on the Canadian continental shelf of the Arctic Ocean. *The Arctic Seas*, pp. 497-569.

Vilks, G., Deonarine, B., Wagner, F.J., Winters, G.V. (1982) Foraminifera and mollusca in surface sediments of the southeastern Labrador Shelf and Lake Melville, Canada. *Geological Society of America Bulletin* **93**: 225-238.

Vinther, B.M., Buchardt, S.L., Clausen, H.B., Dahl-Jensen, D., Johnsen, S.J., Fisher, D.A., Koerner, R.M., Raynaud, D., Lipenkov, V., Andersen, K.K., Blunier, T., Rasmussen, S.O., Steffensen, J.P., Svensson, A.M. (2009) Holocene thinning of the Greenland ice sheet. *Nature* **461**: 385-388.

Vinther, B.M., Clausen, H.B., Johnsen, S.J., Rasmussen, S.O., Andersen, K.K., Buchardt, S.L., Dahl-Jensen, D., Seierstad, I.K., Siggaard-Andersen, M.L., Steffensen, J.P., Olsen, J., Heinemeier, J. (2006) A synchronized dating of three Greenland ice cores throughout the Holocene. *Journal of Geophysical Research-Atmospheres* **111**: D13102, doi: 10.1029/2005JD006921.

Walker, D.P., Brandon, M.A., Jenkins, A., Allen, J.T., Dowdeswell, J.A., Evans, J. (2007) Oceanic heat transport onto the Amundsen Sea shelf through a submarine glacial trough. *Geophysical Research Letters* **34**: L02602, doi:10.1029/2006GL028154.

Warren, C.R. (1991) Terminal environment, topographic control and fluctuations of West Greenland glaciers. *Boreas* **20**: 1-15.

Warren, C.R., Hulton, N.R.J. (1990) Topographic and glaciological controls on Holocene ice-sheet margin dynamics, central west Greenland. *Journal of Glaciology* **14**: 307-310.

Weaver, A.J., Bitz, C.M., Fanning, A.F., Holland, M.M. (1999) Thermohaline Circulation: High-latitude phenomena and the difference between the Pacific and Atlantic. *Annual Review of Earth and Planetary Sciences* **27**: 231-285.

Weidick, A. (1963) Glacial variations in West Greenland in postglacial time. *Bulletin of the International Association of Scientific Hydrology* **8**: 75-82.

Weidick, A. (1968) Observations on some Holocene glacier fluctuations in West Greenland. *Meddelelser om Grønland* **165**: pp. 202.

Weidick, A. (1972a) Holocene shore-lines and glacial stages in Greenland; an attempt at correlation. *Rapport Grønlands Geologiske Undersøgelse* **41**: pp. 39.

Weidick, A. (1972b) Notes on Holocene glacial events in Greenland. In: Vasari, Y., Hyvärinen, H., Hicks, S. (eds.), *Climatic changes in Arctic areas during the last ten-thousand years*. Acta University of Oulu, Finland: A3 geol. 1, pp. 177-204.

Weidick, A. (1985) Review of glacier changes in West Greenland. *Zeitschrift fur Gletscherkunde und Glazialgeologie* **21**: 301-309.

Weidick, A. (1992) Jakobshavn Isbræ area during the climatic optimum. *Rapport Grønlands Geologiske Undersøgelse* **155**: 67-72.

Weidick, A. (1994) Fluctuations of West Greenland calving glaciers. In: Reeh, N. (ed.), *Report on the Workshop on the Calving Rate of West Greenland Glaciers in Response to Climate Change*. Danish Polar Center: University of Copenhagen, pp. 141-168.

Weidick, A. (1995) Greenland. In: Williams, R.S., Ferigno, J.G. (eds.), *Satellite Image Atlas of Glaciers of the World: Greenland*. U.S. Geological Survey Professional Paper 1386-C. United States Government Printing Office, Washington. 141 pp.

Weidick, A. (1996) Neoglacial Changes of Ice Cover and Sea Level in Greenland - a Classical Enigma. In: Grønnow, B. (ed.), *Palaeo-Eskimo Cultures of Greenland: New Perspectives in Greenlandic Archaeology*. Copenhagen: Danish Polar Center, University of Copenhagen, pp. 257–270.

Weidick, A., Bennike, O. (2007) Quaternary glaciation history and glaciology of Jakobshavn Isbræ and the Disko Bugt region, West Greenland: a review. *Geological Survey of Denmark and Greenland Bulletin* **14**: 78 pp.

Weidick, A., Oerter, H., Reeh, N., Thomsen, H.H., Thorning, L. (1990) The recession of the Inland Ice margin during the Holocene climatic optimum in the Jakobshavn Isfjord area of West Greenland. *Palaeogeography, Palaeoclimatology, Palaeoecology* **82**: 389-399.

Weidick, A., Mikkelsen, N., Mayer, C., Podlech, S. (2003) Jakobshavn Isbrae, West Greenland: the 2002-2003 collapse and nomination for the UNESCO World Heritage List. *Geological Survey of Denmark and Greenland Bulletin* **4**: 85-88.

Williams, L.D., Bradley, R.S. (1985) Paleoclimatology of the Baffin Bay Region. In: Andrews, J.T. (ed.), *Quaternary environments: Eastern Canadian Arctic, Baffin Bay, and western Greenland.* Boston: Allen and Unwin, pp. 741-772.

Wollenburg, J.E., Mackensen, A. (1998a) Living benthic foraminifers from the central Arctic Ocean: Faunal composition, standing stock and diversity. *Marine Micropaleontology* **34**: 153-185.

Wollenburg, J.E., Mackensen, A. (1998b) On the vertical distribution of living (Rose Bengal stained) benthic foraminifera in the Arctic Ocean. *Journal of Foraminiferal Research* **28**: 268-285.

Woodroffe, S.A. (2009) Recognising subtidal foraminiferal assemblages: implications for quantitative sea-level reconstructions using a foraminiferal-based transfer function. *Journal of Quaternary Science* **24**: 215-223.

Wu, G., Hillaire-Marcel, C. (1994) Accelerator mass spectrometry radiocarbon stratigraphies in deep Labrador Sea cores: paleoceanographic implications *Canadian Journal of Earth Sciences* **31**: 38-47.

Yashayaev, I., Lazier, J.R., Clarke, R. (2003) Temperature and salinity in the central Labrador Sea during the 1990s and in the context of the longer term change, *ICES Marine Science Symposia* **219**: 32-39.

Young, N.E., Briner, J.P., Stewart, H.A.M., Axford, Y., Csatho, B., Rood, D.H., Finkel, R.C. (2011) Response of Jakobshavn Isbræ, Greenland, to Holocene climate change. *Geology* **39**: 131-134.

Zarudzki, E.F.K. (1979) Interpretation of shallow seismic profiles over the continental shelf in West Greenland between latitudes 64 degrees and 69 degrees 30'N. *Rapport Grønlands Geologiske Undersøgelse* **100**: 58-61.

Zreda, M., England, J., Phillips, F., Elmore, D., Sharma, P. (1999) Unblocking of the Nares Strait by Greenland and Ellesmere ice-sheet retreat 10,000 years ago. *Nature* **398**: 139-142.

Zwally, H.J., Abdalati, W., Herring, T., Larson, K., Saba, J., Steffen, K. (2002) Surface melt-induced acceleration of Greenland Ice-Sheet flow. *Science* **297**: 218-222.

APPENDICES

Appendix 1

Table 1

Foraminifera taxonomic list

Agglutinated species

Adercotryma glomerata (Brady, 1878)
Ammodiscus gullmarensis (Höglund, 1947)
Ammotium spp.
Ammoscalaria pseudospiralis (Williamson, 1858)
Cribrostomoides crassimargo (Norman, 1892)
Cribrostomoides jeffreysi (Williamson, 1858)
Cuneata arctica (Brady, 1881)
Deuterammina lepida Brönnimann & Whittaker, 1986
Deuterammina grahami Brönnimann & Whittaker, 1988
Eggerella advena Cushman, 1922
Paratrochammina spp.
Globotrochammina spp.
Hormosinella spp.
Lagenammina arenulata (Skinner, 1961)
Pelosina spp.
Recurvoides turbinatus (Brady, 1881)
Reophax bilocularis Flint, 1899
Reophax dentaliniformis (Brady, 1881)
Reophax fusiformis (Williamson, 1858)
Reophax gracilis (Brady, 1881)
Reophax guttifer (Brady, 1881)
Reophax pilulifer Brady, 1884
Reophax subfusiformis Earland, 1933
Saccammina difflugiformis Brady, 1879
Saccammina spp.
Silicosigmoilina groenlandica (Cushman, 1933)
Spiroplectammina biformis (Parker and Jones, 1865)
Textularia earlandi Phleger, 1952
Textularia torquata Phleger, 1952
Trochammina globigeriniformis Parker and Jones, 1865
Trochammina ochracea (Williamson, 1858)
Trochammina nana (Brady, 1881)

Calcareous species

Astononion gallowayi Loeblich and Tappan, 1953
Bolivana pseudopunctata Höglund, 1947
Buccella frigida (Cushman, 1922)
Buccella tenerrima (Brady, 1950)
Buliminella spp.
Cassidulina laevigata d'Orbigny, 1826
Cassidulina neoteretis Tappan, 1951
Cassidulina obtusa Williamson, 1858
Cassidulina reniforme Nørvang, 1945
Cibicides lobatulus (Walker and Jacob, 1798)
Dentalina sp.
Elphidium excavatum (Terquem) f. *clavata* Cushman, 1944
Elphidium incertum (Williamson, 1858)
Elphidium spp.
Elphidium subarcticum Cushman, 1944
Fissurina spp.
Globulina sp.
Guttalina sp.
Haynesina orbiculare (Brady 1881)
Islandiella helanae Feyling-Hanssen and Buzas, 1976
Islandiella islandica (Nørvang, 1945)
Islandiella norcrossi (Cushman, 1933)
Lagena sp.
Melonis barleeanum (Williamson, 1858)
Miliolinella spp.
Nonionella auricula Herron-Allen and Earland, 1930
Nonionella turgida (Williamson, 1858)
Nonionella turgida var. digitata (Nørvang, 1945)
Nonionellina labradorica (Dawson, 1860)
Oolina sp.
Pullenia bulloides (d'Orbigny, 1846)
Pyrgo williamsoni (Silvestri, 1923)
Quinqueloculina sp.
Stainforthia concava Höglund, 1947
Stainforthia feylingi Knudsen and Seidenkrantz, 1994
Stetsonia horvathi Green, 1960
Trifarina fluens (Todd, 1947)
Triloculina sp.

Table 2

Foraminifera counts, MSM-343340_G

Sample number	Depth (cm)	Age (cal. yr BP)	*Adercotryma glomerata*	*Ammoscalaria pseudospiralis*	*Cribrostomoides crassimargo*	*Cribrostomoides jeffreysi*	*Cribrostomoides* sp.	*Cuneata arctica*	*Deuterammina lepida*	*Deuterammina grahami*	*Eggerella advena*	*Paratrochammina* spp.	*Recurvoides turbinatus*	*Reophax bilocularis*	*Reophax dentaliniformis*
1	1	40	62	3	2			97		12	2		12	5	1
2	33	1326	41	3	2	2		160	1		4		8	4	
3	65	3076	14	5	1	1		19		1			7	5	
4	97	5924	1	4		1	1	192			13		2	1	
5	129	8773	6	1	1	9		91			38	1	28		
6	161	8956				17		106			70	10	3		
7	193	9139	4			17		46			42	8	24		
8	225	9322	4		2	6		114			15	32	25		
9	257	9505	2				9	103			30		11		
10	289	9688					14	125			1	1	13		
11	321	9871	2				19	188					7		
12	353	10054	6		1		9	207					2		
13	373	10169	6		2			167				4	8		
14	377	10191	1		1	1		122				5	9		
15	385	10237	2				11	145				1	4		
16	417	10420					3	245							
17	449	10603						2							
18	481	10728					18	80					6		
19	513	10836					11	151				1	5		
20	545	10944					87	39				5	23		
21	577	11051					16	1							
22	609	11159					3						1		
23	641	11273													
24	673	11406													
25	705	11539	1				16	3				1			
26	737	11672					2								
27	745	11705													
28	769	11805					5	1							
29	801	11938						1							
30	833	12071					1								
31	865	12204													
32	897	12337													
33	929	12470													
34	951	12562					1								
35	961	12603													
36	993	12736													
37	1025	12869													
38	1057	13002													
39	1061	13019													
40	1073	13069													

Reophax fusiformis	*Reophax gracilis*	*Reophax pilulifer*	*Reophax* sp.	*Saccammina difflugiformis*	*Silicosigmoilina groenlandica*	*Spiroplectammina biformis*	*Textularia earlandi*	*Textularia torquata*	*Trochammina globigeriniformis*	*Trochammina ochracea*	*Trochammina nana*	Unidentified agglutinated sp.	*Astononion gallowayi*	*Bolivana pseudopunctata*	*Buccella frigida*
7	25	13		12	1	9	8	21	3	5	9				
4	19	6		8		16		17	1	5					
3	25	18		57	5	1	2	4		2	2				
	60	4	1	6	2	4		5			4				
	13					35		65							
	7					88		30							
	26			2		47		90			1				
	3					87		27							
	12					115		31							
	92					95		40							
	35					70		9			1				
	15					42		22			1				
	5				1	42		24			1	2	1	3	
	25					55	2	64			2	1			
	86					22		45		1	1				
	20			1		27		15							
						1									
	96					88		17							
	27	1				89		19							
	20					123		8		1					
	2					30		1					1	1	
						8				1				1	
						1									
	1					46		1				1	1		
						4									
						5	2					1			
						10									
	6														
	1					4									
	2				1								1		1
	24				1	8									
						2									
	3					39	9								
	3					22									

Buccella tenerrima	*Cassidulina reniforme*	*Cassidulina neoteretis*	*Cibicides lobatulus*	*Elphidium excavatum* f. *clavata*	*Elphidium* spp.	*Haynesina orbiculare*	*Islandiella helanae*	*Islandiella islandica*	*Islandiella norcrossi*	*Melonis barleeanum*	*Nonionellina labradorica*	*Pullenia bulloides*	*Quinqueloculina* sp.	*Stainforthia concava*	*Stainforthia feylingi*
				2					2		1				2
											1				1
	22		3	11	1		4		18	1	1	1		3	18
	1		5	7			3		12						1
									1						
				1											2
									4						
	15		1	17					7			2			274
1	22		1	22			5		42			2			194
	1														396
	2			1			1		5						385
	41	2	1	3	1		10	2	4				1		351
	41			3			1		26						246
	15			6			31								255
	19		4	16			1	4	17						142
	1														316
	13			1					3						86
	5		3	1				2	1						31
	83		1	12		1			18						
	42		1	23			6		3		1				190
	9								1						
	102		1				2		1						1
	22			2											2

Unidentified sp.	*N. pachyderma (s)*	Total	Test linings	Atlantic species	Intermediate species	Arctic species	Indifferent species	Agglutinated species	Calcareous species	% Agglutinated	Foraminifera concentration (sp./ml)
		309	50	52	0	114	143	309	0	100.0	74.9
		301	265	33	41	176	51	301	0	100.0	60.7
		172	315	95	14	22	41	172	0	100.0	31.3
		301	512	17	1	196	87	301	0	100.0	80.4
	1	295	61	30	6	132	127	288	7	97.6	75.1
		331	29	3	0	194	134	331	0	100.0	326.4
		309	133	27	4	94	184	307	2	99.4	154.0
		315	35	25	4	201	85	315	0	100.0	343.6
		313	12	11	2	218	82	313	0	100.0	385.2
		381	18	13	0	220	148	381	0	100.0	226.9
		331	27	7	2	258	64	331	0	100.0	181.2
		305	54	2	6	249	48	305	0	100.0	235.4
1	3	350	32	13	6	286	45	262	88	74.9	116.7
	5	317	17	9	1	203	104	288	29	90.9	74.0
		319	37	4	2	168	145	318	1	99.7	78.6
		311	12	1	0	272	38	311	0	100.0	67.1
		3	0	0	0	3	0	3	0	100.0	0.3
		305	19	6	0	168	131	305	0	100.0	124.4
		307	28	6	0	243	58	304	3	99.0	139.5
		310	35	23	0	166	121	306	4	98.7	204.2
		368	0	1	0	345	22	50	318	13.6	257.8
2		305	15	3	0	293	9	13	292	4.3	117.5
		398	0	0	0	398	0	1	397	0.3	679.9
		394	0	0	0	394	0	0	394	0.0	570.5
3	3	490	1	2	1	459	28	70	420	14.3	214.2
		323	12	0	0	321	2	6	317	1.9	58.5
		315	0	0	0	314	1	8	307	2.5	504.0
		219	1	0	0	206	13	16	203	7.3	22.3
		324	1	0	0	318	6	7	317	2.2	263.1
		109	0	0	0	107	2	6	103	5.5	8.9
		43	0	0	0	38	5	0	43	0.0	4.0
1		121	2	1	0	114	6	3	118	2.5	10.2
		0	0	0	0	0	0	0	0		0.0
1		301	0	1	0	272	28	34	267	11.3	100.3
		0	0	0	0	0	0	0	0		0.0
	1	12	0	0	0	12	0	2	10	16.7	1.2
		0	0	0	0	0	0	0	0		0.0
	1	158	0	0	0	154	4	51	107	32.3	14.9
	2	51	1	0	0	48	3	25	26	49.0	10.2
		0	0	0	0	0	0	0	0		0.0

Table 3

Foraminifera counts, MSM-343520_G

Sample number	Depth (cm)	Age (cal. yr BP)	*Adercotryma glomerata*	*Ammodiscus gullmarensis*	*Ammoscalaria pseudospiralis*	*Cribrostomoides crassimargo*	*Cribrostomoides jeffreysi*	*Cribrostomoides* sp.	*Cuneata arctica*	*Deuterammina lepida*	*Deuterammina grahami*	*Eggerella advena*	*Paratrochammina* sp.	*Recurvoides turbinatus*	*Reophax bilocularis*	*Reophax fusiformis*	*Reophax gracilis*	*Reophax guttifer*
1	1	18	12	2	6	9			59					1		12	3	5
2	5	91	29			1			6					5	2		5	
3	9	163	14	1		8		2	59	2		3	1	7	3	2	18	
4	17	309	35	1		1			12			2	2	3			9	
5	25	454	14			3			38		1	1		3			27	
6	29	526	9		1	2			58			3		12			101	
7	33	599	2		3	3			68			4	2	3			100	
8	41	744	2		2	9	1		45			2	2	6			25	
9	49	819	4		7	6			63					10			22	
10	57	893	22			4	2		41					12			20	
11	65	968	20			9			37			6		2	1		20	
12	73	1043	31		1	9	1		9			1		12		1	16	
13	81	1118	25	1		5	1	3	9			2		6		1	25	
14	89	1193	45				1	1	16			3		2		1	4	
15	97	1268	31	1		7			16			1		1			4	
16	105	1342	51			6		3	32	24		11		3		1	7	
17	113	1417	28	1	1	7	1		22	2				3			20	
18	121	1492	72		8	3	1	1	58	3		10		4	1		14	
19	129	1567	83	2	1	8			33	24	1	6		4	3	6	8	
20	137	1642	51	4	1	5	1		15	14	1	10		9			7	
21	145	1717	80		1	9			13			2		26			4	
22	153	1791	81	1	2	7			9			2		29	1		10	
23	157	1829	85	1	4	48	4		8			1		21	5	1	3	
24	161	1867	37	1		21	1		11			2		10	1	4	6	
25	165	1936	45		1	6	2		9			4		9	1		7	
26	169	2005	43			2	3		27			3		11	2	1	6	1
27	173	2074	42	1			1		10			2		1			17	
28	177	2144	23			6			15					11			8	
29	181	2213	49	1		6		4	29	1	1	3		3		1	16	2
30	185	2282	26			1	5		11			1		3	1	1	4	
31	189	2351	26			2		2	8	1				6			5	
32	193	2420	18			4			4			1		4	2			
33	197	2490	16			1								1			1	
34	201	2559	14			1			2	1				7				
35	205	2628	30						6			3		9	4		5	
36	209	2697	21			2		1	7			2		4	3		2	
37	213	2766	24			2			4			5		2	1		2	
38	217	2836	42	1					4			1		5	9		2	
39	221	2913	32			4			6			4		1	5		7	
40	225	2990	3						3			1	1	2	4		2	
41	229	3067	41			8			10			4		12	5		2	
42	233	3144	50			4	3		14			9		2	2		11	
43	237	3221	64			5		5	10	1		2		6	8	1		
44	241	3298	3			1			1					1			1	
45	245	3375	22											1	1		6	
46	249	3453	2			1			1					2			1	

Reophax pilulifer	*Reophax* sp.	*Saccammina difflugiformis*	*Silicosigmoilina groenlandica*	*Spiroplectammina biformis*	*Textularia earlandi*	*Textularia torquata*	*Trochammina globigeriniformis*	*Trochammina ochracea*	*Trochammina nana*	*Trochammina* sp.	Unidentified agglutinated sp.	*Astononion gallowayi*	*Bolivana pseudopunctata*	*Buccella frigida*	*Buccella tenerrima*	*Buliminella* sp.	*Cassidulina laevigata*	*Cassidulina obtusa*	*Cassidulina reniforme*	*Cassidulina neoteretis*
5	14	50		9	57	98		1	19	1	15		4							
		1		9	9	16			4										1	
5	2	37	1	20	26	43			4	7	1	4	6	2					4	
	2			17	4	26	1		7		1	1		1	1				3	
1		2		40	3	14	2		5		1		5		1				2	
				33		28			1					7	1				1	10
	1	1		35		23							1	12					9	
1	1			29		12							9	8	3				14	
2		1		27	1	12	1				1		17	11	2				18	
		1	1	24	4	17			2	1	1			8	2				10	
1	1	2	2	12	2	36			6			3	7	1					10	
1		2	2	13	2	18			11			4	10	2	3				23	
1				9	1	20			4			3	10	5	2				14	
5	1	1	3	10	1	25			15			2	4	4	2				18	
5		8	1	10	3	36			10			2	8	5	3				4	
10		16	1	17	8	58	3		33		1	1	6	3	3				1	
2		3	1	3		14	2		6			2	18	2	1			5	9	
6		6		27	1	24	3		6				9	7	2		2	1	4	
8		14		16	4	52	5		22		1	1	11	2					7	
		8		21	9	42	2	1	16		4	2	8	2	1			1	5	
1		3		13	1	25			12		1	2	7	1	2		1	2	25	
2		5	1	15	1	23			14			1	8	2	1		4		21	
		2		7	2	29		2	8				1	3	10				1	
1	1	1		9	1	13			5			9	6	5	8	1			23	
1	1	1		11	3	21			6			1	8	7	5				16	
	1			16	5	14						1		4	1				7	
				5	1	25			6					5						
1		2	1	10		11			3			2	6	9	12				32	
2	3	2		16	2	34			6						3				1	
		1		6		9			5											
	1	1		6	1	8			1											
		2		7		10			7					1					23	
3				4	1	6			1											
				2		1			2				2	1					6	
		1		3	1	4			4										14	2
		2		5	2	11			4				1						4	
		4	1	4	4	15		5	4	2					1				1	
	1	7		5	3	13		2	8			3	1		2				17	1
1		2		5		8		4	9			1			1				2	1
		1				7			1										5	
2		1		5	2	21		3	5						1					
2		2	1	7	2	27		2	6	2										
1	1	2		10	6	26	1		24		1				1					
				3		2													2	
						8			3											
1				1		3														

Cassidulina sp.	*Cibicides lobatulus*	*Dentalina* sp.	*Elphidium excavatum* f. *clavata*	*Elphidium subactum*	*Globulina* sp.	*Guttalina* sp.	*Haynesina orbiculare*	*Islandiella helenae*	*Islandiella islandica*	*Islandiella norcrossi*	*Lagena* sp.	*Melonis barleeanum*	*Miliolinella* sp.	*Nonionella turgida*	*Nonionellina labradorica*	*Pyrgo williamsoni*	*Quinqueloculina* sp.	*Stainforthia concava*
			1					7		1				1	3			1
			4					1		3					2			
			1					1		5								
			7					1		2					3			
			23					1			1				8			
			59		1			2							12			1
		1	73							10				1	22			
			52							14		2			23			1
	1		40		3					10					3			
			22					2		3					33			2
			35		2					15	2			2	21			
			41							10		2		3	37			4
			19							10	1	1		3	48			2
			13		2					21	1	1		3	45			6
			8		2					6		1		1	30			2
			33		4					15	1		1	2	38	1	1	2
	1		12							10					29			1
			9		1					17					27			
	1		12							5					11			1
			24					1		22	1				7			3
	1		20		2			1		17	2			1	13			10
4	1		12		1				2	20			1		38			3
	1		25					1		20				1	24		1	5
			18		3		2	1		14	4			1	16			5
2			13			1				6	2				9			5
4			3							5					1			1
2		1			25					23	1			1	15			8
			1	1				3			1				3		1	
			7							1					2			1
								2										
3			6		3			1		13	1			2	2			2
								2							1			
			2		1					9					5			3
			21		4					18	2			1	11			7
2			11					2		11	1				6			1
			6		2					6	1				8			3
	1		17				2			15	2				16			6
			10		1			1		15				1	24			1
6			3		1			2		7					1			
					1													
		2			2							2			1			
4								1		5					1			

Stainforthia feylingi	*Stetsonia horvathi*	*Trifarina fluens*	*Triloculina* sp.	Unidentified sp.	*N. pachyderma* (s)	Total	Test linings	Atlantic species	Intermediate species	Arctic species	Indifferent	Agglutinated specimens	Calcareous specimens	% Agglutinated	Foraminifera concentration (sp./ml)
						382	10	77	12	125	168	378	4	99	218
				2		104	4	6	29	35	34	87	17	84	22
3		1		1	6	297	14	58	14	124	101	266	31	90	104
				2		138	85	2	35	44	57	123	15	89	25
5				5	3	186	115	12	14	98	62	155	31	83	60
2				1		303	179	27	9	118	149	248	55	82	96
15				4	8	361	98	30	2	189	140	245	116	68	153
81				6	13	365	38	45	2	252	66	137	228	38	1008
18				2	7	317	76	65	4	194	54	157	160	50	157
6				7	6	242	142	17	22	135	68	152	90	63	77
24				3	30	267	152	45	20	117	85	157	110	59	105
12				10	6	271	122	43	31	113	84	130	141	48	131
14				15	16	273	202	58	25	105	85	113	160	41	297
18				1	21	267	131	66	45	96	60	134	133	50	119
8				4	3	260	67	77	31	83	69	134	126	52	262
13				8		370	100	72	51	88	159	285	85	77	470
35					23	286	130	69	28	121	68	116	170	41	1248
14				6	13	346	52	68	72	127	79	248	98	72	1990
5				9		390	88	73	83	92	142	301	89	77	382
19				17	4	306	71	31	51	89	135	221	85	72	283
7				12	21	308	68	22	80	111	95	191	117	62	215
35		1		9	133	352	122	37	81	130	104	203	149	58	253
				2	4	330	116	65	85	53	127	231	99	70	134
17					9	272	47	50	37	121	64	125	147	46	128
15				1	6	245	72	43	45	93	64	128	117	52	70
4				1	1	191	127	17	43	84	47	135	56	71	64
				2		132	107	6	42	25	59	111	21	84	48
50					5	278	45	70	23	140	45	91	187	33	108
1		1		13		210	248	12	49	53	96	181	29	86	92
				6		91	62	5	26	26	34	74	17	81	31
				3		73	33	1	26	17	29	68	5	93	21
1					9	117	20	9	18	57	33	59	58	50	27
				2		39	36	4	16	7	12	34	5	87	15
1				3	2	63	24	9	14	25	15	30	33	48	17
				1	13	151	107	22	30	70	29	70	81	46	52
1				8		114	42	12	21	44	37	66	48	58	31
				4	1	111	61	16	24	28	43	79	32	71	34
4				16	7	206	95	36	42	74	54	103	103	50	60
3				9	12	158	105	35	32	44	47	88	70	56	53
		1				51	22	8	3	20	20	25	26	49	15
1						124	81	10	41	18	55	121	3	98	41
				2		148	100	6	50	23	69	146	2	99	50
				14		196	100	18	64	26	88	174	22	89	59
				2		27	11	1	3	12	11	12	15	44	8
				16		57	41	1	22	0	34	41	16	72	20
						12	8	1	2	2	7	12	0	100	4

Sample number	Depth (cm)	Age (cal. yr BP)	*Adercotryma glomerata*	*Ammodiscus gullmarensis*	*Ammoscalaria pseudospiralis*	*Cribrostomoides crassimargo*	*Cribrostomoides jeffreysi*	*Cribrostomoides* sp.	*Cuneata arctica*	*Deuterammina lepida*	*Deuterammina grahami*	*Eggerella advena*	*Paratrochammina* sp.	*Recurvoides turbinatus*	*Reophax bilocularis*	*Reophax fusiformis*	*Reophax gracilis*	*Reophax guttifer*
47	253	3530	12			1		1	58			10		3			38	
48	257	3607	10			2			67			21		2			21	
49	261	3684	16			1		1	85			16		5			44	
50	265	3761	12		2	5			94			6		1			56	
51	269	3838	12		10	1		2	129			13		2			69	
52	273	3915	23		7	6	2		58			15	2	2	1		9	
53	277	3992	4		4				134			7					118	
54	281	4069	13		2	2			133			26		1		1	56	
55	289	4223	17		1	6	2		37	3		5		3			20	
56	293	4300	1		1	1			121			16		1			130	
57	297	4377	6			4			65			5		5			58	
58	301	4454	14						65			2		3			29	
59	305	4532	9		2	1			23					1			6	
60	309	4609	13		1				145			6		11	1		52	
61	313	4686	11			1		1	125			7		9	1		25	
62	315	4724			2	1			16			1		6	2		6	
63	317	4763	20		6	2		1	116	2		4		13	2		28	
64	321	4840	22		2	1	1		19	9	1	4	2	4	1		20	
65	323	4878			2				2						1		3	
66	325	4917	4		4	1			117			9		1			98	
67	329	4996	4		1	1			93			6		3			51	
68	333	5046	14		6			1	95			7		2	2	1	59	
69	337	5096	7			3		2	129			10		1			79	
70	341	5146	10		2				117			14					127	
71	343	5171	2		1				68			3		1			157	
72	345	5196	13			1			130			11		5			105	
73	349	5245	1		1	1			144			4					138	
74	353	5295	6		4	1			44			11		4			60	
75	357	5345	3		2				95			5					181	
76	361	5395	4		2	2		3	124			6		4			143	
77	365	5445	4		1	1			115			13					145	
78	369	5495	2		1				63			7		3	4		45	
79	373	5545	2						153			6		2			147	
80	377	5595	3		10	1			89			8		3			195	
81	381	5645	1		2	1			95			7		1			172	
82	385	5695	1			1			60			12		3			114	
83	389	5745							94			2		3			202	
84	393	5795	2		1			1	137			4		6			117	
85	397	5845	1		2				137			5					160	
86	401	5895	2		2				35			3		6			57	
87	405	5945	1					1	96			2		3			168	
88	409	5995	2		2			2	80			4					206	
89	413	6044	5		3			1	101					1			159	
90	417	6094	1		3				35					1			62	
91	421	6144	8		3		2	1	95			3		5	1		134	
92	425	6194	1		4			1	119			7		8			111	

Reophax pilulifer	*Reophax* sp.	*Saccammina difflugiformis*	*Silicosigmoilina groenlandica*	*Spiroplectammina biformis*	*Textularia earlandi*	*Textularia torquata*	*Trochammina globigeriniformis*	*Trochammina ochracea*	*Trochammina nana*	*Trochammina* sp.	Unidentified agglutinated sp.	*Astononion gallowayi*	*Bolivan pseudopunctata*	*Buccella frigida*	*Buccella tenerrima*	*Buliminella* sp.	*Cassidulina laevigata*	*Cassidulina obtusa*	*Cassidulina reniforme*	*Cassidulina neoteretis*
2				9		44														
				25		30								7	1				2	1
2				16		27			1									1		
		1		22		53			1											
				23		50														
				30		31			1					9						
				16	3	14														
				32	1	65			1						1					
2		1	3	14	1	13			2				2	5					2	
		1		11		18														
2	1			3	2	8														
1				6	2	13			3											
1		2		7		7								8	2					
		5		20	2	49														
		2	1	23	4	37			3		1			2						
		3	1	4		4							1	3	5				7	2
	1	9	1	29	4	38		1	2		2			2	1	6				
5	2	6	1	3	2	17			4				13	3						
		1	1			1							2	16	2				25	1
1				11		11			1					5						
2		3		12	5	28								5	1					
1				14	1	34					1									
		1		14		10			1											
		2		5	3	24														
				1		5								3						
				10		30		1	2											
				5		12														
				8		7			1				1	12	1				11	
				5		9			1											
				12		22														
				4	2	17														
		1		4		8								22					15	1
				5	1	20														
				5		17														
				2	2	17														
		2		7		20			1				1	3					1	
				5	3	15			1											
2				9	2	40														
				15	1	19														
1		6		8		3			1				1	4					6	
				12		16			1											
				13		14														
				17	1	15														
				11		2								2					13	1
		2		35	2	22			1							1				
1				27	1	33								1						

Cassidulina sp.	*Cibicides lobatulus*	*Dentalina* sp.	*Elphidium excavatum* f. *clavata*	*Elphidium subactum*	*Globulina* sp.	*Guttalina* sp.	*Haynesina orbiculare*	*Islandiella helanae*	*Islandiella islandica*	*Islandiella norcrossi*	*Lagena* sp.	*Melonis barleeanum*	*Miliolinella* sp.	*Nonionella turgida*	*Nonionellina labradorica*	*Pyrgo williamsoni*	*Quinqueloculina* sp.	*Stainforthia concava*
4			52							7					6			
															2			
		1	34		1					6					13			
															1			
1			38		1					20					10			1
			1												1			
			53							3					13			4
															1			
			112							34					22			4
2			25					4							2			
4			26							3					18			3
			152		5					32	1	4			29			6
			44					2							13			
2		1	71									3			7			1
			20					2							2			
			1							1								
		1	19												4			
			2															
			1				1											
			87		1		2			7					17			
	1		63		1		4			18					8			4
			7		1					14					11			
			1															
			91		1		2			22					25			1
															2			
			81				3			4				1	40			1
							1											
							4											

Stainforthia feylingi	*Stetsonia horvathi*	*Trifarina fluens*	*Triloculina* sp.	Unidentified sp.	*N. pachyderma (s)*	Total	Test linings	Atlantic species	Intermediate species	Arctic species	Indifferent	Agglutinated specimens	Calcareous specimens	% Agglutinated	Foraminifera concentration (sp./ml)
						178	259	2	12	67	97	178	0	100	87
					2	258	77	15	10	153	80	178	80	69	112
						215	276	2	16	101	96	214	1	100	98
						253	331	3	12	116	122	253	0	100	215
				1		314	227	12	12	152	138	311	3	99	252
						251	65	31	23	128	69	187	64	75	79
						300	277	4	4	153	139	300	0	100	231
						335	237	5	13	166	151	333	2	99	229
				10	1	220	147	22	17	113	68	130	90	59	73
				1		304	544	3	1	133	167	301	3	99	297
						159	816	2	6	70	81	159	0	100	163
						138	633	1	14	73	50	138	0	100	220
				9		151	144	28	9	90	24	59	92	39	59
1						307	1070	8	13	168	118	305	2	99	386
						253	760	5	11	152	85	251	2	99	203
13		3			5	252	52	43	0	190	19	46	206	18	182
5				6		334	557	22	20	183	109	281	53	84	178
						196	287	48	22	56	70	126	70	64	121
5		1				292	21	64	0	222	6	11	281	4	63
1				2		325	484	23	4	175	123	258	67	79	324
				3		303	459	22	4	182	95	209	94	69	152
				4		266	646	12	14	132	108	238	28	89	292
				1		260	757	1	7	145	107	257	3	99	156
						304	460	4	10	125	165	304	0	100	244
1						266	118	8	2	89	167	238	28	89	384
						310	676	0	13	142	155	308	2	99	197
						308	325	1	1	150	156	306	2	99	253
1				1	1	287	90	36	6	158	87	146	141	51	94
						301	348	2	3	100	196	301	0	100	325
						322	290	2	4	136	180	322	0	100	136
						302	296	1	4	121	176	302	0	100	419
1					1	276	80	38	2	168	68	138	138	50	178
						336	342	0	2	159	175	336	0	100	271
						331	276	10	3	94	224	331	0	100	162
1						301	169	2	1	100	198	300	1	100	226
3						262	118	18	1	92	151	221	41	84	190
						326	269	0	0	103	223	325	1	100	238
						321	291	3	2	148	168	321	0	100	306
				1		341	359	2	1	153	185	340	1	100	280
					2	277	114	40	2	163	72	124	153	45	196
						300	303	0	1	108	191	300	0	100	271
						323	234	2	2	93	226	323	0	100	390
				1		306	126	5	5	119	177	303	3	99	216
4					2	265	45	46	1	149	69	115	150	43	155
						316	108	6	8	132	170	314	2	99	170
						318	0	6	1	147	164	313	5	98	127

Sample number	Depth (cm)	Age (cal. yr BP)	*Adercotryma glomerata*	*Ammodiscus gullmarensis*	*Ammoscalaria pseudospiralis*	*Cribrostomoides crassimargo*	*Cribrostomoides jeffreysii*	*Cribrostomoides* sp.	*Cuneata arctica*	*Deuterammina lepida*	*Deuterammina grahami*	*Eggerella advena*	*Paratrochammina* sp.	*Recurvoides turbinatus*	*Reophax bilocularis*	*Reophax fusiformis*	*Reophax gracilis*	*Reophax guttifer*
93	429	6244	1		1				115			3					141	
94	433	6294	1		3				36			2		1			29	
95	437	6344	4			1			100			6	1	2			159	
96	441	6394	1		3				108			4		4			123	
97	445	6444	2			1			95			6	4				170	
98	449	6494	2		1				51			3		4			49	
99	453	6544	6		4				77			6		1			81	
100	457	6579	7		1	1			118			4		3			112	
101	461	6616	4						108			8	1	5			125	
102	465	6652	9		1				33			6					37	
103	469	6688	8			2			79			7	1	1			105	
104	473	6725	4						70			11	1	2			145	
105	477	6761	8		1				110			11		2			134	
106	481	6802	9						33			11		2			34	
107	485	6841	25		6	2			82			18	1	4			57	
108	489	6880	11		1	1			129			15	1				79	
109	493	6919	12		1	2			96			14		7			69	
110	497	6958	7		1	1			77			9		3			45	
111	501	6996	7						109			36					107	
112	505	7035	2						112			16					122	
113	509	7074	12			1		1	131			13	1	4			93	
114	513	7113	6		2	1	4		57			11	1	6			25	
115	517	7152	6		1	2			88			8	1	3			68	
116	521	7191						1	56			3	1				39	
117	525	7229			3		1	3	125			13		2			97	
118	529	7268	13		1		3		49			6		1			28	
119	533	7307	11	1		1			138			27		4			38	
120	537	7346	20						143			28		1	1		13	
121	541	7385	9						100			20		1			29	
122	545	7424	29				2		77			15		2		1	13	
123	549	7462	21						92			20		2	2	1	16	
124	553	7501	22						113	1		17			1	1	24	
125	557	7540	9						118			19		1	2		25	
126	561	7576	6				1		47			11					3	
127	565	7615	8	1					114			20	2				19	
128	569	7655	3						129			15	1	3	1		21	
129	573	7694	5						89			8			1		14	
130	577	7733	8	1			1		55			8					2	
131	581	7773	3				2		164			6					61	
132	585	7812	24			1	4		119			20		2		1	68	
133	589	7851	14		1				147			11		2			67	
134	593	7891	11			7	2		103			12		7			13	
135	597	7930	25		1		1		143			15	2	8			20	
136	601	7970	11			3	1		137			27	4	4			23	
137	605	8009	34			3	3		145			19	2	10		1	19	
138	609	8048	16			1	3		78			12	1	3			6	

Reophax pilulifer	*Reophax* sp.	*Saccammina difflugiformis*	*Silicosigmoilina groenlandica*	*Spiroplectammina biformis*	*Textularia earlandi*	*Textularia torquata*	*Trochammina globigeriniformis*	*Trochammina ochracea*	*Trochammina nana*	*Trochammina* sp.	Unidentified agglutinated sp.	*Astononion gallowayi*	*Bolivana pseudopunctata*	*Buccella frigida*	*Buccella tenerrima*	*Buliminella* sp.	*Cassidulina laevigata*	*Cassidulina obtusa*	*Cassidulina reniforme*	*Cassidulina neoteretis*
			1	16		30														
				10	1	28							10	7					18	
				17		33														
				20	2	41														
				7		27														
				7		13			2				6	2					6	
				4		18			1					2					1	
				7		32								2					1	
				5		34														
				9		17						1	6	1					31	
				17		33			1					5					1	
				17		28								4		2			1	
				8		24			1					1						1
				7		15						1	19	4					16	
				13		38								2		1				
				22		61														
				17		47										1				
				11		23							4						10	
				16	1	29			2							1				
				18		32														
				25	2	44			2											
				25	2	35			3				15	1	3				16	3
				14	1	24							6	3					10	2
				12		18							7	1					12	
				39		48										1				
1				13		34							6	3	2				15	
				22	7	64			2											
		2		37	11	62			3											
		1		47	8	50			1		1									
8		2	1	16	23	45		1	3				1	3					1	
4		1		8	36	72			4					3		1				
1		3		20	24	47			6											
2	1	2		11	36	72			12											
		6	1	6	7	25			4			4	18	6	3				35	2
1		3		10	10	41			2					1	1				1	
2		1		9	1	32			1					3					3	
3		3		16	8	31			2			1		2	1				10	
1				14		21			2			5	9	3	2				45	5
		3		8		34														
	1	4		17	2	55			1											
				26	2	44														
1		1		38	1	38							4		1				11	1
				48		48														
		1		59	7	46			3				1							
			1	46	1	32			5											
1		2	3	15	1	11			2			3	6		6				39	1

Cassidulina sp.	*Cibicides lobatulus*	*Dentalina* sp.	*Elphidium excavatum* f. *clavata*	*Elphidium subacticum*	*Globulina* sp.	*Guttalina* sp.	*Haynesina orbiculare*	*Islandiella helanae*	*Islandiella islandica*	*Islandiella norcrossi*	*Lagena* sp.	*Melonis barleeanum*	*Miliolinella* sp.	*Nonionella turgida*	*Nonionellina labradorica*	*Pyrgo williamsoni*	*Quinqueloculina* sp.	*Stainforthia concava*
			120				1		3	8					9			1
																	1	
			6												2		1	
			57				1			9					3			1
	1		108							10					15			1
			21				1	1		2					13			
			13							2					1		1	
			56							8					10			7
	1		59							1					3			
	1		33							1					4			1
			10												4			
	1		83			2				12					22			3
			42							14					19			1
			1												3			
			16												24			
			29							4					26			1
			29				1			3					12			1
			9							2					11			3
			22							2					35			1
			3															
			21							5					28			2
			11							6					19			1
			5					1		23					12			
			13							9					20			2
															1			
			25					1		21		1			23			4
	1		19				1	1		34	1	1			21			1
	1		18					2		29		3			23			3
	1	1	39					3		50					24			2
		1	65							54		1			37			3
			7							6					15			1
			4							2		1			2			1
	1		8							4					1			
			17							37					7			4
			1							1					2			
			5							7					1			1
																	1	
	3		30							52					5			1

Stainforthia feylingi	*Stetsonia horvathi*	*Trifarina fluens*	*Triloculina* sp.	Unidentified sp.	*N. pachyderma (s)*	Total	Test linings	Atlantic species	Intermediate species	Arctic species	Indifferent	Agglutinated specimens	Calcareous specimens	% Agglutinated	Foraminifera concentration (sp./ml)
				2		310	132	1	1	131	177	308	2	99	177
42				2	4	332	37	29	1	236	66	111	221	33	738
						324	204	0	4	117	203	323	1	100	176
						306	96	3	1	130	172	306	0	100	161
				1		322	198	2	2	108	210	312	10	97	243
57					3	274	44	12	2	188	72	132	142	48	795
				3		339	88	21	6	201	111	198	141	58	120
				4		330	106	16	7	150	157	285	45	86	105
1				7		315	85	1	4	129	181	290	25	92	200
102					3	334	32	18	9	247	60	112	222	34	183
1				7	1	332	107	8	8	158	158	254	78	77	263
				11	1	336	83	8	4	123	201	278	58	83	335
				2		317	143	7	8	128	174	299	18	94	184
55					20	329	18	45	9	210	65	111	218	34	260
1				17		343	36	27	25	153	138	246	97	72	152
5				1		330	133	4	11	157	158	320	10	97	370
1				11	1	318	104	25	12	130	151	265	53	83	253
67					4	318	26	31	7	199	81	177	141	56	258
3						311	111	0	7	129	175	307	4	99	338
						302	77	0	2	130	170	302	0	100	190
5						334	418	0	12	163	159	329	5	99	602
20					2	282	33	36	6	153	87	178	104	63	735
93				2		357	52	23	6	220	108	216	141	61	245
101				1	1	312	29	43	0	206	63	130	182	42	273
						335	78	3	0	167	165	331	4	99	248
116				2	6	349	30	41	13	221	74	149	200	43	227
						315	183	0	11	167	137	315	0	100	139
						321	245	3	20	191	107	321	0	100	170
		1		18	4	323	180	21	9	173	120	267	56	83	126
13				1	1	298	90	27	29	159	83	238	60	80	146
				48	3	375	76	31	21	160	163	279	96	74	150
				3		283	162	6	22	157	98	280	3	99	223
				13		324	177	7	9	165	143	310	14	96	140
40				5	2	305	31	59	6	190	50	117	188	38	504
8				57		379	77	28	8	198	145	231	148	61	182
19		1		26	1	350	63	34	3	213	100	219	131	63	165
13		1		25	1	353	34	35	5	231	82	180	173	51	232
40				1	9	384	14	58	8	281	37	113	271	29	299
				4	1	314	39	18	3	186	107	281	33	89	247
				5		334	85	8	24	145	157	319	15	96	156
				11		339	71	2	14	187	136	314	25	93	328
8					1	324	14	15	11	219	79	234	90	72	188
						315	52	3	25	193	94	311	4	99	161
				2		343	56	3	11	216	113	326	17	95	239
1						323	35	1	34	193	95	321	2	99	215
33				2	4	336	11	21	16	252	47	155	181	46	260

Sample number	Depth (cm)	Age (cal. yr BP)	*Adercotryma glomerata*	*Ammodiscus gullmarensis*	*Ammoscalaria pseudospiralis*	*Cribrostomoides crassimargo*	*Cribrostomoides jeffreysi*	*Cribrostomoides* sp.	*Cuneata arctica*	*Deuterammina lepida*	*Deuterammina grahami*	*Eggerella advena*	*Paratrochammina* sp.	*Recurvoides turbinatus*	*Reophax bilocularis*	*Reophax fusiformis*	*Reophax gracilis*	*Reophax guttifer*
139	613	8088					1		197			23	4	2			9	
140	617	8127							115			14	2	4			10	
141	621	8166				1	2	3	127			25	7	15			27	
142	625	8206				4	7		65			6		10		1	9	
143	629	8245					6		39			11	1	5			14	
144	633	8285					1		71			25		1			29	
145	637	8324	1				1		20			4		1			14	
146	641	8365	1				11		66			13		2			17	
147	645	8406				2	4		157			68	1	2			30	
148	649	8447					2		164			57		4			53	
149	653	8487					2		165			54	1	4			23	
150	657	8528					12		73			32		3			5	
151	661	8569					14		143			36		6			16	
152	665	8610				1	6		159			75	1	4			23	
153	669	8651				2	8		167			60	6	7			5	
154	673	8691					8		81			23		3			3	
155	677	8732					4		75			33	10	5			8	
156	681	8773					4		54			17	4	3			5	
157	685	8814					13		76			52	7	5			23	
158	689	8854					3		112			57	1	2			16	
159	693	8896					3		61			24	5				8	
160	697	8935							161			42	9	3			8	
161	701	8974				1	4		118			54	13	9			9	
162	705	9013			0	1	6		42			12		1			2	
163	709	9051				1			115			33	15	1			34	
164	713	9090					6		99			24		3			16	
165	717	9129							156			17	19	1			22	
166	721	9167					17		60			10		3				
167	725	9206					30		93			23					11	
168	729	9245							127			13	49	6			19	
169	733	9284							159			16	24	1			11	
170	737	9322					28		105			19		2			3	
171	741	9361							140			12	25	5			21	
172	745	9400					1		119			15	33	1			12	
173	749	9439					20		116			18		7			8	
174	753	9477				1	23		68			6		4		1		
175	757	9516				1			121			8	16	32			55	
176	761	9555							95			15	20	16			22	
177	765	9593				1			58			20	44	10			11	
178	769	9632				2	5		66			7	2	5			3	
179	773	9671							123			3	27	9			16	
180	777	9710							116				31	9			8	
181	781	9748							95				23	7			7	
182	785	9787				4	25		61			1	2	29				
183	789	9826				1	60		94					10			9	
184	793	9864					15		149					2			5	

Reophax pilulifer	*Reophax* sp.	*Saccammina difflugiformis*	*Silicosigmoilina groenlandica*	*Spiroplectammina biformis*	*Textularia earlandi*	*Textularia torquata*	*Trochammina globigeriniformis*	*Trochammina ochracea*	*Trochammina nana*	*Trochammina* sp.	Unidentified agglutinated sp.	*Astononion gallowayi*	*Bolivana pseudopunctata*	*Buccella frigida*	*Buccella tenerrima*	*Buliminella* sp.	*Cassidulina laevigata*	*Cassidulina obtusa*	*Cassidulina reniforme*	*Cassidulina neoteretis*
				33	1	31													4	
				25	1	23							6	6					34	
				73	1	29			1					1					4	
				47		12							4	2	1				63	
				25		18							2	1					40	
		1		25		17							2						20	
				14		7							6	1					61	
				35		9							4	1		5			50	2
				55		20														
				51		27														
				75		29														
				46		10							5			1			36	
				69		34														
				29		24														
				51	1	22														
			1	24		14							6	1					26	6
			1	32	1	10			1				6	2					31	
				26		5							1						6	
				44		17							3						4	
				63		26			1					1					1	
				26		4						1	4						36	1
				54	1														5	2
				54		26			1	3									3	
				36		8							3						36	
				81	5	22			2											
				83	3	28							2	1					16	
		1	4	43	4	19			1										4	
			2	91		15							3						38	
				128	4	23			1											
			1	63	1	35			1											
				77		32														
				57		10							1						11	
				84		29														
			1	74	2	47			1											
				95	1	38													8	
			1	60	2	25							1						76	4
				75		18														
				86	1	10													4	
				120		19			1										12	
				111		10													59	2
				96	2	13							1						21	
				102	1	8													25	
				67	2	11			1				3						72	
				93		26			2				1						15	1
				114		13			3										6	
				146	1	12														

Cassidulina sp.	*Cibicides lobatulus*	*Dentalina* sp.	*Elphidium excavatum* f. *clavata*	*Elphidium subacticum*	*Globulina* sp.	*Guttalina* sp.	*Haynesina orbiculare*	*Islandiella helanae*	*Islandiella islandica*	*Islandiella norcrossi*	*Lagena* sp.	*Melonis barleeanum*	*Miliolinella* sp.	*Nonionella turgida*	*Nonionellina labradorica*	*Pyrgo williamsoni*	*Quinqueloculina* sp.	*Stainforthia concava*
			8							3								
			15							3					1			
			3							3					1			
			41							3					3			
	1		56			1				3					2		1	
			14							1					1			
1	1		29			1		1		7					2			1
	2		17				1			20					3			1
																	3	
			1							1								
			12							2					1			
			1							5					7			
			10							17					1			
	1		14							15		1			4		1	
	1		3			2		1		1					1			
			1							2					4			1
			2							1					2			
	1		9					2		11					10			1
	1		7					1		2					6			
	1		13					1		3					1			
	1		16							4					1			
	1		2							4					1			1
			11							10					7			
	2		9							32					3			1
	1		12		1					10					3			
	1		8							6								
	1		4							16		1			1			1
	1		15				1			14					1			1
			5							1					1			
	2		45							6								
	1		5					1		4					1			
			13							11								
	1		19							7					2			1
	2		1							10								
	1		15							20					1			1
			6							5								
			1							6								

Stainforthia feylingi	*Stetsonia horvathi*	*Trifarina fluens*	*Triloculina* sp.	Unidentified sp.	*N. pachyderma (s)*	Total	Test linings	Atlantic species	Intermediate species	Arctic species	Indifferent	Agglutinated specimens	Calcareous specimens	% Agglutinated	Foraminifera concentration (sp./ml)
4				1	1	321	11	0	0	250	71	301	20	94	266
86					3	345	2	13	0	279	53	194	151	56	625
					2	323	26	2	0	211	110	311	12	96	349
92					3	370	10	11	0	311	48	161	209	44	1140
184				2	3	412	29	5	0	347	60	119	293	29	1411
265				1	7	474	8	4	0	396	74	170	304	36	2314
179				4	21	356	3	9	1	312	34	62	294	17	1795
76				1	1	337	11	10	1	265	61	154	183	46	696
						339	20	0	0	212	127	339	0	100	431
						361	29	0	0	215	146	358	3	99	546
						355	32	0	0	242	113	353	2	99	929
82					1	320	5	6	0	251	63	181	139	57	488
						318	10	0	0	212	106	318	0	100	112
						322	15	0	0	188	134	322	0	100	270
1				3		346	11	7	0	226	113	329	17	95	286
132					1	356	8	14	0	290	52	157	199	44	1092
119				4	6	378	5	13	0	287	78	180	198	48	613
338					2	472	4	2	0	429	41	118	354	25	2856
77						329	28	7	0	205	117	237	92	72	143
40						328	0	3	0	219	106	281	47	86	164
160					7	367	3	15	0	307	45	131	236	36	518
3				8		313	23	8	0	234	71	278	35	89	336
12				2		328	37	1	0	204	123	292	36	89	219
167					1	336	2	4	0	301	31	108	228	32	507
1				6		325	12	1	0	209	115	309	16	95	202
24				9	8	342	25	10	0	246	86	262	80	77	587
				10	2	348	15	4	0	249	95	287	61	82	363
41				1	2	308	12	7	0	252	49	198	110	64	560
				4		317	7	0	0	225	92	313	4	99	389
				7		322	31	0	0	191	131	315	7	98	177
				2		322	28	0	0	236	86	320	2	99	700
40						291	19	1	0	227	63	224	67	77	155
						316	26	0	0	224	92	316	0	100	274
				3		309	23	0	0	195	114	306	3	99	266
1				12	5	348	12	2	0	242	104	303	45	87	288
19					1	324	1	7	0	255	62	191	133	59	650
1				2	1	336	34	1	0	203	132	326	10	97	222
1				8	1	331	11	0	0	238	93	265	66	80	274
				11	3	319	10	1	0	200	118	284	35	89	197
18				3	5	317	2	2	0	278	37	211	106	67	638
					1	341	7	3	0	269	69	289	52	85	325
				2	1	315	1	0	0	255	60	275	40	87	253
6				8	5	340	6	4	0	278	58	213	127	63	208
9					2	280	3	2	0	189	89	243	37	87	425
					2	317	8	0	0	221	96	304	13	96	152
						330	0	0	0	296	34	330	0	100	231

Sample number	Depth (cm)	Age (cal. yr BP)	*Adercotryma glomerata*	*Ammodiscus gullmarensis*	*Ammoscalaria pseudospiralis*	*Cribrostomoides crassimargo*	*Cribrostomoides jeffreysi*	*Cribrostomoides* sp.	*Cuneata arctica*	*Deuterammina lepida*	*Deuterammina grahami*	*Eggerella advena*	*Paratrochammina* sp.	*Recurvoides turbinatus*	*Reophax bilocularis*	*Reophax fusiformis*	*Reophax gracilis*	*Reophax guttifer*
185	797	9903				1	12		127					6			16	
186	801	9942					17		113				1	2			2	
187	805	9981					6		158					13			2	
188	809	10019				5	4		171					8		1	19	
189	813	10058				2	11		135					13			9	
190	817	10097				1	7		116				1	14			8	
191	821	10136				1	5		171					4			8	
192	825	10174					9		216					2			16	
193	829	10213					9		107					4			7	
194	832.7	10249					13		143				1	4	0		8	
195	835.4	10275	1						134				4	6			4	
196	837	10290					2		54					1			2	
197	841	10329					1		64					7			10	
198	845	10368					1		146					2			16	
199	849	10407					4		134					6			20	
200	853	10445							58								28	
201	857	10484							16								12	
202	861	10523					1		25					1			4	
203	865	10561					3		91			1		4			47	
204	869	10600					14		72					6			17	
205	873	10639					1		13					1			2	
206	877	10678					2		57					7			55	
207	881	10716							2							2	1	
208	885	10755							1								2	
209	889	10794												12				
210	893	10833				4			5					6			6	
211	897	10871						1	8					4			2	
212	899	10891					12		1								1	
213	901	10910				2								3			1	
214	903	10929												2			2	
215	905	10949												6				
216	909	10987												2				
217	913	11026											2	3			2	
218	917	11065					3							1			4	
219	921	11104															3	
220	925	11142																
221	929	11181																
222	933	11220																
223	937	11258										1					2	
224	941	11297																
225	945	11336										2						
226	953	11413															1	
227	957	11452																
228	961	11491																
229	965	11530									3							
230	969	11568																

Reophax pilulifer	*Reophax* sp.	*Saccammina difflugiformis*	*Silicosigmoilina groenlandica*	*Spiroplectammina biformis*	*Textularia earlandi*	*Textularia torquata*	*Trochammina globigeriniformis*	*Trochammina ochracea*	*Trochammina nana*	*Trochammina* sp.	Unidentified agglutinated sp.	*Astononion gallowayi*	*Bolivana pseudopunctata*	*Buccella frigida*	*Buccella tenerrima*	*Buliminella* sp.	*Cassidulina laevigata*	*Cassidulina obtusa*	*Cassidulina reniforme*	*Cassidulina neoteretis*
				124	2	16							1	1					15	
				95	2	13							1						50	1
				25	4	23			6				2						36	
				43	11	12			5				1						21	
				74		18			1										33	
				69		14			3										32	1
				83	5	10			1				1						35	
				69	1	17													2	1
				53	3	12			4										1	
	1			42	2	7			5				1						29	1
				51		14			8					2		2			55	
				35	4	2			2										1	
				41	8	19								1					51	
				59	9	21			5				2	1					12	
				64	5	16			6										1	
				37	3	5			4											
				21	10	1			3											
				14	2	4														
				75	2	9			4										7	
				73	5	21														
				12		2							1							
				123	3	11														
				4							1	1				1			7	
				1																
	1	1	2	18		2			79		7								14	
		2		24	1				24	3	1		1						24	
1				21	1	1						1							60	5
				59	3	5			11										55	
			1	40	1				11											
		1		50		1	1		24										104	
		3		36	2				46		3		1						121	
	1			6					11										1	
				45	2	3			39		5								55	
		1		13	1	1			50		7									
3				9	1				1	1									3	
					1															
					1															
					2														5	
	2			4					1			1							21	5
				3	2															
				6	7							5							36	

Cassidulina sp.	*Cibicides lobatulus*	*Dentalina* sp.	*Elphidium excavatum* f. *clavata*	*Elphidium subacticum*	*Globulina* sp.	*Guttalina* sp.	*Haynesina orbiculare*	*Islandiella helanae*	*Islandiella islandica*	*Islandiella norcrossi*	*Lagena* sp.	*Melonis barleeanum*	*Miliolinella* sp.	*Nonionella turgida*	*Nonionellina labradorica*	*Pyrgo williamsoni*	*Quinqueloculina* sp.	*Stainforthia concava*
	1		2							4								
	1		3							32					1			
	1		5							46					1			2
	3		5							5								
			10							13								
			12							23								
			10							21								1
			2							4					2			
										3								
	2		10					2		23					1			
			7					1		30		2			8			2
	2		1				1			15					2			
	5		9							28								1
			15							9					1			2
			1															
												1			2			
			2							13								
			1															
										1								
			2							4	1							1
			1							5					4			
4			18							2						1		
2	1		49							14			1		3	3		1
13	1		113							29					6			
	1		23						4	14		1			3			
			18							9								1
1			32							15								2
			1							1			1					
	1		27							7								
			3							2								
			2							2								
			1							2								
1																		
2										1			43					
																	1	

Stainforthia feylingi	*Stetsonia horvathi*	*Trifarina fluens*	*Triloculina* sp.	Unidentified sp.	*N. pachyderma (s)*	Total	Test linings	Atlantic species	Intermediate species	Arctic species	Indifferent	Agglutinated specimens	Calcareous specimens	% Agglutinated	Foraminifera concentration (sp./ml)
2				7		337	1	2	0	276	59	304	33	90	270
14				2	5	350	8	3	0	309	38	245	105	70	448
10					7	340	8	3	0	286	51	237	103	70	162
4					3	318	11	2	0	260	56	279	39	88	154
4					3	323	10	0	0	269	54	263	60	81	104
6					1	307	7	1	0	258	48	233	74	76	314
9				1	2	366	5	1	0	335	30	288	78	79	148
						341	13	3	0	294	44	330	11	97	71
					2	203	14	0	0	167	36	199	4	98	43
				3	3	298	7	3	0	251	44	226	72	76	102
2					8	333	0	12	1	282	38	222	111	67	78
1				2	1	127	7	2	0	111	14	102	25	80	27
5				2	7	252	2	1	0	207	44	150	102	60	51
32					25	333	18	4	0	284	45	259	74	78	123
					2	256	28	0	0	204	52	255	1	100	71
				1		137	20	0	0	99	38	135	2	99	31
						63	11	0	0	47	16	63	0	100	15
				4		58	25	3	0	41	14	51	7	88	17
1					1	259	44	0	0	191	68	236	23	91	76
						208	32	0	0	150	58	208	0	100	48
1						34	8	1	0	27	6	31	3	91	8
2						261	12	0	0	186	75	258	3	99	55
7				3		37	8	2	0	28	7	10	27	27	11
						14	2	4	0	8	2	4	10	29	3
1				5	0	167	15	1	0	53	113	122	45	73	36
5				1	4	181	29	6	0	123	52	76	105	42	30
5				5	8	277	18	12	0	238	27	39	238	14	89
67					6	260	7	4	0	222	34	92	168	35	45
				3		62	17	0	0	41	21	59	3	95	16
70					5	283	8	1	0	252	30	81	202	29	36
35			1	1	0	305	4	4	0	243	58	96	209	31	124
2				2		28	0	0	0	11	17	20	8	71	6
73	5					269	8	0	0	209	60	101	168	38	55
						86	9	1	0	19	66	81	5	94	19
4				7		36	0	3	0	21	12	18	18	50	7
						3	0	0	0	3	0	0	3	0	1
												0			0
												0			0
						4	0	0	0	1	3	4	0	100	1
												0			0
						3	0	0	0	1	2	3	0	100	1
				3		12	0	0	0	7	5	3	9	25	2
												0			0
			5	31		116	0	0	0	54	1	7	109	6	
	8					17	0	0	0	5	12	8	9	47	3
				1		55	0	0	0	54	1	13	42	24	11

Table 4

Foraminifera counts, MSM-343520_MC

Sample number	Depth (cm)	Age (yr. A.D.)	*Adercotryma glomerata*	*Ammodiscus gullmarensis*	*Ammoscalaria pseudospiralis*	*Cribrostomoides crassimargo*	*Cribrostomoides jeffreysi*	*Cuneata arctica*	*Deuterammina lepida*	*Deuterammina grahami*	*Eggerella advena*	*Globotrochammina* sp.	*Hormosinella* sp.	*Lagenammina arenulata*	*Paratrochammina* sp.	*Pelosina* sp.	*Recurvoides turbinatus*	*Reophax bilocularis*	*Reophax fusiformis*
1	1	2000	41		5	12	1	35									1	21	27
2	2.5	1988	15	1	4	3		55		4	3		3	13			5	16	5
3	3.5	1980	29	2	8	3	1	64		3	6		8	15			2	27	6
4	4.5	1972	6		6			70		6	2		2	35		1	5	21	4
5	5.5	1964	38		16	14	1	75		16	2	3		5		2	7	10	15
6	6.5	1956	21	1	6	10	1	84		14	2			3			10	6	10
7	7.5	1948	26		12	13	2	95		12	5			16			12	5	7
8	8.5	1940	31		27	12	3	76		14	2			5			9	13	4
9	9.5	1931	39	1	10	10	2	125		22	2	13		7			13	10	13
10	10.5	1923	25	1	2	7	1	80		5	1	3		8		1	7	1	2
11	11.5	1915	27		3	12	1	62	1	6	1	8			1		5	5	6
12	12.5	1907	35	3		4	2	49		2	1	11		6		1	11	5	3
13	13.5	1899	22	2		4	3	42		1				1			3		1
14	14.5	1891	32				1	6			1						5		
15	15.5	1883	39	1	1	1		15			1			1		1	8		
16	16.5	1875	23		1			11							1		3		1
17	17.5	1866	24				3	9				1					3		1
18	18.5	1858	18	2			4	19		1	1						2		
19	19.5	1850	16				5	2									5		1
20	20.5	1842	22			2		4		1							4		
21	21.5	1834	18	1				4						1			2		1
22	22.5	1826	21	2				1									5		
23	23.5	1818	31	1	2	3	2	28		1	1						4		2
24	24.5	1810	29		9	4		24	1	13	1					1	8		4
25	25.5	1802	13	2	2	5		14	1	1							1		1
26	26.5	1793	26	1	2	3		71		10				6			7		3
27	27.5	1785	50	1		4	2	23	2	1	1			2	1		2		
28	28.5	1777	35			3	2	12									7		
29	29.5	1769	61	1	2	4	4	17									7		
30	30.5	1761	42	1		4	5	25									3		
31	31.5	1753	20			1	1	15									5		
32	32.5	1745	38			3	1	18									4		1
33	33.5	1737	30	1	9	5	6	46		1							8		1
34	34.5	1728	21		24	1		48	1	5	1						5		
35	35.5	1720	13		29	4		52		3							7		2
36	36.5	1712				2	1	4									3		
37	37.5	1704	16			1		1			2						9		
38	38.5	1696	5			1	2	2									3		
39	39.5	1688	29		1			11											
40	40.5	1680	13	3		4		13											
41	41.5	1672	31			11		4			1						5		
42	42.3	1666	11			2		5									2		

Reophax gracilis	*Reophax guttifer*	*Reophax pilulifer*	*Reophax sp.*	*Saccammina difflugiformis*	*Saccammina subfusiformis*	*Silicosigmoilina groenlandica*	*Spiroplectammina biformis*	*Textularia earlandi*	*Textularia torquata*	*Trochammina ochracea*	*Trochammina nana*	*Trochammina* sp.	*Astononion gallowayi*	*Bolivina pseudopunctata*	*Buccella frigida*	*Buccella tenerrima*	*Buliminella exilis*	*Cassidulina reniforme*	*Cassidulina neoteretis*
0	2	77		20		1	6	21	12		28			4	10	12			
3	2	37	1	35	6		11	20	71	7	15	4		5	1	5			
	5	34		33	3		26	27	65	5	20	3		9	1	8			
	10	17	2	4	2		7	13	34	5	5	5		6	4	2		1	
5	3	8	3	32	3	1	15	16	59	7	16	4		1	1	4		1	
1	3	18		23	3		19	19	60	6	13	2				1			
	5	15		25	8	1	27	13	49	4	17	6			4	1			
	3	15		32	1		10	29	50	5	15	5							
3	2	9	1	39	2	4	26	28	73	10	24	1			1				
3	4			13		3	21	19	75	5	20	1		1	1	2			
8	1	2		26		1	19	17	61	5	20	2			1	4			
4	1	7		13	1		22	19	48	1	20	2			2	2			
10		1		5			24	18	62	3	13	1		6	1			2	
2							11	12	23		6								
2		4		1			14	13	22	1	4								
8		2					18	6	20		4								
10		1		3			24	8	21		2			2	3			1	
5		2		3		1	17	8	24	1	6							1	
13		2		1			14	12	26		1			1	7		2	3	
11					1		8	6	24		1			1				4	
4		2				1	9	4	2		4					1			
				1	1		11	2	34		4				1		1		
5		1		5			17	8	58	1	6				1			1	
4		12		28	6		22	28	54	4	20	2							
1				2		1	13	2	41		6				1	1			
1		23		15	4		23	31	80	3	8				2	1			
1		1		3	1		28	7	49		4					1			
		3				2	13	7	14		5								
4		2		4			23	9	49		5	1							
7		2	1			1	42	5	34		10			1		1			
5		1		2		1	12	1	15		2								
6		6		1	1	1	14	2	23	1	6							1	1
7	5	6		16	1		18	3	22	1	13	2	1	2	2				
1		24		59	6		12	10	22	5	11		1	3		2		3	1
5	2	7		19	1		9	5	13		4	1		1	2			2	1
2							1				1				1			9	
5							3		8		1								
							5	1	9		2								
5				4			18		27	1	6				1				7
12		2			2		16	2	25		2								
12				1			6	1	5		1				2				14
6		4		1			9	1	10		4								3

Cassidulina sp.	*Cibicides lobatulus*	*Dentalina* sp.	*Elphidium excavatum* f. *clavata*	*Elphidium incertum*	*Globulina* sp.	*Haynesina orbiculare*	*Islandiella helanae*	*Islandiella norcrossi*	*Lagena* sp.	*Melonis barleeanum*	*Miliolinella* sp.	*Nonionella auricola*	*Nonionella turgida digitata*	*Nonionellina labradorica*	*Oolina* sp.	*Pullenia bulloides*	*Quinqueloculina* sp.	*Stainforthia concava*	*Stainforthia feylingi*	*Trifarina fluens*
		1	144	2					3	5		2		10	1	1		2	12	
	1	1	5						1	3			1	1					5	
			6										1	4					1	
		1	18			1				1			1	2					9	
			1										1	5					12	
			1		2									1						
					1														1	
			4							1				1						
							1			2										
			1		1	1				1										
			2																	
			2		1					2								1	3	
	1		2		1	1		2						3					7	1
								1												1
			1											3						
								3			1									
					1			5					1	2			1		1	
			2					2		1				2					7	
			1					9									1	1	7	
	1		2		1			3						2						
					1			5						1					1	
			1					5						2						
			2					8	1					1						
			3					2						2						1
								1		1				1						
			6															1	2	
		1	2															1	3	1
			2														1			
								1									2		1	
			2					2		1									4	
1			1																	
4		1	8					1												
			1					5	2	1				4					1	1
	1		3		1			2	1	2			1	1				4	5	1
1	1		6			1		5		1				1					1	1
			2				3	3											3	
								6											1	
							2				2									
	1		3		1			11	1					5					3	
								3											1	
			4					17						2						
			3					4						1				1		

Unidentified calcareous sp.	Corroded specimens	*N. pachyderma (s)*	Total	Test linings	Atlantic species	Intermediate species	Arctic species	Indifferent	Agglutinated	% Agglutinated	Foraminifera concentration (sp./ml)
			519	0	191	41	220	67	310	60	297
		1	368	1	131	15	96	126	339	92	327
2			427	4	148	29	124	126	395	93	214
1		2	309	9	104	6	118	81	262	85	309
			402	7	100	38	120	144	376	94	201
			340	2	73	21	123	123	335	99	272
	1		382	3	94	26	136	126	375	98	229
			367	0	99	31	119	118	361	98	367
1			494	7	93	39	180	182	489	99	198
			316	11	32	25	121	138	308	97	70
			307	4	47	27	100	133	300	98	68
2		2	286	10	42	35	96	113	271	95	57
1		1	244	27	20	22	97	105	216	89	49
			101	0	1	32	30	38	99	98	25
2	4		135	15	10	39	43	43	129	96	34
			102	3	4	23	38	37	98	96	26
		1	127	35	13	24	48	42	110	87	32
		1	129	35	8	18	56	47	114	88	32
		5	130	37	12	16	49	53	98	75	33
			98	32	5	22	27	44	84	86	25
			62	35	7	18	23	14	53	85	16
			92	10	5	21	20	46	82	89	23
			190	67	12	31	64	83	176	93	48
1			283	4	62	29	79	113	274	97	142
			111	46	9	13	30	59	106	95	28
			329	15	56	26	134	113	317	96	123
	1		192	23	9	50	64	69	183	95	48
	1		106	7	3	35	34	34	103	97	27
	2		197	28	8	61	51	77	193	98	49
2			195	45	5	42	80	68	182	93	49
			83	10	3	20	29	31	81	98	21
		1	142	11	10	38	44	50	126	89	36
		6	221	17	43	30	75	73	201	91	55
		27	288	9	124	21	88	55	256	89	432
		24	200	19	65	13	80	42	176	88	50
		2	35	21	1	0	25	9	14	40	9
2			55	22	0	16	11	28	46	84	14
2			36	5	0	5	10	21	30	83	9
			135	43	19	29	46	41	102	76	34
	4		98	59	4	13	35	46	94	96	25
7		1	124	21	19	31	32	42	78	63	31
			67	28	9	11	23	24	55	82	17

Table 5

Foraminifera counts, DA06-139G

Sample number	Depth (cm)	Age (cal. yrs BP)	*Adercotryma glomerata*	*Ammodiscus gullmarensis*	*Ammoscalaria pseudospiralis*	*Cribrostomoides crassimargo*	*Cribrostomoides jeffreysi*	*Cribrostomoides* sp.	*Cuneata arctica*	*Deuterammina lepida*	*Eggerella advena*	*Paratrochammina* spp.	*Recurvoides turbinatus*	*Reophax fusiformis*	*Reophax gracilis*	*Reophax guttifer*	*Reophax pilulifer*
1	1	9	10		3	2		17	81		7		9	2	41		
2	9	85	5		4	14	5	22	71		4		4	1	64		
3	17	161	1		2	8		16	102		7		16		34		
4	25	236	11		2	7	6	20	72	2	3		25		20		
5	33	304			4			6	114		4		8		30		
6	41	368			2	3		22	124		7		22		26	1	
7	49	432	1		5	4	1	1	124		5		14		18		
8	57	496	5		6	1	1	22	63		9		18		21	1	1
9	65	578				6		55	104	3	9				39		
10	73	666			4	1	1	14	136		6	2	11		29		
11	81	754	3		10	5	1	56	96		6	3	16		40		
12	89	842	8		8	4	1	18	85	1	9	8	19		45		
13	97	930	1		3		1	21	89		3		23		27		
14	105	1018	2	1	13	2	3	2	73		5		18		13		1
15	113	1106	6			13		50	64	1	14	1	12		55		
16	121	1194	2		1		9		148		6	2	21		23		
17	129	1282	5		10			14	94		9		20		45		
18	137	1345	6		14	1	13		76		3	1	35	1	9		
19	145	1365	7		8		1		112		6				45		
20	153	1386	1		4	1	12		140		1	11	37		9		
21	161	1407		1	8	7			145		9				28		
22	169	1428			4	3		27	103	1	9		4		14		
23	177	1448	4		5	8		24	113		5				26		
24	184	1499	5	1	7	4	1	8	132		6	1	24		8		
25	193	1596	24		18	15	1		105	1	7				43		
26	201	1680	29		18			7	84		6	1	13		29		
27	209	1754	15		10	2		9	105	1	9		9		98		
28	217	1829	26		10			8	60		4	2	8		10		1
29	225	1904	7		16	4		8	86		10	11	3		32		
30	233	1978	11		15	2		12	128		4	3	10		26		
31	241	2053		1	8	4		5	130		1	4	5		51		
32	249	2127	1		3	2		6	176		8	3	12		16		
33	257	2202			4			15	160		9		1		50		
34	273	2351			10	3		1	142	1	5	6	3		30		
35	281	2425	8		3	1			139		1		1	2	30		1
36	289	2500	2	1	6	1	1	20	135	1	6	5			68		
37	305	2659	10		3	3	1	5	44		3		2		9		
38	321	2894	8		5	2	6		68	1	7		4		36		
39	337	3128	3	1	3		9	2	154	1	8	2	1	1	83		
40	353	3363	2		2	1	4	13	96		2	2			41		
41	369	3597	1		3	1	3	12	175		2				26		
42	385	3832			1	1	2	9	132		9				21		
43	401	4167			3		3		63		8				10		
44	417	4527			2		1	1	116	1	9				43		
45	433	4888			1		1		88		11				58		
46	442.75	5108						2	99		2				14		

Reophax spp.	*Saccammina difflugiformis*	*Spiroplectammina biformis*	*Textularia earlandi*	*Textularia torquata*	*Trochammina ochracea*	*Trochammina nana*	Unidentified agglutinated	*Astononion gallowayi*	*Bolivana pseudopunctata*	*Buccella frigida*	*Buccella tenerrima*	*Cassidulina reniforme*	*Cassidulina neoteretis*	*Cibicides lobatulus*	*Dentalina* spp.	*Elphidium excavatum* f. *clavata*	*Fissurina* spp.	*Globulina* spp.	*Islandiella helanae*
	8	56	1	16					1			1				2			
		95	4	21			1											1	
	1	115		15												2			
	3	100	2	16			1									1			1
		105		8															
	3	96	1	21															
		68	2	6		9										9	1		
	1	74	1	28			2											1	
	1	62	1	33								1				2			
		98	1	14	1		3												
1		79		24			9												
	1	81		22			3												
		40	2	6					2	6		15				60			1
	1	128		16												3			
2		45		18						4	1	3	1						
		83		24	1		1			5	1	1				5			
2	1	52		19	2		2			1	2	5			1	1		1	10
	2	52		16						14	2	1				3			1
1	3	87	3	16	1	11							1			2			
		54		11	1					9						2			
2		72	5	20		11													
		98		18			1												
1	1	111	4	26		2	3												
		59		19					1	6		15				81		2	1
	1	37	1	22		24						2							
	1	40		19						4		2			1	14			
1		36		22	1														
		34		8						4		13		2		19		2	
		34		17		2	1			2	3	12		1		37			14
		31		25		1													
		45		13							4	3				7			11
		35		8						3						2			
		41		15							1				1	3			5
		44	1	17		6					1					35			1
		22	1	7						3	4	1	6		1	26		5	
1		39		9			6					2				4			
		19		9			1	2	7	1	3	79	2	1		78		1	7
1	4	24	2	7				3		2	7	9	1			34		1	1
		14		4	3	1	2		4	4		6		3		24		1	4
		13		7	1		3	1		9		17		1	1	55		2	6
		24	1	9			3				2		3			8			
		17		6						1	3	3	6			33		1	
1		12		3			1		2	4	5	12	4			93		2	4
		8		3	1					3	11		6		1	23		12	
		3		1			3			5	3	4	3	1		55			5
		2		2			1				2		1			21			

Islandiella islandica	*Islandiella norcrossi*	*Lagena* spp.	*Melonis barleeanum*	*Nonionellina labradorica*	*Stainforthia concava*	*Stainforthia feylingi*	*Trifarina fluens*	Unidentified calcareous	Test linings	Total	Atlantic species	Intermediate species	Arctic species	Indifferent	Agglutinated	% Agglutinated	Foraminifera concentration (sp./ml)
				1	1		1		43	260	16	10	142	92	253	97	306
				1				1	22	318	7	5	170	136	315	99	228
	1								28	320	3	1	220	96	317	99	512
								2	8	294	5	11	176	102	290	99	730
									31	279	4	0	219	56	279	100	446
									24	328	5	0	221	102	328	100	410
				2	2				19	272	7	1	205	59	258	95	272
	1							2	44	258	9	5	139	105	254	98	427
			1	1	1				94	319	3	0	171	145	313	98	228
									62	321	4	0	235	82	321	100	642
				1					117	350	11	3	175	161	349	100	354
									129	313	9	8	166	130	313	100	209
6	27		1					15	41	349	12	1	234	102	216	62	349
1								8	30	290	15	2	204	69	278	96	230
3	3			2				8	79	306	8	6	115	177	281	92	153
	8			1	2	1		5	46	350	8	2	248	92	321	92	2218
4				3				1	127	304	18	5	162	119	275	90	193
	36			4		1		12	33	303	37	6	170	90	229	76	946
								3	71	307	12	7	204	84	301	98	156
	9			2				2	61	306	15	1	205	85	282	92	1224
									56	308	8	0	222	78	308	100	176
								1	30	283	4	0	201	78	282	100	470
								1	55	334	6	4	228	96	333	100	134
	15			5		4		5	15	410	21	5	307	77	275	67	1673
									59	301	19	24	145	113	299	99	361
	14	1		9	3			7	38	302	32	29	157	84	247	82	730
				2				1	92	321	12	15	141	153	318	99	321
	24			10	4	1		30	38	280	27	26	155	72	171	61	272
	9			3	1				60	313	24	7	193	89	231	74	176
								9	56	277	15	11	159	92	268	97	54
				1	1			2	137	296	13	0	197	86	267	90	296
	4			3				5	14	287	9	1	217	60	270	94	383
				1				1	39	307	6	0	209	92	295	96	1020
				2	1			3	31	312	13	0	224	75	269	86	1500
	8			7				8	34	285	31	8	197	49	216	76	226
				2				3	107	312	8	2	180	122	301	96	312
	26		2	10	2	9		17	34	356	29	10	266	51	109	31	348
	23		2	5	2			19	48	284	27	8	166	83	175	62	177
	25		5	2		3	1	9	31	383	21	3	230	129	292	76	251
	13			6	2			26	71	326	19	2	203	102	187	57	187
				2				3	49	278	10	1	208	59	260	94	720
				12				12	24	269	24	0	185	60	198	74	67
	14			14	1			9	17	268	34	0	199	35	104	39	804
				11				9	112	261	45	0	147	69	185	71	163
				10				7	246	259	22	0	155	82	166	64	160
								12	85	158	3	0	122	33	122	77	148

Appendix 2

Table 1

Foraminifera isotope analysis, MSM-343520_G

Sample No.	Depth (cm)	Age (cal yrs BP)	δ 13C (PDB)	δ 18O (PDB)
1	4	73	-0.426	3.753
2	8	145	-0.728	3.704
3	12	218	-0.564	3.713
4	21	381	-1.021	3.619
5	25	454	-0.458	3.779
6	27	490	-0.524	3.737
7	29	526	-0.790	3.673
8	33	599	-1.129	3.782
9	35	635	-2.300	3.776
10	37	672	-1.444	3.773
11	39	708	-1.458	3.669
12	41	744	-1.376	3.631
13	43	762	-1.299	3.543
14	45	781	-1.605	3.651
15	47	800	-1.681	3.612
16	49	819	-0.928	3.752
17	51	837	-1.607	3.742
18	53	856	-0.881	3.732
19	55	875	-1.003	3.697
20	57	893	-0.418	3.592
21	59	912	-1.137	3.744
22	61	931	-1.617	3.645
23	63	949	-0.810	4.239
24	65	968	-0.448	3.950
25	67	987	-0.551	3.676
26	69	1006	-0.444	3.680
27	71	1024	-0.588	3.690
28	73	1043	-0.674	3.768
29	75	1062	-0.991	3.505
30	77	1080	-0.363	3.677
31	81	1118	-0.633	3.766
32	83	1137	-0.283	3.829
33	85	1155	-0.192	3.705
34	87	1174	-0.290	3.711
35	89	1193	-0.409	3.748
36	91	1211	-0.435	3.620
37	93	1230	-0.277	3.755
38	95	1249	-0.258	3.736
39	97	1268	-0.570	3.784
40	101	1305	-0.244	3.655
41	103	1324	-0.316	3.756
42	105	1342	-0.576	3.656
43	107	1361	-0.259	3.805
44	109	1380	-0.133	3.727
45	111	1399	-0.266	3.736
46	113	1417	-0.481	3.816
47	115	1436	-0.381	3.684
48	117	1455	-0.928	3.767
49	121	1492	-0.615	3.696
50	123	1511	-0.702	3.666
51	125	1529	-0.318	3.736
52	127	1548	-0.317	3.798
53	129	1567	-0.625	3.712
54	131	1586	-0.086	3.643

Sample No.	Depth (cm)	Age (cal yrs BP)	δ 13C (PDB)	δ 18O (PDB)
55	133	1604	-0.250	3.666
56	135	1623	-0.694	3.851
57	137	1642	-0.223	3.745
58	139	1660	-0.461	3.793
59	141	1679	-0.158	3.618
60	143	1698	-0.558	3.606
61	145	1717	-0.470	3.654
62	147	1735	-0.368	3.801
63	149	1754	-0.622	3.545
64	151	1773	-0.541	3.861
65	153	1791	-0.162	3.581
66	155	1810	-1.230	-0.627
67	157	1829	-0.465	3.853
68	159	1848	-0.415	3.771
69	161	1867	-0.111	3.776
70	163	1901	-0.556	3.780
71	165	1936	-0.209	3.665
72	167	1971	-0.797	3.819
73	169	2005	-0.586	3.871
74	171	2040	-0.328	3.765
75	175	2109	-0.598	3.718
76	177	2144	-0.417	3.801
77	179	2178	-0.079	4.344
78	181	2213	-0.294	3.679
79	183	2247	-0.459	3.728
80	185	2282	-0.103	3.701
81	187	2317	-0.176	3.685
82	189	2351	-0.137	3.762
83	191	2386	-0.657	3.598
84	193	2420	-0.664	3.580
85	199	2524	-0.521	3.724
86	201	2559	-0.580	3.526
87	203	2593	-0.303	3.639
88	205	2628	-0.580	3.525
89	207	2663	-0.241	3.964
90	211	2732	-0.207	4.024
91	213	2766	-0.481	3.614
92	215	2801	-0.207	3.764
93	217	2836	-0.125	4.327
94	219	2875	0.154	4.130
95	221	2913	-0.354	3.594
96	223	2952	-1.157	3.711
97	251	3491	-0.729	3.575
98	257	3607	-0.760	3.703
99	263	3722	-0.472	3.606
100	271	3876	-0.764	3.532
101	273	3915	-1.086	3.763
102	275	3954	-0.927	3.631
103	279	4031	-0.869	3.620
104	283	4108	-0.921	3.673
105	287	4185	-0.926	3.609
106	289	4223	-0.964	3.485
107	291	4262	-0.808	3.582
108	295	4339	-0.908	3.684

Sample No.	Depth (cm)	Age (cal yrs BP)	δ 13C (PDB)	δ 18O (PDB)
109	305	4532	-1.087	3.672
110	307	4570	-0.776	3.608
111	311	4647	-1.131	3.499
112	315	4724	-0.212	4.282
113	319	4801	-0.511	3.927
114	321	4840	-0.612	3.624
115	323	4878	-1.056	3.725
116	325	4917	-1.214	3.767
117	327	4955	-0.710	3.679
118	331	5021	-1.035	3.679
119	333	5046	-1.163	3.560
120	335	5071	-1.021	3.654
121	339	5121	-0.998	3.748
122	351	5270	-0.931	3.626
123	353	5295	-2.188	3.356
124	355	5320	-1.006	3.659
125	367	5470	-1.066	3.671
126	369	5495	-1.374	3.744
127	371	5520	-1.379	3.669
128	375	5570	-3.206	3.501
129	387	5720	-1.023	3.770
130	401	5895	-1.108	3.801
131	413	6044	-1.368	3.732
132	417	6094	-2.263	3.861
133	423	6169	-2.437	3.981
134	427	6219	-2.583	3.950
135	431	6269	-1.967	3.791
136	433	6294	-1.529	3.847
137	435	6319	-2.541	3.820
138	447	6469	-2.166	3.757
139	451	6519	-0.933	3.907
140	453	6544	-0.461	3.954
141	455	6561	-1.783	4.026
142	457	6579	-1.839	3.914
143	459	6598	-1.625	4.019
144	461	6616	-1.273	4.095
145	463	6634	-1.337	4.064
146	465	6652	-1.005	4.132
147	467	6670	-0.752	4.112
148	469	6688	-0.967	3.942
149	473	6725	-2.102	4.056
150	475	6743	-1.859	4.049
151	481	6802	-1.761	3.989
152	483	6822	-1.424	4.042
153	485	6841	-1.513	4.061
154	487	6860	-1.121	4.078
155	489	6880	-0.924	4.010
156	491	6899	-1.388	3.779
157	493	6919	-0.978	4.031
158	495	6938	-1.203	4.068
159	497	6958	-1.671	4.181
160	503	7016	-1.574	3.990
161	511	7093	-1.167	4.095
162	513	7113	-0.607	4.237
163	515	7132	-1.145	4.045
164	517	7152	-0.843	4.040
165	519	7171	-1.646	4.146
166	521	7191	-1.553	4.046
167	523	7210	-0.742	3.997
168	525	7229	-3.075	3.964
169	527	7249	-1.480	4.111
170	529	7268	-1.247	3.906
171	531	7288	-1.312	4.008
172	539	7365	-1.161	4.173
173	541	7385	-1.386	4.062
174	545	7424	-1.164	3.965
175	547	7443	-1.118	4.247
176	549	7462	-1.080	4.286
177	551	7482	-1.105	4.372
178	557	7540	-0.902	4.192
179	559	7556	-0.875	4.303
180	561	7576	-1.232	4.326
181	563	7596	-0.951	4.274
182	565	7615	-0.981	4.323
183	567	7635	-1.358	4.287
184	569	7655	-1.002	4.358
185	571	7674	-1.043	4.295
186	573	7694	-1.017	4.316
187	575	7714	-1.621	4.372
188	577	7733	-1.489	4.256
189	579	7753	-1.742	4.312
190	581	7773	-1.693	4.224
191	585	7812	-1.366	4.274
192	587	7832	-1.593	4.201
193	593	7891	-2.180	4.063
194	617	8127	-3.998	3.920
195	627	8225	-4.272	3.859
196	633	8285	-5.100	3.848
197	635	8304	-4.918	3.952
198	637	8324	-5.932	3.967
199	639	8344	-4.816	4.077
200	641	8365	-1.719	4.348
201	669	8651	-2.528	4.191
202	671	8671	-2.782	4.157
203	673	8691	-2.705	4.224
204	677	8732	-3.003	4.139
205	679	8752	-5.253	3.842
206	681	8773	-4.468	3.877
207	683	8793	-3.741	3.876
208	689	8854	-2.747	4.016
209	691	8875	-1.614	3.985
210	693	8896	-3.144	4.054
211	695	8916	-2.996	4.109
212	697	8935	-2.494	4.030
213	701	8974	-1.218	3.930
214	705	9013	-1.117	4.122
215	713	9090	-1.885	4.262
216	719	9148	-2.405	4.162
217	833.4	10256	-1.150	4.458
218	893	10833	-0.975	4.139
219	899	10891	-1.075	3.880

Table 2 Duplicate isotope sample analyses on *N. Labradorica* specimens.

Depth (cm)	δ 13C (PDB)	Mean δ 13C (PDB)	1σ	δ 18O (PDB)	Mean δ 18O (PDB)	1σ
37	-1.44			+3.77		
	-1.71	-1.58	0.19	+3.66	+3.72	0.08
73	-0.67			+3.77		
	-0.42	-0.55	0.18	+3.70	+3.74	0.05
95	-0.26			+3.74		
	-0.26	-0.26	0.00	+3.67	+3.71	0.05
131	-0.09			+3.64		
	-0.30	-0.19	0.15	+3.49	+3.57	0.11
305	-1.09			+3.67		
	-1.02	-1.05	0.05	+3.58	+3.63	0.06
431	-1.97			+3.79		
	-2.04	-2.01	0.05	+3.93	+3.86	0.10
465	-1.00			+4.13		
	-0.90	-0.95	0.08	+4.13	+4.13	0.00
493	-0.98			+4.03		
	-1.06	-1.02	0.06	+4.02	+4.03	0.01
527	-1.48			+4.11		
	-0.82	-1.15	0.47	+4.03	+4.07	0.06
565	-0.98			+4.32		
	-1.06	-1.02	0.05	+4.31	+4.32	0.01
635	-4.92			+3.95		
	-5.67	-5.29	0.53	+3.78	+3.87	0.12